Ministry of natural resources of the Russian Federation
Russian Academy of Sciences
Russian Academy of Natural Sciences
Moscow State University
Russian Research Institute for the Synthesis of Materials

The International Jubilee Conference

"Single crystals and their application in the XXI century – 2004"

VNIISIMS, Alexandrov, Russia
June 8-11, 2004

Alexandrov
VNIISIMS

Abstracts of the International Jubilee Conference
"Single crystals and their application in the XXI century – 2004"
June 8-11, 2004
Alexandrov, VNIISIMS, 2004, 348 pages

All texts are presented according to authors' original articles.

Conference sponsors:
Anthony&Bryan Lonsdale Charity Foundation,
Moscow Industrial Bank

A HISTORY OF SURFACE ACOUSTIC WAVE DEVICES

D.P.Morgan, UK

Surface Acoustic Waves (SAWs) were discovered by Lord Rayleigh in the 19th century, but their applications in electronics date from the 1960s. As for bulk acoustic waves, SAW's have the major advantages of low velocities and low losses, but in addition the presence of a free surface brings substantial versatility. Thus, a wide variety of SAW components can be used to generate and detect the waves, or to modify them by introducing reflections, waveguiding and so on. This has lead to a substantial range of SAW devices, which are now firmly established in the area of passive analogue electronics.

This paper will review the development of the subject historically. For electronics, the subject was initiated by the invention in 1965 of the interdigital transducer for generation and detection of the waves, exploiting the piezoelectric effect in quartz or lithium niobate crystals. Early efforts were aimed at pulse compression for radar systems, and SAW made this technique practically feasible. Another early aim was the IF bandpass filter for domestic TV, where SAW devices became universal after a few years of development. In the 1970s a considerable variety of devices were developed, particulary for military systems, and SAW technology became established. In parallel with device development, the important topic of suitable materials was investigated, and new crystals were established.

In the 1980's the rise in wireless communications (particularly mobile phones) demanded bandpass filters with low loss, as low as 2 dB at RF (900 MHz). In response, a variety of new SAW filters were invented. RF devices include types of resonator filters using novel 'leaky' waves, and IF devices include transverse-coupled resonators and unidirectional transducers. All of these are now in common use, particularly in mobile phones. The devices exhibit a very high degree of versatility and reproducibility - factors which have made the subject a great success, as shown by the production of about 3 billion devices annually.

A SURVEY OF SAW RESONATORS

D.P.Morgan, UK

Resonators are familiar components in analogue electronics, examples being electromagnetic resonators (cavities, dielectric ceramics, etc.) and bulk acoustic wave resonators usually made of quartz. These components have applications in frequency stabilisation of oscillators and in low-loss bandpass filters.

SAW resonators can serve the same functions, particularly in wireless applications - in fact, the majority of low-loss SAW bandpass filters in mobile phones are based on resonators. However, SAW resonators differ from other technologies in several ways. To obtain strong reflections, SAW devices need gratings consisting of many reflecting strips. The gratings give strong reflections only over a narrow frequency band, and the device only behaves as a resonator in this band. Typically, the cavity length might be 100 wavelengths, giving small mode spacing, but the narrow bandwidth of the reflector gratings is used to select only 1 or 2 of these modes. If quartz resonators are connected electrically to form bandpass filters, the low piezoelectric coupling limits the bandwidth. Consequently, a variety of devices have been developed to overcome this by using direct acoustic coupling between resonators.

Because of these considerations, SAW resonators have many distinct features. This paper will give an overview of the subject, including

1) 'classical' resonators (1- or 2-port) with non-reflective transducers;
2) Effect of electrode reflections in transducers;
3) Transverse-coupled resonators for IF filtering;
4) Impedance element filters for RF filtering, using leaky waves;
5) Longitudinally-coupled resonator (LCR, or DMS) filters.

The last three filter types are common in present-day mobile phones. The paper will discuss these topics descriptively, including device principles and performance.

EVOLUTION OF BAW DEVICES,THEORICAL UNDERSTANDING,TECHNIQUES AND USE OF PIEZOELECTRIC MATERIALS

Raymond J. Besson E.N.S.M.M. 26 Chemin de l'epitaphe 25030

BESANCON cedex France

Piezoelectric crystal resonators are present in almost any frequency control equipment and in many sensors.There has been a strong competition between the needs (more and more demanding) and the improvements to overcome limitations.

Developing resonators and sensors has always been very demanding.New designs and new theoretical understandings together with improved use of piezoelectric matérials have allowed very impressive progress(at a time an order of magnitude per decade). In this paper, piézoéiectric resonators are first presented trying to point out important concepts for developments and new developments. An historical review providing general ideas is presented.Some détails are also given on the effort devoted to the production and use of matérials.During decades matérial was essentially quartz, but the search for substitutes to quartz has been recently rather successfull and will be outlined here.

The various steps of progress will be presented and, in conclusion ,the improvements in results will be discussed pointing out possible future

DYNAMIC ROTARY TORQUE MEASUREMENT USING SURFACE ACOUSTIC WAVES

A. Lonsdale - Technical Director

Sensor Technology Ltd

ABSTRACT

The subject of torque measurement has previously been addressed extensively. Most of the existing transducers either rely on low voltage analogue systems (e.g. conventional resistive strain gauge) or complicated mechanical assemblies by physically assessing displacement, i.e. optical systems.

This paper identifies a new, potentially low cost, non-contact, frequency domain strain torque sensor[1] utilising SAW (Surface Acoustic Wave) Technology for surface strain measurement. The sensor has a short axial length making it flexible in terms of integration into a variety of applications, encompassing both static and dynamic measurement. The paper presents a technical description of the resulting transducer, regarding its operation and construction.

1.0 Background

The stress-strain relationship is fundamental to the study of the mechanics of materials and is used to measure many physical quantities such as axial force, bending moment, torque, pressure, acceleration and temperature. In order to practically assess the stress state in a specimen it is imperative to measure the strain. Simple computation[2] of the strain, along with material properties, provides a method for determining the stress state. Effective practical measurement of strain has long been a problem. The following is a summary of the existing methodologies for strain assessment.

Mechanical devices evolved as the first type of strain gauge e.g. extensometer, which relies on the displacement of levers to indicate the strain. Another example is that of the photoelectric strain sensor, which utilises the displacement of light passing through gratings separated at a set distance; sensing of variation in light intensity by photocells provides a signal indicative of the strain. On the whole, such methods are bulky, difficult to use and mostly limited to static strain analysis.

Optical techniques, such as photo-elasticity, holography or Moire' methods for strain analysis prove to be both accurate and sensitive. However, the apparatus and intricacy of the optical processes generally restricts the practise of such methods to specially prepared laboratories.

Existing electrical devices for measuring strain can utilise any of the following methods; capacitive, inductive, piezoelectric, resistive and piezo-resistive techniques can be identified as the main contributors to the solution of practical strain measurement. However, all rely on the interrogation of low power density analogue signals, highly susceptible to amplitude-modulated noise.

Of all the techniques described, resistive strain gauges have emerged as the dominating technique for strain measurement. The gauge is generally bonded onto the specimen and provides a low cost solution with the following characteristics: short gauge length, small physical size, small mass, moderate signal error resulting from temperature fluctuations and capability of measuring both static and dynamic strain. However translation to non-stationary applications e.g. a rotating shaft, demands expensive slip rings or large low frequency transformers.

It is apparent, therefore, that there is great demand for a low-cost, unobtrusive, high performance, non-contact strain sensor. This paper will identify a new, potentially low cost, non-contact, frequency domain strain sensor utilising SAW (Surface Acoustic Wave) Technology for surface strain measurement. The fundamental behaviour of the device will be discussed along with brief attention to its construction.

2.0 Non-Contact Strain Measurement Utilising Rayleigh Waves

2.1 Surface Acoustic Waves (SAW) - Rayleigh Waves

In 1885, the English scientist, Lord Rayleigh, theoretically demonstrated[3] that waves could be propagated over the plane boundary between a linearly elastic half-space and a vacuum (or a sufficiently rarefied medium e.g. air), where the amplitude of the waves decays exponentially with depth. Rayleigh predicted such waves to be a major component of earthquakes, a fact to be confirmed much later in the 1920's due to the advent of seismographic recordings.

Some forty-five years later, Voltmer and White, of the University of California, generated such waves[4], which are more commonly referred to as Surface Acoustic Waves (SAW) or Rayleigh Waves, on the free surface of an isotropic, elastic substrate, namely, quartz.

Figure 1.
Surface Acoustic Wave

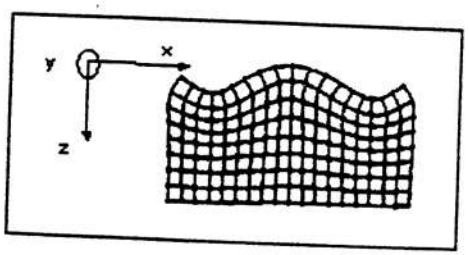

The action of the wave on the solid produces a pattern of displacements as illustrated in figure1., where the dots indicate material particles, nominally equidistant both vertically and horizontally in the absence of wave motion. The components of displacement along the x and z axes are given by equations (1) and (2) respectively[5].

1) $$U_R = Ak_R\left[e^{-q_R z} - \left(\frac{2q_R S_R}{k_R^2 + S_R^2} \right) e^{-S_R z} \right] \sin(k_R x - \omega$$

2) $$W_R = Aq_R\left[e^{-q_R z} - \left(\frac{2k_R^2}{k_R^2 + S_R^2} \right) e^{-S_R z} \right] \cos(k_R x - ($$

Where:

A is an amplitude constant,

k_R is the Rayleigh wave number,

$k_L = \omega(\rho/(\lambda+\mu))^{1/2}$ are the wave numbers for longitudinal modes,

$k_T = \omega(\rho/\mu)^{1/2}$ are the wave numbers for transverse modes,

λ and μ are the elastic Lame constants, ρ the material density and ω the circular frequency,

$q_R = (k_R - k_L)^{1/2}$, $s_R = (k_R - k_T)^{1/2}$,

t is the time, x the in-plane displacement and z the vertical displacement.

Since the displacement components U_R and W_R in the Rayleigh wave along the x and z axes, respectively, are shifted in phase by $\pi/2$, the mode of oscillation of particles supporting a Rayleigh wave is a retrograde ellipse whose normal (vertical) displacement reaches its maximum amplitude at a depth of approximately $0.2\lambda_R$ (where λ_R is the Rayleigh wavelength) and then decays to zero within two wavelengths from the surface. It also contains a component of displacement in the plane of the solid surface.

The influence of the material properties of the surface layer of a sample on the velocity and attenuation of Rayleigh waves permits the latter to be used for the assessment of residual stresses in the surface layer, as well as the thermal and mechanical properties of the surface layer of the sample. Upon this is based the application of Rayleigh waves for the non-intrusive surface testing of components and of particular interest strain measurement. The requirement is for a transducer design capable of measuring such phenomena.

2.2 Surface Acoustic Wave Transducer Construction

An important property of a surface acoustic wave is that its phase velocity is somewhat smaller than the phase velocity of a bulk wave in that direction. The Rayleigh wave velocity is

approximately 10^5 times slower than the velocity of electromagnetic radiation in vacuo, and thus, for the same frequency, the wavelength of the elastic wave is less than the wavelength of the corresponding electromagnetic wave by a factor of 10^5. This result has immediate importance on the geometry of the resulting gauge and is the philosophy behind surface wave technology, since the devices themselves can be much smaller than their electromagnetic counterparts, with the additional advantage that the surface wave can readily be sensed anywhere along its path. Importantly, it can be shown[3] that the Rayleigh wave does not exhibit phase velocity dispersion, i.e. there is no dependence of velocity on frequency.

The Rayleigh waves are produced by metallic film transducers on the surface of a piezoelectric material as illustrated in figure 2. These transducers have an interdigital configuration, which is readily fabricated using standard integrated circuit technology. The period of the fingers determines the period of the wave generated. An alternating voltage applied to the transducer causes the surface of the piezoelectric material to undulate periodically, thus producing waves. These waves are reflected by a similar array and form a one-port structure whose impedance can be set at a given frequency, normally 50Ω.

Saw sensors can be made of quartz as shown in Fig.3.

Figure 2.
Outline of a Basic Saw Transducer

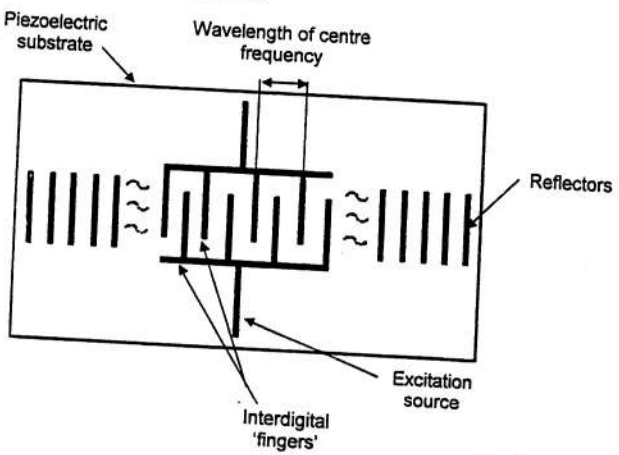

Figure 3.
200MHz SAW Resonator shown on thumbnail

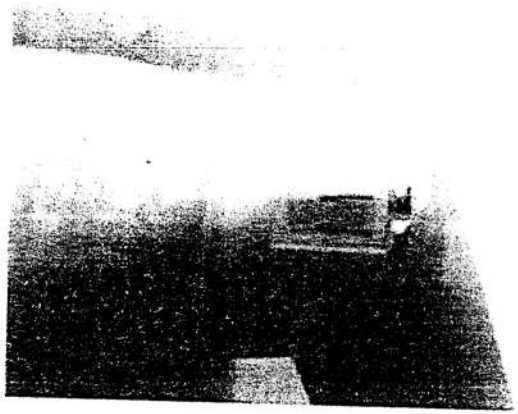

The operation of a SAW transducer for strain measurement depends on the choice of a suitable piezoelectric substrate, which can be attached to the material to be stressed. The stress induces a strain, which can be in either a state of tension or compression. The sensitive axis of the transducer is longitudinal in the direction of wave propagation. Strain will change the spacing of the interdigital electrodes and hence the operating frequency. For example, for an excitation frequency of 500 MHz, 1000 με of tension will decrease the frequency by 500 KHz [simply: $1000.e^{-6}.500.e^{6}$], conversely a compressive strain will increase the frequency by the same amount. The quality factor (Q) of the transducer is high, typically 10^4, therefore, by measuring the impedance, a tracking oscillator can be controlled; this can represent the resonant frequency within a few hertz.

Figure 4
Schematic Of Frequency Domain SAW Signals

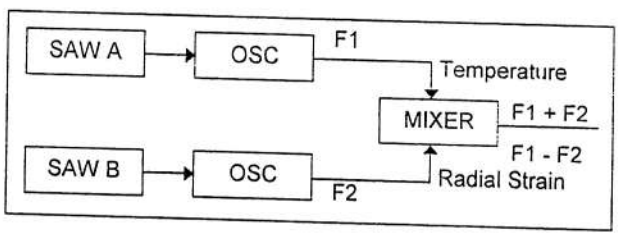

From the technique described it is apparent that the output signal will be in the frequency domain as shown in figure 4. This has many advantages from an application viewpoint; particularly in variable speed electrical machines where low frequency signals can be easily contaminated by drive electronic generated noise. The SAW impedance, designed at the 50 Ω standard, means there is generally less noise than in its classical resistance gauge counterpart (resistance usually 100 - 350Ω). The maximum power of the SAW signal is in the region of 25mW, and so when compared with say a 10V half bridge resistive strain gauge system where the total power of the output strain signal is in the region of 1μW the SAW offers a more robust solution to strain measurement. Piezoelectric transducers are available for dynamic strain sensing but with the disadvantage of having a high output impedance and poor temperature performance.

2.3.0 Application of SAW Devices For Measuring Strain

2.3.1 Torque Measurement

Torque (radial strain) transducers are one of the more common devices used by development engineers. Knowledge of torque and rotational speed can be used to indicate power, from which the efficiency of gearboxes, transmissions, electrical machines and many other systems can readily be assessed. To apply the SAW element principle, two devices are used in a half bridge, analogous to the classic resistive strain gauging configuration; one positioned so as to be sensitive to the principal compressive strain and the other positioned to observe the principal tensile strain. Note that in the absence of bending moments and axial forces, the principal stress planes lie perpendicular to one another at 45° to the plane about which the tensional moment is applied. This is illustrated in figure 5.

Figure 5
SAW Gauge Arrangement For Torque Measurement

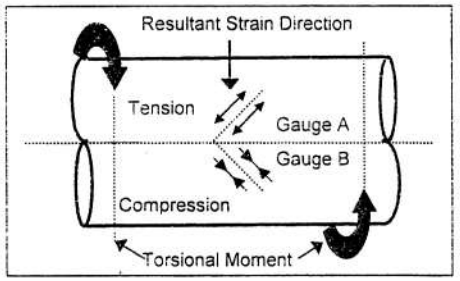

A typical structure is shown with 2 saws attached, like the one in Figure 6.

Figure 6
Shaft with two SAWs attached

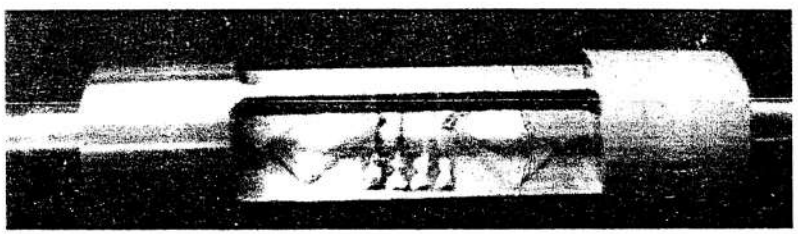

The two frequencies produced by the Saw's are mixed together to produce the difference and / or sum signals. The difference signal is a measure of induced strain due to the twisting moment and hence, from a knowledge of the material properties and the governing equations, the torque is implied. The sum signal is a measure of shaft temperature.

Coupling of the signals to and from the machine shaft is achieved via an electromagnetic coupling device comprising of two concentric loops, separated by a suitable distance, one fixed to the shaft housing and the other fixed to the rotating shaft providing non contact interrogation which is intrinsically safe. This coupling is shown in Figure 7.

Figure 7
Electromagnetic coupling device mounted onto the shaft

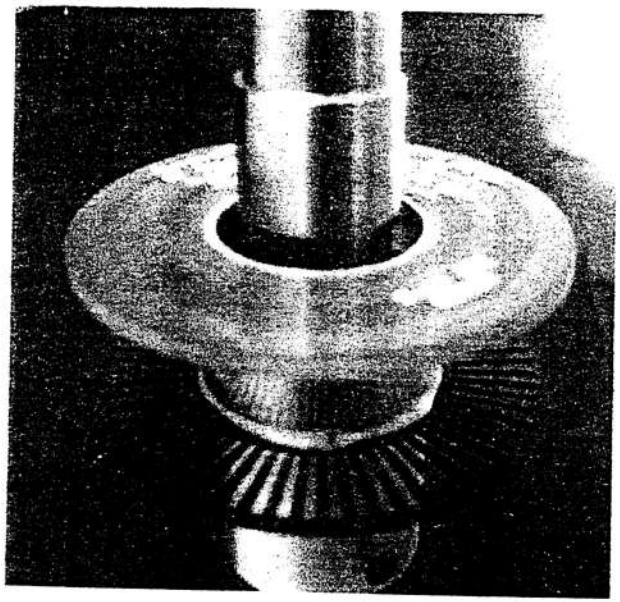

The primary frequency of oscillation can be chosen to lie between 100 - 1000 MHz with the difference frequency varying up to 1MHz. Such a transducer has the following specification:

Resolution: 1 part in 10^6.

Linearity: 0.1%.

Bandwidth: >1MHz.

3.0 Conclusions

It has been demonstrated that SAW devices can be used as strain gauges functioning in the frequency domain. An increase in sensitivity over prior art by two orders of magnitude is not unrealistic. The low power requirements coupled with low impedance make these devices superior to conventional resistance gauges. Due to their simplicity and ease of manufacture it

is not improbable that these devices will serve well into the 21st Century, as the resistance gauge has served during the 20th Century.

4.0 References

1. A Lonsdale & B Lonsdale EU Patent EP518900, USA Patent 5585571
2. 'Theory Of Elasticity', Timoshenko, S. P., & Goodier, J. N., Third Ed., 1970, McGraw-Hill inc.
3. Lord Rayleigh (J. Strutt): 'On waves propagated along the plane surface of an elastic solid', Proc. Lon. Math. Soc., (17): 4-11, 1885.
4. White, R.M. and Voltmer, F.W. : 'Direct piezoelectric coupling to surface elastic waves', Applied Physics. Letters, (7): pp 314-316, 1965.
5. Viktorov, I.V. : 'Rayleigh and Lamb Waves - Physical theory and applications', Plenum Press, New York, 1967.

B-LI-CE SCINTILLATION GLASS FOR NEUTRON DETECTION

M. Ishii[1)*], Y. Kuwano[1)], T. Asai[1)], S. Asaba[1)], M. Kawamura[1)], T. Kito[1)], N. Senguttuvan[2)$], T. Takagi[2)], T. Hayashi[2)], M. Kobayashi[3)], M. Nikl[4)], S. Hosoya[5)], K. Sakai[6)#], T. Adachi[6)], T. Oku[6)#], H.M. Shimizu[6)]

1 Dai-Ichi Kiden Co., Ltd., Shimo-ishihara, Chofu, Tokyo 182-0034, Japan

2 SIT, Shonan Institute of Technology, Fujisawa 251-8511, Japan

3 KEK, High Energy Accelerator Research Organization, Tsukuba 305-0801, Japan

4 Institute of Physics, AS CR, Cukrovarnicka 10, 16200 Prague, Czech Republic

5 Yamanashi University, Takeda, Kofu 400-8510, Japan

6 RIKEN, Wako, Saitama 351-0198, Japan

Abstract

The luminescence property of Ce containing oxide glass having B and Li with large absorption coefficient for neutron was investigated by optical transmittance, alpha particle, and neutron irradiation. The light output of the B_2O_3-Li_2O-CeO_2 glass system increased with the increase in B_2O_3 and CeO_2. It was observed that the decay time which showed composition dependence varied in the range 40 - 45 ns. Although the light output by neutron irradiation is 8.5% of Li-glass, small atomic number, low density and short decay time make this new boron based glass scintillator useful for neutron detection.

Corresponding author. Tel.: +81-424-88-3312; fax: +81-424-88-3420; e-mail: m-ishii@d-kdn.co.jp

Present address: $ Hitachi Chemical Co., Ltd., Tsukuba 300-4247, Japan.

JAERI Tokai, Ibaraki 319-1195, Japan

PHYSICAL PROCESSES IN SCINTILLATORS STUDIED USING SYNCHROTRON RADIATION

V.V.Mikhailin

Physics Faculty, Moscow State University, Moscow, 119992 Russia

Transformation of energy of ionizing particle or high-energy photon in scintillators is the result of several consecutive relaxation processes, starting from the creation of primary high-energy electronic excitations and ending by photon emission or defect creation or direct heating by phonon emission. Hot relaxation stage results in the creation of secondary electronic excitations of intermediate energies similar to those created after the absorption of VUV or XUV photons. Thus synchrotron radiation in this energy range provides an unique tool for direct investigation of the majority of energy conversion stages in scintillators and luminescent detectors of ionizing radiation.

The results of investigation of various crystals with heavy ions (lead tungstate, cerium and barium fluoride, lutetium and ytterbium compounds, etc.) using synchrotron radiation are reviewed. These scintillators have short decay time, good radiation hardness and high density and therefore can be used in manifold medical and high energy physics applications. The main investigation methods discussed in the presentation are decay kinetic analysis and study of luminescence excitation spectra under VUV and XUV excitation.

ANOMALOUS TRANSIT-TIME DISPERSION IN NATURAL DIAMONDS

V. Kvaskov

Polaron Ltd., Moscow. E-mail: kvaskov-v@nm.ru

Results are presented of some optoelectronic properties studies which characterised of natural diamond as a disordered semiconductor. The reason is random space and energy level distributions of the localized electronic states. These states created of nitrogen defects, with content to 1 *pm*. Thus, the natural diamonds are among the highly doped compensated semiconductors.

It is shown that photocurrent decay non-exponentialy. With UV-Lasers (248, 222, 203 nm) stimulated transient-current trace was non-Gaussian (with constant velocity of charge packet moving "plateau" with following exponential "tail"). A log-log plot indicating the current I(t) associated with a packet of carriers moving, in electric field, with a hopping-time distributen functin. The continuous reduction of the current is observed. This reduction obeys an equations

$$\log I(t) \sim [-(1-\alpha)] \quad \text{for a propagating packet}$$

$$\text{and} \quad \log (I) \sim [-(1+\alpha)] \quad \text{for a long-time "tail"}$$

The dispersion factor α satisfy an condition

$$-[(1+\alpha)+(1-\alpha)] = -2$$

The experimental data corroborate the non-classical nature of photocurrent relaxatoin. Pulse UV-photoconductivity of natural diamond is a stohastic prozess with dispersion in the hopping-time distribution function. Normalized transient-current trace expected for a non-Gaussian, non-Markoffian transport. This trace is known as a "Continuous Time Random Walk". The quantative features of CTRW model discussed.

New experimental data on S-shaped optoelectronic switching in natural diamond are presented. Several features of phenomena (I-W, I-V-characteristic and delay time) are studied by applying a Laser pulse with difference power and voltage. The possible physical mechanism of switching phenomena in connection with random structure in the impurity band and nature of defects are discussed.

SCINTILLATION MATERIALS ON A BASE OF OXIDE CRYSTALLINE COMPOUNDS. STATUS AND DEVELOPMENT.

M.Korzhik

Institute for Nuclear Problems, 220050, Minsk, Belarus

A phenomenon of scintillation as an instrument of ionizing radiation parameters detection and measuring has played a prominent role in the development of a modern physics. Visual observation of scintillation in ZnS has allowed to E. Rutherford to observe alpha-particles and became a starting point in an experimental nuclear physics and has predetermined its development. Historically, alcali-halide scintillation crystals have received the greatest distribution in detecting technique since the extremity of the fortieth years of the last century. At the same time already in the beginning of the eightieth, with the development of fast response photodetectors, electronics and acquisition systems, became apparent limits of these crystals, especially in experimental high energy and particle physics. On the other hand, the fast development of production technology and intensive study in the field of laser media on the base of oxide and fluoride crystalline materials boosted development and have made routine high-temperature production technology of crystals. Luminescent crystalline oxide high quality single crystals became available in great quantities since the eightieth years. It has led to discovering of a number of new prospective scintillation materials. Scintillators on the basis of oxide compounds have several advantages. By virtue of that our world is oxygen, crystals on the basis of oxide compounds are not subject to degradation due to anionic spontaneous diffusive substitution while halide crystals, especially fluorides, are subject to spontaneous degradation in an oxygen environment. Thus the majority of oxide single crystals which are potentially applicable for scintillator making, are rigid, not hygroscopic and chemically inert. Oxygen compounds allow to create single crystals with density of 7–10 g/cm^3 that predetermines their high potential for dominating use in detecting systems for high-energy particles and γ-quanta. Classification of the scintillation materials, scintillation mechanisms in undoped and doped single crystals, further development of the new materials will be discussed.

LANGASITE SAW RESONATOR FOR OPTICAL COMMUNICATION

Sean Wu and Yeong-Chin Chen

Department of Electronics and Information Engineering, Tung-Fang Institute of Technology, 110 Tung-Fung Road, Hunei Shiang, Kaohsiung 829,Taiwan, R.O.C.

Abstract

Today the Internet has become essential global communication system and the Internet users are glowing dynamically in the world. By applying the WDM (Wavelength Division Multiplexing) technology, it is possible to transmitter a large volume data. The CDR (Clock Data Recovery) must be connected with each wavelength signal. To transmit the data in high speed, high clock frequency is required. In the optical transceiver, the most important part is the clock generator of transmitter and the clock recovery circuit of receiver. To ensure the correct of transmission, photo electronic receiver retrieves the data clock with clock recovery circuit, and the judgment circuit takes samples with that clock. To minimize the error rate, judgment circuit shall sample at appreciate time; therefore the clock recovery circuit shall supply accuracy clock without jittering. VCSO (Voltage Controlled Surface acoustic wave Oscillator) is a good choice. A fast accuracy voltage controlled oscillator has those important properties, such as, temperature stability, low jitter and large tunability. Large tunability will make the CDR easy to synchronize the input signal. To get large tunability, it needs a high frequency fundamental resonator. The tradition primary material for SAW resonator is ST-cut quartz. It will be known, ST-cut quartz has high quality factor and very good temperature stability. Langasite ($La_3Ga_5SiO_{14}$) crystal has an electromechanical coupling coefficient approximately 3 times larger than that of ST-cut quartz and shows good temperature stability. In this research, we use ST-cut quartz and Langasite ($La_3Ga_5SiO_{14}$) crystal (0°, 138.5°, 26.5°) to be the substrates for the one-port SAW resonator. We design two frequencies are 155 MHz (OC-3/STM1) and 622 (OC-12/STM4) MHz, and simulate the frequency response. The results show the Δf (f_r□f_a) on LGS based have at least twice as those on quartz based. That means the tunaility of LGS VCSO will larger than quartz. It was evident from the theory and simulation results. LGS also has high quality factor and very good temperature stability. We think LGS crystal family are very suitable on the VCO applications for optical communications.

GROWTH AND DIELECTRIC PROPERTIES OF SINGLE CRYSTAL $Pb_5Ge_3O_{11}$

M.V. Provotorov (1), T.N. Trushkova (1), A.A. Bush, (2), K.E. Kamentsev (2)

(1) D. Mendeleev University of Chemical Technology of Russia 125480, Moscow, Russia

(2) Moscow state institutes of a radio engineering, electronics and automatics (technical university) 119454, Moscow, Russia

E-mail: (1) mailto:mvprovo@rambler.ru ; (2) abush@ranet.ru

Ferroelectric crystals of lead germanate $Pb_5Ge_3O_{11}$ are promising materials for different technical applications [1]. However, nature of the appearance of the strong low frequency dielectric dispersion at temperatures below Curie point (450 K) remain debatable.

Single crystals $Pb_5Ge_3O_{11}$ up to several cubic centimeter in volume have been grown by Chzochralski technique from own melt with coefficient of its utilization equal to 0,1. Repeated growth from the same melt result in change of the trigonal unit cell parameters (*a*: 10,226(4) Å → 10,214(5) Å; *c*: 10,664(3) Å → 10,649(4) Å). This indicates on the presence of the narrow homogeneity range in PbO-GeO_2 system and on deviation of the melt composition to the boundary of this range in consequence of evaporation of the more volatile component (most likely PbO). Such deviation from the initial stoichiometry results to appearance of the own impurity composition and noticeable darkening of the brown coloring of crystals. Accordingly, the electrical conductivity of crystals is increased. The pulling rate was equal to 2-4 mm/h, growth direction was directed along an axis "*c*" or along an axis "*a*". The grown crystals have brightly expressed facet and pseudo facet forms. The first oriented seeds were obtained by hybrid method (directional crystallization from continuously feeding melt through a platinum spinneret). The crystal rods1-2 mm in diameter were obtained by means of expansion growth of microscopic crystals $Pb_5Ge_3O_{11}$, obtained earlier by hydrothermal synthesis. The last crystals are easy oriented by use of natural facet. Besides, orientation of crystals have been tested by x-ray diffraction studies. To minimize the growth banding, all crystals were synthesized in a condition of a free (no controllable) growth at stabilization of power. This method exclude the necessity of the stabilization of a crystal diameter with the use of an electronic controller.

The dielectric and electric properties of crystals were studied on the platelet single crystal samples with different thickness in the range 0,5-3 mm. The plates were oriented perpendicular to an axis "*c*" or on an axis "*a*". Temperature varied in the range 100-600 K, frequency and amplitude of a ac measuring voltage varied in the ranges of 0,1-100 kHz and 0,04-2,0 V. On the temperature dependencies of the dielectric constant apart sharp peak in the range of Curie point it is observed the less expressed peaks in the ranges 230 K and 100 K. The data about influence on low temperature dielectric anomalies different factors (frequency, polarization of crystals, its sintering at different temperatures and various gas environments and other) were obtained. It was found that these dielectric anomalies have relaxation character and are related to processes of charges localization on defect centers. They are caused by semiconductor properties of the ferroelectric crystals $Pb_5Ge_3O_{11}$ and are connected to the dynamics of thermally localization of charge carriers at defect levels with formation of local polarized states. Therefore, the studies of the dielectric properties of these crystals in this temperature range are effective method of controlling of the defect state of these crystals.

The present work was supported by Russian fund of basic researches (Project No 02-02-17798).

1. A.A. Bush, Yu.N. Venevtsev. Single crystals with ferroelectric and related properties in system PbO-GeO_2 and possible areas of their applications. Moscow, NIITEHIM. 70 p. (1981).

METASTABLE PHASES AND MICROSTRUCTURE PARTICULARITIES IN PROTON EXCHANGED WAVEGUIDES LAYERS

Denis I. Shevtsov[1], Irina S. Azanova[1], Il'yas F. Taysin[1], Ivan E. Kalabin[2], Victor V. Atuchin[2], Anatoliy B. Volyntsev[3],

[1] Perm scientific-industrial instrument-making company 614990, Perm, 25-October st., 106 root@ppk.perm.ru

[2] Institute of Semiconductor Physics SB RAS, [3] Perm State University

Proton exchanged layers and channels in lithium niobate (H:$LiNbO_3$), with chemical composition $H_xLi_{1-x}NbO_3$, are the challenging medium for making various integrated optic components. Evidently, the reliability of the devices is defined by the stability and reproducibility of waveguide optical properties, refractive index in particular. The formation and decay of high temperature phases in waveguide layers, representing α-, β_l- phases of solid solution $H_xLi_{1-x}NbO_3$ on X and Z-cut $LiNbO_3$ and pure $LiNbO_3$ have been studied by means of IR transmission spectroscopy, waveguide mode spectroscopy and high resolution X-ray diffractometry. It is shown now that the phase transitions between the equilibrium and high temperature phases in $H_xLi_{1-x}NbO_3$ layers at high x~0.47 are reversible and accompanied by variations of crystal structure of the layer as high as ~16% in reference to deformation created by doping. It may be supposed that the structural transformations are governed by some configuration redistribution of the protons within the possible crystal lattice positions.

The refractive index profiles and crystal structure of X-cut H:Ti:$LiNbO_3$ layers have been studied in the present study with different content of hydrogen. The estimated surface Ti content was ~6 mol% that is far below the upper concentration boundary of solid solution of titaniun in $LiNbO_3$. It has been shown that the presence of Ti impacts the crystal lattice deformation induced by proton exchange.

The structural defects had been found out on surface H:$LiNbO_3$ of the waveguides produced on substrates $LiNbO_3$ containing residual internal strain by optical microscopy. The defects represent, apparently, lamellar areas thickness ~100 nm containing one of the phases of solid solution $H_xLi_{1-x}NbO_3$ with higher parameter of a crystal lattice in perpendicular direction to substrate plane. These lamellar areas are distributed deep into $H_xLi_{1-x}NbO_3$ waveguide layer that proves to be true the data of scanning electronic microscopy and interfaced to a matrix by means of a grid of dislocations of discrepancy. These lamellar areas leave on substrate surface of a depth waveguide layer and extracting external border of a monocrystal that was revealed by optical interferometer profilometer. The residual internal strain in substrate $LiNbO_3$, apparently, promotes formation of the found out lamellar areas.

DYNAMIC ELECTROCALORIC EFFECT IN FERROELEKTRICS.

Мокejev A.A., Мокejev An. A.

Private laboratory, 210035, Vitebsk, street. Smolensk 5-1-18, Byelorussia.

The ferroelectric phase transition of displacement type is relaxation of a cristal srtucrure, of soft sublattice elasticity and the avalanche decay of the polarization P~X, which is proportional to the coherent displacement of the soft sublattice ions at action of the feedback between polarization and Lorentz - Wise field with intensity $El = P / \varepsilon o \cdot \gamma l$. in motion equation of soft sublattice ions for its displacement X from the equilibrium place, which is removed on pseudo - spin shoulder X2 from neutral center of elementary cells this feedback is expressed by the negative friction - h (X-Xs) dX/dt, that is replaced by positive friction with displaces greater than Xs, corresponding to spontaneous polarization Ps [1]

$$\frac{d^2X}{dt^2}+\left(g-f\cdot\left(X-X_s\right)\right)\frac{dX}{dt}+\left[A\cdot\left(X-X_2\right)+G\cdot X\right]\cdot e^{W\cdot(X_1-X)\cdot\tau}+B\cdot X\cdot e^{v\cdot(T-T_t)\cdot\tau}=0 \quad (1)$$

The feedback of P and El together the nonlinear dependence of soft sublattice elasticity on displacement X of these ions results in occurrence of auto- oscillations of polarization near the phase transition with temperature T near phase transition temperature Tt(Ed(X1-X) which dependes on a depolarizing field which intensity Ed ~ X. The chose of shunting resistor R relative to internal Ri of a sample establishes the average deviation of transition temperature and sample temperature Tt-T so auto-oscillations do not stop. The power tacked away by oscillations of polarization from a sample, is absorbed in shunting resistor. The decrease of transition temperature owing to amplification of a depolarizing field stabilizes the auto-oscillations

$$Ed = Edo - \frac{Ri\cdot\varepsilon o\cdot\gamma d}{(R+Ri)\cdot h\cdot C}\cdot Edo \quad (2)$$

where Edo - intensity of the depolarized field for free crystal, γd – depolarizing form factor, h - wide of crystal, εo – electric permeability of vacuum, C - electric capacity.

Because the voltage arising on shunting loading stops the growth of depolarizing field.

In a significant part of the oscillation period the an abnormal heat capacity appears small.

It provides strong electrocaloric effect proportional to a square of amplitude of polarization oscillations

$$\Delta T = \frac{\beta}{Cp} \cdot T \cdot \Delta P^2 \qquad (3)$$

With temperature close to transition temperature arises a strong frequency dispersion of absorption. The maximum of absorption with T ~ Tt is replaced by a minimum on high frequencies of electric field oscillations. This minimum tries to negative meanings. The negative absorption could be revealed with the best temperature resolution [2].

1. Mokejev A.A., Mokejev An.A. Auto-oscillations of polarization of ferroelectrics. Proceedings of the VI international conference «Crystals: growth, property, applications . Alexandrov, VNIISIMS, 2003.

2. Acoustic crystals. Edit. Shaskolskaia M.P. M. Sience, 1982.

3. Mokejev A.A. www. Avtoferelrheo.narod.ru

PHOTO- AND THERMOELCTRIC PHENOMENA IN THE SANDWICH STRUCTURE OF METAL-FERROELECTRIC-METAL

Ivanov V.I., Karpets Yu.M., Klimentyev S.V., Marchenkov N.V.

Far-Eastern State Transport University

47 Serysheva Street, Khabarovsk, Russia 680021

(kjum@festu.khv.ru, тел. (4212)359114)

In [1], the thermoelectric response in the highly alloyed lithium niobate crystals with different electrodes including a slow component caused by a presence of the thermo-stimulated EMF proportional to the crystal temperature has been studied.

In the same place, the electret model of the effect which is qualitatively consistent with the experimental dependences of the EMF values on admixture concentration and crystal geometry has been proposed. In this work, the more detailed comparison of the model computations with the experimental results considering, in partial, the Mott character of the dependence of the electroconductivity of the highly alloyed lithium niobate crystal on temperature was carried out.

Based on the outlined effect of the non-pyroelectric thermo-EMF in the alloyed $LiNbO_3$ crystals with electrodes of different metals, the pre-production model of detector for recording of radiation of the wide spectral range with the infra-low modulation frequencies. The detector's sensitivity was 6 V/W at noises comparable with the Johnson's ones.

[1]. Ivanov V.I., Karpets Yu.M., Klimentyev S.V., Marchenkov N.V. Proceedings of the VI International conference "Crystals: growth, properties, real structure, application". Aleksandrov: VNIISIMS, 2003.-P. 243-244.

LIFE TIME OF HIGH TEMPERATURE PHASES IN $H_xLi_{1-x}MO_3$ (M=Nb, Ta).

I.E. Kalabin, T.I. Grigorieva, L.D. Pokrovsky and V.V. Atuchin

Laboratory of Optical Materials and Structures, Institute of Semiconductor Physics, Novosibirsk, 630090, Russia.

Lithium niobate and lithium tantalate (LN, LT) are well-known ferroelectric mediums for integrated optics devices fabrications. The most suitable technique for waveguide formation in these mediums is ion exchange reaction in some organic acids melt. Temperature of proton reaction limited only melting temperature of acid and it's approximately 200-240°C, which far below Curie temperature (1210°C for LN and 620°C for LT). Produced $H_xLi_{1-x}MO_3$ (M=Nb, Ta) compounds have a large electro- and acousto-optic coefficients, low optical damage and are the promising mediums for electrooptical modulators, frequency converters and integrated lasers [1, 2]. But applicability of this kind of waveguide in practical systems is limited by variations of refractive index depending the cooling regimes. The variations of refractive index caused by high temperature, metastable in room conditions phases formation-decay process [3, 4]. In this connection arise the question about life time of high temperature phases, determining the time of device characteristics variation.

The $H_xLi_{1-x}MO_3$ (M=Nb, Ta) waveguide layers were fabricated in benzoic acid melt at 240°C for different times. After this, annealings were applied to decrease the hydrogen concentration in the layer to the level that belongs to the composition range of the desired equilibrium phase. As criteria of phase assignment, the surface value of refractive index increase $\Delta n_e(0)$ was used. To force the systems transit to high temperature state quenching technique has been applied. To observe refractive index profile vs. depth of the sample the standard prizm coupling technique [5] and inverse WKB method [6] was utilized. The surface structure was traced by reflection of high energy electron diffraction.

It has been shown that the life time of high temperature phases in wide hydrogen concentrations is very large. In k_2-phase of $H_xLi_{1-x}NbO_3$ high temperature phase totally decay for ~300 hours. In α-phase of $H_xLi_{1-x}TaO_3$ layers halved decay was achieve after 1500 hours and only heating up to 100°C allow to completely decaying the high temperature phase. In δ-phase of $H_xLi_{1-x}TaO_3$ decay process is slower and after the lapse ~10000 hours decay is not complete.

So, the processes of decay of high temperature phases in $H_xLi_{1-x}MO_3$ (M=Nb, Ta) waveguide layers are very slow. Therefore, relaxation of formed high temperature phases in integrated optics devices could generate long time instabilities of their optical properties.

1. T. Findakly, P. Suchoski and F. Leonberger, Optics Lett. 13 (1988), p. 797.
2. P. Baldi, M.P. De Micheli, K. El Hadi, S. Nouh, A.C. Cino, P. Aschieri and D.B. Ostrowsky, Opt. Eng. 37 (1998), p. 1193.
3. V.V. Atuchin, D. Dimova-Malinovska, T.I. Grigorieva, I.E. Kalabin, I. Savatinova, I. Savova, E.V. Spesivtsev, S. Tonchev, C.C. Ziling, Metastable phases in $H_xLi_{1-x}TaO_3$ waveguide layers and pure $LiTaO_3$, Appl. Phys.B.73 (2001) 559-563.
4. I.E. Kalabin, V.V. Atuchin, T.I. Grigorieva, Formation and decay of high temperature phase in $H_xLi_{1-x}NbO_3$ layers, Optical Materials, 23(1-2), 2003, 283-286.
5. H. Onodera, I. Awai, J. Ikenoue, Refractive-index measurement of bulk materials: prism coupling method, Appl. Opt. 22 (8) (1983) 1194-1197.
6. V.G. Pankin, V.U. Pchelkin and V.V. Shashkin, Kvant. Elect. 4 (1977), p. 1497 (in Russian).

ANISOTROPIC ABSORPTION IN DOPED $LINbO_3$ CRYSTALS

V.A. Maksimenko, Yu. M. Karpets

Far-Eastern State Transport University, 47 Serysheva Street,
Khabarovsk, Russia 680021
Tel. (4212) 359-114, E-Mail: fizika@festu.khv.ru

Lithium niobate crystals are broadly used in applied optics. On their base designed and are used in practice second harmonic generators and electro-optic modulators of light. Also lithium niobate is a perspective material for holography. High optical quality of crystals is required for all these areas. Usually it is understood as sufficient transparency and optical homogeneity of material. Lithium niobate crystals, used in applied and scientific purposes answer such requirements. However, absorption of lithium niobate depends on polarizations of light. To take account of this phenomenon is important in experiments on photorefractive characteristics study and holographic record in lithium niobate crystals. Particularly powerfully anisotropy of absorption is in doped crystals. However, an influence of one or other alloying additives on the anisotropy of absorption is poorly known. In order to determine this influence we have studied the anisotropic absorption of the light in $LiNbO_3$ crystals with additives of Fe, Rh, Fe+Rh, Fe+Cu, Ru. Anisotropy of absorption is determined as ratio of absorptance for e-beam and o-beam accordingly.

Anisotropy of absorption in $LiNbO_3$ crystals depends on wavelengths of light and on kind of dopes. In the $LiNbO_3$:Fe crystals on the wavelength 630 mcm absorptance for e-beam approximately in 1,5 times more, than for o-beam. But in the crystal $LiNbO_3$:Rh absorptance e-beam on same wavelength in 2,5 times less, than o-beam. That is to say anisotropy of absorption in $LiNbO_3$:Fe and $LiNbO_3$:Rh crystals has different value and character.

Above possible to expect that analysis of spectrums to anisotropy of absorption will allow relatively simply and safely identify admixtures in optical crystals.

PECULIARITIES OF DESIGN OF SAW FILTERS WITH TRANSVERSALLY COUPLED RESONATORS ON QUARTZ AND LITHIUM TETRABORATE

V.S.Orlov, V.B.Chvets, A.L.Scwartz
Moscow Radiocommunication Research Institute
Nizhegorodskaya 32, Moscow, 109029

SAW filters with transversally coupled resonators (TCR) made on quartz wafers are widely used at frequencies from 80 to 1000 MHz. They provide high rejection level in the stop band UR=45-60 dB, shape factor SH=1.5-1.8 and fairly low insertion loss IL=2.5-6.0 dB. The typical structure of TCR filter includes two tracks, each formed by a pair of identical acoustically coupled resonators. An external inductivity with precise tuning is usually used as an element which provides electrical coupling between the tracks. Such TCR filters with electrically coupled tracks are characterized by the sensitivity to the inductivity value which grows with increasing bandwidth. It results in limitation for maximum bandwidth of a filter. Usually the relative bandwidth of TCR filters lies within the interval BW3=0.05-0.1%. Besides, additional inductivity results in higher loss and degradation of temperature performance of SAW filter.

The present paper describes the peculiarities of a design of TCR filters with relative bandwidths BW3=0.15-0.3%. To realize wider bandwidth we suggest to use acoustic and electrical coupling between resonators, but without additional external elements. In this case, the coupling only depends on accuracy of photolithography process. The widest bandwidth BW3=0.2-0.3% and the lowest loss IL=2.0-3.0 дБ can be obtained for triple-resonator TCR filters with pure acoustic coupling between resonators. TCR filters with four acoustically coupled resonators provide bandwidth BW3=0.15-0.2% and insertion loss IL=3.0-4.0 dB.
The best shape factor SH=1.3-1.5 and high rejection level UR=60-70 dB can be obtained for TCR filters consisting of two pairs of acoustically coupled resonators and direct electrical coupling between these pairs, when the bandwidth varies within the interval BW3=0.1-0.15% and insertion loss is IL=3.5-5.5 dB. The mechanisms which provide maximum achievable bandwidths are considered for each TCR filter structure mentioned above.

Design of the described filter structures is illustrated by the experimental examples: 315 MHz filter (BW3=827 kHz or 0.28%) and 868 MHz filter (BW3=1.4 MHz or 0.16%) fabricated on quartz for car alarm systems; filters for radio phones of PHS standard with

frequency 244 МГц (BW3=448 kHz or 1.8 %) and GSM standard with frequency 360 MHz (BW3=380 kHz or 0.1%), filters for mobile communication systems with frequency 133 MHz (BW3=80 kHz or 0.05%). Extended bandwidths 0.4-0.6 % can be achieved if lithium tetraborate is used as a wafer, for example in GSM filter with frequency 71 MHz (BW3=280 kHz or 0.4 %).

E-mail : filcrys@rinet.ru

FREQUENCY DISPERSION OF DIELECTRIC PERMITTIVITY OF RELAXOR $(Pb,Sr,Bi)TiO_3$ SOLID SOLUTIONS

K. Bormanis[1], V.A. Latovin[2], A. Kalvane[1], A.V. Shil'nikov[2], and A.I. Burkhanov[2]

[1]Institute of Solid State Physics, University of Latvia, Riga, Latvia
[2]Volgograd State Architectural and Engineering University, Volgograd, Russia

The growing interest in disordered relaxor ferroelectrics is due to unusual properties mainly related to the existence of broad phase transitions characteristic to the systems.

Original ternary solid solutions $0.85Pb_{0.6}Sr_{0.4}TiO_3$-$0.15Bi_{2/3}TiO_3$ (a) and $0.9Pb_{0.3}Sr_{0.7}TiO_3$-$0.1Bi_{2/3}TiO_3$ (b) have been produced. Powders of solid solutions were obtained by solid state synthesis from high purity grade oxides at 1280-1300 ^{0}C, 2h. Ceramic samples presented for studies were produced by conventional ceramics technology at 1360 ^{0}C, 2h. The samples were furnished with fired silver paste electrodes.

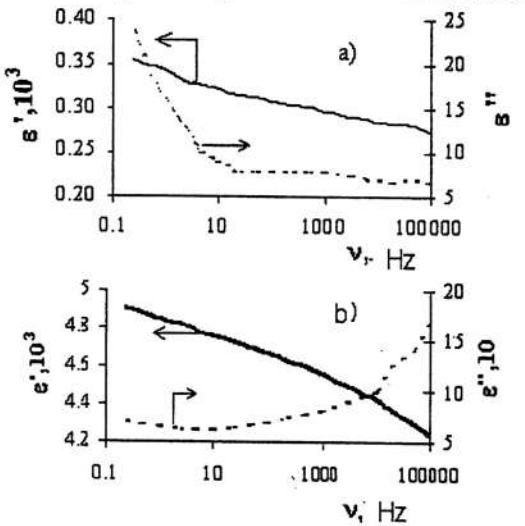

Figure 1. Complex dielectric permittivity as a function of frequency of ferroelectric solid solutions $0.85Pb_{0.6}Sr_{0.4}TiO_3$-$0.15Bi_{2/3}TiO_3$ (a) and $0.9Pb_{0.3}Sr_{0.7}TiO_3$-$0.1Bi_{2/3}TiO_3$ (b)

Differential thermal analysis and X-ray diffraction were used to examine the synthesis and phase constitution. The effects of dielectric response are studied as functions of temperature and frequency (10^{-1}-10^5Hz) at week a-c fields (1 V/cm). Measurements of complex dielectric permittivity (Fig.1.) shows dispersion at different frequency regions: in composition (a) the dispersion takes place at low frequencies – below 10 Hz, but in composition (b) – dispersion shifts to high frequency region – above 1000 Hz. Analysis of frequency behaviour of dielectric permittivity reveals essential relaxation processes related to dynamics of domain boundaries. Results are discussed in terms of domain boundary interaction with point defects, such as lead and oxygen vacancies, with account for relaxor properties.

The studies have been financially supported by Latvian Scientific Council grant 01.0818 "Nonequilibre thermodynamic, crystallographic properties and external factors induced phase transitions in ferroelectrics with different degree of ordering", and by the NIR grant No. 202.03.02.044. of the Russian Federation.

GROWTH AND PROPERTIES OF $LiNbO_3$ SINGLE CRYSTALS DOPED WITH RARE EARTH ELEMENTS

K. Bormanis[1], M.N. Palatnikov[2], N.V. Sidorov[2], and I.V. Biryukova[2]

[1]Institute of Solid State Physics, University of Latvia, Riga, Latvia

[2]Institute of Chemistry, Kola Science Centre RAS, Apatity, Murmansk Region, Russia

Lattice defects and considerable diversity of the degree of ion ordering formed at substitutions in lithium niobate structures by dopant ions of different valences make for a wide-range variation of material properties.

Single crystals of lithium niobate containing Er, Tb, Dy, Eu, Gd, Pr, and Y dopants within a wide range of concentrations have been grown by Czochralsky method from congruent mixtures. Results of chemical and physical analysis and Raman studies of the obtained crystals are reported.

Coefficients of admixture penetration in the growing crystals as functions of the dopant concentration in the melt have been determined. The coefficient of Er penetration is found to change within the range of 0.9 -- 1.5 in the range of admixture concentrations of 0.1 - - 4.0 %w. The pattern of the dependence of crystal properties on Er concentration in the melt points to a change of the mechanism of Er penetration in the crystal structure. Conditions of $LiNbO_3$:Er single crystal growth providing a macroscopically homogeneous distribution of erbium in the crystal are determined. Dependence of penetration coefficients on concentration of Tb and Pr being 0.9-1.0 and ca.0.1, respectively, is rather weak.

A model is proposed that allows to judge from dependence of physical characteristics on dopant concentration about positioning of the rare earth admixture cations in the single crystal structure.

Raman spectra of nominally pure $LiNbO_3$ single crystals, within the limits of homogeneity, are found to exhibit single-mode behaviour. In case of rare earth admixtures they show single-mode behaviour at small concentrations and transform into two-mode pattern as the concentration increases. In the latter case two distinct bands, 873 cm-1 and 900 cm-1 are observed in the region of stretch vibrations of the oxygen bridge. It is possible under conditions of non-equivalent positioning of identical cations within the oxygen octahedrons, e.g., as a result of formation of clusters of basic and admixture ions in the cation sublattice pointing to the change of the mechanism of admixture ion penetration into the crystal structure as the dopant concentration in the melt increases. It also may suggest formation of some ordered superstructure of defects in the cation sublattice.

The studies has been partly financially supported by Latvian Scientific Council grant No. 01.0818. and by RFFI grant No. 03-03-32964.

LOW FREQUENCY MEASUREMENTS IN LEAD TITANATE FERROELECTRIC SOLID SOLUTIONS

K. Bormanis[1], A.I.Burkhanov[2], S.A.Satarov[2], A. Kalvane[1] A. Sternberg[1], and A.V.Shil'nikov[2]

[1]Institute of Solid State Physics, University of Latvia, Riga, LV-1063, Latvia

[2]Volgograd State Architectural and Engineering University, Volgograd, 400074, Russia

Ferroelectric $(1-x)Pb(Sc_{1/2}Nb_{1/2})O_3$-$xPbTiO_3$ (PSN-PT) solid solutions being of theoretical and practical interest have a morphotropic boundary between rhombohedral and tetragonal phases within the concentration range of x = 0.35 – 0.43 [1]. Existence of the monoclinic phase has also been observed between the rhombohedral and tetragonal phases [2].

The dielectric and piezoelectric parameters are known to have extremely high values near the morphotropic phase boundary (MPB) in ferroelectric solid solutions (FESS) of lead titanate [3] for which reason the PSN-PT ceramics is a promising material for transducers and ultrasonic drivers requiring a strong electromechanical coupling and a large piezoelectric modulus. Dielectric studies at low- and infra-low frequencies (LF-ILF) [4] of materials like PSN-PT are of special interest since the PT component is a disordered ferroelectric exhibiting slow relaxation of polarization.

The present LF-ILF polarisation and polarisation switching studies of the 0.58PSN–0.42PT ferroelectric solid solution [5] produced by conventional ceramic technology have been performed on a modified Sowyer-Tower bridge at different intensities of the applied field E_o over a wide range of temperature.

Dielectric relaxation associated with movements of domain and phase boundaries in ferroelectrics is well illustrated, along with effective dielectric loss factor [6], by the half-width of polarisation loops (PL) E_{hw} (Fig. 1.). At extremely high field intensities E_o the half-width of PL is comparable to the coercive field E_c and some features of polarisation switching related to ageing of the material may be erased at restoration of the sample by field. The effect of dielectric field memory has been detected at $E_o < E_c$ in relaxor PLZT in the region of phase transition.

A broad local minimum on the $E_{hw}(T)$ curves (Fig.1.) is observed around room

temperature (20 ^{0}C) at increasing of the measuring field intensity. As seen from the PL obtained at different temperatures, a small constriction of PL during the polarisation cycle is observed only at T=+20 ^{0}C, which suggests of dielectric memory (of the ageing temperature of samples) in the PSN-PT ceramics. Such memory effects [7] are manifested by materials of different coexisting phases (polar and non-polar or polar phases of different symmetry). Existence of dielectric memory in the 0.58PSN–0.42PT ceramics suggests of a rather broad MPB – coexistence of different polar phases since transition to the paraelectric phase at T_m ~310 ^{0}C is far from the room temperature.

Behaviour of the effective conductivity at temperatures over the temperature of dielectric permittivity maximum T_m follows Arrhenius law $ln\ \sigma = f(1/T)$ with activation energy U=0.97 eV characteristic to ion conductivity that, in the given case, is due to defects such as lead and oxygen vacancies.

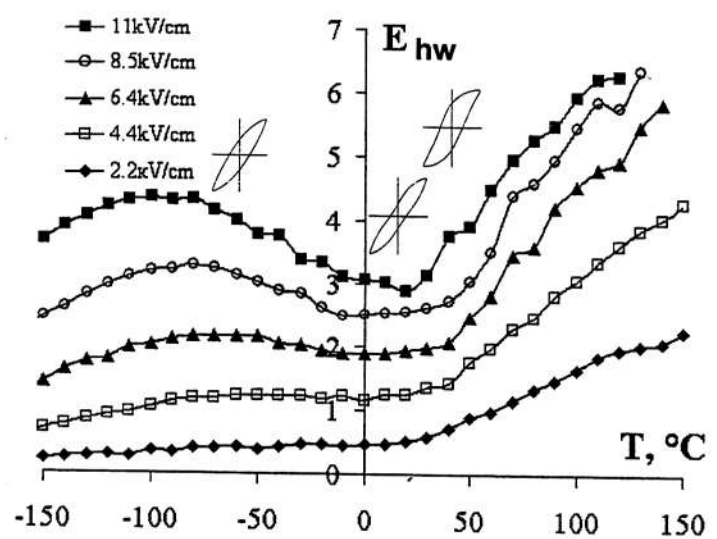

Figure 1. The half-width of polarisation loops as a function of temperature at measuring frequency 0.1 Hz and different field intensities; polarisation loops at –70 ^{0}C, 20 ^{0}C and 50 ^{0}C, accordingly.

The studies has been financially supported by Latvian Scientific Council grant 01.0818 "Nonequilibre thermodynamic, crystallographic properties and external factors induced phase transitions in ferroelectrics with different degree of ordering", and by RFFI (grant #02-02-16232), the contest centre of the Ministry of Education of the RF (grant #E02-3.4-424), the "Research by Higher Education in Priority Directions of Science and Technology" grant # 202.03.02.04, and grant HIII-1514.2003.2 of the support to higher education.

References

[1] Y.-H. Chen, K. Uchino, M. Shen and D. Viehland. J. Appl. Phys., **90**, 3, p. 231, (2001).

[2] J-M. Kiat, Y. Uesu, B. Dkhil, MX. Matsuda, C. Malibert, G. Calvarin. Cond-mat., **1**, 12, p. 1093, (2001).

[3] M. Lejeume and J.P. Boilot. Mater. Res. Bull., **20**, 493, p.1265, (1985).

[4] A.V.Shil'nikov. Proc. ASc. USSR, Ser.Phys., **51**, 10, pp.1726-1735, (1987), in Russian.

[5] V.J. Tennery, K.W.Hang and R.E. Novak. J. Am. Ceram. Soc., **51**, 671, p. 2672, (1968).

[6] A.I.Burkhanov, A.V.Shil'nikov, S.A.Satarov, K.J.Bormanis, A.R.Sternberg, A.Kalvane International Conference "Intermatic - 2003" 9-12 June 2003. Moscow, MIREA, Proceedings, pp.96-99, in Russian.

[7] Burkhanov A.I., Shilnikov A.V., Dimza V. Ferroelectrics, **131**, pp. 267-273, (1992).

STRUCTURAL PERFECTION OF STOICHIOMETRIC LITHIUM NIOBATE SINGLE CRYSTALS

M.N. Palatnikov[1], N.V. Sidorov[1], K. Bormanis[2], and V.T. Kalinnikov[1]

[1]Institute of Chemistry, Kola Science Centre RAS, Apatity, Murmansk Region, Russia
[2]Institute of Solid State Physics, University of Latvia, Riga, Latvia

Lithium niobate is one of the materials widely used in devices of nonlinear, electronic, and integral optics. It is a typical non-stoichiometric crystal the congruent melt composition of which is not stoichiometric. Commercially available crystals usually have a congruent and macroscopically homogeneous composition along the growth axis. However, for a series of practical applications the stoiciometric $LiNbO_3$ crystals (Li/Nb=1) have essential advantages as compared with crystals of a congruent composition. Application of stoichiometric lithium niobate in optic devices requires methods by which the crystal composition and the degree of structural perfection can be controlled.

The paper reports studies of Raman spectra with respect to features of the cation sublattice in real lithium niobate single crystals of various chemical compositions (both nominally pure and doped). Formation of rather ordered basic and impurity clusters in the cation sublattice of non-stoichiometric crystals is suggested as the source of weak "excess" Raman bands. Sublattices of defects are shown to be absent in highly ordered stoichiometric crystals.

The 100-120 cm^{-1} Raman bands in the lithium niobate crystal corresponding to two-particle states of acoustic phonons are found to be sensible to structural ordering in the cation sublatttice since there are no Raman bands in the 100 – 120 cm^{-1} range in stoichiometric crystals of a high degree of structural perfection. The absence of Raman bands in the 100 – 120 cm^{-1} interval may be assumed as an experimental criterion of of conformity to the stoichiometric composition and a high degree structural perfection of the lithium niobate crystals. Any deviation from stoichiometry results in appearance of the band in the Raman spectrum. Introduction of a small amount of impurity ions into the structure of a stoichiometric crystal destroys the ideal order of cation alternation, brings a deviation from the stoichiometric composition and causes appearance of the 103 and 117 cm^{-1} Raman bands.

The study has been financially partly supported by RFFI grant № 03-03-32964.

RAMAN STUDIES OF PHASE TRANSITIONS IN FERROELECTRIC $Li_{0.12}Na_{0.88}Ta_{0.4}Nb_{0.6}O_3$ SOLID SOLUTIONS

N.V. Sidorov[1], M.N. Palatnikov[1], and K. Bormanis[2]

[1]Institute of Chemistry, Kola Science Centre RAS, Apatity, Murmansk Region, Russia
[2]Institute of Solid State Physics, University of Latvia, Riga, Latvia

Lattice defects and considerable diversity of the degree of ion ordering formed at substitution of ions of different valences in complex $(A'A'')(B'B'')O_3$ oxide structures make for a wide-range variation of material properties. The complex perovskite structures of double oxides are currently known not only to be relaxors but ion superconductors as well.

By varying the ratio of components in ferroelectric (Li, Na)(Ta, Nb)O_3 perovskite structures formation of BO_6 octahedrons and AO_{12} polyhedrons is also varied. The state of ion superconductivity is attained at the Na:Li=7:1 ratio. The regions of morphotropic transitions between the rhombic and rhombohedric phases are changed with the change of the Ta and Nb proportion.

Raman studies of $Li_{0.12}Na_{0.88}Ta_{0.4}Nb_{0.6}O_3$ have shown the ferroelectric - antiferroelectric (FE–AFE) phase transition to be of the ordering type and related to the increase of anharmonicity of symmetric vibration. The change of the intensity of the B-O-B vibration suggests disagreement with the second order phase transition as described by the Landau theory. It shows that the FE–AFE phase transitions are related to the increase of anharmonicity of vibrations of the BO_6 octahedrons and belong to the first order transitions.

The curves of thermal behaviour of the intensity of the mentioned vibrations of oxygen atoms have maximums at 60–100 ^{0}C suggesting existence of a structural phase transition and a morphotropic phase region at room temperature. With rise of the temperature intensity of the vibration becomes zero at 250 ^{0}C where the FE–AFE phase transition occurs.

The study has been partly supported financially by the RFFI № 03-03-32964 grant.

THE CRYSTAL PRODUCTION OF LAYERED PEROVSKITE-LIKE FERROELECTRICS $A_2B_2O_7$:PHYSICAL AND CHEMICAL FEATURES

Zakharov N.A., Zakharova T.V., Kalinnirov V.T.

Kurnakov Institute of General and Inorganic Chemistry RAS,
Leninskjj pr., 31, 119991, Moscow, RUSSIA
E-mail: zakharov@igic.ras.ru, (095) 955-48-84, (095) 954-12-79

The ferroelectrics with layered perovskite-like structure $A_2B_2O_7$ (FLPS $A_2B_2O_7$) are a perspective stuffs for piesotechnique and optoelectronics. In this connection an actual problem is the production of their crystals, definition of factors that determine their structural perfection, the physical and chemical characteristics.

We report the data on synthesis and crystal production of FLPS $A_2B_2O_7$ – $Sr_2Ta_2O_7$, $A_2Nb_2O_7$ (A=Ca, Sr), $Ln_2Ti_2O_7$ (Ln = La, Ce, Pr, Nd), series of solid solution on their basis and phases of high pressure by similar structural type. On examples for series of FPLS $A_2B_2O_7$ the conditions of their crystal production by methods of spontaneous crystallisation from solutions and melts, crystal growth by methods of Cochralsky, Bridgmen, a direct high-frequency melting in cold container and method optical-zone are considered. The effect of some factors (temperature of heating, temperature gradient in crystallization zone, composition of solution and gas medium, features of thermal block design, rate of motion of crystal/melt surface) were estimated.

The results allow to carry out a choice of procedures for FLPS $A_2B_2O_7$ production that has specific complex of physical and chemical properties. The problems of FLPS $A_2B_2O_7$ crystals practical application (detectors of emission, devises of laser technique and piezotechnique) are discussed.

CONCENTRATIONAL AND THERMAL PHASE TRANSITIONS IN SYSTEMS OF $Li_xNa_{1-x}Ta_yNb_{1-y}O_3$ SOLID SOLUTIONS

N.V. Sidorov, M.N. Palatnikov, N.A. Golubyatnik, V.T. Kalinnikov
Institute of Chemistry and Technology of Rare Elements and Mineral Raw Materials, Kola Sceince Centre RAS, 26a Fersman Str., 184209, Apatity, Murmansk region, E-mail: palat_mn@chemy.kolasc.net.ru

B.N. Mavrin, V.V. Asonov
Institute of Spectroscopy RAS, 142190, z.Troitsk, Moscow region, Russia E-mail:mavrin@isan.troitsk.ru

The results of an investigation into concentrational and thermal phase transitions in systems of solid perovskite ceramic solid solutions (SS) with the common formula of $Li_xNa_{1-x}Ta_yNb_{1-y}O_3$ (LNTN), obtained by using Raman spectroscopy, are presented. The structure, ordering of structural units in various sublattices and SS LNTN properties are shown to considerably change both within one SS multicomponent system and on transition from one system to the other. When establishing the composition–structure-property regularities we were particularly interested in processes of structural disordering of LNTN cation sublattices responsible both for dipole ordering and SS ferroelectric properties and the mechanisms of structural phase transitions (PT) typical of LNTN SS.

Concentrational dependencies of Raman spectra have revealed that in the $NaTa_yNb_{1-y}O_3$ system that the increasing y transforms the structure of lithium niobate to that of lithium tantalate continuously throughout the area of enhanced structural disordering at $0.2<y<0.8$, whereas the sodium niobate structure is transformed to that of sodium tantalate in the $LiNa_{1-x}Ta_yNb_{1-y}O_3$ ss system through the PT at y~0.55. The system of $Li_{0.12}Na_{0.88}Ta_yNb_{1-y}O_3$ SS, interesting as superionic conductors, has revealed concentrational transitions near y ~ 0.2; 0.55; and 0.8 accompanied by serious changes in the structural ordering of cation sublattices and oxygen carcass deformations.

Raman spectra provided an insight into the ferroelectric-antiferroelectric PT in the $Li_{0.12}Na_{0.88}Ta_yNb_{1-y}O_3$ system. Temperature increase to the transition point has shown a broadening of lines corresponding to the vibrations of cations located in octahedral and cubic octahedral hollows of the structure, as well as oxygen carcass vibrations (suggesting a substantial growth in disordering of cation sublattices). The 875 cm^{-1} line intensity,

corresponding to bridge valent vibrations of the octahedral anion BO_6, near the transition point is seen to diminish to zero.

The temperature dependence of the 875 cm^{-1} line intensity in the transition area was used to study the behaviour of the in function of the phase transition order parameter. The n behaviour showed disagreement with Landau theory of y-dependent second-kind order transitions. The discrepancies are shown to be caused by increased disordering in the niobium and tantalum sublattices in $Li_{0.12}Na_{0.88}Ta_yNb_{1-y}O_3$ solid solution system with y increase. In this case the kind of phase transition is decreased.

The work was performed with the support of RFBR. Grant № 03-03-32964.

PHOTOREFRACTIVE EFFECT IN LITHIUM NIOBATE CRYSTALS OF DISSIMILAR COMPOSITION

N.V. Sidorov, P.G. Chufyrev, M.N. Palatnikov, V.T. Kalinnikov, Institute of Chemistry and Technology of Rare Elements and Mineral Raw Materials KSC RAS, 184200 Apatity, Russia,**N.N. Melnik** Lebedev Institute of Physics RAS, 117904 Moscow, Russia,**Yu.A. Zheleznov** Center of Scientific Instrumentation of the Institute of Problems of Electrophysics. 117993 Moscow, Leninskiy pr. 32A.

The electro-optic and nonlinear optic photorefractive lithium niobate $LiNbO_3$ crystal is unmatched among the acoustooptic materials applied nowadays. The diversity of its optic applications is based on high values of electro-optic and nonlinear-optic coefficients and the possibility of achieving laser generation with self-duplicating frequencies. Lithium niobate is characterized by a broad field of homogeneity on the phase diagram and represents a phase of variable composition. Interestingly, the changing composition (during alloying or stoichiometry variation) brings about changes in the structural units and the state of defectiveness of only the cation sublattice forming the ferroelectric and nonlinear-optic properties of the crystal. Hence the controllability of lithium niobate crystals optic quality and, consequently, their optic properties, which is achieved by varying their composition over a broad range and makes them attractive for integral optic devices.

When affected by laser radiation, the lithium niobate crystal changes its photo-induced refraction indices. This phenomenon was called 'the photorefractive effect' or 'optical damage'. The photorefraction effect limits the application of lithium niobate crystals in optics as a frequency converter, electro-optic modulators, etc. The photorefractive effect is usually diminished through heavy alloying (up to 6 w/o) of the crystal with nonphotorefractive impurity cations (for example and others) which, unlike the photorefractive cations (Cu, Mn, Ni, etc.), do not change their charge state in the crystal structure.

Owing to recently developed approaches to growing of perfect crystals with a composition close to stoichiometric (Li/Nb=1) it was found that own structural defects appreciably affect the photorefractive properties as well.

One of the most informative methods for investigating the crystal structure, defects and photorefractive effect is Raman spectroscopy. If both the spectrum and photorefraction are excited by the same laser radiation, the emergence of photorefraction-induced exciting radiation in the crystal, differing from laser radiation falling on the crystal in the direction of both propagation and polarization, should result in the appearance of Raman lines prohibited by the rules of selection for the given scattering geometry. The parameters of lines ('prohibited lines'

in particular) in the spectrum of photorefractive crystals depend on the polarizing scattering geometry, the exciting radiation density and also on composition and degree of the crystal's structural perfection. Moreover, the Raman line parameters are highly sensitive to interactions between the crystal's structural units and, consequently, to all fine restructurings in the crystal structure, such as those emerging when the crystal is alloyed or the stoichiometry of nominally pure crystals is changed. So, by studying the behaviour of concentration dependencies of spetral line parameters one can obtain important information on how structural unit ordering affects the crystal's photorefractive features.

The paper presents the results of Raman spectroscopy-based research comparing the photorefractive effect in various lithium niobate crystals (nominally pure, with varying Li/Nb ratio and alloyed) differing in the ordering of structural ordering in the cation sublattice. The studied spectra included:

1) those in polarized radiation of nominally pure single crystals of congruent (Li/Nb = 0.946) and stoichiometric compositions grown by two methods (from a melt with excess Li_2O and from a stoichiometric melt doped with K_2O);

2) Raman spectra of alloyed congruent single crystals: $LiNbO_3$:Gd (C_{Gd}=0.002; 0.003; 0.005; 0.44 w/o), and the spectra of stoichiometric $LiNbO_3$:Gd (C_{Gd}=0.001 w/o).

The behavior of line basic parameters (frequency, width, intensity and shape) depending on the concentration of alloying components Mg^{2+}, Gd^{3+} and Y^{3+}, has been studied. It is shown that in a certain interval of Mg^{2+} and Gd^{3+} small concentrations structural units tend to arrange. The value of photorefractive effect is shown to diminish. Further increase of Mg^{2+} and Gd^{3+} concentration disorders the cation sublattice, which is evident in broadened spectral lines. Meanwhile the photorefractive effect increases. Among the nominally pure lithium niobate crystals the stoichiometric single crystals feature the highest photorefractive effect. An explanation for this fact has been found. Small defectiveness of highly ordered stoichiometric crystals causes the number of electronic traps ('adhesion levels' near the bottom of the conductivity zone) associated with these defects to diminish. This dams/ the alternative channel of radiation-induced/ rearrangement of photoexcited carriers related to the 'adhesion levels', the photoelectrons being captured by deeper traps thus enhancing the photorefraction effect.

It is discovered that the intensity of the line corresponding to bridge valent vibrations of oxygen atoms in NbO_6 octahedra is sensitive to dipole ordering of the lithium niobate crystal cation sublattice. When through varying the crystal's composition the degree of dipole ordering of the cation sublattice is increased (increased spontaneous polarization), this line intensity also increases.

The work was performed with the support of RFBR. Grant № 03-03-32964.

SAW SENSORS BASED ON QUARTZ RESONATOR WITH "NONTRADITIONAL FORMATS" OF OUTPUT SIGNAL

R.G. Kryshtal and A.V. Medved

Institute of Radio Engineering and Electronics of Russian Academy of Sciences, Vvedensky sq., 1, Fryazino, Moscow region, RUSSIA 141190

Abstract

Some new experimental results on gas and temperature sensors based on ST-quartz two port SAW resonator with "nontraditional formats" of output signal are presented. Usually frequency shift is used as an output signal in SAW sensors based on SAW resonator. In our work we used phase shift as sensor response both of a transmitted and reflected signals (S_{21} and S_{22} parameters, respectively) of SAW-resonator sensor treated as a standard four port device.

Practical possibility of use of the SAW gas sensor with phase format of transmitted signal as output signal is demonstrated using procedure of the determination of the water contents in gaseous nitrogen as an example. Water concentration in nitrogen less than 10^{-7} g/m^3 was detected. The essential influence of SAW power on sensor response has been discovered.

Extremely high sensor sensitivity was obtained when using phase format of reflected signal as a sensor output. Using such a format of sensor output we have reliably measured the change of temperature of ST-quartz SAW sensor substrate as small as 0.01 °C.

These results can appear to be useful to designers of sensors devices by the way of broadening of functional possibilities of existing SAW - sensors.

DOUBLE ELECTRONIC FANO RESONANCE IN FERROMAGNETIC IMPURITY COMPLEXES IN SAPPHIRE CRYSTALS

Dicova E.E., Gerasimov V.P., Levin D.M.

Absorption spectra of $Al_2O_3:Ti^{4+},Fe^{3+}$ sapphire crystals with impurity molecular complexes (IMC) feature wide absorption bands in the visible range having maximums at 600 and 700 nm (σ- and π-polarization), a high-intensity band with the maximum at 560 hm, and Fano resonance that occur as maximums and minimums on the absorption band's outline caused by the $Ti^{4+}\rightarrow Ti^{3+}$ charge transformation [1]. Wide absorption bands in sapphire relate to electronic density transfer $Fe^{3+}\rightarrow Ti^{4+}$ in the complex's exited state. Weak and symmetric Fano resonance the band's shape is distorted; very strong resonance the band's displacement may occur. The inoculating level of Fano resonance is the initial (non-split, non-displaced) position of the current level. The goal of the present work is development of methodology for experimental measurement and transition wavelength calculation for various kinds of Fano resonance.

It has been found that under high concentration of impurities that cause high internal stress in the crystals and $Ti^{4+}\rightarrow Ti^{3+}$ transformation of ions charged state IMC occur with super-exchange interaction as well as an impurity state zone based on the Ti^{3+} ion level because IMC in sapphire crystals possess mobile electrons. In the impurity states area with localized energy levels of Ti^{3+} and Fe^{3+} ions double electronic resonance occurs, whose components are Fano resonance and spin resonance interaction of Ti^{3+} and Fe^{3+} ions. As a result antiresonance happens as a collapse near 480 nm at the wide absorption band's outline with a maximum at 560 nm. The present IMC can be represented in ferromagnetic $Fe^{3+}\downarrow Fe^{3+}\uparrow\otimes\uparrow Ti^{3+}\downarrow O^{1-}$ or anti-ferromagnetic $Fe^{3+}\uparrow Fe^{3+}\uparrow\otimes\uparrow Ti^{3+}\downarrow O^{1-}$ kind, where ⊗ is a free electron. The work proposes a methodology for measuring the transitions' positions for the inoculating levels that are involved into Fano resonance; wavelengths for transitions from the inoculating levels of Fano resonance have been calculated. For Fano strong, symmetric and anti-resonance the wavelengths for transitions to the inoculating levels are 626, 630, 482, and 472 nm, correspondingly. The results are in good match to the results of quantum-chemical calculations made with the expanded Hukkel's method.

[1]. Levin D.M., Gerasimov V.P., Guseinov F.Kh, Dicova E.E. Influence of mechanical stress upon the structure of impurity-vacancy complexes with charge transfer // X International Conference "Defects Interaction and Non-elastic Phenomena in Solids". Proceedings. Tula, Sep. 13-15, 2001. –Tula, 2003. - p. 36.

PROSPECTS OF LANGASITE FAMILY CRYSTALS APPLICATION IN PIEZORESONANT SENSORS.

Domoroshina E., Dubovskiy A., Semenkovich G., Smuk Ya., Tsegleev A.

Crystals with structure of lanthanum-gallic silicate (langasite $La_3Ga_5SiO_{14}$- LGS), grown in VNIISIMS are perspective material for manufacturing devices on the base of volumetric and surface acoustic waves. For its piezoelectrical properties langasite and its analogues occupy intermediate state among well-known piezoelectrics – quartz, possessing temperature-stable cuts and low electomechanical coupling coefficients and lithium niobate (tantalate), which has high values of electromechanical coupling coefficients and piezomodules, but low temperature stability. The peculiarity of langasite crystals and its analogues is absence of phase transitions up to melting temperature. This fact becomes main idea for development of piezoelectrical sensors on the base of langasite crystals at temperatures up to 1000 °C.

Growing of high-quality langasite analogues determines by original chemical reagent purity, conditions and method of charge preparing, qualitative seed manufacturing, optimal control of crystallization front form and process parameters of growing.

When piezoelectrical sensors on the base of volumetric ultrasonic waves are producing, crystal elements should have stable piezoelectrical properties: small dependence of elastic constants and density on temperature and external effects, low coefficients of thermal expansion and internal friction. At the same time elastic, piezo- and dielectrical characteristics of piezocrystals should have minimal nonlinearity.

Manufacturing of highly sensitive sensors, working up to 1000 °C with conductance 1×10^{10} Om*cm at 300 °C is possible on the base of piezoelement data.

Piezoelectrical resonators on frequencies 10 MHz, made in VNIISIMS showed low values of dynamic resistance, temperature-frequency coefficients in the range of temperatures between – 40 °C and + 75 °C and quality factor increase on the third and fifth harmonics. Such values of technical parameters allow us to develop thermostable resonators on frequencies up to 210 MHz and highly sensitive piezoresonant sensors of vibration, force, pressure, viscosity and various chemical sensors.

EFFECT OF K_2SO_4 AND LI_2SO_4 MINERALIZERS ON MORPHOLOGY OF FLUX GROWN $KTIOPO_4$ CRYSTALS

M. Nikitina, V. Maltsev, N. Leonyuk

Deptartment of Crystallography & Crystallochemistry

Geological Faculty, Moscow State University, 119992/GSP-2 Moscow, Russia

$KTiOPO_4$ crystal, named as KTP, is a well known commercial material for non-linear optical applications (See, for example, Ref. [1]). These non-hygroscopic and chemically inert crystals have high conversion efficiency of second harmonic generation. They also used for parametric conversion of radiation, and electro-optic modulation.

Since KTP melts incongruently, these crystals can be grown from high-temperature solutions based on the $K_4P_2O_7$ and $K_6P_4O_{13}$ fluxes. At the same time, the phosphate fluxed melts possess a high viscosity, and it restricts in mass transportation at the solid-liquid interface. It becomes problematic to obtain these crystals with high optical homogeneity. In Ref. [2], an attempt was made to improve crystallization conditions by modification of phosphate fluxes using the potassium sulphate because of its capability to break the titanate-oxygen and phosphorous-oxygen chains. However, there is no systematic data about the influence of sulphate fluxes on the morphology and homogeneity of grown crystals. In this paper, morphology of KTP crystals was studied depending on growth conditions from $K_6P_4O_{13}$-K_2SO_4 and $K_6P_4O_{13}$-Li_2SO_4 high-temperature solutions.

KTP crystals were grown from the $K_6P_4O_{13}$ based fluxed melt as well as with an excess of K_2SO_4 and Li_2SO_4 resulted in the following molar fractions: $4K_6P_4O_{13}$:$1K_2SO_4$ and $4K_6P_4O_{13}$:$1Li_2SO_4$.

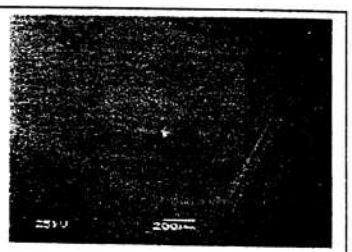

Fig.1.Growth layers on the (011) plane

The morphology of crystals grown in the first series, i.e. using pure $K_6P_4O_{13}$ flux, consists of {100}, {201}, {011} simple crystallographic forms. In this case, development of the pinacoid restricts dimensions of the (011) face. Characteristic feature of these crystals is their twinning. The electronic microscopy shows, presumably, disintegration structures, from porous to linear. The crystal surface also exhibits large blocs and striations on the (100) face, dendrites on the (201) plane, growth sectors and "negative" case-like pentagonal growth layers on the (011) face (Fig.1). It implies the crystal growth from a periphery to the centre.

The external morphology of the crystals grown from the fluxed melts modified with K_2SO_4 is characterized by the same crystallographic forms, i.e. {100}, {201} and {011}. The crystals of this series are shown in Fig. 2. Some crystals edged with another solid phase, presumably, having different composition. In the meantime, there are growth striations and pentagonal growth layers on the (100) and (011) faces respectively. Smooth surface (100) was also observed on KTP crystals. Disintegration structures of the porous edge, probably, another composition, were observed in some arias of grown crystals, by analogy to experiments with pure $K_6P_4O_{13}$.

Fig.2. KTP crystals grown from $K_6P_4O_{13}$-K_2SO_4 based solutions

The external morphology of the crystals grown with an addition of Li_2SO_4 mineralizer is realized in the same crystal forms as it is mentioned for above mentioned two series. No twins were observed in these experiments. The surface morphology is characterized by growth striations and dendrites on the (100) face, pentagonal growth layers and dendrites on the (011) and (201) planes respectively. Some crystals show well developed (110) face with triangle growth layers. The (031) face also presents on some crystals.

This research was supported, in part, by the RFBR Grant № 04-05-64709 and the Grant of the Russian President for Young Scientists MK-1430.2003.05. The authors thank Dr. E.V. Koporulina for electron microscopy of grown crystals.

References

[1] P.F. Bordui, J.C. Jacco, G.M. Loiacono, R.A. Stolzenberger, J.J. Zola, J. Cryst. Growth 84 (1987) 403

[2] R.J. Bolt, M.H. van der Mooren, H. de Haas, J. Cryst. Growth 114 (1991) 141.

PECULARITIES OF DEFECT FORMATION IN LANGASITE CRYSTALS.

Domoroshina E., Dubovskiy A., Semenkovich G., Kuzmicheva G., Tsegleev A.

The production of new highly effective piezoelectric crystals is a crucial factor in the development of piezoelectric an acoustoelectric instrument making. Development and manufacture of electronic components require crystals with stable parameters and perfect characteristics.

The quality of crystals frequently depends on pecularities of the methods used to grow crystals and the formation of defects which determine stability and homogeneity of the properties in the volume of a crystal. Study of formation and behavior of defects allows not only to find out the range of changes in technical parameters but also to purposely correct them by means of external impacts. Recently in some areas of piezotechnics and acoustoelectronics quartz crystals have been replaced by langasite crystals (langasite – lanthanum gallium silicate, $La_3Ga_5SiO_{14}$), due to their higher density ρ=5,75 g/cm^3, dielectric constant

$\varepsilon_{11}/\varepsilon_0$=18.9, $\varepsilon_{33}/\varepsilon_0$=52.0 (for quartz $\varepsilon_{11}/\varepsilon_0$=4.51, $\varepsilon_{33}/\varepsilon_0$=4.63), piezoelectric coefficient d_{11}=-6,16 pC/N, d_{14} = 5,36 pC/N (for quartz d_{11} = 2,31 pC/N, d_{14} = -0,727 pC/N) and electromechanical coupling coefficient k_{12} = 16%, k_{26} = 13,4%.

Wide application of LGS crystals is hindered by considerable changes of physical properties in the volume of crystals what can be connected with structural defects.

Langasite crystals and its analogs have been studied by IR spectroscopy, major oscillation states connected with the oscillation of tetrahedral and octohedral polyhedrons have been determined. The band 3400 cm^{-1} is predicated by the formation of hydrogen centers which decompose after exposure to temperature 1000 °C.

The edge of optical transmission of langasite is in the UV range beginning from 41000 cm^{-1} (244 nm) due to direct interzone transfer which is determined by the width of the bandgap.

According to the character of transmission spectra crystals are divided into three groups.

LGS samples have some common regularities: increase in transmission after annealing in vaccuum at 1000 °C; introduction of germanium admixtures leads to the growth of optical transmission in UV and visible ranges. Changes in LGS composition both in the volume of crystals and between crystals and their link with the spectra of optical transmission have been determined.

X-ray study of langasite $La_3Ga_4(GaSi)O_{14}$ with different proportion of Ga:Si (Ga>Si and Si>Ga) in the composition of crystals gives evidence about the formation of point defects on the following quasichemical reactions:

$Ga_{Ga}^{x}+M_M^{x}+O_O^{x}\leftrightarrow 2Ga_M^{'}+V_O^{\bullet\bullet}$, where M=$Si^{4+}$, Ge^{4+}

$La_{La}^{x}+Ga_{Ga}^{x}+M_M^{x}\leftrightarrow 3M_{Ga}^{\bullet}+V_{La}^{'''}$,

$La_{La}^{x}+Ga_{Ga}^{x}+M_M^{x}\leftrightarrow 3M_{Ga}^{\bullet}+V_{Ga}^{'''}$,

$Ga_{Ga}^{x}+O_O^{x}\leftrightarrow 2V_{Ga}^{'''}+3V_O^{\bullet\bullet}$, .

$La_{La}^{x}+O_O^{x}\leftrightarrow 2V_{La}^{'''}+3V_O^{\bullet\bullet}$.

Growth of crystals in argon or thermal treatment in vaccuum increases the content of $V_O^{\bullet\bullet}$ in crystals, what allows to obtain colourless crystals. Orange colour appear when crystals are grown in argon atmosphere with 1% oxygen and intensifies in two times when annealing in oxygen at 1000 °C. As far as LGS crystals of stoichiometrical composition (Ga=Si) are concerned colourless crystals can be formed when there are no oxygen vacancies $V_O^{\bullet\bullet}$, while a small number of these vacancies will cause a colouring on the account of the associates $(V_O^{\bullet\bullet},2e')^x$.

CRYSTAL GROWTH OF STRONTIUM CUPRATE-BORATE

V.V. Maltsev, N.I. Leonyuk

Deptartment of Crystallography & Crystal Chemistry

Geological Faculty, Moscow State University, 119992/GSP-2 Moscow, Russia

A discovery of high-temperature superconductivity stimulated intensive investigations of magnetic properties of cuprates as well as a search of new doped antiferromagnetics. As a result, compounds with spin gap were discovered. Among them, so-called strontium copper borate, or $SrCu_2(BO_3)_2$ (SCB) has a sharp decrease of magnetic susceptibility at 20 K, and the spin gap at ~ 30 K [1]. Various series measurements of SCB physical characteristics were obtained from the experiments on ceramic samples or very small crystals. Since any ceramics practically always contain an amount of initial components and other subsidiary solid phases, the growth of singe crystals with sufficient sizes and quality has significant importance. It should be noted in this connection, a crystalline road of SCB containing high-quality single crystal domains up to 6мм x 6мм x 3мм was successfully obtained by a travelling solvent floating zone method using $LiBO_2$ as a flux [2]. The present work reports on a new advance in the growth of crystals of spin lattice materials.

Based on the earlier results, sodium tetraborate $Na_2B_4O_{10}$ was used as a flux. All experiments on the crystal growth of SCB from high-temperature solutions were performed in a resistive heated furnace. First of all, SCB ceramics were prepared by heating stoichiometric mixtures of strontium nitrate, copper (II) and boron oxides with 99,99% purity. Starting chemicals were carefully mixed, ground, followed by heat treatment in Pt crucibles at 850°C in air atmosphere during a few days with several intermediate grindings, until blue mono-phase crystalline specimens of the title compound were obtained. In the meantime, the sodium tetraborate solvent was also calcinated at 400°C within a day or two.

At the next stage, a mixture of SCB and $Na_2B_4O_{10}$ in the weight ratio from 2/1 to 1/2 was heated in a Pt crucible to 900°C, cooled at 6-10°C/day to 750°C, then quenched by removal from the furnace. Crystallization products were boiled in distillated water, and SCB single crystals were separated from the crucible.

The best results in this series of SCB flux crystallization were obtained when the weight ratio of SCB/$Na_2B_4O_7$ was varied from 1:1 to 2:3. The maximum yield of SCB single crystals is observed in the case of the solute/flux ratio of 5:6 by mass.

SCB crystals are usually formed on the top of fluxed melt in the center of the crucible. As one would expect, their size increases with a lower cooling rate of fluxed melt. There is the following correlation between the growth rate of different faces of the SCB crystals: {001} < {110} < {100}. The crystals grown at walls of the crucible have strongly developed plate-like habit.

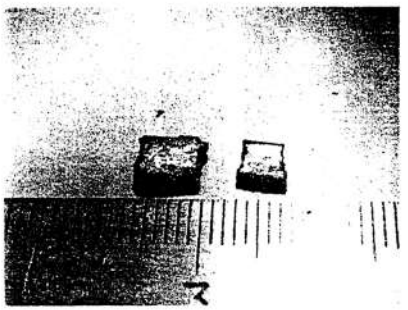

Fig. 1.Flux grown SCB single crystals.

SCB single crystals with good quality have been successfully grown from $Na_2B_4O_7$ based high-temperature solutions, as a result of lowering temperature within 900-750°C at a cooling rate of 6-10°C/day (Fig.1). Their size increases with a lower cooling rate of fluxed melt. Some SCB crystals displayed strongly developed growth striations on the {001} faces.

In the meantime, a major problem which awaits clarification concerns the detailed nature of SCB crystallization processes which occur in the fluxed melts. A choice of the optimal flux composition may be a way to avoid formation of inclusions and cracks in the SCB crystals. Also, these and other defects can be reduced by decreasing the growth rate of crystals in the case of top-seeded solution growth. Further refinements of the crystal growth parameters are in progress.

This research was supported, in part, by the RFBR Grant № 04-05-64709 and the Grant of the Russian President for Young Scientists MK-1430.2003.05. The authors thank Dr. E.V. Koporulina for ASEM analysis of grown crystals.

References

[1] R.W. Smith, D.A. Keszler, J. Solid State Chem. 93 (1991) 430.

[2] H. Kageyama et al., J. Cryst. Growth 206 (1999) 65.

MANIFESTATION OF PHOTOREFRACTIVE EFFECT IN RAMAN SPECTRA OF LITHIUM NIOBATE CRYSTALS OF DISSIMILAR COMPOSITIONS

N.V.Sidorov*, P.G.Chufyrev*, M.N.Palatnikov*, N.N.Melnik **, Yu.A. Zheleznov***

*Institute of Chemistry and technology of Rare Elements and Mineral Raw Materials KSC RAS, 184200. Apatity, Russia

** Levedev Institute of Physics RAS, 117904. Moscow, Russia

*** Center of Scientific Instrumentation of the Institute of Problems of Electrophysics, 117993 Moscow, Russia

(submitted to the editor on 2004 r.)

The Raman spectra application in studies of the structural units ordering in the cation sublattice and the photorefractive properties of lithium niobate single crystals of dissimilar compositions, i.e. nominally pure ones with varying Li/Nb ratios and crystals alloyed with nonphotorefractive cations Mg^{2+}, Gd^{3+} and Y^{3+} is discussed. It is shown that at small Mg^{3+}, Gd^{3+} and Y^{3+} concentrations the photorefractive effect value is essentially controlled by the structural units ordering in the cation sublattice. It is found that the line intensity corresponding to bridge valent vibrations of oxygen atoms in NbO_6 octahedra is sensitive to the cation sublattice dipole ordering.

Laser radiation is known to produce photoinduced changes in the refraction indices of lithium niobate crystal ($LiNbO_3$). This phenomenon was called the "photorefractive effect" or "the optical damage effect" [1,2]. The photorefraction effect hinders the use of this unique crystal in optics as a frequency transformer, electrooptic modulators, etc. [1-4]. The photorefractive effect value can usually be decreased by heavy alloying (up to 6 w/o) of the crystal with nonphotorefractive impurity cations (for example, Mg^{2+}, Zn^{2+}, In^{2+}, Sc^{3+} and other cations) which, unlike the photorefractive cations (Cu, Nb, Ni, etc), do not change their charge in the crystal lattice [1-4]. Recent studies, developing new approaches to growing perfect single crystals with a composition close to stoichiometrical (R=Li/Nb=1), have also disclosed a noticeable effect of own structural defects on the photorefractive properties [2].

In this work, the photorefractive effect in lithium niobate crystals of various compositions (including the slight alloying with nonphotorefractive cations) was studied using the Raman spectra. The Raman spectra make the photorefractive effect visible through the appearance in the spectrum of lines prohibited for the given scattering geometry [5-10].

Moreover, the intensity of 'prohibited' lines increases with the growth of the optic distortion value. We have studied the following spectra: a) those of nominally pure single crystals of congruent (R=0.946) and stoichiometric (R=1) composition grown by two methods (from melts with 1) excess Li_2O and 2) of a stoichiometric composition doped with K_2O); b) those of congruent crystals alloyed with nonphotorefractive impurities $LiNbO_3$:Gd (C_{Gd}=0.002; 0.003; 0.05; 0.44 w/o), $LiNbO_3$:Y (C_Y=0.24; 0.46 w/o); c) and also the spectra of stoichiometric $LiNbO_3$:Gd (C_{Gd}=0.001 w/o). The methods of crystal growth and sample preparation are described in detail in works [11-12]. Both the Raman spectra and photorefraction were simultaneously excited by the same laser radiation using the Ar^+- ILM-120 laser with the generation line and power of about 0.2 Wt. The spectra were recorded by spectrometers Ramanor U-1000 and DFS-24 at room temperature. Since the photorefractive spectra may feature temporary variations [2,5,9], they were recorded about one hour after the onset of sample radiation, when these changes are essentially reduced to zero.

Figures 1(a, b) and 2 present fragments of Raman spectra of crystals of varying compositions and scattering geometries Y(ZX)Z. The spectra are noticeably different, the difference being of a fundamental character and determined by fine peculiarities of structural unit ordering in the lithium niobate sublattice. The photorefraction effect was expected to be minimal in stoichiometric crystals due to the best ordering of their cation sublattices. However, our experiments have shown that nominally pure, highly ordered lithium niobate stoichiometric crystals have a more pronounced photorefractive effect than the congruent crystals. This is evident in Fig.1 representing the spectra in the low-frequency region (a) and in the region of oxygen octahedra NbO_6 vibrations (b). According to the Raman tensor [2, 12], these spectrum regions should develop only the lines with frequencies of ≈ 150 and 580cm^{-1}, corresponding to E(TO) phonons. However, the photorefractive effects creates in the scattering geometry Y(ZX)Z additional lines with the frequencies of ≈ 172, 605 cm^{-1} corresponding to prohibited A_1(TO) phonons (Fig. 1, a, b). In the spectra of nominally pure and slightly alloyed with Cd^{3+} stoichiometric crystals grown from a melt with appreciable excess of Li_2O (curves 1 and 2, respectively) the intensity of 'prohibited' lines is higher than that of similar lines in the spectra of crystals grown from congruent melts doped with K_2O (curves 3), or congruent crystal spectra (curves 4).

Fig.1 (a, b) also shows the variation of 'prohibited' lines intensity (and, consequently, the photorefractive effect) with changing crystal composition. It should also be noted that in a certain region of alloying impurity concentrations the intensity of 'prohibited' lines in

congruent crystal spectra (curves 6, 8) and, consequently, the photorefractive effect, are substantially lower than in the spectrum of nominally pure stoichiometric and congruent crystals. Further increase of alloying impurity concentrations in congruent crystals (>0.4 w/o) results in broadening and enhanced intensity of 'prohibited' lines (curves 7, 9) due to increasing photorefractive effect, alongside with a noticeable broadening of all the other spectrum lines likely to be brought about by disordering in the cation sublattice caused by alloying impurities.

These findings also suggest that the photorefractive effect in stoichiometric and congruent, both conventionally grown and K_2O alloyed, crystals has different values. The difference in 'prohibited' line intensities suggests (Fig. 1, a and b) that the photorefraction value in congruent and stoichiometric, K_2O unalloyed, crystals is about 1.5-3 times as high as the value in similar crystals grown with K_2O addition.

The result of either alloying or changing of the crystal stoichiometry becomes evident not only in the changed structural unit ordering in the cation sublattice but also the dipole moment of oxygen octahedra BO_6 and, consequently, their polarizing ability. These changes should also affect the intensity of the line corresponding to bridge valent vibrations (BVV) of oxygen atoms in the octahedral anion BO_6. This vibration is active in the Raman spectrum of noncentrosymmetrical oxygen octahedra and is prohibited in the spectrum of centrosymmetrical (ideal) octahedra [14].

Fig.2 shows the transformation of the line shape corresponding to BVV of oxygen ions B_1-O-B_2 (where B_1 and B_2 are basic (Li^+, Nb^{5+}) or impurity ions) with the changing crystal composition. As is seen from the Figure, the line has an intricate contour. Analysis involving the contour separation reveals only one line (curves 1, 2, 4-6, 8) in both the spectra of crystals with fairly ordered cation sublattices (such as the spectra of nominally pure congruent and stoichiometric crystals) and in congruent crystals alloyed with relatively small amounts of Gd^{3+}, Y^{3+} ions in the B_1-O-B_2 BVV . Moreover, this line is the narrowest for stoichiometric, the best-ordered, crystals. So, the nominally pure homogeneous lithium niobate crystals can be regarded as unimode ones. The unimode behaviour of alloyed lithium niobate crystals becomes obvious at those small alloying concentrations which exert an ordering effect on the cation sublattice of a congruent crystal thus increasing the photorefraction effect [2, 15].

The spectra of both stoichiometric crystals slightly alloyed with Gd^{3+} and congruent crystals alloyed with appreciable amounts of Gd^{3+} and Y^{3+} in the region of oxygen atom BVV have two distinct lines with frequencies of 850 and $\approx$ 900 cm^{-1}, namely

curves 3, 7 and 9. The line with frequency 900 cm^{-1} in Fig. 2 is highlighted with dotted lines.

The authors express their thanks to V.T. Gabrielyan for the lithium niobate single crystals alloyed with K_2O kindly presented to carry out these investigations.

The work was funded by RFBR. Project № 03-03-32964.

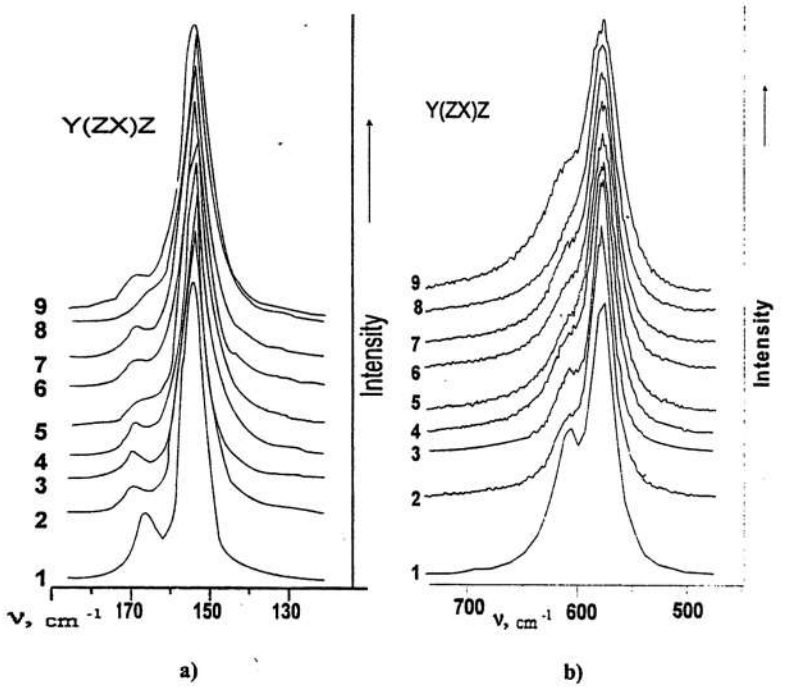

Fig. 1 Fragments of Raman spectra of lithium niobate crystals of varying compositions:
a) in the low-frequency region; b) in the region of oxygen octahedra NbO_6 vibrations;
1.- $LiNbO_3$ stoich. 2.- $LiNbO_3$ stoich: Gd(0.001%) 3.- $LiNbO_3$ stoich. (K_2O).
4.- $LiNbO_3$ cong. 5.- $LiNbO_3$ cong. (K_2O). 6.- $LiNbO_3$ cong: Gd(0.002%).
7.- $LiNbO_3$ cong: Gd(0.44%). 8.- $LiNbO_3$ cong: Y(0.24%): Mg. 9.- $LiNbO_3$ cong: Y(0.46%).

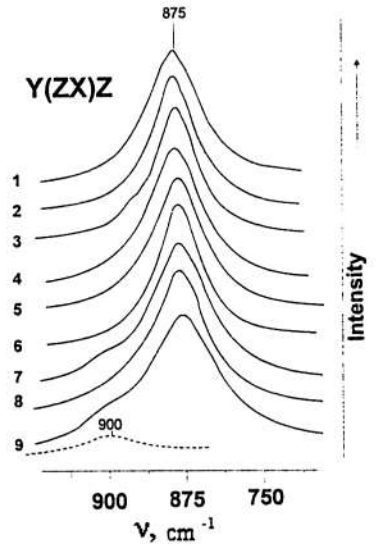

Fig. 2 Fragments of Raman spectra of lithium niobate crystals of varying compositions in the region of oxygen atom BVV;

1.- $LiNbO_3$ stoich. 2.- $LiNbO_3$ stoich: Gd(0.001%) 3.- $LiNbO_3$ stoich. (K_2O).

4.- $LiNbO_3$ cong. 5.- $LiNbO_3$ cong. (K_2O). 6.- $LiNbO_3$ cong: Gd(0.002%).

7.- $LiNbO_3$ cong: Gd(0.44%). 8.- $LiNbO_3$ cong: Y(0.24%): Mg. 9.- $LiNbO_3$ cong: Y(0.46%).

References

1. Kuzminov Yu.S. Electrooptic and nonlinearoptic lithium niobate crystal M., 1987, 264 p.

2. Sidorov N.V., Volk T.R., Mavrin B.N., Kalinnikov V.T. Lithium niobate: its defects, photorefraction, vibration spectrum, polaritons. M., 2003. 256 p.

3. Blistanov A.A. Crystals of quantum and nonlinear optics. M., 2000. 432 p.

4. Rauber A. Chemistry and Physics Of Lithium Niobate. Current Topic in Materials Science // E. Kaldis E. Amsterdam: North-Holland. 1978. V.1 501p.

5. Semyonov A.E., Cherkasov E.V.//ZhPhCh 1980. V. 54. B??10. 2600-2603 p.

6. Korotkov P.A., Obukhovsky V.V., Dmitrik G.N. et al.// Optics and Spectrosopy. 1984. V. 57. N4, p 572-574.

7. Kostritsky S.M., Semyonov A.E., Filipov I.V. // Optics and Spectroscopy. 1984. V. 57. N4. P. 759-761.

8. Dmitril G.N., Korotkov P.A., Radchenko P.S. // Optics and Spectroscopy. 1985. V. 58. N6. P. 1355-1357.

9. Semyonov A.E., Filipov I.V. // Optics and Spectroscopy. 1984. V. 56. N5. P. 833-835.

10. Malovichko G.I., Grachev V.G., Yurchenko L.P., Proshko Y.Ya., Kokanyan E.P., Gabrielyan V.T. // Phys. Stat. Solidi A.1992. V.133. P. K29.

11. Palatnikov M.N., Sidorov M.N., Sidorov N.V., Stefanovich S.Yu., Kalinnikov V.T. Proceedings of the Third international conference 'Crystals, growth, properties, real structure, applications'. V.1, Aleksandrov, VNIISIMS. 1997. P. 349-374.

12. Palatnikov M.N., Sidorov N.V., Stefanovich S.Yu., Kalinnikov V.T. // Inorganic Materials. 1998. V.34. №8. P.903-910.

13. Application of Raman spectra / Ed. by A. Anderson and K.I. Petrov. M., 1977. 586p.

14. Nakomoto K. Infrared spectra of inorganic and coordination compounds. M., 1966. 441p..

15. Sidorov N.V., Serebryakov Yu.A. // Ferroelectrics. 1994. V.160. P.191-105.

DOUBLE ELECTRONIC FANO RESONANCE IN FERROMAGNETIC IMPURITY COMPLEXES IN SAPPHIRE CRYSTALS

Dicova E.E., Gerasimov V.P., Levin D.M.

Absorption spectra of $Al_2O_3:Ti^{4+},Fe^{3+}$ sapphire crystals with impurity molecular complexes (IMC) feature wide absorption bands in the visible range having maximums at 600 and 700 nm (σ- and π-polarization), a high-intensity band with the maximum at 560 hm, and Fano resonance that occur as maximums and minimums on the absorption band's outline caused by the $Ti^{4+}\rightarrow Ti^{3+}$ charge transformation [1]. Wide absorption bands in sapphire relate to electronic density transfer $Fe^{3+}\rightarrow Ti^{4+}$ in the complex's exited state. Weak and symmetric Fano resonance the band's shape is distorted; very strong resonance the band's displacement may occur. The inoculating level of Fano resonance is the initial (non-split, non-displaced) position of the current level. The goal of the present work is development of methodology for experimental measurement and transition wavelength calculation for various kinds of Fano resonance.

It has been found that under high concentration of impurities that cause high internal stress in the crystals and $Ti^{4+}\rightarrow Ti^{3+}$ transformation of ions charged state IMC occur with super-exchange interaction as well as an impurity state zone based on the Ti^{3+} ion level because IMC in sapphire crystals possess mobile electrons. In the impurity states area with localized energy levels of Ti^{3+} and Fe^{3+} ions double electronic resonance occurs, whose components are Fano resonance and spin resonance interaction of Ti^{3+} and Fe^{3+} ions. As a result antiresonance happens as a collapse near 480 nm at the wide absorption band's outline with a maximum at 560 nm. The present IMC can be represented in ferromagnetic $Fe^{3+}\downarrow Fe^{3+}\uparrow\otimes\uparrow Ti^{3+}\downarrow O^{1-}$ or anti-ferromagnetic $Fe^{3+}\uparrow Fe^{3+}\uparrow\otimes\uparrow Ti^{3+}\downarrow O^{1-}$ kind, where ⊗ is a free electron. The work proposes a methodology for measuring the transitions' positions for the inoculating levels that are involved into Fano resonance; wavelengths for transitions from the inoculating levels of Fano resonance have been calculated. For Fano strong, symmetric and anti-resonance the wavelengths for transitions to the inoculating levels are 626, 630, 482, and 472 nm, correspondingly. The results are in good match to the results of quantum-chemical calculations made with the expanded Hukkel's method.

[1]. Levin D.M., Gerasimov V.P., Guseinov F.Kh, Dicova E.E. Influence of mechanical stress upon the structure of impurity-vacancy complexes with charge transfer // X International Conference "Defects Interaction and Non-elastic Phenomena in Solids". Proceedings. Tula, Sep. 13-15, 2001. –Tula, 2003. - p. 36.

SWITCHING PROCESSES IN TGS and DTGS CRYSTALS IRRADIATED BY HIGH-CURRENT PULSED ELECTRON BEAM.

[1)]Ivanov V.V., [1)]Makarov V.V., [1)]Klevtsova E.A., [1)]Markova T.A., [1)]Samsonova O.V., [2)]Tutunnikov S.I., [2)]Efimov V.V.

[1)] Tver State University, Tver

[2)] Joint Institute for Nuclear research

Introduction

In the present time are the measurements of the polarization reversal occurring after some type of external influence – electric field, temperature, mechanical strain.

Authors [1] were carried out spectroscopical researches of TGS crystals irradiated with an impulse electron beam. At work [2] an electronic irradiation effect on dielectric behaviors of single TGS and DTGS crystals was investigated. Introduction in ferroelectric material crystalline structure of a different impurities, and also action on crystals various types of the ionizing irradiation essentially influence their switching.

The collective of our faculty together with the Joint Institute for Nuclear research Dubna had been carried out complex research of an irradiation influence by a high-current impulse electron beam on physical properties TGS and DTGS. In the present paper the switching processes outcomes of irradiated crystals TGS and DTGS are represented by a Barkhausen effect method [3].

Subjects

Model uniaxial ferroelectric TGS and its deuterated analog DTGS had been selected as the subject of research. Samples are plane-parallel plate Y - section, subjected to an irradiation along a polar axis impulse electronic streams. The areas and width of all explored samples made 250 мм^2 and 0,8 mm accordingly. Electrodes were rendered on samples by a sputtering technique of silver in vacuo.

Experimental procedure

Barkhausen effect method as the most responsive to domain structure reorganization has been selected. The irradiation was carried out on an impulse high-current electronogen and ions in physics laboratory of particles in the Joint Institute for Nuclear research, Dubna. Samples were irradiated from both sides. The electrons fluence was defined by the number of pulses enumerated on electrons amount. The kinetic energy of an electron in a pulse made

250 keV, pulse duration τ = 300 nanoseconds, an impulse frequency - 0,2 Hz, the electrons fluence N_e at irradiation crystal of one pulse corresponds the value 10^{15} electron·cm^{-2}.

Results

The integral curves of Barkhausen jumps number at change of a sample electrical condition by a steps method from "-" to "+" (fig. 1a) and from "+" to "-" (fig. 1b) for unirradiated DTGS crystals (the curve 1) and irradiated with an impulse electron beam various electron fluence (curves 2-5) are shown.

It was shown with an electron fluence increases (from 0 up to $400 \cdot 10^{15}$ electron·cm^{-2}) the Barkhausen jumps total number in DTGS crystals at the beginning grows and then decreases.

It is possible to explain by formation of dot charged imperfections under action of an irradiation by an impulse electron beam. Reduction of the Barkhausen jumps total number at an irradiation an impulse electron beam we can explain domain structure fixing on the charged dot defects.

It was shown an electronic irradiation promotes increasing unipolarity degree in DTGS crystals. It was studied the influence of an irradiation on Barkhausen jumps total number in TGS (fig. 3). With increase of at electrons fluence from 0 up to $60 \cdot 10^{15}$ electron·cm^{-2} the Barkhausen jumps total number at switching TGS crystals by steps method is incremented. Similar association is observed in all an explored temperatures interval (fig. 4). It happens because with increase of an electrons fluence in TGS crystals the number of imperfections, and thereof also number of Barkhausen jumps are increased. The similar relative position of Barkhausen jumps total number curves of the irradiated and unirradiated DTGS crystals is observed in an interval of an electrons fluence from 0 up to $70 \cdot 10^{15}$ electron·cm^{-2}.

Also researches of a polarization reversal in TGS crystals at switching an exterior electric field had been carried out. On fig.5-6 time profiles of Barkhausen jumps total number is represented. It was shown increasing an external electric field accelerates the process of polarization reversal as unirradiated TGS, and for irradiated with different fluence value and as increase total number of Barkhausen jumps (fig.7-8). Mathematical calculation of experimental outcomes has shown the curves of following of Barkhausen jumps are well approximated by the law $N \sim 1 - \exp\left(-\left(\frac{t}{\tau}\right)^{\alpha}\right)$, where τ and $0<\alpha\leq 1$ – constants.

From tab. 1 it is visible, that for unirradiated TGS crystals and irradiated with a fluence $10 \cdot 10^{15}$ electron·cm^{-2} pulses the law represents the routine exponential curve with one

relaxation time, for the irradiated crystals with the fluence $30 \cdot 10^{15}$ and $60 \cdot 10^{15}$ electron·cm^{-2} there is justified a supposition about existence of a relaxation spectrum.

1. Efimov V.V., Ivanov V.V., Klevtsova E.A., Novikova N.N., Sikolenko V.V., Tiutiunnikov S.I., Vinogradova E.A., Yakovlev V.A. Particles and nuclei, letters, 6[115] - 2002, p. 65-71.
2. Sogr A.A., Kopulova I.B. Izv. RAS. Ser.phys.-1996, T.60, 10, p.150-152. (in Russian)
3. Rudyak V.M. Switching processes in nonlinear crystals. –M.:Nauka, 1986.-248 p.

This work was supported by the program "Universities of Russia"
№ УР01.01.053.

TEMPERATURE DEPENDENCE OF GROWTH RATES FOR {0001} AND {01$\bar{1}$1} FASES IN QUARTZ

Ostapenko G.T., Mitsyuk B.M., Institute of Magnetism, NAS of Ukraine, Kiev
ostap@imag.kiev.ua факс: (38044) 424-10-20 тел: (38044) 424-12-66

Growth rates of {0001} and {01$\bar{1}$1} faces in alkali aqueous solutions (4% NaOH) were determined in autoclave experiments within 300 - 360°C temperature interval and at 1 kbar pressure. Method of temperature difference (ΔT) between dissolving and growth zones [Laudise, 1959; Khadzi et al., 1987] was applied, ΔT being 10°C.

Between 300°C and 360°C, growth rates exponentially grew from 0.18 to 0.67 mm/day and 0.05 to 0.3 mm/day respectively for {0001} and {01$\bar{1}$1} faces. Same values of activation energy, E, were obtained for growth rates of both faces: 20 ± (1-2) kcal/mol (or 84 ± (4-8) kJ/mol). The above E values coincide with activation energy for {0001}, but differ from E for {01$\bar{1}$1} (14 kcal/mol) in [Laudise, 1959]. Actually, the obtained values of E control rates of surface crystallization reactions.

TWINS FORMATION IN SYNTHETICAL CRYSTALS OF QUARTZ.

Stepanova T.A.
VNIISIMS, Alexandrov

Brazil twins belong to either (together with twins) of the most wide-spread types of twins in quartz. These twins are also wide-spread in synthetical crystals of quartz.

Contrast of twinning border is explored in different reflections by diffractive contrast method with the use of x-ray topography (for macrotwins) or under the electronic microscope.

Probability of Brazil twins formation in α-quartz should decrease during crystallization if temperature increases. That's why, the presence of Brazil twins in natural quartz samples can point to its initial low-temperature origin (certainly, it's necessary to take into account a possible complicated influence of impurities). It was repeatedly mentioned in mineralogical literature that Brazil twins are found especially often in quartz crystals, which have low-temperature genesis. A well-known fact about the presence of twins in the outward parts of crystal also witnesses about it. Brazil twins are formed in almost all growth pyramids (although with various probability for different pyramids)during quartz crystal growth. Twins are formed in pyramids of positive basic rhombohedron <R> and pyramids of trigonal prism <-X>. Twin formation in pyramids <-X> is observed often enough. In this case they have a characteristic morphological mark on the surface –X, masking veritable R-orientation of twin individuals. Considerably higher rate of surface +X growth in comparison with –X leads to formation of inlet angle between twins and matrix. Healing of such angles creates characteristic morphological habit of such formations. However, R-orientation of this type twins is clearly revealed after cutting down of twinning accessory and etching. Brazil twins have roof-like shape [1].

Nature of Brazil twins formation has growth origin, it cannot be obtained in deformated way.

Twins are often formed during growing on passivated screens in real conditions of the hydrothermal synthesis of synthetical crystal material. It is well agreed with the theoretical suppositions about complicating influence of impurities, promoting appearence of these defects. As it is generally known, passivation of autoclave wall equipping promotes the formation of acmite ($NaFeSi_2O_6$) protective layer, which is generated as a result of interaction between hydrothermal alkaline solutions and iron of apparatus. On the other hand, crystals grown on passivated screens are cleaner as for mechanical inclusions, their grade is higher. It drives us to a conclusion that twins formation accumulates this kind of inclusions on itself.

The cycle, in which we fix the seed plates for piezoquartz synthesis on passivated and new screens in correlation 1:1 is the confirmation of influence of twins appearence on face -X. Practical data, accumulated as a result of many cycles, carried out on SVD vessels also proves this fact. Study of samples, conducted in the department of hydrothermal synthesis by Belimenko F.A., allowed us to make a conclusion that twinning in saleable crystals of optical quartz is caused by dropout of solid inclusions in growth pyramids <-X>,<+X> and dislocation structure formation on its base.

But the mechanism of twins origin is very difficult. Probably, the insertion regime influences the formation of twins on face –X. This is a very important factor of any kind of synthesis. The insertion should be done fluently, without temperature drops or power changes because any sharp change in power leads to perturbation of streams, causing precipitation of solid inclusion lines in crystal-traps, allowing to study the influence of the above-stated factors in depth.

References:

1. Synthesis of minerals.Vol.1, VNIISIMS, Alexandrov, 2000, p.662.

BRITTLE FRACTURE KINETICS OF QUARTZ SINGLE CRYSTALS.

Zhoga L. V.[1], Shilnikov A. V.[1], Shpeizman V. V.[2],
[1)] State Architectural and Engineering academy, Volgograd, Russia
[2)] A. F. Ioffe Phisico-Technical Institute of Acad. Sci., St.-Petersburg, Russia

The results of measurements of strength and durability of quartz single crystals are given. The beams (2×2×20 mm) oriented along Y-axis were tested by a three-point bending method with a stepwise loading. Measurements are carried out at temperatures from 20 up to 400°C. The weak dependence of durability on the test temperature is observed and the dispersion of durability decreases with temperature increase. The durability of samples of natural and synthetic quartz is measured at 20, 300 and 400°C. The large dispersion of strength and durability of samples, which is typical for brittle fracture, is possible to explain by the various speed of an overstress relaxation in a local zone of destruction, therefore the kinetic parameters of fracture are calculated on the base of the model offered in [1, 2]. The integral distribution of bending strength and the curve of probability of destruction at $\sigma = \text{const}$ on each step are constructed by the results of statistics of destruction at stepwise loading. On the basis of these data the parameters A and B in the formula for durability τ: $\lg\tau = \lg A - B\sigma$ are obtained by the equations: $\lg\frac{A}{\tau_{min}} = \frac{\bar{\sigma}\lg\tau_{max}/\tau_{min}}{\int_{-\infty}^{\infty} W d\sigma}$, $B = \frac{\lg A/\tau_{min}}{\bar{\sigma}}$, where $\lg A$ and B are constant for the given test temperature. The factor A defines the activation energy of the fracture, and B defines the effective activation volume. The calculated value of activation energy does not depend on temperature (U_0 = 3.5 eV) and coincides with the energy of the bond Si-O (E=3.9 eV), determined by the thermochemical experiments on quartz [3]. This fact confirms that the fracture kinetics of quartz is determined by the bonds breaking process, therefore only effective activation volume, being structurally sensitive characteristic, depends on temperature. This confirms as well the assumption, that the main reason of durability and strength dispersion is distinctions in structure of different samples.

This work is supported by the RFBR (Grant № 02-02-016232) and by the Competitive center of Russian Ministry of Education (Grant E 02-34-424).

1. V.V. Shpejzman, V.A. Stepan, L.V. Zhoga. Problems of durability and plasticity of materials. Л.: Science, 1979, with. 43-55.
2. V.A. Stepan, N.N. Peschanskaja, V.V. Shpejzman. Durability and релаксационные the phenomena in firm bodies. Л.: Science, 1984, 246 with.
3. Gimblett F.G. Inorganic hjlymer chemistry, London, Butterworths,1963.

INVESTIGATING INFLUENCE OF GRATINGS ON GAAS/ALGAAS QWIP PHOTOSENSIVITY SPECTRA

.Pavel Y. Pak, Anatoliy P. Savchenko, Marina M. Kachanova and Valeriy V. Shashkin

Development of high-sensitive, homogeneous two-dimensional IR photodetectors for long wavelength IR (LWIR) spectrum is a very attractive task worldwide. Using MBE technology for growth QWIP on A^3B^5 compounds giving precise barrier composition and number of monolayers as well as high range of doping concentration in final QWs. However, photosensitive structures, based on two-dimensional QWs with two discrete electron levels absorbing only TE mode of normal incident IR radiation. This leads to necessity of development of matching structures on two-dimensional photosensitive arrays.

In this work a three-dimensional difractive gratings, formed in n^+-GaAs top conductive layer were investigated. A several dimensions of grating step were applied on single GaAs/AlGaAS 30-period QWIP structure with own 9,0 μm peak photocurrent wavelength. A dry etching through aluminium mask technology was used for creating low-dimensional defractive shapes with a vertical walls and defined depth. Grating structures were investigated using optical and electron microscopy. Test mesastructures, consists of GaAs/AlGaAs 30-period multilayer structure with 200x200 μm^2 area with etched on top n^+-GaAs layer ordered multielement grating structure were investigated on photosensivity spectra shape and absolute peak ampere-watt sensity.

This experiences defined a high dependence of photosensivity spectra shape, absolute peak and integrated sensity on step of array of etched and nonetched shapes with predefined relation of areas in grating structure, that is coinsides with theoretical assumptions.

NEW NONCENTROSYMMETRIC SULFIDES PROMISING FOR HIGH OPTICAL NONLINEARITY

V.V. Atuchin[1], B.I. Kidyarov[1] and N.V. Pervukhina[2]

[1] Institute of Semiconductor Physics, SB RAS, Novosibirsk, 630090, Russia.

[2] Institute of Inorganic Chemistry, SB RAS, Novosibirsk, 630090, Russia.

Many simple and binary sulfides possess high nonlinear optical, electrooptical and piezoelectric properties and used as a basic materials for optoelectronic device applications [1-3]. Nevertheless, material properties of the dominant part of the compounds remain unknown because of great efforts needed for growth of single crystal with dimensions and quality enough for physical characteristics observation. Evidently the most wide information is available on nonlinear optical properties of the compounds due to the fact that average level of nonlinear optical susceptibility $\chi^{(2)}$ can be estimated through powder SHG intensity with using relatively simple technique proposed in [4]. So, the problem is how to ascertain a priory the acentric crystals exhibiting the most promise for high nonlinear optical properties. The characteristics of ideal crystal are evidently defined by sort and number of atoms included into elementary cell and chemical bonds between them [5]. So, it seems be reasonable to search for some universal correlation between nonlinear optical properties of the compound and some key characteristics of the chemical bonds generated on crystal lattice formation. The absence of inversion center in crystal lattice is defined by two factors, namely the distortion of sulphur environment around cation M and asymmetric linkage of MS_x groups with the sulphur polyhedra containing another cations. As it appears, the length of the shortest chemical bond L(M–S) can be reasonably used as a parameter to characterize the acentricity of MS_x structural units. The rules governing the linkage of polyhedra of different cations in crystal lattice, however, are less clear and it is a difficult task to formulate suitable geometrical parameter for numerical description of the "acentricity rate" [6]. The aim of this study is the comparative observation of noncentrosymmetric binary sulfides to test the validity of the rule for this set of the compounds. The relation between the magnitude of $\chi^{(2)}$ and chemical bond lengths for presently known simple and binary noncentrosymmetric and sulfides, omitting the compounds containing halogens, will be considered also.

At the moment our collection of noncentrosymmetric simple and binary sulfides includes 375 compounds for which crystal structure has been refined by experimental

methods of X-ray and neutron analysis. Chemical composition of binary sulfides can be described by formulas $M_nM_mS_t$, $M_nE_mS_t$ or $E_nE_mS_t$ in which cation types E and M are defined by the relation L(E-S) ≤ A < L(M-S), where A is some transition value of bond length. In Fig.1 the sulfides are shown as points on the plane of the shortest chemical bonds. In this figure, because of arbitrariness in the choice of the first cation in chemical formula for binary sulfides , any compound containing two cations E or M is displayed by two points positioned symmetrically in reference to the bisectrix of the coordinate angle. The points related to simple sulfides lie on the bisectrix. As it is evident, near all points may be covered by a rossete of two big partly crossing ellipses of "acentricity". Only few simple noncentrosymmetric sulfides put away the ellipses. Furthermore, principally dominant part of the compounds ispositioned into a rossete of twinternal ellipses with lower dimension. Few noncentrosymmetric sulfides $E_nE_mS_p$, $M_nM_mS_t$ locate into the belt between external and internal ellipses but, up to now, measurable acentric properties have not been reported for them. Another specific feature is the absence of noncentrosymmetric sulfides with very short bonds L(E–S). As it may be supposed such compounds should contain P, B, C or N cations. Thus, this representation permits us to understand the ranges of the shortest bonds between cations and oxygen under which the formation of noncentrosymmetric crystals is probable. All sulfides with measurable optical nonlinearity $\chi^{(2)}$ >0.05 pm/V lie inside internal ellipses of "acentricity" in the range ~151pm<L(E-S)<253pm. So, for binary sulfides the value of A, right boundary of vertical internal ellipse of "acentricity", can be estimated as A_s~253pm, and for vertical external ellipse- A_s~275pm.

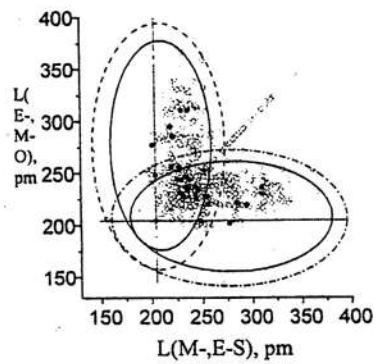

Fig.1. The plane of the shortest chemical bonds for noncentrosymmetric simple and binary sulfides. Dark colour show the crystals posessing optical non-linearity $\chi^{(2)}$ ≥ 0.05 pm/V.

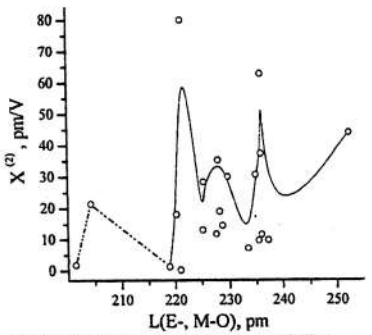

Fig.2. Nonlinear optical susceptibility $X^{(2)}$ as a function of the shortest chemical bond length L(E,M-S) in sulfides.

In Fig.2 the dependence of $\chi^{(2)}$ on L(E-S) is presented for the compounds listed in Table I. Thus, similar to oxides, strong $\chi^{(2)}$ >4pm/V is detected for limited intervals of L(E–S)= ~205, 221-236 and ~252pm. This range covers such cations as Ag, Zn, Hg, Cd, Al, Ga, In, Fe, Co, Ni, Au, Pt, Pd, Ti, V, As, Sb, Nb, Ta and Mo; particularly U, Zr, Hf, Sc, Cr, Tl, Sn, Cu, and it appears that binary sulfides with these metals are most promising for high $\chi^{(2)}$. Only one sulfide, $InPS_4$, with pronounced $\chi^{(2)} \approx 21.4$ pm/V has been found in the range ~L(E–S)≤205pm and in this region the dependence of $\chi^{(2)}$ on L remains unclear. As to simple sulfides, its number can not be large and evidently the compounds were searching very intensively in the past. So, the discovery of new noncentrosymmetric simple sulfides with measurable $\chi^{(2)}$ seems be unlikely. As it is known, the value of $\chi^{(2)}$ essentially increases with chemical bond length growing. From comparative crystal structure analysis it has been found that sulfur effective anion radius is higher than that of oxygen and, respectively, sulfides are waiting for higher optical polarizability [7].

So, the criterion of the shortest chemical bond length is used for definiton of the fields of noncentrosymmetric binary sulfide crystals. This approach yields the estimations of bond length characteristics promising for high optical nonlinearity. For sulfides available information on nonlinear optical properties is very limited and only less defined list of cations promising for high $\chi^{(2)}$ can be formulated. At present this set includes Ag, Zn, Hg, Cd, Al, Ga, In, Fe, Co, Ni, Au, Pt, Pd, Ti, V, As, Sb, Nb, Ta and Mo; particularly Cu, Sc, Cr, Tl, Sn, Zr, Hf, U.

[1] Dmitriev V.G., Gurgazyan G.G., Nikogosyan D.N., *Handbook of nonlinear optical crystals. Springer series in optical sciences*, Berlin: vol. 64 (Second edition), Springer-Verlag, 1994.

[2] Rashkeev S.N., Lambrecht R.L., *Phys. Rev.* 2001, v. B63, p. 165212.

[3] Andreev Yu.M., Geiko P.P., Badikov V.V., Bhar G.C., Das S., Chaudhury A.K., *Nonlinear Optics* 2002, v.29, n1. p.19-27.

[4] Kurtz S.K., Perry T.T., *J.* structures, *Phys. Rev.* 1973, v.7, n6. p. 2600-2626.

[6] Atuchin V.V., Kidyarov, B.I. *J. Kor. Cryst. Growth Cryst. Techn.* 2002, v. 12, n6. p. 323-328.

[7] R.D. Shannon, *Acta Cryst.* 1976, v. A32, p. 751-787.

THE CATHODOLUMINESCENSE OF CuCl

Zakharova T.V., Zakharov N.A., Kalinnikov V.T.

Kurnakov Institute of General and Inorganic Chemistry RAS,
Leninskjj pr., 31, 119991, Moscow, RUSSIA
E-mail: zakharov@igic.ras.ru, (095) 955-48-84, (095) 954-12-79

The luminescent characteristics of copper chloride CuCl during series of years were object of steadfast attention of the explorers. Fixed, that at temperature of fluid nitrogen the radiation spectrum CuCl near to edges of own absorption is characterized by bands of radiance free excitons Z1, 2 (377,0 nm) and Z3 (385,0 nm), by a band I_1 (387,8 nm) of linked exciton, and also band 390,0 nm, referred to emission of exiton molecules. In more long-wave region of a spectrum there is a violet band luminescense with a maximum at 425 nm. Besides in emission of CuCl films the wide bands 450, 490, 530 and 650 nm were found.

By the purpose of the present work was the experimental research luminescense of CuCl crystals in a spectral region 300-900 nm at excitation of luminophor by an electron beam and study of temperature dependence of a radiation spectrum in range of temperatures 80-400 K. The objects of research was CuCl crystals with cubic crystalline structure that were grown by Bridgmen method. The excitation was carried out by an electron beam by output power 10 kW at density of a current of a beam about $2 \cdot 10^{-5}$ A / cm^2.

In result of investigations were estimated bands of emission with maximums 393,5; 700; 780 and 830 nm. In addition dependence of spectral composition of emission from temperature and anomalous displacement of Z_3 – exciton emission.

OPTICAL AND LUMINESCENT PROPERTIES OF THE SCHEELITE TYPE CRYSTALS: $SRWO_4$, $SRMOO_4$ AND $CAMOO_4$

I.V. Kitaeva*, L.I. Ivleva, V.N. Kolobanov*, V.V. Mikhailin*, D.A. Spassky***, I.S. Voronina****

* Synchrotron Radiation Laboratory, Physics Faculty, Moscow State University, 119992 Moscow, Russia
** Laser Materials and Technology Research Center of GPI, Vavilor str. 38, Bdl. "D", 119991, Moscow, Russia
*** Skobeltsyn Institute of Nuclear Physics, Moscow State University, 119992 Moscow, Russia

The following scheelite-type crystals: $SrWO_4$, $SrMoO_4$ and $CaMoO_4$ were investigated in the present work. Strontium tungstate is a promising laser crystal [1] and calcium molybdate is used in tuneable acousto-optical filters [2].

To our knowledge the luminescent properties of these compounds are studied extremely poor. Also there is no information about the electronic density of the energy bands of these crystals. The study of it's energy band structures by means of absorption spectra is embarrassed in the region of fundamental absorption, therefore in the present work the reflectivity spectra were measured using synchroton radiation (SR) in the energy region of 4-40 eV in order to obtain information about electronic structure of these crystals. Then, using Kramers – Kronig relations absorption as well as optical functions were obtained from the reflectivity. The anisotropy of crystal structure of the investigated compounds was also taken into account in the experiments. That is important for the analysis of the measured reflectivity spectra of the scheelite type crystals, because its profile strongly depend on the relative orientation of the optical axes of the sample and vector **E** of the linearly polarized SR incident radiation [3].

Reflectivity, photoluminescence and luminescence excitation spectra at UV-VUV region as well as X-ray excited luminescence were measured. The measurements in the photon energy range of 4 - 40 eV were carried out on the Superlumi station (DESY, Hamburg, Germany) at the room and nearly liquid helium (8 K) temperature and at the set-up in the X-ray channel of the synchrotron radiation of the "Siberia" storage ring at the Kurchatov Center of Synchrotron Radiation (Moscow, Russia) at the room temperature. The

investigated crystals were grown using Czochralski method in the General Physics Institute, RAS, Moscow.

The analysis of reflectivity spectra of $SrWO_4$, $SrMoO_4$ and $CaMoO_4$ allowed to explain some fundamental features of the electronic structure of these crystals. Particularly, it was shown that calcium electronic states don't participate in forming of the bottom of the conduction band. The conclusions about the nature of the luminescence center of the investigated crystals were also made.

References

1. L.I. Ivleva, T.T. Basiev, I.S. Voronina, et al Optical Materials, **23** (2003), 1-2, 439-442
2. A.A. Blistanov, Crystals of quantum and non-linear optics. Moscow. MISIS. 2000. p.431.
3. V.N. Kolobanov, I.A. Kamenskikh, V.V. Mikhailin et al NIM **A 486/1-2** (2002) pp. 496-503.

e-mail: Irina_Kitaeva@rambler.ru

Moreover, the intensity of 'prohibited' lines increases with the growth of the optic distortion value. We have studied the following spectra: a) those of nominally pure single crystals of congruent (R=0.946) and stoichiometric (R=1) composition grown by two methods (from melts with 1) excess Li_2O and 2) of a stoichiometric composition doped with K_2O); b) those of congruent crystals alloyed with nonphotorefractive impurities $LiNbO_3$:Gd (C_{Gd}=0.002; 0.003; 0.05; 0.44 w/o), $LiNbO_3$:Y (C_Y=0.24; 0.46 w/o); c) and also the spectra of stoichiometric $LiNbO_3$:Gd (C_{Gd}=0.001 w/o). The methods of crystal growth and sample preparation are described in detail in works [11-12]. Both the Raman spectra and photorefraction were simultaneously excited by the same laser radiation using the Ar^+- ILM-120 laser with the generation line and power of about 0.2 Wt. The spectra were recorded by spectrometers Ramanor U-1000 and DFS-24 at room temperature. Since the photorefractive spectra may feature temporary variations [2,5,9], they were recorded about one hour after the onset of sample radiation, when these changes are essentially reduced to zero.

Figures 1(a, b) and 2 present fragments of Raman spectra of crystals of varying compositions and scattering geometries Y(ZX)Z. The spectra are noticeably different, the difference being of a fundamental character and determined by fine peculiarities of structural unit ordering in the lithium niobate sublattice. The photorefraction effect was expected to be minimal in stoichiometric crystals due to the best ordering of their cation sublattices. However, our experiments have shown that nominally pure, highly ordered lithium niobate stoichiometric crystals have a more pronounced photorefractive effect than the congruent crystals. This is evident in Fig.1 representing the spectra in the low-frequency region (a) and in the region of oxygen octahedra NbO_6 vibrations (b). According to the Raman tensor [2, 12], these spectrum regions should develop only the lines with frequencies of ≈ 150 and 580cm^{-1}, corresponding to E(TO) phonons. However, the photorefractive effects creates in the scattering geometry Y(ZX)Z additional lines with the frequencies of ≈ 172, 605 cm^{-1} corresponding to prohibited A_1(TO) phonons (Fig. 1, a, b). In the spectra of nominally pure and slightly alloyed with Cd^{3+} stoichiometric crystals grown from a melt with appreciable excess of Li_2O (curves 1 and 2, respectively) the intensity of 'prohibited' lines is higher than that of similar lines in the spectra of crystals grown from congruent melts doped with K_2O (curves 3), or congruent crystal spectra (curves 4).

Fig.1 (a, b) also shows the variation of 'prohibited' lines intensity (and, consequently, the photorefractive effect) with changing crystal composition. It should also be noted that in a certain region of alloying impurity concentrations the intensity of 'prohibited' lines in

congruent crystal spectra (curves 6, 8) and, consequently, the photorefractive effect, are substantially lower than in the spectrum of nominally pure stoichiometric and congruent crystals. Further increase of alloying impurity concentrations in congruent crystals (>0.4 w/o) results in broadening and enhanced intensity of 'prohibited' lines (curves 7, 9) due to increasing photorefractive effect, alongside with a noticeable broadening of all the other spectrum lines likely to be brought about by disordering in the cation sublattice caused by alloying impurities.

These findings also suggest that the photorefractive effect in stoichiometric and congruent, both conventionally grown and K_2O alloyed, crystals has different values. The difference in 'prohibited' line intensities suggests (Fig. 1, a and b) that the photorefraction value in congruent and stoichiometric, K_2O unalloyed, crystals is about 1.5-3 times as high as the value in similar crystals grown with K_2O addition.

The result of either alloying or changing of the crystal stoichiometry becomes evident not only in the changed structural unit ordering in the cation sublattice but also the dipole moment of oxygen octahedra BO_6 and, consequently, their polarizing ability. These changes should also affect the intensity of the line corresponding to bridge valent vibrations (BVV) of oxygen atoms in the octahedral anion BO_6. This vibration is active in the Raman spectrum of noncentrosymmetrical oxygen octahedra and is prohibited in the spectrum of centrosymmetrical (ideal) octahcdra [14].

Fig.2 shows the transformation of the line shape corresponding to BVV of oxygen ions B_1-O-B_2 (where B_1 and B_2 are basic (Li^+, Nb^{5+}) or impurity ions) with the changing crystal composition. As is seen from the Figure, the line has an intricate contour. Analysis involving the contour separation reveals only one line (curves 1, 2, 4-6, 8) in both the spectra of crystals with fairly ordered cation sublattices (such as the spectra of nominally pure congruent and stoichiometric crystals) and in congruent crystals alloyed with relatively small amounts of Gd^{3+}, Y^{3+} ions in the B_1-O-B_2 BVV . Moreover, this line is the narrowest for stoichiometric, the best-ordered, crystals. So, the nominally pure homogeneous lithium niobate crystals can be regarded as unimode ones. The unimode behaviour of alloyed lithium niobate crystals becomes obvious at those small alloying concentrations which exert an ordering effect on the cation sublattice of a congruent crystal thus increasing the photorefraction effect [2, 15].

The spectra of both stoichiometric crystals slightly alloyed with Gd^{3+} and congruent crystals alloyed with appreciable amounts of Gd^{3+} and Y^{3+} in the region of oxygen atom BVV have two distinct lines with frequencies of 850 and ≈ 900 cm^{-1}, namely

CONOSCOPE FIGURES OF OPTICALLY ACTIVE CRYSTALS

Pikul O.J., Rudoj K.A., Stroganov V.I.

Far East state transport university, Khabarovsk, Russia

The spiral structure in conoscope figures of optically active crystals, differing from Eire's figures was found out. The reason of appearance of spiral structure is the radiation polarized circularly.

The conoscope method plays special role in research of crystals's optical properties. Lissajous (conoscope) figures appeared from passage of the converging light beam through the crystal plates, placed between a polarizer and the analyzer, contain the significant information about properties of crystals.

For linearly polarized radiation the conoscope picture of monoaxial optically active crystal which has been cut out of perpendicularly optical axis, represents the system of isochromatic fringe (rings). The black "cross wheel" in the field of some angular diameter is absent. Diameter of rings varies with rotation of the analyzer: increases or decreases depending on a direction of rotation of the analyzer and from a sign of rotation of the crystal. It allows to form the beams like besselian beams, if to pass slightly a polarizer – a crystal – an analyzer.

In this work the results received by circularly and elliptically polarized radiation are represented.

To find out circularly polarized radiation, the quarter - wave phase plate which made of quartz crystal (thickness about 3 mm) was used. In experiment single-mode helium - neon laser (λ = 0.6328 microns) with radiation divergence of 3,5 minutes was used The azimuth of linearly polarized radiation on the input into the plate was 45° depending on the one of main directions of the plate. The control of the optical signal at the output from the plate was carried out by the photometric method. Polarization of radiation on the output from a plate was near circular one.

It was possible to receive the radiation polarized elliptically at an inclination of the quartz plate. The eccentricity degree could be adjusted. It is necessary to note that even small changes of orientation of the quarter- wave plate result to eccentricity deviations from one.

Conoscope pictures was observed on crystal plates TeO_2 (thickness of 3,10 mm; 1,23 mm; 0,36 mm) and $LiJO_3$ (thickness of 5,94 mm and 1,18 mm), cut out perpendicularly to optical axis.

Characteristic conoscope pictures varied depending on the optical polarization were observed for each of the specified plates. For circularly polarized radiation conoscope picture will be transformed to the figure consisting of two spirals, one placed into another.

This picture differs from Eire's spirals observed in two optically active plates with different sign of rotation. The cross wheel is absent in observed pictures. If to look towards to a beam, the direction of spiral's cockling at a crystal TeO_2 (from the beginning) – counter-clockwise, at a crystal $LiJO_3$– clockwise. That agrees with fixed sign of rotation for crystal's model of TeO_2 and $LiJO_3$ used in experiment.

It is typical, that spirals get the form close to "square" for thin crystal plates.

With turn of the analyzer clockwise after the crossed position – the nearest to the center isochromatic "rings" (the parts of spirals) diverge, if the spiral is turned round counter-clockwise; or converge, if the spiral is turned round clockwise. The conoscope figure is appeared with turnover (180°C) of the analyzer.

This conoscope figures can be applied in quantum electronics for definition of a direction of rotation the circularly polarized radiation and for fast qualitative definition of the polarization's degree.

Such method is convenient for use in system: a polarizer – a crystal – an analyzer of the diffuser (before crystal), It allows to receive large-scale conoscope figures. For the circularly polarized radiation, depending on the right or left rotation, the straight line which has been drawn in the beginning of two spirals, differs in 90 degrees.

Application of the concrete crystal, TeO_2 for example, allows to characterize polarizing properties of used radiation by visual conoscope picture.

SPECTRAL PROPERTIES OF CdF_2 SINGLE CRYSTALS IN SHORT WAVELENGTH SPECTRAL REGION

D.N. Karimov, I.I. Buchinskaya, B.P. Sobolev, A.A. Artyukhov*, S.P. Chernov**

Institute of Crystallography RAS, 59 Leninskii Prospect, 119333, Moscow, Russia
karimov_d@rambler.ru
* RRC «Kurchatov Institute», 1 Kurchatov Square, 123182, Moscow, Russia
** Physics department. Moscow State University, 119899, Moscow, Russia

Cadmium fluoride single crystals are present of interest as base for creation of optoelectronic materials. Crystals of the solid solutions gallium and indium fluorides in CdF_2 demonstrate of gigantic photorefractive effect [1, 2]. Such materials functionality in UV-VIS spectral ranges demand knowing of their fundamental absorption characteristics. Data of the cadmium fluoride crystals spectral properties are very scarce in this spectral region.

Transmission of crystals in a short wavelength spectral region is determined by the first peak of fundamental absorption position. Gap band for CdF_2 crystals is 7.6 eV [3] that has to provide the high transparency of these materials in UV spectral region. But optical properties of CdF_2 crystals considerably depend on chemical purity of starting materials and on conditions of crystal growth.

In the present work the UV-VIS transmission spectra of CdF_2 crystals were studied. The crystals were grown from different charge: 1) the powder of commercial "highly pure" grade CdF_2 reagent were purified of oxygen impurity by polytetrafluoroethylene pyrolysis products; 2) the same reagent, fluorinated by XeF_2 at temperature about 400 °C and pressure about 3-4 Torr ; 3) the CdF_2 powder obtaining by reaction of metallic Cd with elementary fluorine at temperature about 400 °C.

Optical grade CdF_2 single crystals were grown by Bridgman technique in opened multi-channel graphite crucible. Rate of crucible lowering was 9.5 mm/h in 50 °C/cm temperature gradient. All growing crystals were yellowish coloring independently on kind of starting charge. This coloring was not controlled and had different intensity and shade from lightly yellow to dark red and brown. It is note, that coloring intensity was decrease in the some measure with increasing of fluorine agent quantity in growth atmosphere, duration of melting and overheating degree of the CdF_2 melt. But full coloring illumination was not achieved.

Direction crystallization is effective method for purification CdF_2 crystals from yellow color. Optical centers due to color reveal during crystal growth like impurity with distribution coefficient < 1. Practical colorless crystals CdF_2 were obtained after three times recrystallization in the fluorinating atmosphere with rate crucible lowering 3,5 – 4 mm/h and removal every time the most colored part.

Crystals were cut perpendicularly to direction axes from different part of crystals rods into samples with 0.5 - 5 mm thick and polished. RT spectra transmission of CdF_2 in visible wavelength region were made on Specord-type spectrophotometer, UV transmission spectra were obtained in the vacuum by a VMR-2 monochromator (with the inverse linear dispersion of 1,6 nm/mm) with hydrogen lamp as a light source.

Transmission spectra of CdF_2 single crystals are shown in Figure. These spectra demonstrate some following features:

1.) UV transmittance limit (with transmission level less then 1%) were located at 197 nm for the sample thickness of 0.5 mm (curves 1, 3). CdF_2 single crystals growing from charge obtaining by reaction of metallic Cd with elementary fluorine show highest transmission level (curve 1).

2.) Well-resolution absorption band at 220 nm is presented in practically all spectra. Distribution and accumulation of defects during crystal growth process result in the increasing of this band absorption and shifting of transmission limit toward long wavelength region (curves 2, 4).

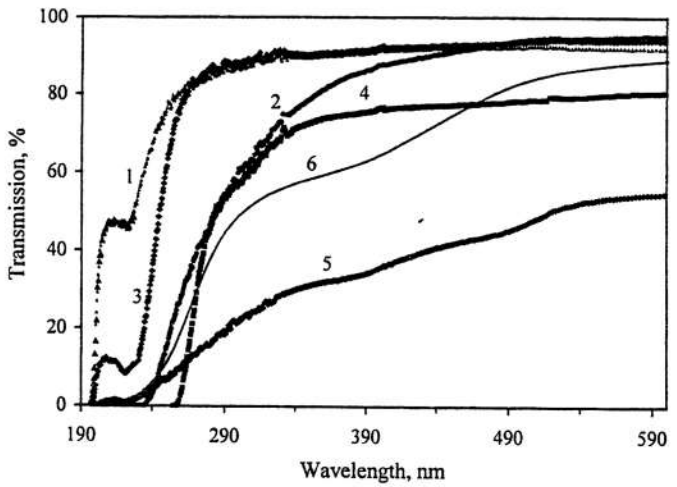

Fig. Transmission spectra of CdF_2 single crystals, growing from different charge: bottom (1) and middle parts (2) of the crystal rod, obtaining by reaction of metallic Cd with molecular fluorine; bottom (3) and top parts (4) of the crystal, obtaining from CdF_2 charge fluorinated by XeF_2; top of crystal (5) obtaining from CdF_2 charge fluorinated by thermal decomposition products of polytetrafluoroethylene; (6) data from literature [4]. Thickness was 0.5 and 5 mm for 1, 3–5 and 2, 6 samples, respectively.

3.) The yellowish coloring of the top crystals rod naturally enough attribute to decreasing there transmission in blue-violet spectral region without any selective absorption bands appearance.

4.) Also two weak broad absorption bands with maxima at 380 and 480 nm are observed for intense yellow coloring crystals obtaining from CdF_2 charge fluorinated by thermal decomposition products of polytetrafluoroethylene (curve 5). Nature of these absorption bands is demanded in additional investigation. Transmission decreasing in these regions was demonstrated previously in [4], where CdF_2 crystals were obtained slowly cooling of the melt in inert growth atmosphere (argon).

This work was performed with the support under ISTC (grant № 2136) and RFBR (grant № 04-02-16241).

References

[1]. Ryskin A.I., Shcheulin A.S. et al., J. Appl. Phys., 1994, V.67(1), P. 31-33
[2]. Ryskin A.I., Shcheulin A.S. et al., Appl. Rhys., 1998, V. 83, No. 4, P. 2215-2221
[3]. Albert J.P., Jouanin C., Gout C., Phys. Rev. B, 1977, V. 16, No.10, P. 4619-4629
[4]. Haendler H.M., Wheeler C.M. et al., J. Opt. Soc. Amer. 1953, V. 43, No. 1-3, P. 215-216

GROWTH AND SPECTROSCOPIC INVESTIGATIONS OF YB:ER:GDCA$_4$O(BO$_3$)$_3$ SINGLE CRYSTALS.

I.Voronina, L.Ivleva, B.Denker, V.Osiko, B.Galagan, S.Sverchkov

General Physics Institute, Vavilov Str., 38, 119991, Moscow, Russia

e-mail: IrinaVoronina@yandex.ru

The crystals of rare-earth calcium oxoborate family RECa$_4$O(BO$_3$)$_3$ (RE = Y, Gd, La) represent a new class of perspective nonlinear-optical materials. Nd-doped RECOB crystals combine properties of nonlinear and laser active media. Recently the data were published concerning to using Yb:Er:YCOB as active laser medium [1]. Yb:Er:GdCOB is an isostructural analogue of this material and can be considered as active matrix for lasers working in 1.5 μm diapason. Such active media are of great interest because of the fact they have better thermophysical properties in comparison with widely used for 1.5 μm spectral range erbium glasses. Their technology gives practical advantages; large crystals of good optical quality can be grown by Czochralski method.

In present work we report the results of study of crystallization processes of GdCOB doped with Yb, Er in different concentrations. The spectral and luminescence characteristics are presented.

The relatively low melting temperature (1480°C) of GdCOB enables crystal growth using platinum (instead of iridium for other oxoborates) crucibles in the air atmosphere. In GdCOB gadolinium can be substituted by Yb and Er ions. In our Czochralski growth experiments the concentration of Yb ions in the melt varied from 15 to 38.5%; the concentration of Er ions was constant of 2.5%. 1wt.% Cr_2O_3 was added into the melt to obtain Cr:Yb:Er:CdCOB. The crystals doped with Er; Yb-Er; Cr-Yb-Er were grown up to 30 mm in length and up to 15 mm in diameter using the seed of [010] orientation. The crystals of optical quality were obtained at crystallization rate of 0.15 cm^3/h.

The dependence of Yb → Er energy transfer rate versus Yb concentration in GdCOB crystal is measured. For $Yb_{0.385}Gd_{0.59}Er_{0.025}Ca_4O(BO_3)$ $^4I_{13/2}$ Er^{3+} level lifetime τ_1 = 1.2 μs, $^4I_{11/2}$ Er^{3+} level $\tau_2 \leq 0.25$ μs. Efficient 1.54 μm laser action was obtained at wavelength 1.54 μm at continuous and pulsed pumping due to low value of τ_2 and relatively high τ_1. The slope efficiency about 15% was obtained under diode laser pumping and under Ti:Al_2O_3 laser pumping. The average output power was 80 mW, the peak output power was more than 150 mW.

The possibility to incorporate Cr ions in GdCOB crystal host was shown, but no Cr luminescence or energy transfer from Cr to Yb or Er was observed.

1. P. Burns, J. Dawes, P. Dekker, J. Piper, H. Jiang, J. Wang. "CW diode-pumped microlaser operation at 1.5-1.6 μm in Er,Yb:YCOB". IEEE Photonics Technology lett. V.14, #12, Dec.2002, pp.1677-1679.

GROWTH, PHYSICAL PROPERTIES AND APPLICATION OF THE ISOMORPHOUS OF CADMIUM AND ZINC DIPHOSPHIDES.

V. Trukhan, T. Haliakevich

Institute of Solid State and Semiconductors Physics, NASB, 220072, P.Brovki str.17, Minsk, Belarus

The physical-chemistry properties of the grown high degree optical perfection single crystals of cadmium and zinc diphosphides of the tetragonal modification became the basis for building of elements and instruments of laser and optical-electronic technology, which is examined in the present work.

Bridgeman's method is suitable for growth of the single crystals of $CdP_{2(T)}$, however, the optical strength of crystals almost two times decreases with the cultivation from the fusion, therefore the massive single crystals CdP_2 with a diameter up to 20 mm and with a length of 40-50 mm were obtained by paraphase method. Optimum combination of three factors: crystallization temperature, critical supercooling values and displacement speed of ampoule ensured continuous single-crystal growth of cadmium diphosphide [1].

Growth of zinc diphosphide tetragonal modification (α-ZnP_2) was produced in those evacuated to 10^3Pa and sealed quartz ampoule with diameter up to 50 mm and length of 500 mm [2]. Conditions for the formation of α-ZnP_2 crystals of tetragonal modification are determine by the variation of the evaporation and crystallization zones temperatures. Table 1 gives the phase composition of substance in the crystallization zone with different temperature conditions. Predominantly tetragonal ZnP_2 is crystallized in the middle of the indicated temperature range.

Table 1.Dependence of phase composition in the zone of crystallization on the temperature conditions of furnace.

№	Substance	Vaporization temperature,K	Crystallization temperature, K	Composition of phases in the crystallization zone
1	Polycrystalline ZnP_2	1073	1033	β
2	-//-	1080	1045	α+β
3	-//-	1090	1060	α+β
4	-//-	1100	1070	α
5	-//-	1110	1078	α
6	-//-	1120	1090	α+β
7	-//-	1145	1120	α+β
8	-//-	1155	1130	β

Influence of the radial temperature gradient on the anisotropy of the rate of growth α-ZnP_2 is studied at optimum temperatures in the working chamber of furnace. It is established, that the relatively small radial gradient of the temperature in the zone of crystallization is necessary to create for an increase in the transverse sizes of single crystals α-ZnP_2. The length of the grown single crystals α-ZnP_2 reached 50 mm.

It is established, that the amount of the deviation of laser beam cadmium and zinc diphosphides is directly proportional to the thickness of active region and composes ~1,8 deg/mm during the supplying of pulses with the duration of 10 milliseconds with the amplitude of 500V and fixed distance from the contact equal to 2 mm. Strong dependence of refractive index on the temperature, low thermal conductivity (λ=7,5 W/m*K) makes it possible to create on the basis of single crystals CdP_2 and ZnP_2 the deflector of laser beam with the characteristics given in Table 2.

Table 2.

Active region	active region thickness, mm	Pulse duration, ms	deflection angle, deg	Required power, W	Transparence range, μm	Distance of ray from the contact, mm
CdP_2 or ZnP_2	0,25	10	0,46	10^{-3}	0,6-15	2

It is determined, that the threshold sensitivity in λ=0,3 μm for CdP_2 composes P=10^{-14}W/Hz$^{1/2}$, current sensitivity in the wavelengths range 0,24-0,40 μm is equal to 0,025 A/W, the spectral sensitivity λ=0,240–0,62 μm. Time constant for CdP_2 is equal τ~10^{-4} sec. High threshold sensitivity of single crystals CdP_2 it makes it possible to create photosensitive elements with the high speed operation in the ultraviolet spectrum range.

The value of thermal-optical coefficient in cadmium diphosphide is given in Table 3, which is considerably above, than in the glass and other semiconductor materials, which makes promising the application of crystals CdP_2 as the temperature detectors of the different physical quantities sensors.

In particular, the work of the sensor of liquid level can be based, both on a change of the refractive index of termooptical crystal in the dependence on the temperature, and on the temperature dependence of its own optical activity.

The temperature coefficient of optical activity in CdP_2 and ZnP_2 is 5,74 and 2,3 deg/cm*K respectively, for λ=0,612 nm in the temperature range of 300-500K. It is possible to

Table 3.

Material	dn/dT, 10^{-5}, 1/K	λ, μm
Glass KB	0,31	0,63
KRS	-25,0	0,63
Polymethyl methacrylate	-11,5	0,63
$LiNBO_3$	+4,6	0,63
ZnS	+7,5	0,63
SnSe	+11,1	0,63
$GaAs_2$	+18,7	1,15
CdTl	+14,7	1,15
Ge	+26,8	3,39
CdP_2	+60,0	0,63

create noise-immune temperature sensors (accuracy $\pm 10^{-4}$) on basis of CdP_2 and ZnP_2 using linear temperature dependence of optical activity. Sensor measures the temperature with the presence of electromagnetic LF, HF, SHF fields and vibrations, for example, the temperature control of living tissues with the treatment by SHF- warming, or measurements in the volumes, where the conclusion of electrical wires is hindered or undesirable.

It is possible to smoothly increase the duration of monopulse from 20-25 ns to 150-350 ns by placing the single crystal plates CdP_2 and ZnP_2 into the resonator of ruby and neodymium laser. The elements for control of the ruby and neodymium laser generation pulses duration are prepared in ISSS NASB (together with IP NAS of the Ukraine) (table 4).

Table 4.

Laser	Maximum duration, nc		Nonlinear element parameters				
	without plates	with plates	compound	E_q, eV	Thickness, мм	Linear losses coefficient, cm^{-1}	Coefficient of two-photon absorption, cm/MW
ruby	20	360	CdP_2	2,02	0,5 – 1,5	1,25 – 2	0,80
ruby	20	290	ZnP_2	2,15	0,6 – 1,6	0.9 – 1.9	0,68
neodymium	25	190	CdP_2	2,02	0,5 – 1,5	1,3-2	0,16
neodymium	25	150	ZnP_2	2,15	0,6 – 1,6	1,19	0,20

It is determined, that for CdP_2 and ZnP_2 the Verde constant with λ=0,63 μm is V=0,550 min/Oe·cm and V=0,279 min/Oe·cm respectively. High value and the linear dependence of Verde constant on the magnetic induction, both in the constants, and in the pulse magnetic fields up to 22Тл, indicates to the possibility of use CdP_2 as the light modulators in the neighbor IR-range, and also as the sensors of magnetic induction.

A property of ZnP_2 to change into ~10^5 times resistance during the influence of the specific voltage can be used for creating the switching instruments. The effect of switching from the high-resistance state into the low-resistance is saved also in the diode structures on the basis of amorphous CdP_2. Restoration from the low-resistance state into the high-resistance is accomplished by an action of the short-term electric pulse of any polarity, amplitude of which exceeds the switching voltage.

Thus, using high optical quality single crystals of cadmium and zinc diphosphides it is possible to create: the laser emission deflectors, stabilizers and the attenuators of the laser emission monopulses, temperature sensors, photosensitive elements, switches and other elements of optical electronics.

References:

1. V.Trukhan, A. Sheleg. Method of obtaining of the cadmium diphosphide single crystals of tetragonal modification. Claim for invention № a2003 0693 from 30.06.2003.

2. V.N.Yakimovich, V.M.Trukhan. Growth of the single crystals of the tetragonal ZnP_2 from the vapor phase//Inorganic materials, 1998, v.34, №11, p.1292-1294.

X-RAY OPTICAL SYSTEM OF INTERACTIVE MANAGEMENT OF A X-RAY RADIATION

V.N. Trushin, A.A. Zholudev, A.S. Markelov, E.V. Chuprunov
Nizhiny Novgorod State University
603950, Nizhny Novgorod, Russia, trush@phys.unn.runnet.ru

Creating some elements of spatial and temporal modulation of X-ray radiation is one of current problems in X-ray optics. There may be various ways for solving this problem. For instance, high-frequency time modulation of X-ray radiation can be implemented in the process of X-ray diffraction with the use of surface acoustic waves [1-3]. In [4] it was shown that the external influences can lead to significant changes in the intensity of X-ray diffraction maxima (XDM) of crystals. It was established experimentally in [5] that the effect of reversible change of crystal parameters under the influence of crystal surface illumination by optical radiation can be used to form an X-ray image. It was shown that the spatial structure of XDM under certain conditions can correspond to the structure of the external influence, i.e. it can represent an X-ray image functionally related to the optical image, used as a template.

On the basis of researches by us the technology and a control system of x-ray radiation (XFormer) for radiology is developed. Technology XFormer this new perspective decision in development of x-ray optical systems. The basic purpose of such systems is decrease of a doze of an irradiation during a diagnostic session. The device XFormer also may be used in proton and neutron optics that uncloses new perspective areas of his application.

XFormer makes it possible to form any spatial distribution of intensity in the X-ray beam, which allows the user:

- to reduce the radiation dose received by the patients without affecting the self-descriptiveness of the X-ray images;
- to use methods of early diagnostics of oncological diseases;
- to form half-tone X-ray images of any shape;
- to improve the contrast of X-ray images;
- to operate the XFormer in coordination with other medical devices, USI for example;
- to form the spatial distribution of X-ray intensity in accordance with the X-ray dose chart of the patient;
- to create systems of automatic and semi-automatic, as well as remote diagnostics.

The XFormer installed in mammographs will make it possible to reduce the radiation dose by 30-80% compared to the present-day methods used in mammography. The radiation dose is reduced here due to the diminution of the irradiated areas, as well as due to the radiation impact on a patient's tissues being strictly localized and dosed.

On a fig.1 the scheme of work of system XFormer is submitted.

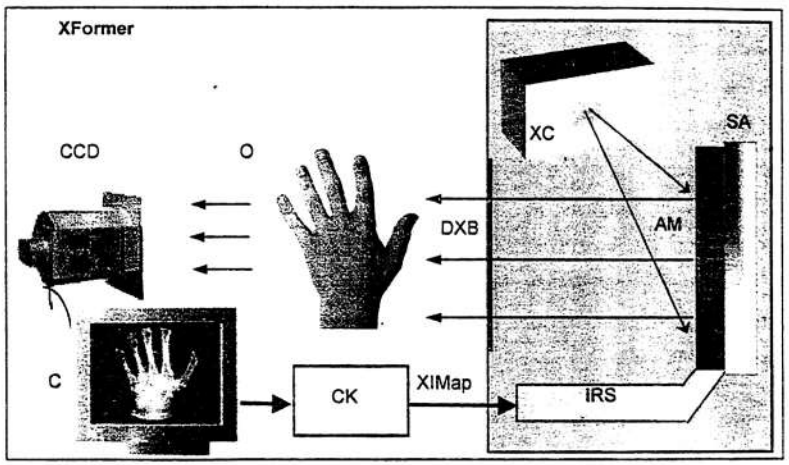

Fig.1. The scheme of work of the XFormer.

XC – the X-ray corrector;
AM – the active medium unit with the temperature stabilizing unit;
SA – the AM positioning unit;
IRS – the image replicate system;
CK – the coupling device between the computer and the IRS;
O – the biological object;
CCD – the X-ray CCD camera (two positions of the CCD camera are shown);
C – the computer of radiological system;
XS – the X-ray source;
DXB – the diagnosing X-ray beam.
XIMap – the X-ray intensity map in the DXB.

The distribution of intensity in the Diagnosing X-ray Beam (DXB) may be monitored in the following way. The X-ray beam is transmitted from the X-ray emitter XS to the XFormer device.

The X-ray corrector (XC) functioning as a monochromator forms a monochromatized X-ray beam, which falls onto the active medium (AM). The crystal monochromator is the basic component of the XC and is designed with allowance to the X-ray beam aperture and the focal size of the X-ray tube.

The AM forms the DXB, which falls onto the diagnosed object O. The beam is formed due to the local unbalance of the Bragg reflection from the AM. The unbalance of the Bragg reflection is invoked by the change of the AM characteristics. The operating principle, material and the technology of manufacturing of the AM are the know-how of the scientific group CrOX. The AM characteristics and accordingly the distribution of intensity in the DXB are controlled by the image replicate system (IRS). The IRS changes the AM parameters and forms the preset intensity distribution in the DXB automatically or in the interactive mode.

The IRS input receives an X-ray intensity map (XIMap). The AM forms the intensity distribution in the DXB according to the XIMap. The XIMap may be presented as a standard graphical file (for example, jpg.). On the basis of the XIMap the IRS unit forms AM control signals, which modify its parameters locally. Thus the spatial distribution of intensity in the DXB is functionally connected with the spatial distribution of brightness in the image, presented as a graphical file. When the graphical file is changed, it causes the spatial distribution of intensity in the DXB to change too. In other words, the brightness of a certain area of the graphical image XIMap determines the intensity in the corresponding area of the DXB.

The CCD camera registers the X-ray image of the object O. The computer (C) software composes a graphical file, which is then used for monitoring the distribution of intensity in the DXB. The graphical file is transmitted to the IRS by the coupling device CK. To compose the graphical file we can use the information acquired by different methods (non-X-ray as well), for example USI or a digital camera.

Working in the manual mode the operator can set the area and the contours of the diagnosing with the help of the graphical interface, using the tentative data about the object. The interactive mode is possible only with the help of the CCD camera. It is not necessary to use the CCD camera in a standard mode.

The XFormer performance can be modified if necessary. For instance, a crystal analyzer may be placed between the object O and the CCD camera, which increases the self-descriptiveness of the X-ray images.

References

1. D.V. Roshchupin, I.A. Schelokov, R.Tucoulou, M. Brunel, *IEEE Trans. Ultrason. Ferroelectric Freq. Continue,* **42** (1995) 127.

2. R.Tucoulou, I.A. Schelokov, D.V. Roshchupin, M. Brunel, L.Ortega, P. Chevallier, *Optic Communications*, **118** (1995) 175.

3. F. Snigirev, V. Kohn, Snigireva, B. Lengeler, "A compound refractive lens for focusing high energy X-rays", *Nature* **384** (1996) 49-51.

4. V.N. Trushin, T.M. Ryzhkova, M.A. Faddeev, E.L. Chistjakova, E.V. Chuprunov, A.F. Khokhlov, *Kristallografiya* **38**(4) (1993) 213-218 (see Sov.Phys.Crystallography).

5. V.N. Trushin, A.A. Zholudev, Y.V. Chuprunov, M.A. Faddeyev, A.F. Khokhlov "Investigation of internal inhomogeneity effects on the X-ray and optical parameters of LiNbO3 and SBN crystals" Materials Structure, vol. 6, number 2, (1999) 143 –145.

THE INFLUENCE OF Cr-IONES ON PHYSICAL PROPERTIES OF SILLENITE-TYPE SINGLE CRYSTALS

Goraschenko N.G., Stepanova I.V.

The Mendeleev University of Chemical Technology of Russia (Moscow, Russia)

nggor@rctu.ru , iris@rctu.ru

Sillenite-type single crystals have a number of valuable physical properties. The presence of elektrooptical effect, the wide range of transparency and high symmetry make them useful materials for electronic applications.

These properties depend on the nature of dopants. Bismuth germanate $Bi_{12}GeO_{20}$ has an "ideal" sillenite-structure [1]. The replacement of Ge^{4+}-iones by cations with other valences leads to appearance in atomic structure different types of defects, and as a consequence – various physical properties [2].

Single crystals of solid solutions $Bi_{12}GeO_{20}$-Cr_2O_3 were grown by Czochralski technique in open air. The concentrations of Cr-iones varied from 0 to 4at.%.

The transmission spectra were obtained. In the range of wave length 0.39-1 mcm crystals doped Cr^{3+} have supplementary adsorption strips comparatively with pure $Bi_{12}GeO_{20}$. The presence of impurity extends considerably the transmission range in the longwave part of spectrum.

Paranormal dispersion of optical activity with maximum at λ=0.5 mcm was revealed.

Cr-doped sillenites electrical conductivity decreases in comparison with undoped $Bi_{12}GeO_{20}$.

The perfection of crystals obtained investigated with chemical treatment method to turn up the dislocations. The crystal wafers cut out perpendicularly to <100> and undergone mechanical and chemical treatment consecutively. The dependence of quantity of dislocations from concentrations of Cr-iones was revealed.

The Cr-doped sillenite crystals are more resistant to γ-irradiation than pure $Bi_{12}GeO_{20}$. The resistance rises up when Cr-iones concentration increases. We suppose optical centers induced by γ-irradiation as well as by visual light have the same nature.

1. Radaev S.F., Simonov V.I. Sillenites structure and atomic mechanisms of isomorphous replacement. J. Crystallography, Moscow: 1992, V.37, N.4, P.914-941 (in Russian)

2. Craig D.C., Stephenson N.C. Structural Studies of Some Body-Centered Cubic Phases of Mixed Oxides Involving Bi_2O_3: The Structures of $Bi_{25}FeO_{40}$ and $Bi_{38}ZnO_{60}$. J. Solid State Chemistry: 1975, V.15, N1, P.1-8

FLUX GROWTH AND MORPHOLOGY OF $NDTA_7O_{19}$ AND $YTA-O_{19}$ CRYSTALS

A.V. Alexeev, E.A Volkova, N.I. Leonyuk

Deptartment of Crystallography & Crystallochemistry

Geological Faculty, Moscow State University, 119992/GSP-2 Moscow, Russia

Rare earth (RE) heptatantalates $RETa_7O_{19}$ (RE=La, Ce, Nd, Sm, Dy, Y, Tm) are of interest for miniature laser components with high concentration of active ions. These compounds have a high level of thermal and chemical stability as well as rather high concentration of rare earth elements. In this paper, phase formation in the systems RE_2O_3 – Ta_2O_5 – B_2O_3 – $K_2Mo_3O_{10}$ (RE – Nd, Y) and morphology of $NdTa_7O_{19}$ (NHT) and YTa_7O_{19} (YHT) crystals were studied.

NHT and YHT crystals were obtained by spontaneous nucleation from $K_2Mo_3O_{10}$ – B_2O_3 based high-temperature solutions in the temperature interval 1150-850°C at a cooling rate of fluxed melt within 0.5-5 °C/h. RE_2O_3/Ta_2O_5 ratio corresponded to their stoichiometry in the NHT and YHT formulas (1:7). Molar fractions of $K_2Mo_3O_{10}$ and B_2O_3 in the flux were the followings: 1:1, 5:1, 10:1.

Three types of NHT crystals were grown in the system Nd_2O_3 – Ta_2O_5 – B_2O_3 – $K_2Mo_3O_{10}$: plate-like (3 mm), short-prismatic (2 mm) and long-prismatic (1mm). Except of NHT, four subsidiary phases also crystallize in this system: 0.03 mm dark-brown cubic crystals of $Nd_{0.33}TaO_3$, $Ta_{12}MoO_{33}$ crystals (2.5 mm) with pillar-like habit. In the last case, their color usually varies from honey-yellow to dark-brown. The third phase is represented by yellow-green transparent crystals (0.1 mm). As a result of qualitative EMPA, this phase consists of tantalum oxide. However, no similar compound was found in ICDD database. Also lilac non-transparent crystals of $KNd(MoO_4)_2$ were obtained.

Taking into consideration the field of NHT stability in the system Nd_2O_3 – Ta_2O_5 – B_2O_3 – $K_2Mo_3O_{10}$, YHT crystals were obtained in the yttrium-containing tantalate system under the same temperature regimes. On this base, a comparison was made for both systems. Size of plate-like and short-prismatic YHT crystals was up to 2.5 mm. In case when $K_2Mo_3O_{10}$ /B_2O_3 was equal to 5/1, $Ta_{12}MoO_{33}$ crystals were found.

The facetting of NHT crystals is characterized by a small number of simple crystallographic forms: strongly developed pinacoid {0001}, two hexagonal prisms {1010} and {1120} and hexagonal pyramid {1121}. NHT crystal morphology depends on the $K_2Mo_3O_{10}$ /B_2O_3 ratio in the fluxed melt. Increase of

$K_2Mo_3O_{10}$concentration in the $K_2Mo_3O_{10}$ /B_2O_3 solvent promotes the development of {0001} faces in the NHT crystals. There are growth spirals on pinacoids of plate-like NHT crystals (Fig. 1). According to literature data, these spirals are related to dislocations.

The facetting of YHT crystals is also characterized by four simple crystallographic forms: {0001}, {1010}, {1120} and {1121}. All crystals have pinacoidal faces. YHT crystal morphology also depends on the $K_2Mo_3O_{10}$ /B_2O_3 ratio in the fluxed melt. In case of $K_2Mo_3O_{10}/B_2O_3$ = 1/1, plate-like and short-prismatic YHT crystals were obtained. However, if $K_2Mo_3O_{10}/B_2O_3$ = 5/1 or 10/1, only plate-like YHT crystals were grown. Also, there are growth spirals on pinacoids of plate-like YHT crystals (Fig. 2).

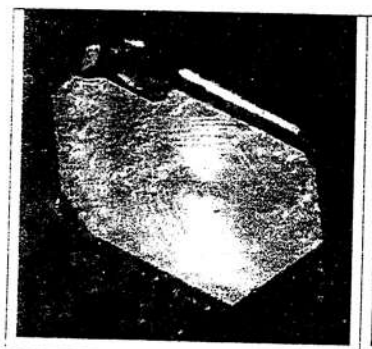

Fig. 1. Growth spirals on {0001} faces of NHT crystals

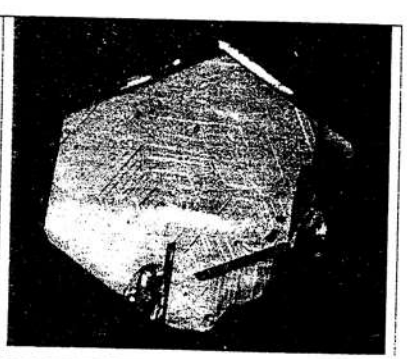

Fig. 2. Growth spirals on {0001} faces of YHT crystals

{0001} faces of NHT long-prismatic crystals contain less than 0.09 wt% of Mo, but plate-like samples have 0.13-0.79 wt% of Mo. On this base, it was supposed that increasing $K_2Mo_3O_{10}$ concentration in the solvent leads to blocking {0001} face. As a result, the pinacoidal face becomes the dominant simple crystallographic form.

This research was supported, in part, by the RFBR Grant № 04-05-64709. The authors thank Dr. I.A. Bryzgalov for ASEM analysis of grown crystals.

AHP CRYSTALLIZATION OF CONCENTRATED ALLOY CDZNTE

Bykova S.V., Golyshev V. D., Gonik M.A., Tsvetovsky V.B.

Center for Thermophysical Researches "Thermo" (Alexandrov, Russia)
E-mail: Bykova@thermo.vladimir.su ; phone/fax(095) 584-58-16

Cadmium zinc telluride (CZT) is of great technological interest and strategic importance. In order to enable the continued advance of technologies based upon CZT substrates, large, high-quality, single crystals of CZT are required. Infrared detector material is most commonly grown via the horizontal Bridgman method, while nuclear detector material is generally produced using the high-pressure vertical Bridgman technique. To date, CZT grown by both processes has been plagued by low yields that have been attributed to crystalline defects such as grain boundaries, twins, inclusions, precipitates, and microcracks, as well as compositional inhomogeneity resulting from segregation.

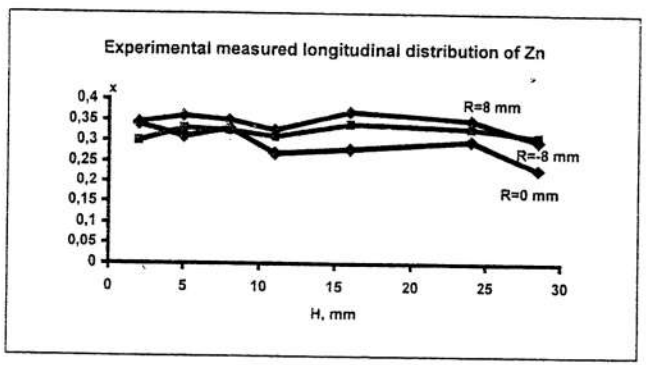

To overcome these problems the melt crystal growth method at axial heating process (AHP method [1]) was used. This method used an additional heater (AHP heater) that is submerged in the melt and that is placed close to the solid-liquid interface. By properly balancing thermal flux from this heater and from a set of background heaters, it is possible to establish an axial heat flux close to the interface and maintain constant interface shape, position, and velocity throughout the growth run.

The zone-leveling approach (optimum charge composition in upper (above AHP heater) and lower (below AHP heater) melt zones) is applied to provide optimal axial segregation.

The high-pressure (100 atmosphere of Argon) AHP technique was applied. Result of the AHP crystal growth of $Cd_{07}Zn_{03}Te$ alloy are described in the presentation. The some results on the lateral and on the longitudinal composition of AHP grown CZT are shown in Figure.

This research is supported by the U.S. Civilian Research & Development Foundation under CRDF grant № RE1-2480.

1. V.D. Golyshev, M.A. Gonik, A temperature field investigation in case of crystal growth from the melt with a plane interface on exact determination thermal conditions, Cryst. Prop. and Preparation, 36-38 (1991) 623-630.

FLUX GROWTH OF $NDAL_3(BO_3)_4$ AND $YAL_3(BO_3)_4$ CRYSTALS DOPED WITH SC^{3+} AND GA^{3+}

M.A. Fedotova[a], E.V. Koporulina[a], V.V. Maltsev[a], A.V. Mokhov[b], O.V. Pilipenko[a], N.I. Leonyuk[a]

[a]Deptartment of Crystallography & Crystallochemistry
Geological Faculty, Moscow State University, 119992/GSP-2 Moscow, Russia
[b]Institute of Ore Deposits Geology, Petrography, Mineralogy
& Geochemistry, 109017 Moscow, Russia

Non-centrosymmetric crystals $NdAl_3(BO_3)_4$ (NAB) and $YAl_3(BO_3)_4$ (YAB) doped with Tm, Yb, Eu, Er are of most interest as a promising solids for lasing and non-linear optical applications [1,2]. Since these compounds decompose before melting, they can be grown by $K_2Mo_3O_{10}$ based flux method [1]. However, their solubility in this flux is limited by 20 wt.%. The temperature solubility coefficients of NAB and YAB are also small ($\Delta C/\Delta T$ = 0.03 wt%/°C and 0.06 wt%/°C respectively), and it implies low growth rates and crystal yield. Moreover, NAB crystallizes in acentric $R32$ sp. gr. (low-NAB) below 880-890°C and in centrosymmetric $C2/c$ sp. gr. (high-NAB) at elevated temperatures [1]. On the other hand, the low-temperature structure of $NdSc_3(BO_3)_4$ (NSAB) is stable up to about 1450-1480°C, and the phase transition into monoclinic modification takes place at temperature closed to its melting point [3]. In this connection, replacement of Al^{3+} by some amount of Sc^{3+} and Ga^{3+} seems to be studied. For this reason, the present work is focused on investigations of $Nd(Sc_xAl_{1-x})_3(BO_3)_4$ (x = 0.01, 0.05 and 0.1) (NSAB), $Y(Ga_xAl_{1-x})_3(BO_3)_4$ (x = 0.05, 0.15, 0.2, 0.4) (YGaAB) and $Y(Sc_xAl_{1-x})_3(BO_3)_4$ (x =0.1 and 0.15) (YSAB) crystals depending on flux growth conditions.

At the first stage, NSAB crystals were prepared by spontaneous nucleation under different conditions using a $K_2Mo_3O_{10}$ based flux. The initial concentration of NSAB crystalline substance in fluxed melts was 20 and 30 wt%. Platinum crucibles with the starting mixture were kept at 920-1120°C for 10-12 hours, depending on the borate concentrations and compositions, and cooled down to 900°C at a rate of 12-24°C/day. Then, the temperature was lowered to 350°C.

The composition, homogeneity and external morphology of grown crystals were studied by the analytical scanning electron microscope (ASEM) JSM-5300 + Link ISIS and

JSM-5610LV. Microprobe analysis of polishing samples was performed with an accuracy of 0.2-0.3 wt %. A Cameca analyzer was used for study of crystal with a minor dopant concentration. In this case, the accuracy has been increased up to 0.02-0.03 wt.%. The X-ray powder diffraction pattern of solids was obtained using Rigaku D/Max-2200.

Low-temperature NAB modification was obtained in the system 20 wt% NSAB – 80 wt% ($K_2Mo_3O_{10}$-B_2O_3-Nd_2O_3) in the temperature range of 920-700°C. Based on X-ray diffraction study and scanning electron microscopy, it was found that only subsidiary phases, neodymium aluminium metaborate

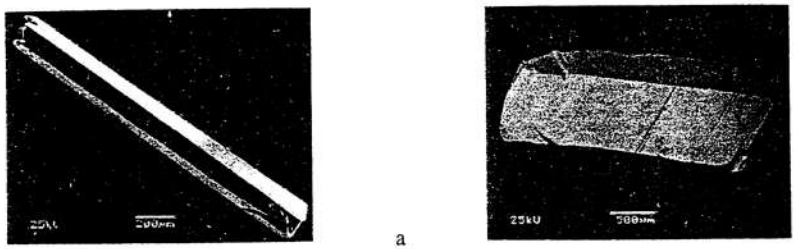

a b

Fig.1 Crystals of low (a) and high (b) NAB

$NdAl_{2.07}[B_4O_{10}]O_{0.9}$ and some molybdates, crystallize. An increase in initial crystallization temperature (up to 1037°C) leads to formation of an amount of small transparent violet NAB crystals strongly elongated along *c* axis (Fig 1a). Apparently, they formed jointly with molybdates $KNd(MoO_4)_2$ at the final stage of crystallizaton. Increase in borate concentration in starting fluxed melts up to 30 wt% results in crystallization of NAB high-temperature modification in the temperature range of 1037-700°C. Grown NAB crystals have characteristic growth striations (Fig 1b). The typical sizes of YAB:Sc (Ga) crystals in all runs were about 2-3 mm. Among subsidiary phases, only $Al_{18}B_4O_{33}$ were found.

SEM photographs show the splitting of trigonal prisms and this phenomenon is characteristic most of all grown crystals (Fig. 2a). In the case of YGaAB, splitting becomes stronger with an increase in Ga_2O_3/Al_2O_3 ratio in the initial mixture. Further growth of these splitted crystals often results in formation of twisted aggregates (Fig. 2b). Splitting is weakly developed only on faces of low-NAB crystals, if the Sc_2O_3 concentration does not exceeds 5 wt. % in initial fluxed melts Probably, huntite R32 structure becomes unstable in this case. However, X-ray pattern of the splitted crystals is similar to those for huntite type of structure. This morphological feature should be studied in detail, depending on dopant type and growth conditions to understand the nature of this splitting.

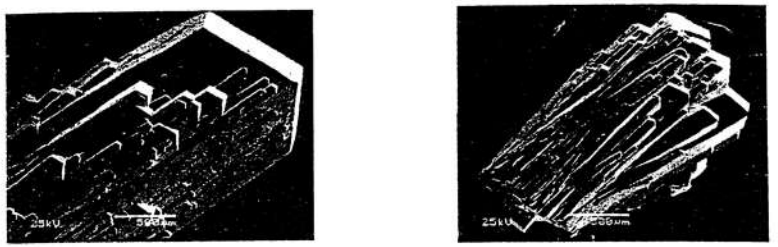

a b

Fig. 2. Splitting of trigonal prism faces of YGaAB crystals (a); twisted YGaAB crystal (b)

From ASEM data, it was found that the average Ga distribution coefficients in YGaAB crystals slightly rises from 0.84 to 0.98 with increase of Ga concentration in the initial borates from 5 to 15 at % (from Al^{3+} site). Further increase in starting Ga concentration up to 20 and 40 at% leads to sharply decreasing distribution coefficient to 0.68 and 0.32 respectively. Apparently, limit for aluminium substitution by gallium in YAB crystals is close to 15% of Al^{3+} site. In contrast to that, no scandium found neither in YAB nor in NAB crystals. This fact may probably be caused by high Sc_2O_3 solubility in B_2O_3-$K_2Mo_3O_{10}$ fluxes. Hence following to the Ruff rule it will be accumulate in the residual melt.

Comparative crystallochemical and morphological analysis Nd-metaborate $NdAl_{2.07}[B_4O_{10}]O_{0.9}$ [8] with mineral peprossiite with ideal formula $(Ce,La)Al_2B_3O_9$ [9] was showed practically identity of these compositions. Differences in their genetic data has allowed to suppose at least a polygenetic nature of this mineral.

The research described in this publication was supported, in part, by RFBR grant № 04-05-64709 and grants of Russian President for young scientists № MK-229.2003.05 and MK-1430.2003.05.

References

1. N.I. Leonyuk, Prog. Crystal Growth and Charact. 31 (1995), p. 279.
2. H. Jiang et al. J. Crystal Growth 233 (2001) p. 248.
3. V.B.Rybakov et al. Russian Journal of Inorganic Chemistry 42 (1997) 1453.
4. D.Yu.Puscharovskyi et al. Sov. Phys. Dokl. 23 (1978) 814
5. Della Ventura et al. Eur. J. of Mineral 5 (1993) 53

OPTICAL AND RAMAN SPECTRA OF SINGLE-WALL CARBON NANOTUBES

A.G. Ryabenko[1*], T. N. Moroz[2], V.G. Kostrovsky[3], A.V.Krestinin[1], G.I. Zvereva[1]

[1]Institute of Problems of Chemical Physics RAS, 132432 Chernogolovka, Moscow Region. Russia: E-Mail: aryabenk@icp.ac.ru

[2]United Institute of Geology, Geophysics and Mineralogy, 630090 Novosibirsk . Russia: E-mail: moroz@uiggm.nsc.ru

[3] Institute of Solid State Chemistry and Mechanochemistry, *Novosibirsk*, Russia: E-Mail: kostrovsky@solid.nsc.ru

Abstract A comparative spectroscopic analysis of single-wall carbon nanotubes (SWNT) samples with different diameter distribution by using UV-Vis-NIR optical absorption and Raman scattering is presented. The samples with different diameter distribution of SWNTs were produced by arc discharge with Ni, Co, Ni/Y and Ni/Gd catalysts. It was found that all UV-Vis-NIR spectra of water surfactant dispersions of solitary SWNTs have the similar shape, which are produced by almost the same diameter set of SWNTs, but they have different distribution. Comparison of Raman spectra of solitary SWNTs solution and solid samples shows that RBM peaks have the same position, but different relative intensity. Shifting of absorption bands occurs due to agglomeration leads to changing of Raman resonance conditions. Values of absorption peaks and Raman shifts of RBM modes for Ni/Y, Co and Ni/Gd catalyst samples differ strongly from those predicted by R. Weisman and S. Bachilo (Appl. Phys. A 78 (2004) 1111).

Comparison of the absorption spectra of different samples shows correlations between the peaks, which belong to v2->c2 and v1->c1 transitions of the same semiconducting nanotubes.

Single-wall carbon nanotubes (SWNT) are an important class of material for the development of novel electronic and optical devices. Recent advances in the spectral assignments [1-4] can give researchers new tools to understanding of SWNT electronic structure. In this report, we describe comparative spectroscopic studies of SWNT samples with different diameter distribution, which were purified by successive centrifuging [5], on the last stage at 200000g. Spectra of these samples are shown on Fig. 1. Purity of samples produced by Co, Ni/Y and Ni/Gd catalysts was 95-98%, and by Ni catalysts it was 30% due to low abundance in a raw soot (< 0,1%). All absorbance spectra (Fig.1a) are normalized to equal absorbance at 941 nm (in particular spectrum 4 multiplied by 2,3). The normalization results in spectra overlapping at 1658 nm. It means that absorption at 941 and 1658 nm caused by the same nanotubes. The similar overlapping takes place at 646 nm, and that is surprising because the absorption at 646 nm is caused by metallic nanotubes, and at 941 nm by semiconducting ones. 5 semiconducting nanotubes and 5 metallic ones are clearly seen (814, 873, 941, 1010, 1064 nm and 553, 601, 646, 693, 730 nm). The correspondence of

absorbencies at 941 and 1658 means that it is caused by nanotube (11,9) in accordance with [3]. As absorption at 646 nm corresponds with Raman shift at 195 cm^{-1}, it is caused by nanotube (9,9) [2]. Therefore, the beginning of growth of (9,9) and (11,9) nanotubes is somehow connected.

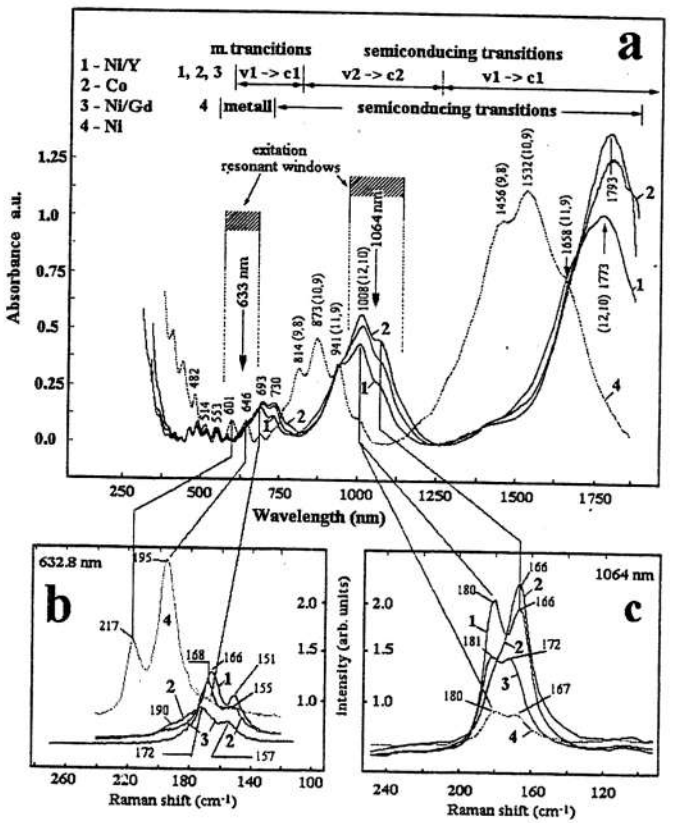

Fig. 1. Absorption spectra and Raman spectra of nanotubes produced by Ni/Y (1), Co (2), Ni/Gd (3), and Ni (4) catalysts (1a), Raman spectra at 633 nm (1b) and 1064 nm (1c) excitation.

The Stokes and anti-Stokes resonant NIR FT-Raman spectra of the SWNT and the first and second-order (Fig. 2b) for the SWNT bundles with known absorption spectrum are shown on Fig. 2a and 2b, responsible. Unpolarized Raman spectra were obtained in a back-scattering

geometry using Bruker FT-Raman RFS 100/S spectrometer with the Nd:YAG laser excitation 1064 nm lines.

An analysis the first and second-order, the Stokes and anti-Stokes resonant NIR FT-Raman spectra of these SWNT bundles (solid and mixed with KBr powder) and nanotubes dispersed in D_2O solution and their relationship with a fluorescence background in 1200 -1800 nm region are presented and discussed.

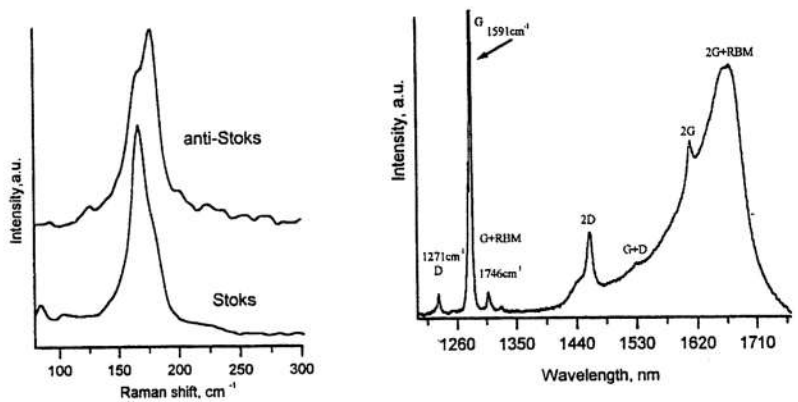

Fig. 2. A: Observed Raman spectrum of the Stoks and anti-Stoks RBM powder sample 1. B: First- and second- order Raman spectra of sample 1 for 1.17 ev (1064 nm) superimposed by the fluorescence background.

Acknowledgements: The authors are indebted to Dr S. Bukalov, the head of the Raman Center, Moskwa, Russia, for obtaining Raman spectra at 633 nm excitation. This work was supported by Russian Foundation of Basic Research, Grant No. 03-03-96404-r2003, Grant No. 04-03-97200r and the Siberian Branch of RAS project No. 6.4.1.

References

1. S M. Bachilo, M S.Strano, C Kittrell, R H.Hauge, R E.Smalley, R.B Weisman Science **298** (2002) 2361-2366.

2. MS Strano, SK Doorn, EH Haroz, C Kittrell, RH Hauge, RE Smalley NANO LETTERS **3**: (8) (2003) 1091-1096.

3. R.B. Weisman S.M. Bachilo D. Tsyboulski. Appl. Phys. A 78, 1111–1116 (2004)

4. S.Lebedkin, K.Arnold, F.Hennrich, R. Krupke, B.Renker and M.M.Kappes New Journal of Physics **5** (2003) 140.1–140.11.

5. A.G. Ryabenko, T.V. Dorofeeva, G.I. Zvereva Carbon, 42 in press.

THE GROWTH OF LARGE SINGLE CRYSTALS WITH THE GARNET AND PEROVSKITE STRUCTURES FOR LASERS.

L.I.Kazakova, S.A.Smirnova

VNIISIMS,Alexandrov, Vladimir reg., 601650, Russia

$Y_3Al_5O_{12}$:Er , $YAlO_3$:Er (till 50% at.) and $Y_3Al_5O_{12}$:Er,Ho,Tm , $YAlO_3$:Er,Ho,Tm single crystals are promising materials for the lasers in 2-3 μm region. All the crystals have been grown in vacuum from the melt by the horizontal directed crystallization techniques at rates 2-4 mm\h, using oriented in [111] direction seeds. Thermal conditions in the growing chamber varied by changing the position of the reflecting screens to the heater during the seeding and the growth processes. All these measures provided the decrease of temperature gradients on the interface and its changing from angular to perpendicular to the growth axes. Optical polarization and X-ray methods have been used to study the quality of the crystals: growth striations, twins, inclusions of foreign phases and the unit sell parameters.

The best quality garnets have been obtained at low crystallization rates, but perovskite crystals need sufficient superheating of the melt during the seeding and the growth processes. Obtained crystals had a plane shape up to 80×160×20 mm in size.

Optically transparent single crystals with low oscillation threshold and high enough energy output had been grown. For instance, in $Y_3Al_5O_{12}$:Er laser rods the threshold was reduced to 25 J with the increase of the generation efficiency up to 0,6%. The efficiency of the lasers, doped by holmium, depended on the active ion concentration and the quantities of the co-active ions.

INVESTIGATION OF PHASE EQUILIBRIA IN THE CaF_2-BaF_2 SYSTEM

P.P. Fedorov, I.I. Buchinskaya, N.A. Ivanovskaya, S.V. Isaev, B.P.Sobolev

Institute of Crystallography, Russian Academy of Sciences, Moscow 199333

< ppf@newmail.ru>

Alkali-earth elements fluorides solid solutions are interesting as optical materials. Literary data on CaF_2-BaF_2 system are conflicting, reported versions of phase diagrams break the phase rule sometimes.

We studied phase equilibria in this system by differential-thermal (DTA) and X-ray powder diffraction analysis. We used optical single crystals as starting materials. DTA experiments were carried out in special setup designed in Institute of Crystallography RAS. Vacuum furnace with graphite resistant heater and system of molybdenum radiation shield was supplied by special feeder to change the analyzed compound composition without explosion conditions (helium atmosphere, graphite and molybdenum crucibles) withdrawal. W/Re thermocouples were used.

Solid solutions based on the components form in the system. The solubility maximums of BaF_2 in CaF_2 is 8 mol. % and CaF_2 in BaF_2 – about 60 mol. %. Probably, the minimum exists on $Ba_{1-x}Ca_xF_2$ solid solution melting curves at x = 0.5. The peritectic triple-phase equilibrium is to be found. Solid solution $Ba_{1-x}Ca_xF_2$ decomposes according to eutectoid phase reaction at temperature decreasing.

The solid solutions single crystals in the system should be grown up by melt crystallization just for limiting (some percents) concentrations of CaF_2 in BaF_2 and BaF_2 in CaF_2.

This investigation was maintained by Russian Foundation of Fundamental Research, grant # 04-03-32836.

Top-seeded solution growth of non-linear LiB_3O_5 crystals with a pulling

A.E. Kokh, N.G. Kononova

Branch of the Institute of Mineralogy and Petrography

43, Russkaya str., 630058, Novosibirsk, Russia

kokh@mail.ru

Last years the significant progress was achieved at crystals growth of lithium triborate (LiB_3O_5 or LBO) from the Li_2O-B_2O_3-MoO_3 ternary system [1]. The crystals are characterized by improved optical quality in comparison with that grown from more viscous system with B_2O_3 excess. The unique physical and nonlinear-optical properties of LBO crystals foretoken its use in broad-aperture laser systems in the near future. For this purpose it is necessary to increase the size of grown crystals with preservation of its high optical quality.

The technique for LBO crystal growth described in [1] requires the crystal cross size to be less than 0.95 of crucible diameter. Hence the crystal height can reach no more than 0.5-0.6 of crystal cross size (Fig.1a). We use the precision heating furnace for LBO crystal growth with a pulling [2]. It allows to create high-symmetry heat fields. The crystal growth was carried out on a seed oriented along the [001] crystallographic axis from the 80 mm in diameter Pt-crucible. The equilibrium temperature was defined by repeated touches of the melt-solution surface by the seed. The contact was fixed by an electrical signal. In that way the decreased height of the seed can be determined. The decrease of the seed height was followed by lowering of the melt-solution temperature. After definition of a equilibrium point crystal growth was carried out at a cooling rate 0.5-1.0 C/day and with the 0.5 mm/day pulling velocity.

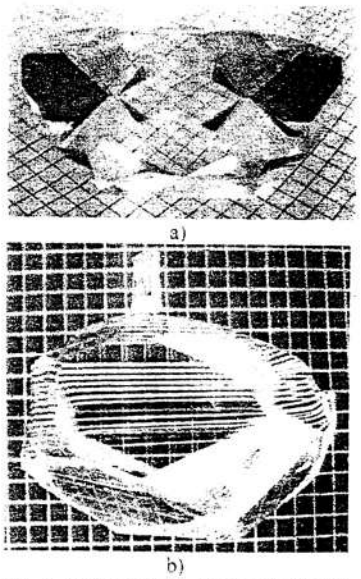

Fig. 1. LBO crystals, grown without (a) and with a pulling (b) from the crucible of 80 mm in diameter. Cells size is 5x5 mm^2.

As a result the high-quality LBO crystals were grown with height reached 0.8-0.9 of its cross size (Fig.1b). Such crystal size allows to make non-linear optical elements of various orientation up to 30 30 (20 30) [3].

References:

1. N.A. Pylneva, N.G. Kononova, A.M. Yurkin et al., J. Crystal Growth 198-199 (1999) 546.
2. A.E. Kokh, V.E. Kokh, V.A. Gets, and N.G. Kononova, Instr. Exp. Tech. 41(4) (1998) 587.

SOLVOTHERMAL SYNTHESIS OF NANOCRYSTALLINE ALUMINUM NITRIDE

A.I. Motchanyy, A.A. Reu, P.P. Chvanski, V.S. Kovalenko, V.G. Balakirev
All-Russian Research Institute for Synthesis of Minerals (VNIISIMS).
1 Institutskaya St., 601650 Alexandrov, Vladimir Distr., Russia

III-Nitride (GaN, AlN and other compounds) have attracted vast interest due to their unique properties and potential applications in optoelectronic devices operating in the blue and UV spectral regions and for the construction of electronic devices capable of operating under high power and high temperature conditions [1-3].

In the paper, we report on the synthesis of nanocrystalline AlN in supercritical ammonia at low temperature by ammonothermal method (AMMONO method), which utilizes ammonia as fluid rather than water as in the hydrothermal process.

Nanocrystalline AlN powder were obtained by AMMONO method, in which nitridization of Al metal occurs in highly chemical active supercritical ammonia and recrystallization of AlN powder in NH_3 using both NH_4X (X=Cl, I) as mineralizers. Mineralizers were added to the autoclave in order to accelerate the chemical reactions rate by increasing the amount of anions in the supercritical NH_3 solution. The experiment were performed in the temperature range of 350-550 °C and pressure of 80–120 MPa in stainless steel autoclaves for up to 5 days. Nanocrystalline AlN were spontaneously nucleated on the lower walls of the autoclaves. The obtained AlN powder was characterized by X-ray diffraction. The morphology and size of the nanocrystalline aluminum nitride was observed using both optical microscopy and scanning electron microscopy (SEM). Nanocrystalline AlN powders with average crystallite size 20-30 nm were produced in the temperature range of 450-550 °C. The preliminary results of the lattice parameter gave a = 3,1114 (2) Å and c = 4,9792 (4) Å. Details of characterization of the AlN are also presented.

References

[1]. S.J. Pearton, R.J. Shul, F. Pen, MRS Internet J. Nitride Semicond. Res. 5 (2000) 11.

[2]. S. Nakamura, Science 281 (1998) 956.

[3]. H. Morkoc, Nitride Semiconductors and Devices, (Springer, New York, 1999).

ReALO$_3$:CE (RE=Y, LU) SCINTILLATION CRYSTALS AND THEIR APPLICATION IN RESEARCH AND INDUSTRY.

A.Fedorov[1], A.Annenkov[2], M.Korzhik[1], V.Ligoun[2], O.Missevitch[1], S.A.Smirnova[3]
1- Institute for Nuclear Problems, 11 Bobruiskaya, 220050, Minsk, Belarus
2- Bogoroditsk Technical Chemical Plant, Tula region, Bogoroditsk-4, Russia
3-VNIISIMS, 1 Institutskaya, 601650, Alexandrov, Vladimir Region, Russia

$REAlO_3:Ce^{3+}$ (RE=Y, Lu) scintillation crystals have impressive prospects for wide application in many branches and are now being actively investigated. Here we report the scintillation properties of crystals with perovskite structure which mass production technology have been developed by us last decade. $YAlO_3$:Ce scintillation material now is widely used for detecting of soft γ- and X-rays. New $(Lu_{0.5}$-$Y_{0.5})AlO_3$:Ce and $(Lu_{0.7}$-$Y_{0.3})AlO_3$:Ce scintillation crystal properties obtained to date have been discussed. The former possesses density of 6.5 g/cm^3, 370 nm luminescence band maximum, light yield of 35-38% to NaI(Tl) and scintillation decay times of 23(50%), 70(25%), and 500(25%) ns, the latter with density of 7.2g/cm^3 shows the luminescence band maximum at 375 nm, light yield of 40% to NaI(Tl) and scintillation decay times of 20 (50%), 80(25%) and 400(25%) ns. The scintillation properties and crystals application in medical imaging technique, well logging and specialized detecting systems have been discussed.

LARGE SCALE PRODUCTION OF PWO SCINTILLATION ELEMENTS

A. Annenkov[1], M. Korzhik[2], V.Kostylev[1], O.Kovalev[1], V.Ligoun[1], O. Missevitch[2], A.Dossovitski[3]

1 - Bogoroditsk Techno Chemical Plant, Tula region, Russia

2 -Institute for Nuclear Problems, Minsk, Belarus

3 – NeoChem, Moscow, Russia

The design and construction of new experiments to be installed in accelerator facilities with high luminosity similar to the Large Hadron Collider, LHC at CERN require a scintillation materials able to maintain a high stability of their parameters under long-term exposure to ionizing radiation. The lead tungstate $PbWO_4$ (PWO) scintillator is a material which allows to perform precise electromagnetic calorimetry in irradiation environment. Currently, PWO scintillation crystal is used to build the Electromagnetic CALorimeter (ECAL) of CMS and the Photon Detector of ALICE experiments at CERN. The crystal production technology has been transformed from the production of a few samples to the mass production of more than one thousand of certified scintillation elements per month within last five years. Bogoroditsk Technical Chemical Plant from Russia carries out the crystal mass production for CMS and ALICE experiments at CERN. Lead tungstate crystals are produced with high yield by Czochralski method using standard equipment of "Crystal 3M" or "Lazurit". Crystals, are grown from specified raw material. An additional pre-crystallization to grow high quality and hard to ionizing radiation crystals is required. Ingots of 250 mm length and cross section close to ellipse from 36 to 86 mm long axis are available. Pulling rate and rotation speed at the crystal growth can be varied in wide range depending on required ingot diameter. Crystal ingots are annealed in atmosphere in non-gradient industrial ovens to minimize radial and axial stresses of ingots before mechanical treatment. At present, mass produced crystal scintillation properties satisfy the LHC experiments requirements. The current level of technology of PWO crystals allows bright, rather fast, optically clear scintillation elements to be produced with good radiation hardness. Here we report a peculiarities of the crystal mass production and further improvement of the crystal scintillation properties.

PRODUCTION OF SPECIFIED RAW MATERIAL TO GROW RADIATION HARD SCINTILLATION SINGLE CRYSTALS.

A.E.Dossovitski[1], A.L. Mikhlin[1], A.A.Annenkov[2], M.V.Korzhik[3]

[1]-JSC "NeoChem", Profsojznaja str., 115-2-331, Moscow, 117647, Russia

[2]-Bogoroditsk Techno Chemical Plant, Tula region, Bogoroditsk-4, Russia

[3]-Institute for Nuclear Problems, 11 Bobruiskaya str., Minsk 220050, Belarus

The design and construction of new generation of medical imaging technique and detectors for high energy physics and particle experiments to be installed at high luminosity accelerators require a scintillation materials able to maintain a high stability of their parameters under long-term exposure to ionizing radiation. It creates a set of the requirements to raw material to be used for the production of radiation hard scintillation single crystals. Here we discuss our experience to produce stochiometric compounds $PbWO_4$, $CdWO_4$, $CaWO_4$ with specified parameters. The specification for the raw materials to produce high quality perfect single crystals also has been discussed.

CHARGE-TRANSFER LUMINESCENCE OF YTTERBIUM-DOPED SESQUIOXIDES

Krasikov Dmitry Nikolaevich

Guerassimova N. V., Kamenskikh I. A., Mikhailin V. V.

Synchrotron radiation laboratory, Physics Department,

M. V. Lomonosov Moscow State University

kdn@hotbox.ru

Ytterbium-doped sesquioxides of yttrium, scandium and lutetium are promising laser materials. One of typical features of these crystals is the IR luminescence caused by radiative f-f transitions in the Yb^{3+} ions. Such luminescence is characterized by radiative lifetime of the order of milliseconds. Recently ytterbium-doped materials became the object of investigation because of the charge-transfer luminescence (CTL). CTL is characterized by lifetime of few to tens nanoseconds and can be used in fast scintillators.

The luminescence spectra of sesquioxides in the spectral range from 1.1 to 5 eV, CTL excitation spectra and CTL decay curves under synchrotron UV- and VUV-radiation excitation has been measured. The measurements were carried out at the SUPERLUMI station of HASYLAB at DESY, Hamburg. The single crystals Lu_2O_3 – Yb 2%, Y_2O_3 – Yb 3%, Sc_2O_3 – Yb 0.7% were grown in the Institute of Laser-Physics (University of Hamburg) by the Heat-Exchanger-Method derived from the Bridgman method.

The CTL bands of ytterbium-doped sesquioxides due to the radiative transitions from the charge-transfer state (the state formed by the hole transition from the Yb^{3+} ions to the oxygen ligands) to the ytterbium levels $^2F_{5/2}$ and $^2F_{7/2}$ are observed in the spectral range 1.8 - 4.5 eV. Measurements with different time windows show that there are two luminescent components, which differ by kinetics and spectral location of the CT bands in the spectra of luminescence as well as excitation of luminescence. It is known that rare-earth ions in the sesquioxide crystal lattice occupy two sites with different symmetry types C_2 and C_{3i}. Therefore it was concluded that ytterbium in the two crystallographic sites forms effective centers of CTL. The measurements of f-f luminescence under excitation to the CT absorption band were used to identify the CTL components.

PHYSICAL BACKGROUND OF INDUSTRIAL TECHNOLOGY OF GROWING LEAD TUNGSTATE (PWO) FOR HIGH-ENERGY PHYSICS APPLICATIONS

S. Burachas[a,b], S. Beloglovsky[a], Yu. Saveliev[a], M. Ippolitov[b], V. Manko[b], A. Vasiliev[b], G. Tamulaitis[c], A. Apanasenko[d]

[a]«North Crystals» Company, Apatity, Murmansk Region, Russia

[b]RRC «Kurchatov Institute», Moscow, Russia

[c]IMSAR, Vilnius University, Vilnius, Lithuania

[d]Kharkov University, Kharkov, Ukraine

We report on development of technology for growth of lead tungstate (PWO) crystals on industrial scale for CERN projects ALICE and CMS, which is based on revealing the origins of the PWO basic properties important for application of this material as scintillator in high-energy physics experiments. It is generally believed that an ideal PWO monocrystal does not absorb in UV region, is insensitive to thermal treatment, and does not gain color under irradiation. The whole variety of dynamical properties is determined rather by "weak spots" in the ideal crystal. In crystals grown from high-purity recrystallized row materials, the "weak spots" develop by formation of molecular clusters, the composition of which depends on specific growth conditions and doping of the PWO crystals. Our study shows that the undoped PWO crystals contain clusters of tungsten oxides with variable valency WO_{3-x} ($0< x <1$). Thus, these inclusions determine the color of PWO crystals in correspondence to the color of the oxides WO_3 (yellow), $WO_{2.96}$ (green), $WO_{2.8\text{-}2.88}$ (blue), $WO_{2.7\text{-}2.75}$ (violet), and WO_2 (brown). In the processes of growth, annealing, and irradiation the clusters WO_{3-x} easily change their valency and, consequently, the properties of the whole crystal. The clusters also enhance the absorption in UV region. Doping of PWO by oxides L_2O_3 (L = Y, La, Gd etc.) results in formation of clusters with composition $W_{1-y}L_yO_{3-x}$ ($0< x <0.3$), where oxygen is bound stronger than in WO_{3-x}. These clusters increase transparency in UV region. Doping of the melt with CdO, MoO, and similar oxides causes formation of inclusions of $CdWO_4$, $PbMoO_4$ etc. resulting in the green component of PWO radioluminescence. In a pure PWO crystal, the green component may be observed only from the surface layer, where certain structural defects responsible for this emission can be formed under appropriate conditions.

The conclusions of the study are substantiated by their application in the PWO growth and annealing technology on industrial scale at the company "*North Crystals*", where PWO crystals with optical and scintillation properties meeting specifications of CERN for the projects ALICE and CMS are produced with the yield of 100%.

SPECTROMETRY OF FAST NEUTRONS BY MEANS OF NEW INORGANIC LBO-GLASS SCINTILLATORS

Zadneprovski B.I.[1], Eremin N.V.[2], Arkhipov M.A.[1], Paskhalov A.A.[2], Shakhovsky V.V.[3], Klimov S.V.[4], Pomazan Yu.V.[4]

[1]All-Russian Research Institute for the Synthesis of Materials (VNIISIMS), Alexandrov
[2]Skobeltsyn Institute of Nuclear Physics (NIIYAF MSU), Moscow
[3]Central Physical-Technical Institute (ZFTI), Sergiev Posad
[4]Applied Problems Section at Presidium of Russian Academy of Science (SPP RAN), Moscow

At the present time the increasing interest to search of new inorganic scintillators for fast neutron spectroscopy is observed. It is stipulated by new problems of a high-energy particles physics, dosimetry, space investigations, military aspects of neutron sources inspection and so on. The series of crystalline materials adequate in a different degree to new requirements was offered by the various authors [1]. For example the crystals of lithium tetraborate ($Li_2B_4O_7$) doped by some activator additions are one of such offered recently materials [2]. However the obtaining of large defectless $Li_2B_4O_7$ crystals has essential technological difficulties. At the same time it is well known, that in the system of oxides Li_2O-B_2O_3 there is a wide area of formation of transparent glasses. The glasslike state of material provides the flexible possibilities of scintillation parameters increase with the help of optimization of material composition. At that the main mechanism of neutrons registration by means of LBO-glasslike scintillator is the same as by $Li_2B_4O_7$ crystals. It is the reactions of (n,α)-type on nucleuses of ^{6,7}Li and ^{10,11}B and also the different processes of neutrons scattering. These all interactions are accompanied by ionization of the medium with carry of energy to activation centers of its highlighting.

For experimental check of the indicated assumptions we have synthesized the glasses of Li_2O-n·B_2O_3 composition (pure and doped by Cu, Ni, Tl, Ce, Eu, Tb, Yb and some other active additions) (fig. 1).

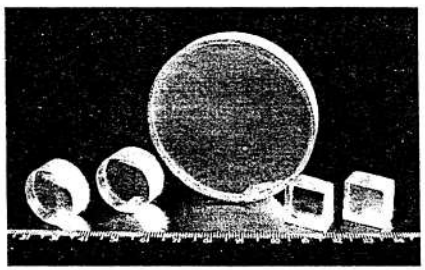

Fig.1 The LBO-glass scintillation elements.

Density of the obtained LBO-glasses is 2.28 g/cm^3. Refractive index is 1.54. The area of optical transparency starts from 280-290 nm. The wavelength of a luminescence maximum of doped LBO-glasses varies from violet up to red area of a spectrum depending on a type of activator (from 375 nm for Cu^{1+} to 615 nm for Eu^{3+}).

The sources of neutrons Pu(Be) and of gamma-irradiation ^{60}Co were applied by us at the testing of the LBO-glasses scintillation properties. It was used two types of photoreceivers – AVP-150 photomultiplier (maximum of sensitivity 380-480 nm) and Si-pin-diodes "Hamamatsu S 3204-05" (maximum of sensitivity 600-1000 nm). For an estimate of neutrons registration efficiency we have entered the coefficient of gamma-radiation damping: $K_{damp} = \varepsilon_n / \varepsilon_\gamma$ (where ε_n – is the absolute coefficient of neutron detection from Pu(Be)-source, ε_γ – is the absolute coefficient of gamma-ray detection from ^{60}Co-source). The testing of obtained LBO-glasses with various dopants has shown, that the spectrum of gamma-radiation is present in low channels only, and it does not overlap a main region of a neutrons spectrum (see for example fig. 2). Thus the LBO-glasses provide complete separation of attendant gamma-radiation in region of the neutrons maximum spectrum. The damping coefficient depends from kind of activator and its value lays in the limits from one to two orders – for example for Cu^{1+} and Ce^{3+} K_{damp} = 25±15; Tl^{1+} 210±20; Tb^{3+} 215±14; Yb^{3+} 330±70. The traditional organic scintillators (anthracene, polystyrene and stilbene) have K_{damp} from 2 to 6. We measured the level of background neutron radiation with the help of LiBO-glass-detector directly without any additional discrimination of gamma-radiation by means of fast-slow light pulse components. The obtained value of background neutron flow was equal (1,5±0,2)·10^{-2} neutron/(cm^2·sec) at the time of measurements about 17.5 hours.

Also the measurements showed the decay time of pure glass has two components τ_1=1.5 ns, τ_2=0.34 μs and it varies to several microseconds depending on a type of activator. Therefore we hope that distinction between yields of fast and slow components will be useful for discrimination of different kinds of nuclear particles.

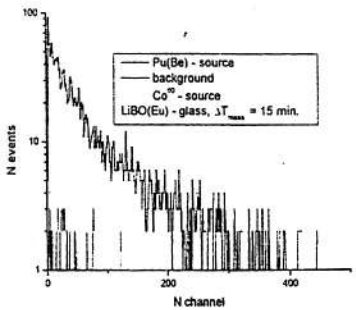

The obtained results demonstrate that the scintillators on the basis of LBO-

glasses can be perspective alternative for known gas, fluid, plastic and crystal detectors of neutrons. This material has high enough efficiency of neutrons registration and low sensitivity to other sorts of radiation. Doping by different activators allows to vary over a wide range both kinetics of light emission and wavelength of emission depending on a type of used photodetector. The LBO-glasses can be produced of big volume that is important for creation of large-sized detectors of neutrons.

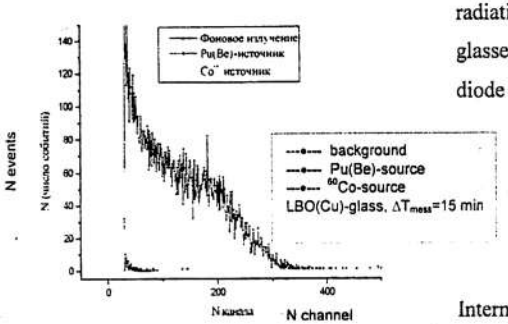

Fig. 2. The energy spectrums of different radiation sources detected by means of LBO-glasses and photomultiplier (a) and Si-pin-diode (b).

References

1. C.W.E. van Eijk. Proc. of the 5-th Intern. Conf. on Inorganic Scintillators and their Application, SCINT'99. Moscow. MSU. 2000. P. 22-32.

2. N. Senguttuvan, M. Ishii, M. Shimoyama et al. Nucl. Instr. and Meth. in Phys. Res. A 486 (2002) P. 264-267.

NON-STOICHIOMETRY DEFECTS AND RADIATION HARDNESS OF $PbWO_4$ AND $NaBi(WO_4)_2$ CRYSTALS

Zadneprovski B.I.[1], Nefedov V.A.[1], Polyansky E.V.[1], Devitsin E.G.[2], Kozlov V.A.[2], Potashov S.Y.[2], Terkulov A.R.[2]

[1]All-Russian Research Institute for the Synthesis of Materials (VNIISIMS), Alexandrov

[2]Lebedev Physical Institute of Russian Academy of Sciences, Moscow

It has been stated many times that the formation of radiation infringements in annealing $PbWO_4$ (PWO) and $NaBi(WO_4)_2$ (NBW) crystals is a big extent stipulated by the non-stoichiometry defects of the crystalline matrix, arising in the process of their growth and annealing. To refine the idea of characteristics of the non-stoichiometry defects and their effect on the radiation hardness of PWO and NBW, the current study is aimed at the melt composition infringements during growth of crystals, influence of annealing atmosphere and at optical transmission of crystals obtained in these conditions after their irradiation. On the basis of the experimental data on melt evaporation while growing PWO and NBW crystals, the formation of non-stochiometry and most probable types of dot defects of the crystals have been considered. Also NBW crystals were grown from non-stoichiometric melt containing surplus of WO_3 or lack of Bi_2O_3. The crystals were irradiated from sources of ^{137}Cs (PWO) and ^{60}Co (NBW) with the dose rate of 2.6-3.0 Gy/h. In the optical transmission measurements along with traditional techniques a method "in situ" was used for the PWO crystals, which provided the measurements in fixed points of the spectrum (380, 470 and 535 nm) directly in the process of the irradiation.

The obtained results demonstrate, that the radiation degradation of PWO and recovery after irradiation have complex character. Fitting of experimental curves points to formation not less than three types of radiation-induced absorption centers in unannealed PWO crystals. According to this the kinetics of induced absorption increasing has three components: fast (τ_f = 0.19-0.72 hour) , middle (τ_m = 2.0-9.7 hours) and slow (τ_s = 33-56 hours). The annealing of PWO in argon medium eliminates fast and middle components of a degradation and increases radiation hardness. It is supposed, that the fast degradation is defined by absorption centers forming on the initial non-stoichiometry defects of a crystalline matrix, the slow one occurs through centers on new radiation defects.

The annealing of NBW crystals influences feebly their optical transmission and their radiation hardness as against PWO crystals. The irradiation induces in NBW a wide absorption band with a maximum in the region of 400-430 нм. The creation in the initial melt of WO_3-surplus increases the radiation hardness of crystals, at that the intensity of a band 400-430 нм is reduced three times. The lack of Bi_2O_3 decreases radiation hardness of NBW. It is supposed that defects determining the radiation-induced absorption are the initial growth defects in (NaBi)-sublattice of crystals.

LUMINESCENCE OF THE TUNGSTATE CRYSTALS CONTAINING DIVALENT IONS

Blistanov A.A.[1], Zadneprovski B.I.[2], Ivanov M.A.[1], Kochurikhin V.V.[1], Petrakov V.S.[1], Yakimova I.O.[1]

[1]Moscow State Institute of Steel and Alloys (MISIS), Moscow

[2]All-Russian Research Institute for the Synthesis of Materials (VNIISIMS), Alexandrov

The interest to tungstate crystals of divalent metals $Me^{2+}WO_4$ (Me^{2+}=Mg, Ca, Zn, Sr, Cd, Ba, Pb) is defined by the practical problems of them application as phosphors and scintillators for registration of ionizing radiations and high energy particles. The representatives of this materials have high density, transparency for own luminescence, some of them have high quantum yield of luminescence and short decay time. In this connection the further refinement of representations about types of luminescence centers in tungstates and of the mechanism of their excitation and relaxation, and also about a role of crystalline matrix ions and of structure defects in creation of optical centers is a high-priority task. The solution of these problems is necessary for the optimization of emission properties by that this crystals possess.

The numerous previous researches of the tungstate crystals testify to existence of two main spectral areas of their luminescence, namely of short-wave band (blue) in the field of 390–420 nm and of one or two long wavelength bands (green) in the region of 480–520 nm. However the causal relationship of these features of a luminescence remains not clear as with the type of divalent matrix cations (Me^{2+}), and with influence of oxygen vacancies at creation of luminescence centers in $MeWO_4$. The further improvement of this connection is the task of a present paper.

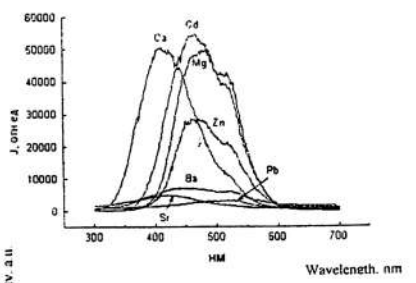

Fig. The luminescence spectrums of tungstate crystals

The spectrums of the luminescence were measured for the indicated tungstate crystals in identical conditions at X-ray excitation. All samples have the maximum of long-wave luminescence in the field of 510–520 nm (fig.). The position of this band does not depend on a type of divalent cation. However wavelength of maximum corresponding to

short-wave luminescence (λ_{blue}) differs for various cations Me^{2+}. The value of λ_{blue} changes from 400 nm for Ca- up to 480 nm for Mg-cations (fig.).

The correlation of λ_{blue} maximum with melting point of crystals and with a position of Me^{2+} cations in subgroups of the elements periodic system was determined. This fact is evidence about connection of blue luminescence with energy of a crystal lattice and with properties of divalent cations, in particular, with their bonding energy in $MeWO_4$ crystals.

$PbWO_4$ and $CaWO_4$ crystals were irradiated with electrons and annealed in vacuum for increase of oxygen vacancies concentration. However these influences have not changed a relation of peaks intensity corresponding to blue and green luminescence. It allows to presume, that the vacancies of oxygen do not promote formation of luminescence centers defining short-wave cr long-wave bands. The role of these vacancies as centers producing luminescence quenching is more probable. Thus, our experiments do not confirm the point of view about the conditionality of a green luminescence by presence of WO_3-groups having oxygen lack.

$AgGaS_2$ CRYSTAL GROWTH BY BRIDGMAN-STOCKBARGER TECHNIQUE UNDER ROTATING HEAT FIELD OF NONCYLINDRYCAL SYMMETRY

K.A. Kokh[a], B.G. Nenashev[b], A.E. Kokh[b]

[a]Novosibirsk State University, 2, Pirogov str., 630090, Novosibirsk, Russia

[b]Branch of the Institute of Mineralogy and Petrography, 43, Russkaya str., 630058, Novosibirsk, Russia

kostya@demakova.net

Crystals used in optical and semiconductor devices have to be of excellent quality, i.e. containing no cracks, inclusions, twins etc. The search of the ways how to improve these parameters is still a topical question for the most of compounds. In spite of discoveries of many IR materials with high figures of merit for nonlinear applications, $AgGaS_2$ (AGS) still has not lost its importance [1]. That compound was chosen for crystal growth experiments using HFRM (Heat Field Rotation Method) proposed by [2].

The growth was performed under rotating heat field with the L_1 symmetry, i.e. $rotL_1$. The rotation of heat field with the decreased symmetry in the short middle zone of the growth setup was produced by the partial switching on of the vertically aligned heaters placed around the lowering ampoule. One switched on/off heater creates overheated/overcooled zones which are situated on the opposite sides of the ampoule walls. Under certain conditions that may result in the formation of two types of axial temperature gradient in the melt, i.e. positive along the overheated wall and negative along the overcooled one. The positive gradient results in the formation of buoyant flow arising along the overheated wall, which in turn is likely to provide a single convective cell in the melt. Also the distortion of the heat field originates the primary direction of the convective flows along the maximum radial temperature gradient [3]. Then, the sequential switching off the adjacent heater and switching on the current one originates the rotation of the convective cell providing the better mixing of solidifying melt. It must be noted that the period between switching appears to be the main parameter governing the rate of distortion of the heat field symmetry.

In order to reach a maximum homogenization of the melt, the melted charge of synthesized $AgGaS_2$ was exposed to the heating procedure under large period between switching. Growth rate and axial temperature gradient at the melting point of $AgGaS_2$ was 5 mm/day and ~15°C/cm, respectively. The great dependence of the crystal quality on the

switching frequency and hence the amplitude of temperature oscillations was observed. Large periods of switching during growth process produced thermal stress in crystal resulting in the formation of many cracks. A high-quality crystal of conical shape 30 mm in diameter and 80 mm in length was obtained under the frequency of heat field rotation equal to 1/210 sec^{-1}. It confirms the supposition that periodic temperature oscillations of appropriate amplitude near the growth interface favors the convective regime in the melt improving the quality of grown crystal.

References

1. S. Haidar, K. Nakamura, E. Niwa, K. Masumoto, H. Ito, Appl. Optics 38(9) (1999) 1789.
2. A.E. Kokh, Thesis for a Doctor's Degree (Prochorov's Inst. of General Physics RAS, Moscow, 2003) 271 p.
3. A. Bachran, P. Reinshaus, W. Seifert, Cryst. Res. Technol. 33(1) (1998) 27.

CRYSTAL CHEMISTRY OF DICHALCOGENIDES

N.V. Podberezskaya, N.V. Pervukhina, S.A. Magarill, I.G. Vasilyeva, S.V.Borisov,

Nikolaev's Institute of Inorganic Chemistry SB RAS, Novosibirsk, Russia,

podberez@che.nsk.su

Dichalcogenides of stoichiometric composision and those with deficient chalcogen atoms have long ago become objects of active interest of researchers. This interest arises from their practically useful combinational of optical, magnetic, and semiconducter properties and also from their specific crystal structure determined by some structural fragments such as covalently bonded chalcogen atomic pairs and chalcogen ions [1–6].

The crystal structures of dichalcogenides MX_2 (M is metal, X = S, Se, Te) may separated into three basic groups with metals in 2+, 3+, and 4+ formal oxidation states and different X-X bond nature. The basic structure types of the first group, containing only covalently bonded chalcogen pairs, are pyrite and marcasite – cubic and orthorhombic modifications of FeS_2, respectively, with NaCl packing of the cations and $(X_2)^{2-}$dumbbell centers. The second group includes compounds of Ln or Ac as a metal and both X^{2-} and $(X_2)^{2-}$ ions with prototype structures of tetragonal matlockite, PbFCl. The third type contains the chalcogen X^{2-} alone and has the metal of group IV-VIII with formal oxidation state 4+. The basic structure types are hexagonal double-layer CdI_2, three-layer $CdCl_2$ and four-layer MoS_2. Symmetry, unit cell metrics and interatomic distances have been analyzed for all groups.

Analysing the pyrite type of structure we note that the metal atoms lie in the X–M–X octahedra formed by the X atoms of six $(X_2)^{2-}$ groups and having regular distances but distorted angles. The angular distortions are generally within ±5° of the ideal values. The environment of the X atom is a pyramidally distorted tetrahedron with the three M atoms at the base and one of the atoms of the $(X_2)^{2-}$ dumbbell at the apex. The formal degree of oxidation of the metal must be 2+, and the observed anomalies of physical properties must be associated with its variation. Then the symmetry may be lowed due to separation of the positions of metal atoms with different degrees of oxidation.

Many compounds have modification of orthorhombic FeS_2 belonging to the marcasite structural type. This is the second structural type among the the known structures of Group II, VII, and VIII dichalcogenides. The specific features of the packing of the $(X_2)^{2-}$

centres of chalcogenide pairs and metal ions may be described by the *I* lattice law, but the (X_2) pairs violate the *I* law, because at the center they have a different orientation. A packing following *F* lattice (neglecting the orientation of the $(X_2)^{2-}$ pairs and taking into account only their centres) may be derived in monoclinic pseudocell with the parameters 110/1-10/001 of the marcasite cell and with β equal to the angle between the diagonals of the (001) face. Doubling the cell along [001] leads to dimentions close to those in a pyrite type cell.

As a radius of Group II element increases along with the coordination number, the structural type of dichalcogenide changes. The structures of strontium and barium disulfides and barium diselenide and ditelluride are currently known. The tetragonal SrS_2 and $BaTe_2$ are $CuAl_2$ type structures isostructural to each other. The packing of cations and anions (the $(X_2)^{2-}$ dimer orientation ignored) generally follows *I* lattice law. BaS_2 and $BaSe_2$ belong to the family of ThC_2.

The covalently bonded pairs (X–X), X = S, Se, Te are absent in the structures of Group III – VIII metal dichalcogenides. Formal charge compensation in these compounds is due to the fact that the metals are in oxidation state 4+. Analysis of all data shows that distribution according to the structural type has clear maxima relative to the CdI_2, $CdCl_2$, and MoS_2 types and polytypes on their basis. In CdI_2 – type structures, the packing of the chalcogenide ions follows the two-layer hexagonal (or distorted hexagonal) motif of *AB* type. In $CdCl_2$ structures, the packing is three-layered, *ABC*. The octahedral voids are occupied by the metal ions. The molybdenite type of structure is a four-layered packing of the chalcogenide ions with the metal surrounded by a trigonal prism. In this group of compounds, the peculiarity lies in the fact that X^{2-} ...X^{2-} distances are shortened compared to the sum of ionic radii S^{2-}, Se^{2-}, Te^{2-}.

The last group are compounds in which the chalcogenide ions are in ionic and covalently bonded states, i.e., these are rare-earth and actinide dichalcogenides. The basic structural type in this group is tetragonal PbFCl (matlockite). The basic structure-forming units in them are layered packets ...$Ln^{3+} – X^{2-} – X^{2-} – Ln^{3+}$ ... in which the squares of metal and chalcogen ions are offset relative to one another by ½ of square diagonal and geometrically commensurate. The shortest $Ln^{3+} – Ln^{3+}$ and $X^{2-} – X^{2-}$ distances in the layers correspond to the square sides and approximate the sum of ionic radii of the corresponding elements. The packets alternate with the layers in which the covalently bonded pairs $(X_2)^{2-}$ also form squares, but these are now rotated through an angle of 45° relative to the

neighboring square layers of the packet. As a matter of fact, the energy factor is responsible for the rather rigid structure of the four-layered packet, and the geometrical factor dominates the combination of the packets and interpacket layers. The different orientational possibilities for $(X_2)^{2-}$ covalent pair in the layer create the structural diversity of compounds from this class belonging to the structural type PbFCl or anti-Cu_2Sb.

THE LIST OF LITERATURE

1. Podberezskaya, N.V., S.A. Magarill, N.V. Pervukhina, I.G. Vasilieva, S.V. Borisov, // J. Struct. Chem. V. 37, No. 6, p.p. 963 – 985, (1996). Translated from *Zhurnal Strukturnoi Khimii,* V.37, No. 6, p.p. 1140 –1170 (1996).

2. Podberezskaya, N.V., S.A. Magarill, N.V. Pervukhina, S.V. Borisov, // J. Struct. Chem. V. 42, No. 4, p.p. 654 – 681, (2001). Translated from *Zhurnal Strukturnoi Khimii,* V.42, No. 4, p.p. 783 – 917 (2001).

3. Mitcheil,K., R.C. Somers, F.Q. Huang, J.A. Ibers,. // J. Solid State Chem. V. 177, p.p. 709 – 713, (2004).

4. Borisov, S.V., N.V. Podberezskaya, N.V. Pervukhina, S.A.Magarill, // Z. Kristallogr., V. 213, p.p.253-258, (1998).

5. Vasilyeva I.G. // in: Hand Book on the Physics and Chemistry of Rare Earths, V. 32, Ch. 209, p.p. 567 – 609. *Ed. K.A. Gscheidner, Jr., L. Eyring and Y.H. Lander, 2001. Elsevier Science B.V.*

6. Kuznetsov, F.A., P. Klevtsov, S.V. Borisov, A Pavluk, Ya. Vasiliev, L. Kozeeva, A. Kamarzin, V. Sokolov, and I.G. Vasilyeva, I.G., // in: Proc. Int. Symp. on Laser and Nonlinear Optical Materials, Singapore, 1997, *ed. T. Sasaki* (Data Storage Institute, Singapore) p.p. 211 – 217

RESEARCH OF THE MORPHOLOGICAL INSTABILITY OF (111) Ge FACET AT HIGH LEVEL OF Sb DOPING.

Svetlana V. Bykova, Vladimir D. Golyshev, Michael A. Gonik, Vladimir B. Tsvetovsky

Centre for Thermophysical Researches "Thermo", Institutskay St. 1, 601650 Alexandrov, Russia E-mail: Bykova@thermo.vladimir.su ; phone/fax: (095) 584-58-16

Germanium with high impurity concentration is a perspective material for cells of solar batteries. Therefore, obtaining of perfect high quality single crystals with high impurity concentration is an actual problem. It is well known that a facet is morphologically more stable than an interface growing by the rough growth mechanism. Therefore, there is an opportunity to grow crystals with a higher impurity concentration due to the absence of a disturbance to the morphological stability.

The present work is dedicated to description of experimental research on morphological instability conditions in faceted growth of Ge, as well as to discussion of phenomena observed in experiment, which are involved into formation of faceting interface and morphological instability of a facet (111).

A crystal of germanium doped with Sb was grown by a method of the Axial Heat flux close to the Phase interface (AHP method) [1] on a seed in the direction [111]. The deviation from a plane (111) was no more than 1 minute. The AHP method allows to obtain a well-known weak AHP forced melt flow along the melt/crystal interface [2]. The necessity of generating such a weak flow is caused by the fact that the melt flow influences facet morphological instability if the velocity of melt flow is comparable to the rate of spreading of macrosteps [3].

The grown single crystal of Ge was cut into plates in the longitudinal direction. To visualize the melt-crystal interface and structure of a crystal, the Ge plate was etched by the method of anode etching. The experimental researches of lateral and longitudinal macroheterogeneity in the distribution of Sb were carried out with the spreading and four probe technique.

To find conditions of facet morphological instability a 1D numerical model together with experimental data were utilized to predict the facet dynamics and solute concentration features of the grown crystal.

On the basis of comparison between the facet-free interface shape without a facet and the interface shape with a facet, a dependence of singular facet (111) growth rate on supercooling has been found. Comparison of the melt flow velocities with the rate of spreading of

macrosteps has shown that these values are close to each other and that the morphological instability for this experiment is connected with the melt flow direction.

These researches were sponsored by INTAS (Project No. 99 – 01814), as well as NASA (Project # 98-HEDS-05092).

[1] V.D. Golyshev, M.A. Gonik // Cryst. Prop. Preparation. 1991. V. 36-38. P. 623.

[2] S.V. Bykova, I.V. Frjazinov, V.D. Golyshev, M.A. Gonik, M.P. Marchenko, V.B. Tsvetovsky, J. Crystal Growth. V. 237-239 (2002) 1886-1891.

[3] A.A. Chernov, Proceeding of NASA Microgravity Materials Science Conference held at Hantsville, Alabama, June 10-11 (1996), p.p. 57-60.

PRODUCTION AND PROPERTIES OF DIAMOND P-N - JUNCTION

V.I. Polakov[1] , A.I. Rukovishnikov[1], V.A.Laptev[2], A.V. Pomchalov[2], S. A. Martynov[2], E. V. Polyansky[2], Yu.N. Pal'yanov[3], Yu.M. Borzdov[3], V.P. Varnin[4],I.G. Teremetskaya[4]

[1] Institute of Radio Engineering & Electronics, RAS, 11 Mohovaya str, Moscow 103907, Russia.

[2] All-Russia Institute for the Synthesis of Minerals, Alexandrov, Vladimir region, Russia

[3] Institute of Mineralogy and Petrography, Siberian Branch of RAS, Novosibirsk, Russia, [4] Institute of Physical Chemistry, RAS, Moscow, Russia

Abstract

A novel electronic device using diamond p-n junction has been fabricated and studied. The electrical characteristics have been obtained and investigated at different temperatures and air conditions. The current-voltage (I-V) characteristics of diamond p-n junction exhibited good rectifying with rectification ratios greater than 106 at 5 V. The differential capacitance-voltage (C-V) and 1/C"2 characteristics of the space-charge region of the diamond p-n junction were typical for good p-n junction with uniform concentration of the uncompensated carriers in the better part of the space-charge (depletion) region. A strong sensitivity of the reverse current of the I-V characteristics to the presence of the water vapor was found. Deep level transient spectroscopy was used for study trapping centers in diamond p-n junction and obtained information about their density, activation energy and capture cross-section. An energy band model was proposed for explanation of the experimental results.

1. INTRODUCTION

For many years, diamond was considered to be very perspective for development of different electronic devices [1]. Based on the success of synthesizing diamond films by several methods [1-3] and controlling the concentration of doping atoms, such as boron, phosphorus or arsenic, which determine the conduction type of diamond films, the idea of fabricating diamond p-n junction with a good electrical characteristics can be realized.

In the past, there have been reports on electronic devices with p-n junction using both single-crystalline and polycrystalline diamond materials [3,4]. Diamond p and n-type films were doped by boron (B) and phosphorus (P), respectively, and were grown using single-crystalline diamond or nondiamond materials as the substrate.

In the present work, we study diamond p-n junction fabricated by growing homoepitaxial boron-doped CVD diamond film on the surface of synthetic semiconductor n-type diamond crystal. Semiconductor n-type arsenic-doped diamond single crystal was synthesized by high pressure high-temperature technique in a "split-sphere" type of apparatus (BARS). Diamond p-type film with

about 2 urn thickness was grown by hot-filament method using methane-acetone mixture as the feed-gas and trimethylborate as the boron atom source. The B-doped film had a monocrystalline structure and low surface roughness of down to 10 nm. Ohmic contacts to diamond were formed by depositing metal on heated crystal surface.

2. EXPERIMENTAL DETAILS

A newly developed computerized system for electrical measurements ASEC-3 was used for diamond p-n junction characterization. This system allows to obtain current-voltage (I-V), capacitance-voltage (C-V), 1/C"^{2}-V characteristics, and perform charge-based deep level transient spectroscopy - Q-DLTS [5,6]. C-V characteristics were obtained in the 10~^{3} - 250 kHz frequency range and, as I-V characteristics, at different temperatures and in the dark.

The measured value of the Q-DLTS signal by the ASEC-3 apparatus can be written as AQ = Q(t,) - Q(t_2), where t, and t_2 are the times from the beginning of discharge. The charge AQ flowing through the circuit during the time period, At = t_2 - t,, is measured as a function of parameters of the bias pulse, temperature, and rate window, x_m = (t_2 -tjVlnft-j/tj). If we keep the ratio t2/t, = oc constant (in our measurements a = 2) and vary t_m = t}(a - l)lna, the functional dependence AQ(i_m) has a maximum which can be used to determine the trapping center parameters. The maximum in AQ(t_m) occurs at the rate window equal to the emission rate of the traps, i.e. In o/(a - l)t, = e. Using our method, the emission rate of the traps can be found without recourse to temperature scanning, which takes considerable time. Furthermore, the trapping center concentration can be obtained from Q-DLTS spectra AQ(im) done under isothermal conditions (at room temperature) as Nt = 4 AQW/qA, where AQmax is the maximum value of the DLTS signal, q is the electron charge, and A is the contact area. Q-DLTS spectra were obtained with the computerized system ASEC-3 in which the charge sensitivity is AQmJn = 10"16 Coulomb. All electrical characteristics were measured in air and also in the presence of the water vapor.

3. RESULTS

Schematic view of fabricated diamond p-n junction with Ti ohmic contacts is shown in Fig.1.

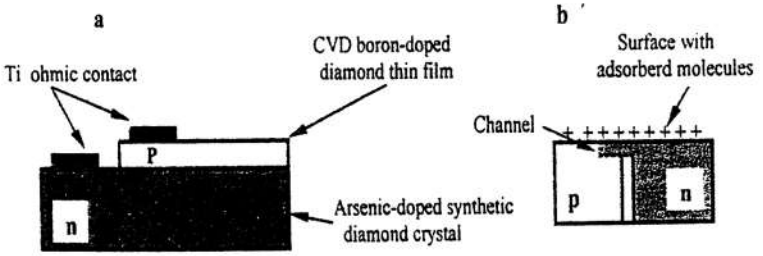

Fig. 1. Schematic view of diamond p-n junction.

The room temperature typical I-V characteristic for different range of applied voltage is shown in Fig.2. The I-V curve of diamond p-n junction exhibit rectifying characteristic with rectification ratios greater than 106 at 5 V.

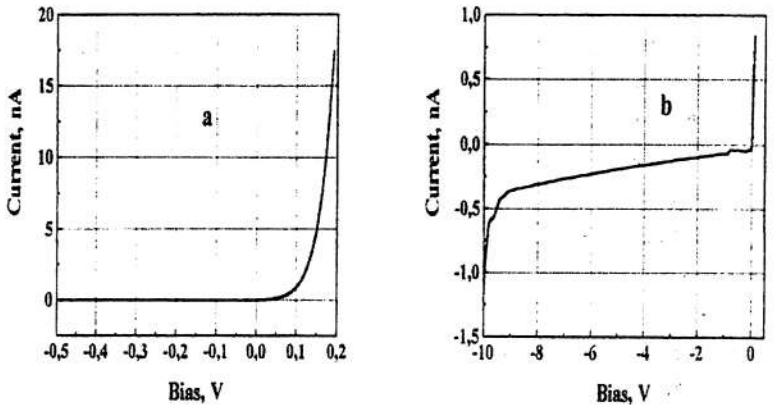

Fig.2. Current -voltage characteristic of the diamond p-n junction at room temperature.

The room temperature differential C-V characteristics of the space charge region of diamond p-n junction were measured in the frequency range from IHz to 250 kHz and were dependent on the test signal frequency evidently due to the presence of trapping centers in the bulk of diamond and at the interface. With increasing frequency, when influence of the trapping centers are decreased, the saturation of capacitance data was observed. The high frequency C-V

characteristic diamond p-n junction at 250kHz and $1/C^{n2}$-Vplot are shown in Fig. 3. C-V data were obtained with the pulse-scan method which allowed to avoid the bias voltage screening affects. The uncompensated acceptor

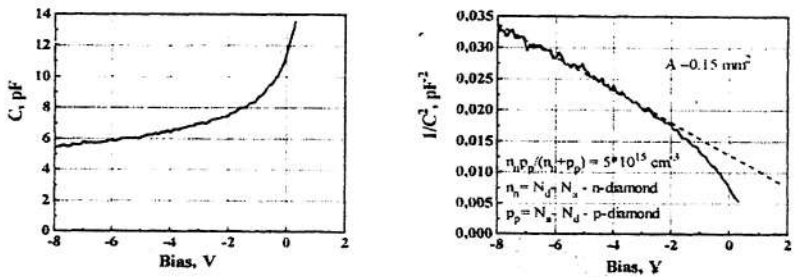

Fig.3. Capacitance-voltage and $1/C^2$ -V characteristics of the diamond p-n junction at room

temperature. A is the area of the contacts.

(N_a- N_d) and donor (N_d - N_a) concentration can be determined from the slop of the $1/C^{n2}$-V plot (Fig.3.) The linearity of the inverse capacitance plot shows the homogeneity of doping (acceptor and donor) concentration within the range of depletion region at reverse bias voltage > -2. A slope change in the $1/C^{n2}$-V plot near forward bias may result of the nonuniformity of the doping concentration profile or processing induced traps [7]. The I-V characteristics of the diamond p-n junction were measured at different temperatures (Fig.4.). The

observed

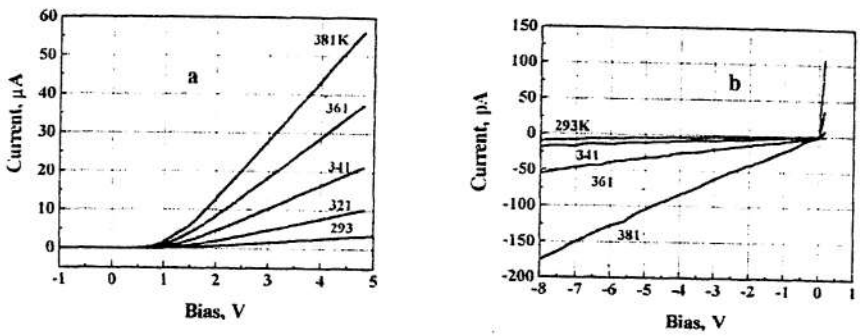

Fig.4. Current-voltage characteristics of the diamond p-n junction at different temperatures.

temperature dependence can be result of diffusion current transport in fabricated diamond p-n diode. It was found that forward I-V characteristic of the diamond p-n junction strongly sensitivity to presence of the water vapor. The Fig.5. shows a large (about two order) change in the I-V characteristics for different concentration cf the vapor at room temperature. The effect is reproducible and repeatable upon adsorption/desorption of water molecules. It seems probable that the adsorbed molecules forma surface dipole (see Fig. 1b), change surface band bending and, as result, induce conduction channel across p-n junction for carriers.

The charge-based deep level transient spectroscopy of diamond p-n junction showed that micro defects with low density are acting as trapping centers (point defects) and have the continuous energy spectrum with two maxi-mums at different energies. From temperatures dependencies of the Q-DLTS peaks two activation energies E_A« 0.4 eV, E_D «0.8 eV and two related capture cross-sections a_A«10^{n14}cm^2, a_D« 0^{n14}cm^2 were obtained. Analysis of the Q-DLTS spectra measuring at different conditions was shown that parameters E_A, O_A characterize point defects induced by boron in p-type CVD diamond film, and E_D, O_D - induced by arsenic in n-type synthetic diamond crystal.

The strong sensitivity of Q-DLTS spectra to the presence of the water vapor was found also. For example, the Q-DLTS signal of diamond p-n junction was changed more then in order in water vapor. This effect may be explained by changing of the p-n junction size and density of surface trapping centers with adsorbed molecules.

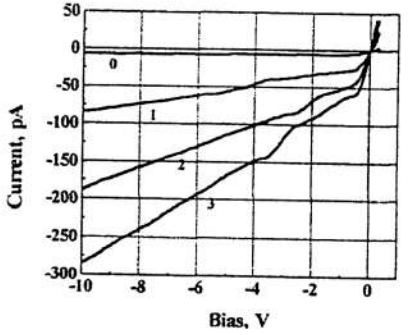

Fig.5. Current-voltage characteristics of the diamond p-n junction before (0) and in water vapor (1-3) at different concentration

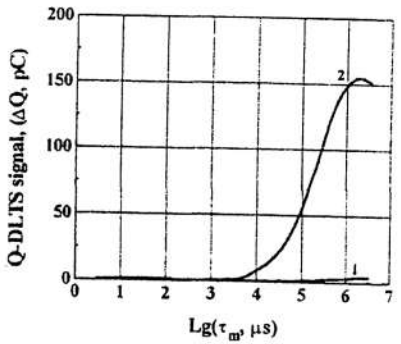

Fig.6. Q-DLTS spectra of the diamond p-n junction: 1 - in air, 2 - in water vapor.

3. CONCLUSION

Performance of the new diamond-based electronic device has been demonstrated. The study of the electrical characteristics shows that fabricated diamond p-n junction can be used as a good diodes or gas sensors.

It should be emphasized, that the study of the current transport and the point defect formation on diamond p-n junction is a real way to operate those parameters and improve characteristics of all possible novel diamond electronic device applications.

4. ACKNOWLEDGEMENTS

This work was supported by Russian Foundation of Fundamental Research (Grant No 98-02-16679).

5. REFERENCES

1. MRS Bulletin, Diamond Films: Recent Development, **23** (1998).

2. V.A. Laptev, V.P. Butuzov, Yu.M. Rotner, et al., DAN USSR, 228 (1976) 1080.

3. K. Okano, H. Kiyota, T. Iwasaki, Y. Nakamura, Y. Akiba, T. Kurosu, M. Iida, T. Nakamura, Appl. Phys., A 51 (1990) 344; and Solid-State Electron., **34** (1991) 139.

4. K. Okano, H. Kiyota, T. Iwasaki, T. Kurosu,, M. Iida, T. Nakamura, Appl. Phys.Lett, 58 (1991) 840.

5. V.I. Polyakov, A.I. Rukovishnikov, N.M. Rossukanyi, V.P. Varnin, I.G. Teremetskaya, B.L. Druz, E. Ostan, A. Hayes, Mater. Res. Soc. Proc., Pittsburg, PA, 442 (1997) 687.

6. V.I. Polyakov, N.M. Rossukanyi, A.I. Rukovishnikov, S.M. Pimenov, A.V. Karabutov, V.I. Konov, J.Appl. Phys., **84** (1998) 2882.

7. M.W. Geis, N.N. Efremow, J.A. von Windheim, Appl.Phys.Lett, **63** (1993) 952.

STRUCTURE-FORMING FACTORS IN SUPRAMOLECULAR ARCHITECTURE OF NIDO [9-C_5H_5N-11-I-7,8-$C_2B_9H_{10}$]

T. M. Polyanskaya

A.V. Nikolaev Institute of Inorganic Chemistry of SB RAS, Novosibirsk, 630090, Russia

e-mail: polyan@che.nsk.su

Intermolecular hydrogen bonding is a major factor involved in supramolecular self-assembly motifs. The molecular rigidity and the topological versatility of carboranes make carborane derivatives the attractive candidates for crystal engineering.

We now report the solid-state structure of the title compound **1**. Crystal species **1** displays photoluminescence under UV irradiation with the wavelength of the fluorescence maximum 476 nm and the band width at semi-height 84 nm [1]. Compound **1** crystallizes as clear yellow monoclinic crystals which gave the molecular structure shown in Figure 1. The molecule consists of the {C_2B_9}icosahedron with one vertex removed and with the pyridine fragment attached to the B9 atom on the open face of the cage through the N1 atom. The B_{cage}

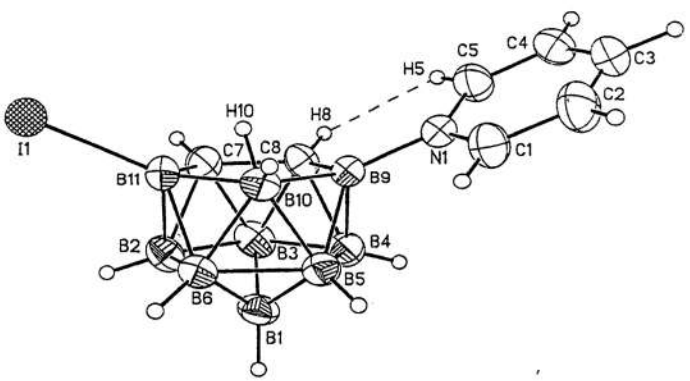

–N bond

Fig. 1

length is 1.546(3) Å, similar to that of 1.543(3) Å found for 9-(4-MePy)-7,8-$C_2B_9H_{11}$ **2** [2]. The carbon-carbon bond length within the cage is 1.549(4) Å, longer by about 0.024 Å than that observed in **2**. The boron-boron bond lengths range from 1.734 to 1.840 Å with an

average of 1.774(4) Å. The carbon-boron bond lengths range from 1.589 to 1.740 Å with an average of 1.680(4) Å. The *exo* terminal boron-hydrogen bond lengths range from 1.01 to 1.12 Å with an average of 1.06(2) Å. The observed boron-iodine bond length of 2.197(3) Å is identical to that of 2.196(6) Å found for 12-iodo-1-(4-pentylquinuclidin-1-yl)-1-carba-*closo*-dodecaborane $C_{13}H_{33}B_{11}IN$, which is zwitterionic derivative of monocarborane $CB_{11}H_{12}$(-1) ion [3]. This value is almost equal to 2.209(9) Å found for monoiodinated 11-vertex carborane cage anion in $[(CH_3)_3NH][nido\text{-}9\text{-}I\text{-}7,8\text{-}C_2B_9H_{11}]$ **3** and 2.201(5) and 2.203(5) Å in diiodo *nido*-carborane cage structure in $[(CH_3)_3NH][nido\text{-}9,11\text{-}I_2\text{-}7,8\text{-}C_2B_9H_{10}]$ **4** [4]. It is intermediate between those obtained for iodo derivatives of *p*- and *o*-carboranes (mean 2.16 Å and 2.168 Å, respectively) [5-7] and $B_{12}H_{11}I$(-2) (2.226(4) Å) [8]. This trend in the bond lengths can be related to the cage electron density; the more electron deficiency of the cage, the shorter the B–I bond.

An important influence of iodine substitution upon the open face of the *nido*-C_2B_9-cage in **1** is the existence of the distinct asymmetrical B–H–B bridge between B10 and B11. The H10–B10 bond length is 1.09(3) Å and the H10–B11 bond length is 1.51(3) Å. In fact, H10 is the *endo*-hydrogen atom, which is directed toward the empty 12th vertex with the H10–B10–H10B bond angle of 111.3°, approaching the tetrahedral geometry about the B10 atom. These characteristics are consistent with previous studies of the structures which contain the $\{BH_2\}$ vertices. It had previously been shown by X-ray crystallography and NMR studies that the unsubstituted $[nido\text{-}7,8\text{-}C_2B_9H_{12}]$(-1) ion exhibits a symmetrical *endo*-H atom at the B10 position [9, 10]. In structure **2,** the B–H–B bridge is symmetrical with the B–H bond lengths of 1.23(3) and 1.24(3) Å. In the anion of **3** and **4,** the bridge H–B–H is asymmetrical in the same way as in **1** with the B–H distance of 1.26(18), 1.55(17) and 1.07(6), 1.50(6) Å , respectively.

The nitrogen-carbon bond lengths within the pyridine cycle range from 1.342 to 1.352 Å with an average of 1.347(3) Å. The carbon-carbon bond lengths range from 1.363 to 1.374 Å with an average of 1.369(4) Å. The carbon-hydrogen bond lengths range from 0.89 to 1.00 Å with an average of 0.93(3) Å. The pyridine cycle forms the 34.4° dihedral angle with the open face of the cage. In the molecular complex **1,** the cluster *nido*-11-vertex $\{C_2B_9\}$ polyhedral skeleton has one nearly planar six-membered B9C8H8H5C5N1 ring of *exo*-polyhedral cyclization by pyridine with the shortened intramolecular contact(a dashed line in Fig. 1) between the H5 and H8 atoms of 2.18 Å. The torsional C8B9N1C5 angle is 4.4° only. In the unsubstituted complex **2,** analogous but ideally planar six-membered ring of *exo*-

polyhedral cyclization has the shortened intramolecular $(C_{Py})H\ldots H(B_{cage})$ contact of 2.24 Å. Such an arrangement leads to the back-bonding interaction between carborane and pyridine fragments producing the yellow colour of the species.

The crystal structure of **1** reveals two orientations of molecules (head-to-tail) arranged in infinite zigzag chains running parallel to the *c* crystallographic axis (Figure 2). Each molecule

Fig. 2

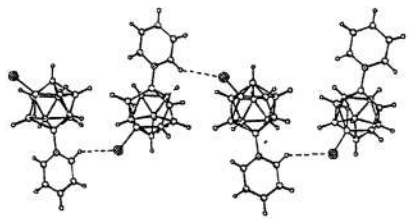

is linked to two neighbors *via* $C5_{Py}$–H…I interactions 3.13 Å, $C5_{Py}$–H…I 140.3°. Two carborane C–H and B–H_{exo} vertices link adjacent zigzag chains *via* C_{cage}–H…I and B_{cage}–H_{exo}…I hydrogen bonds to generate a pattern of self-assembly shown in Figure 3 (for clarity, only hydrogen atoms involved in hydrogen bonding are shown and hydrogen bonds are indicated by dashed lines). These hydrogen bonds are 3.24 and 3.19 Å, respectively, C7–H7…I 175°, B10–H10B…I 132.9°, and trifurcated linkage at I, H7…I–B11 112.9°, $H5_{Py}$…I–B11 100.4°, H5…I–H10B 88.7°, H10B…I–H7 56.2°, B11–I…H10B 168.7°, H7…I…H5 140.0°. In effect, each molecule is linked to four neighbors *via* X–H…I (X=B, C) interactions. Separately these intermolecular interactions are clearly weak, since the sum of the van der Waals radii of H and I is only 3.35 Å. However, the adjacency of the C7–H7 and B10–H10B groups to the I-substituted boron atom B11 along with another functional pyridine C5–H5 group obviously afford a molecule that can maximize its intermolecular X–H…I bonding in a very efficient cooperative fashion by adopting a pattern shown in Figure 3. Certainly this is the original reported example of the *nido*-carborane derivative self-assembly

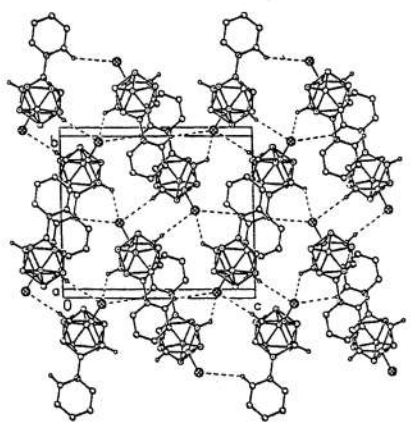

Fig. 3

via X–H…I interactions. This highly ordered structure attests to the ability of

iodinated *nido*- carborane derivatives to build suramolecular assemblies and participate in self-assembly processes *via* X–H…I interactions.

The author is grateful to Dr. O.V. Volkov and Prof. V.V. Volkov for the disposable single crystals of **1.**

1. *Volkov O.V., Il'inchik E.A., Volkov V.V., Voronina G.S. and Yur'eva O.P.* // Koordinats. Khim. 1997. V. 23. N 11. P. 824-827.

2. *Polyanskaya T.M., Alekseev V.I., Volkov O.V.* // Zhurn. Struktur. Khimii. 1993. V. 34. N4. P. 149-153.

3. *Douglass A.G., Janousek Z., Kaszynski P. and Young V.G., Jr.* // Inorg. Chem. 1998. V. 37. N 24. P. 6361-6365.

4. *Pak R. H., Kane R.R., Knobler C.B. and Hawthorne M.F.* // Inorg. Chem. 1994. V. 33. N 23. P. 5355-5357.

5. *Zheng Z., Jiang W., Zinn A.A., Knobler C.B. and Hawthorne M.F.* // Inorg. Chem. 1995. V. 34. N 8. P. 2095-2100.

6. *Jiang W., Knobler C.B., Curtis C.E., Mortimer M.D. and Hawthorne M.F.* // Inorg. Chem. 1995. V. 34. N 13. P. 3491-3498.

7. *Barberà G., Viñas C., Teixidor F., Rosair G.M. and Welch A.J.* // J. Chem. Soc., Dalton Trans. 2002. P. 3647-3648.

8. *Haeckel O., Preetz W.* // Z. Anorg. Allg. Chem. 1995. V. 621. N 9. P. 1454-1458.

9. *Buchanan J., Hamilton E.J.M., Reed D. and Welch A.J.* // J. Chem. Soc., Dalton Trans. 1990. N 2. P. 677-680.

10. *Fontaine X.L.R., Greenwood N.N., Kennedy J.D., Nestor K., Thornton-Pett M., Heřmánek S., Jelínek T. and Štíbr B.* // J. Chem. Soc., Dalton Trans. 1990. N 2. P. 681-689.

STRUCTURE-FORMING FACTORS IN SUPRAMOLECULAR ARCHITECTURE OF (N-Me-Bipy)($B_9C_2H_{12}$)

T.M. Polyanskaya

A.V. Nikolaev Institute of Inorganic Chemistry of SB RAS, Novosibirsk, 630090, Russiae-mail: polyan@che.nsk.su

The design of supramolecular assemblies using nonvalent intermolecular interactions has evolved as a powerful tool for the synthesis of new materials with designed characteristics. We have carried out single-crystal analysis of the title compound **I**. A formula is established by X-ray study. Crystal species **1** has the yellow colour and displays photoluminescence under UV irradiation with the wavelength of the fluorescence maximum 540 nm and the band width at semi-height 107 nm [1]. The crystal structure **I** consists of (N-Me-Bipy)$^+$ cations and ($B_9C_2H_{12}$)$^-$ anions. The X-ray density indicates four formula units in the unit cell. Thus, in space group $P2_1/c$ the asymmetric unit contains one formula unit. Geometry of both the cation and anion has no unexpected norms (Figure 1). The cation is *cisoid* in the disposition of the nitrogen atoms, with twisting of pyridine rings by *ca.* 42°.

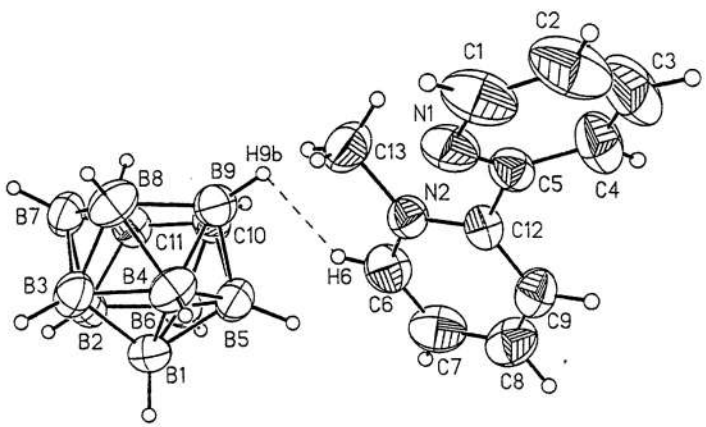

Fig. 1

The methyl group is directed towards the neighbouring Py ring. CNC angle at unprotonated nitrogen atom N1 (sp^2) (116.9°) is much smaller than that for N2 (sp^3) atom containing Me group which is 120.2°.

Figure 2 shows crystal structure of **1** viewed in the *ac* plane. The cation (Cat) and the anion

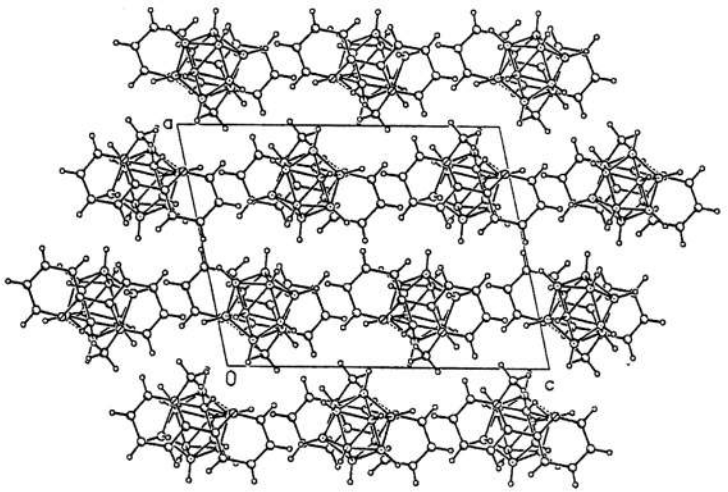

Fig. 2

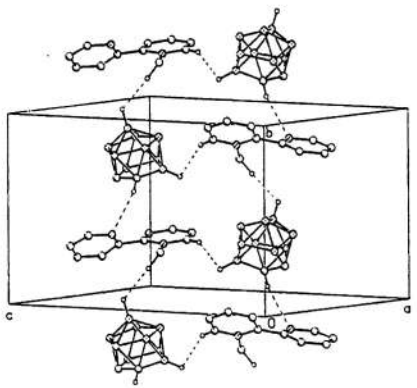

Fig. 3

(An) are arranged one above the other alternating in the ...Cat...An...Cat...An... manner (Fig.3. For clarity, only hydrogen atoms involved in hydrogen bonding are shown and hydrogen bonds are indicated by dashed lines). The packing ions involve $C_{cluster}$–H...N, C_{Py}–H...H–B and C_{Me}–H...H–B interactions with short distances H...N, 2.57 Å, (C_{Py})H...H(B) 2.28 Å and. (C_{Me})H...H(B) 2.22 Å. Each borane cluster interacts with three cations and in turn, each cation is hydrogen bonded to three borane cluster anions forming an infinite hydrogen-bonded ladder structure in which the building blocks surround a 2_1 screw axis.

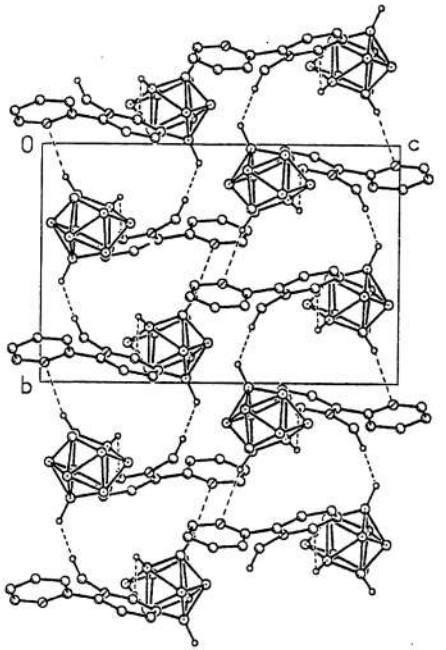

The Fig. 4 shows the ladder structure packing viewed in the *bc* plane.

Cetainly this the original reported example of the *nido*-carborane derivative and protonated aromatic heterocyclic base self-assembly *via* C–H...N and C–H...H–B interactions.

This study attests to the ability of *nido*-carborane derivatives and protonated aromatic heterocyclic bases to build supramolecular assemdlies of hydrogen-bonded ladders in the solid state.

Fig. 4

The author is grateful to Prof. V.V. Volkov for the disposable single crystals of **1**.

1. Volkov V.V., Il'inchik E.A., Volkov O.V. and Yuryeva O.P. // Chemistry for Sustainable Development. 2000. V. 8. N 1–2. P.185-191.

ANALYSIS OF ELECTRONICS MATERIALS IN STATE CENTER (SC) «BELMICROANALYSIS»

V. N. Ponomar, L. D. Buiko, G. G. Chigir, V. A. Filipenya
Minsk, RPC «Integrab», Kazintsa Sq.

In order to enhance efficiency of application, development of the new monocrystalic and other electronics materials it is required to possess a complex of the analytical equipment for the comprehensive analysis of their parameters. As the spectrum of the analyzed materials is very wide, the complex of equipment should have a possibility to analyze a wide range of the physical parameters with the possibility, if need be, to obtain the required information quickly and reliably. The fastest and most efficient rate of such operations can be accomplished, when all required analytical equipment is concentrated at one location, as, for instance, at the State Center «Belmicroanalysis».

State Center «Belnicroanalysis» of RPC «Integral» of the Republic of Belarus is furnished with the contemporary computerized analytical equipment to perform the qualitative and quantitative analysis of composition, analyses of the structural-morphological and electrophysical characteristics of various materials, microelectronics devices and other objects.

<table>
<tr><th colspan="2">Techniques of Element, Phase and Structural Analysis of Materials</th></tr>
<tr><td>Secondary-ion Mass-Spectrometer IMS-4F by company "Cameca" (France) ensures:
• Analysis of element surface composition and element depth distribution (from H to U).
• Depth resolution 5 ~ 30 nm.
• Sensitivity $10^{12} \sim 10^{16}$ at/cm^3.</td><td>Electron Auger Spectrometer PHI-660 by company «Perkin Elmer» (USA) ensures:
• Analysis of element surface composition and depth distribution (from Li to U).
• Depth resolution ≤ 3 nm.
• Locality ≥ 0,1 mcm.
• Sensitivity 0,1 ~ 1,0 at.%.</td></tr>
<tr><td>Scanning Electron Microscope Stereoscan-360 by company Cambridge Instruments (England) with the built-in power spectrometer AN 10000 by company «Link Analytical» (England) ensures:
• Analysis of element composition (from B to U).
• Sensitivity 0,2 atom.%.
• Locality ≥ 1mcm^3.</td><td>Transmission Electron Microscope H-800 by company «Hitachi» (Japan) with Analytical System AN 10000 by company «Link Analytical» (England) ensures:
• Analysis of the surface microrelief (replica).
• Microstructure transparancy examination.
• Electron-diffraction analysis.
• Examination of split structure on transparancy at magnification ≤500 000x with resolution of ≥ 1 nm.
• Analysis of element composition (from B to U).</td></tr>
<tr><th colspan="2">Electrophysical and Optical Control Techniques</th></tr>
<tr><td>Software-Hardware Complex of Volt-Ampere (I V) and Volt-Farad (C-V) Characteristics Precision Measurements of IC Ele-ment Base, consisting of:
• Microprobe manipulator with microscope 1500˟ and ultrasound cutter.
• Precision analyzer of semiconductor devices HP4156B by company «Hewlett-Packard». (USA).
• Precision LCR tester HP4275 by company «Hewlett-Packard». (USA).
• TV-cameras with monitor.
• Work station HP715 with software ICCAP by company «Agilent» (USA).
• Microprobe manipuilator for C-V measurement.
• Electron unit of LCR tester control.
• Computor.
Ensures:
• Fully automated measurement of volt-ampere characteristics in the current ranges from 1fA to 100mA and voltage from 2μV to ±100V at dissipated power of measured element up to 2W
• Capacity measurement from 1fF to 100μF. inductance from 1pH to 200mH, resistance from 0,01mΩ to 20MΩ at voltages ±30V.
• Time-dependent I-V measurements.
• Digitizing and graphical processing of measurement results.
• Analysis of the electrophysical characteristics and semiconductor layers and separation boundaries between them on the base of C – V measurements.
• SPICE-parameters extraction.</td><td>Laser Ellipsometer ЛЭФ-3М-1 (Russia) ensures:
• Measurement of thickness (over 0.5 nm) and optical characteristics (refraction and absorption coefficient) super-thin optically transparent films on silicon, gallium arsenide and other substrates, and also parameters of clear substrates.
• In-process inspection of surface treatment quality.

Software-Hardware Complex for Digitizing Images, consisting of::
• Optical microscope «Leica INM100».
• Digital camera «Polaroid DMC Ie».
• Precision automated scanning table 200x200 mm with control unit LSTEP13.
• Graphical station.
• Printer «Tektronix Phaser 840 DP».
• Stand for macro photography (Copy Stand).
• Ensures:
• Obtaining digital, "combined" from a large number of frames (up to 1000 pcs), video images of IC layers layout and other objects with minimum element size of over 0,5 micron
• Analysis of defect formation in semiconductor structures.
• IC failures analysis.
• Measurement of geometrical sizes of layout elements.</td></tr>
<tr><td>Spectrophotometers: MPV-SP by company «Leica» (Germany); Specord - M40; Specord - M80 by company «Carl Zeiss» (Germany) ensure:
• Analysis of materials optical characteristics, thin films thickness in wave length range 0,2 ~ 50 mcm with locality up to 5×5 mcm^2 (for λ = 400 ~ 800 nm).
• Qualitative and quantitative comparative analysis of optically transparent materials composition.</td><td>Thermovision System «Thermovision 880» by company «Agema» (Sweden) ensures:
• Temperature distribution control on surface of micro and macro objects in real time scale in temperature range from -20 °C to +1500 °C with resolution ±0,1 °C on area ≥ (20x20) mcm^2.

Chemical laboratory and special technological; equipment for samples preparation to analysis.</td></tr>
</table>

As an example, the work indicates the analysis results of the pyroelectric sensor element of the IR range. Pyroelectric element converts the incident IR-irradiation (thermal irradiation of object) into the electric voltage (electric signal). There were examined the

following peculiarities of the pyroelectric element: geometry, ceramic composition, external appearance. Element has the following geometrical sizes sizes: thickness – 95 mcm, width – 3.1 mm and length – 2.6 mm. Pyroelectric element is fabricated from ceramic on the basis of zirconate titanate lead with the various additives. As the additives in the given case there were used Mn and Ni. The ceramic structure images on chip, formed on the raster electron microscope at magnification of 800^x, are listed in Fig.1, the ceramic surface structure – in Fig. 2, the chrome electrode structure on the ceramic surface – on Fig. 3. Ceramic element composition is indicated in Fig. 4.

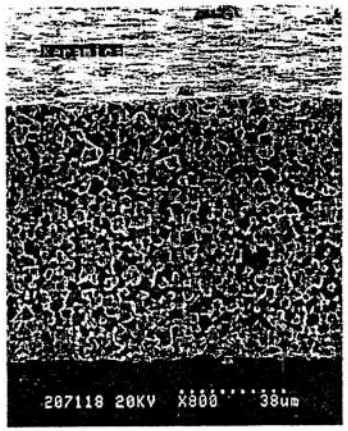

Fig.1 Ceramic chip structure at magnification of 800^x

Fig.2 Ceramic surface at magnification of 3000^x

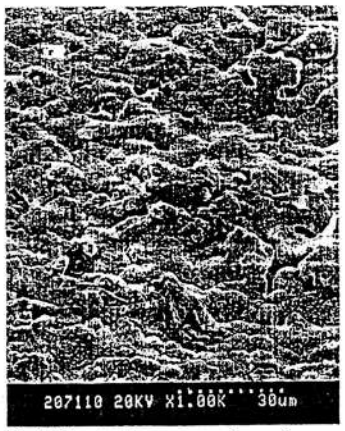

Fig.3 Electrode on ceramic surface at magnification of 1000^x

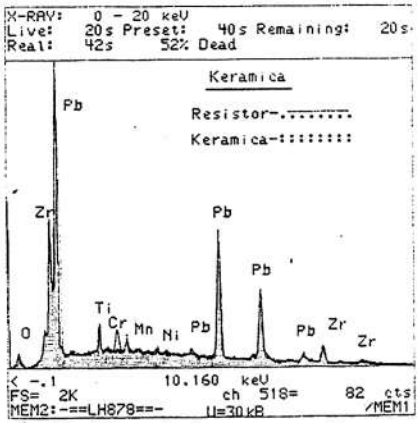

Fig.4 Ceramic element composition

APPLICATION OF VISUALIZATION TECHNIQUE FOR STUDY AND CONTROL OF HEAT AND MASS TRANSFER IN CRYSTAL GROWTH

Michael A. Gonik*, Mark M.. Gonik**

**CTR "Thermo", Department of Crystal Growth, 601650 Alexandrov, Russia*

***Moscow State Technical University named after Bauman, 107005, Moscow, Russia*

Investigation of convection nature in crystal growth is of great importance for the purposes of obtaining perfect crystals. In the conventional growth methods, when a strong forced or thermocapillary convection takes place, a complex flow unstable by its nature is formed. Thus, it is extremely difficult to realize quantitative correlation between experimental and calculated data. In this connection, solidification from a thin melt layer [1,2], when low laminar flows are initiated, is of a special interest.

A novel AHP method of crystal growth under conditions of Axial Heat flux close to Phase interface characterized by an additional heater placed inside in the melt close to the solid-liquid interface was previously proposed [2]. A submerged AHP-heater divides the melt into two zones. Processes in these zones do not affect each other. The zone above the AHP-heater serves for feeding the solidification zone with the melt (under the heater). In crystallization zone, natural convection of the melt is suppressed and a low melt flow, arising due to movement of the crystal with the crucible relatively to the AHP-heater, is laminar and steady-state. It allows controlling the basic technological parameters: position and shape of the solid-liquid interface, actual growth rate of a crystal and temperature gradient at the solidification front during the growth run resulting in high homogeneity of crystal.

Particle image velocimetry (PIV) as well as particle image thermometry (PIT) are used as a quantitative determination of the velocity and temperature map in a convective flow field. These measurements are performed using image analysis software. PIT is used for testing measuring technique with modeling liquids and studying of the temperate field, while PIV is an instrument for investigation melt flow pattern directly in crystal growth process. With the aim to observe the behavior of low AHP flow, an experimental AHP setup for visualization of $NaNO_3$ crystal growth [3], employing 20 μm particles of aluminum powder as tracers, was designed.

It has been shown that crystal growth by the AHP method is characterized by low laminar flows. This allows obtaining experimental benchmarks and testing of 2D and 3D codes for simulation of convection under conditions of phase change. Such flows can be considered as benchmark ones and employed as tools for studying the effect of convection behavior on growth of a crystal and formation of its structure. Hardware on base of high precision multimeter HP34970A of Agilent company and software developed using universal LabView package for computer control of the process of crystal growth itself by AHP method and of operation of digital camera and image processing on-line are discussed.

Obtaining of experimental benchmarks will be considered as a key achievement of investigation in this area. But implementation of visualization technique can be used as a way for feedback in loop of crystal growth control too. This method has a great prevalence in Czochralski crystal growth of dislocation free silicon or Stepanov technique for sapphire crystallization. Possibility of employing of such an approach together with control of temperature distribution over the melt-crystal system for the crucibleless AHP method [3] is under consideration of the work.

The research was sponsored by INTAS-99-01814 and by CRDF RE1-2480.

[1] Ostrogorsky, A. Diffusion-controlled distribution of solute in Sn-1%Bi specimens solidified by the submerged heater method. *Journal of Crystal Growth*, 110, 950-954, 1991

[2] V.D. Golyshev, M.A. Gonik, A temperature field investigation in case of crystal growth from the melt with a plane interface on exact determination thermal conditions, *Cryst. Prop. and Preparation*, 36-38, 623-630, 1991.

[3] V.D. Golyshev, M.A. Gonik, A.N. Kovalenko, E.V. Zharikov. Study of low melt flows during $NaNO_3$ solidification by AHP method. *Abstracts of Int. Symp. on Visualization and Imagining in Transport Phenomena*, May 5-10, 2002, Antalya, Turkey, p. 61-63., 2002.

[4] V.D.Golyshev, M.A. Gonik and Tsvetovsky V.B. Problems of Bi4Ge3O121 and Li2B4O7 single crystals growth by crucibleless variant of AHP method, *J. Cryst. Growth* 198/199 (1999), 501-506.

THE BEHAVIOR OF MODIFIED FULLERENE C_{60} IN CASE OF SUPERHIGH PRESSURE AND TEMPERATURE

Pushkin A.N.[1], Gulish O.K.[1], Gentchel V.K.[1], Lushov A.A.[1], Rudenko A.P.[1], Medovoy A.I.

[1] *Department of Chemistry, Moscow State University, Leninsky Gory, 119899 Moscow, Russia*

According to [1 - 3], simultaneous application of heat and high pressure up to 10 GPa allows C_{60} to retain its molecular structure while forming crystalline polymerized phases. These three different phases are of hexagonal, tetragonal and orthorhombic indexation corresponding to bonding of one molecule to its first six, four or two neighbours in the (111), (100) planes or <100> direction of the *fcc* lattice, respectively.

We report on the investigation of the chemically modified crystalline C_{60} fullerene samples by means of chromatomass spectrometry. The samples were prepared by two methods: (i) C_{60} fullerene was partly oxidized by oxygen at 100 °C and (ii) C_{60} fullerene was kept under hydrogen atmosphere at 100 °C; and then both samples were exposed to high pressure (7 GPa) and temperature (900 °C). Oxygen-modified sample (sample 1) contained a mixture of the linear saturated carbonic acids C_6-C_{16} and linear saturated hydrocarbons C_{21}-C_{28}; whereas in the mass-spectrum of hydrogen-modified sample (sample 2) only hydrocarbons C_{21}-C_{28} were present, the quantity being five times lower then for sample 1. The transition of C_{60} into diamond phase was observed only for sample 2. Obtained results can be tentatively explained by the C_{60} disproportionation during fragmentation of the carbon cage, the main features are similar to the earlier observed process of the formation of hydrogen (oxygen) containing products during the partial O_2 oxidation of C_{60} at 500 °C and atmospheric pressure in the presence of water[4].

It was inwestigated the influence of Mn, Fe, Ni on the phase trasformation of C_{60} at 500°C and 4 GPa during 15 minutes as well. The results of X – ray diffraction analysis illustrate that the treatment of initial C_{60} by transition metal compound caose the transformation and stabilization of polymer phases of C_{60} in idicated condition. All examined samples contain a mixture of rhombohedral (with hexagonal orientation of the molecules) and orthorhombic polymer of C_{60}. In case of Mn the picks of tetragonal polymer are present in difractograms as well.

[1] Marques L., Hodeau J-L., Perroux M. // Electrochem. Soc. Inc. !995. V.2. 95 – 10. P.906.

[2] Agafonov V., Davidov V.A., Kashevarova L.S. et al. // Chem. Phys. Lett. 1997. V.267. P.193.

[3] Moret R., Launoia P., Persson P.-A., Sundqvist B. // Europhys. Lett. 1997. V.40. P.55.

[4] Zenin N.N., Pushkin A.N., Rudenko A.P. et al. Zh. Fiz. Chim. 2000. V.74. №12. P.2142.

ARHIMED HAS NOTHING TO DO WITH IT.

Artemjev G.G., Gerasimenko N.I.

Russian Academy of Economics named after G.V. Plekhanov, Moscow, Russian Federation

It is important to receive the information on density of a chip or metal fast and rather exactly when doing identification and expertise of jeweler products.

Method using the law of the Arhimed has been more often applied nowadays. This method involves sequential weighing of researched substance in air and liquid (better in distiliratig water). The method is exact but rather expensive and not very fast, which makes it difficult for mass application.

Is it possible to combine these two incompatible criteria quickly and precisely? We offer to our readers the technique that has been approbated in the educational process at faculty of Physics of Russian Academy named after G.W. Plekhanov since 2000 and has given brilliant results. Even the most careless students do not write off the results, they carry out the research with pleasure. They have feeling of experts and really become them.

The author's program with the intuitively clear and amicable interface supplements this useful pleasure.

Density, as known, is the ratio of a mass of substance to volume, occupied by it, densities - ratio of weight of a body to volume. In one point of an earth surface both values are strictly proportional to each other. As, unit of a mass of a water almost coincides with unit of its size (If a temperature equal 4^0C volume of one gram of water equal one milliliter), density and densities referred to water, practically are equal and on numerical value. But, certainly, they are various in a physical sense. Finding density needs definition of two values - mass and size. The definition of the ratio can be produced in three ways: or determine a mass of known size, determine size of a known mass, or, at last, on an arbitrary sample determine both mass and size.

A mass of a researched sample is defined with the help of electronic device for weighting

to within the third decimal sign. And as for the size of a sample of the arbitrary geometrical form, it can be received numerical value as follows: the sample is suspended on an independent suspension bracket, as is indicated on fig.1, and small size with distillating water is placed on the scales.

We have revived an old technique on of definition of density of an extremity XIX centuries. It is based on the theorem of the return law of the Archimedes. « Any body immersed in a liquid, heavy and were in an equilibrium, renders on it vertical pressure from above downwards, equal to weight of the superseded liquid ».

It is possible to express that less correctly, but intuitively more clearly, by telling, that the weight lost by an immersed body, is gained with a liquid.

The theoretical explanation of this phenomenon is rather simple. It can be considered or as a corollary from the main law of equality of operation to a counteraction (if the immersed body undergoes pressure on the part of an enclosing liquid, this last should be exposed precisely to same pressure in an opposite direction); or simpler it is possible to notice, that with imbedding of a body in a liquid, the level it in a vessel rises; equal in effect pressure on walls increases, therefore, on such amount, as though the size equal is added to a liquid superseded; this increment of pressure, obviously, is equaled to weight of the superseded size.

For definition of density of a jeweler stone by an offered method, we place on device for weighting small vessel with water and dropped in it up to a fixed point a small basket, made from thin wolfram wire. The observations of on device for weighting we make equal to zero. We drop in a chip to the basket. Device for weighting will show a mass of the superseded water numerically equal to size of a chip. Now it is easy to count up the value of density to within the second decimal sign. The given way is suitable for the express train - definition of density not only stones and precious metals, but also many hard substances not soluble in water.

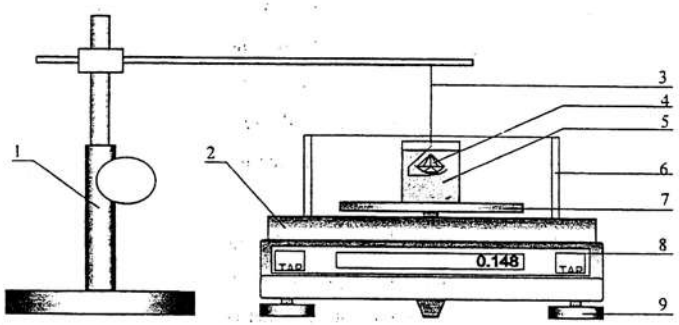

Fig.1. The scheme of device for definition of density: 1 - support, 2 – an electronic device

for weighting, 3 - filament basket, 4 - researched chip, 5 - vessel with distillating water, 6 - show-window glass, 7 - cup of the device for weighting, 8 - toolbar, 9 - screws adjusting

Let's try at once to answer inevitable objections of physicists, that any scales are for measurement of only forces. But physics will agree with the following reasoning: when the speech goes about lever device for weighting there are first of all measurement standards of a mass, and that therefore weighing is manipulation of definition of a mass of a body by matching its weight with weight of a body, which mass unit. As the mass of bodies in the given place is proportional to weight, we and shall receive valid numerical value of a mass in any location of device for weighting, if only etalon of weight. By the way, some models of electronic scales use just this principle.

Shall we use the same method to define the density of liquids? As the scales show the weight of a liquid superseded by a body, let's this very body make the size equals 1 cm^3. Now we will put on the scales the sample with the researched liquid and dropped into it a standard cubic centimeter on a rope. Now we will put the scales on 0 point. Then we will insert the standard cubic centimeter made from invar into the basket. The scales will show the value of density of the researched liquid

Because of methodical reasons standard cubic centimeter should be executed as a cube. In practice it is easier to turn it as the cylinder. In that and other case it is better to have a small store on size and grind this "store" until the exact value of size will be obtained.

Advantage of the offered technique is the comparative cheapness and, that the speed of obtaining of a finite outcome with desirable accuracy.

Nowadays installation working on the above described principle, even more simplified, is started in production and it is possible to gain in JST " Klio-technique" by the address: 119991, Moscow, Leninsky Prospect, 7, Ph: 237-48-42, 237-39-96, 237-67-66. Fax: 236-94-56.

CRYSTAL STRUCTURE OF NEW STRONTIUM MICA

N.I. Bryanchaninova[1], A.B. Makeyev[1] and N.V. Zubkova[2]

[1]Institute of geology Komi Science Centre Ural Division of RAS, Syktyvkar, Russia;

[2]Moscow State University by M.V. Lomonosov

New sodium-strontium variety of mica has found in 2002 in Rubinovy Log (well known many mineralogists object) in Rai-Is ultrabasite massif (the Polar Urals, Russia). The green strontium mica is associated with ruby, oligoclase, talc, pargasite, chlorite, two varieties of chromite $(Fe_6Mg_2)_8(Cr_{12.8}Al_{2.9}Fe_{0.3})_{16}O_{32}$ and $(Fe_6Mg_2)_8(Cr_{8.4}Al_{7.0}Fe_{0.6})_{16}O_{32}$ and gold-brown mica Na,Ba,Al,Cr-bearing phlogopite. All minerals of ruby sequences contain isomorphic admixes of chromium and are enriched with aluminum. Simplified formula of Na,Sr-mica is $Na_{0.50}Sr_{0.25}Al_2(Na_{0.25}\square_{0.75})[Al_{1.25}Si_{2.75}O_{10}](OH)_2$ or $(Sr_nNa_{1-2n})Al_2(Na_n\square_{1-n})[Al_{1+n}Si_{3-n}O_{10}](OH)_2$. Ruby plagioclasite with Na,Sr-mica was formed at the final stage of ultrabasic system evolution by means of solid rock recrystallization with active participant of volatile components.

Crystal structure of Na,Sr-mica has been defined on the basis of single-crystal data (Syntex P $\bar{1}$ diffractometer, graphite-monochromated MoK_α radiation, λ=0.71069 Å) using the program Shelx-97 (R = 0.075). Like other minerals of mica Group the crystal structure of Na,Sr-mica is formed by TOT layers, where octahedral (O) sheet is sandwiched by two tetrahedral (T) grids consisting of (Si. Al)-tetrahedra. Tetrahedral grids are formed by two non-equivalent tetrahedra, which are characterized by similar distribution of Si and Al atoms. In comparison with Paragonite, there was defined an additional position in O sheet partially occupied by Na cations in the crystal structure of Na,Sr-mica. In spite of the presence of this additional position in octahedral sheet in the structure of Na,Sr-mica it should be considered as dioctahedral variety of mica Group according to the classification of IMA. Atoms of Na and Sr statistically occupy large octahedra in the interlayer space.

Strontium is absent among speciation cations of micas. Our foundation testifies that Sr is one more speciation cation and he list of cations in the common formula $\mathbf{IM_{2-3}\square_{1-0}T_4O_{10}A_2}$ of micas in position **I** – Cs, K, Na, NH_4, Rb, Ba, Ca – **Sr** is also added.

REFERENCES

Bryanchaninova N.I., Makeyev A.B., Zubkova N.V., Filippov V.N. Natrium-strontium mica – $Na_{0.50}Sr_{0.25}Al_2(Na_{0.25}\square_{0.75})[Al_{1.25}Si_{2.75}O_{10}](OH)_2$ from Rubinov' Log // Docl. RAS. Vol. 395. №3. 2004. pp.101–107.

AHP CRYSTALLIZATION OF CONCENTRATED ALLOY CDZNTE

Bykova S.V., Golyshev V. D., Gonik M.A., Tsvetovsky V.B.

Center for Thermophysical Researches "Thermo" (Alexandrov, Russia)

E-mail: Bykova@thermo.vladimir.su ; phone/fax(095) 584-58-16

Cadmium zinc telluride (CZT) is of great technological interest and strategic importance. In order to enable the continued advance of technologies based upon CZT substrates, large, high-quality, single crystals of CZT are required. Infrared detector material is most commonly grown via the horizontal Bridgman method, while nuclear detector material is generally produced using the high-pressure vertical Bridgman technique. To date, CZT grown by both processes has been plagued by low yields that have been attributed to crystalline defects such as grain boundaries, twins, inclusions, precipitates, and microcracks, as well as compositional inhomogeneity resulting from segregation.

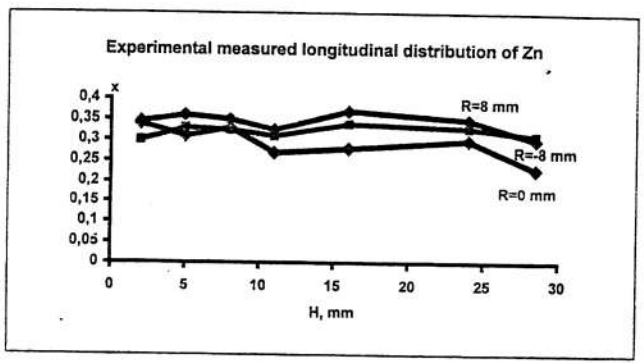

To overcome these problems the melt crystal growth method at axial heating process (AHP method [1]) was used. This method used an additional heater (AHP heater) that is submerged in the melt and that is placed close to the solid-liquid interface. By properly balancing thermal flux from this heater and from a set of background heaters, it is possible to establish an axial heat flux close to the interface and maintain constant interface shape, position, and velocity throughout the growth run.

The zone-leveling approach (optimum charge composition in upper (above AHP heater) and lower (below AHP heater) melt zones) is applied to provide optimal axial segregation.

The high-pressure (100 atmosphere of Argon) AHP technique was applied. Result of the AHP crystal growth of $Cd_{07}Zn_{03}Te$ alloy are described in the presentation. The some results on the lateral and on the longitudinal composition of AHP grown CZT are shown in Figure.

This research is supported by the U.S. Civilian Research & Development Foundation under CRDF grant № RE1-2480.

1. V.D. Golyshev, M.A. Gonik, A temperature field investigation in case of crystal growth from the melt with a plane interface on exact determination thermal conditions, Cryst. Prop. and Preparation, 36-38 (1991) 623-630.

RESEARCH OF THE MORPHOLOGICAL INSTABILITY OF (111) Ge FACET AT HIGH LEVEL OF Sb DOPING.

Svetlana V. Bykova, Vladimir D. Golyshev, Michael A. Gonik, Vladimir B. Tsvetovsky

Centre for Thermophysical Researches "Thermo", Institutskay St. 1, 601650 Alexandrov, Russia E-mail: Bykova@thermo.vladimir.su ; phone/fax: (095) 584-58-16

Germanium with high impurity concentration is a perspective material for cells of solar batteries. Therefore, obtaining of perfect high quality single crystals with high impurity concentration is an actual problem. It is well known that a facet is morphologically more stable than an interface growing by the rough growth mechanism. Therefore, there is an opportunity to grow crystals with a higher impurity concentration due to the absence of a disturbance to the morphological stability.

The present work is dedicated to description of experimental research on morphological instability conditions in faceted growth of Ge, as well as to discussion of phenomena observed in experiment, which are involved into formation of faceting interface and morphological instability of a facet (111).

A crystal of germanium doped with Sb was grown by a method of the Axial Heat flux close to the Phase interface (AHP method) [1] on a seed in the direction [111]. The deviation from a plane (111) was no more than 1 minute. The AHP method allows to obtain a well-known weak AHP forced melt flow along the melt/crystal interface [2]. The necessity of generating such a weak flow is caused by the fact that the melt flow influences facet morphological instability if the velocity of melt flow is comparable to the rate of spreading of macrosteps [3].

The grown single crystal of Ge was cut into plates in the longitudinal direction. To visualize the melt-crystal interface and structure of a crystal, the Ge plate was etched by the method of anode etching. The experimental researches of lateral and longitudinal macroheterogeneity in the distribution of Sb were carried out with the spreading and four probe technique.

To find conditions of facet morphological instability a 1D numerical model together with experimental data were utilized to predict the facet dynamics and solute concentration features of the grown crystal.

On the basis of comparison between the facet-free interface shape without a facet and the interface shape with a facet, a dependence of singular facet (111) growth rate on supercooling has been found. Comparison of the melt flow velocities with the rate of spreading of macrosteps has shown that these values are close to each other and that the morphological instability for this experiment is connected with the melt flow direction.

These researches were sponsored by INTAS (Project No. 99 – 01814), as well as NASA (Project # 98-HEDS-05092).

[1] V.D. Golyshev, M.A. Gonik // Cryst. Prop. Preparation. 1991. V. 36-38. P. 623.

[2] S.V. Bykova, I.V. Frjazinov, V.D. Golyshev, M.A. Gonik, M.P. Marchenko, V.B. Tsvetovsky, J. Crystal Growth. V. 237-239 (2002) 1886-1891.

[3] A.A. Chernov, Proceeding of NASA Microgravity Materials Science Conference held at Hantsville, Alabama, June 10-11 (1996), p.p. 57-60.

CRYSTALLIZATION OF BORATE COMPOUNDS FROM THE MELTS OF NEAR STOICHIOMETRIC BIB_3O_6 COMPOSITIONS

F.Yu. Zavartsev, S.A. Koutovoi, V.V. Voronov,A.I. Zagumennyi, I.A. Shcherbakov

General Physics Institute of RAS, Moscow, fzavart@lsk.gpi.ru

The major problem of BiB_3O_6 crystals growth results from a tendency of borate melts to a glass-forming. According to the equilibrium binary phase diagram in the Bi_2O_3 - B_2O_3 system, the BiB_3O_6 compound occurs only in a small region of composition neighbouring with $Bi_3B_5O_{12}$ and $Bi_2B_8O_{15}$ compounds between 72.5 mol% B_2O_3 and 77.5 mol% B_2O_3, [1]. The bismuth tetraborate has two polymorphous modification, a first one is a high-temperature monoclinic α-$Bi_2B_8O_{15}$ compound having the $P2_1$ space group and another is a low-temperature β-$Bi_2B_8O_{15}$ compound, which structure is not defined at present. The temperature of polymorph α-β transition is 696°C. Growth of single crystals from the vitrifying melts is complexified when a range of temperatures of liquation is near solidification range.

To control a basic components contents in melt and crystal, a proximate method of determining of Bi_2O_3 / B_2O_3 ratio was developed. A method is based on a hydrostatic weighing of specially prepared samples transformed into hardened glass state. The determining of component ratio was carried out in terms of empirical dependence of a density on the Bi_2O_3 / B_2O_3 ratio. An accuracy of measurements was ±0.018 gram/cm^3, thus the composition of samples of melt and crystals had been defined with an accuracy not less than ±0.1 mol%.

It is established that a phase composition of compounds crystallized from a melt of near stoichiometric BiBO compositions depends on a heat prehistory of substance in a stage of its synthesis. After synthesis at temperature above 1200^{0}C a degeneracy of BiBO compound and a formation of metastable equilibrium of two phases $Bi_3B_5O_{12}$ and β-$Bi_2B_8O_{15}$ takes place. A merging of neighboring to BiBO eutectics is explained by a stable rearrangement of BiBO melt structure, while an endless network of boron tetrahedrons is formed, a so-named phenomena of polymerization of melt. As known, a structure of triborate melt contains the $[BO_4]$-tetrahedrons and $[BO_3]$-trigonal pyramids in a ratio of 1:2. A deficiency of $[BO_3]^{3-}$-motifs and a high bond energy of $[BO_4]^{5-}$-tetrahedrons in a melt result in a dissipation of triborate nucleation centers impeding to BiBO crystal growth.

[1]. E.M. Levin, C.L. McDaniel, J. Am. Ceram. Soc. 45, # 8, (1962) 335.

CRYSTALLIZATION OF MONOPHASE SOLID SOLUTIONS BASED ON BERYLLIAN INDIALITE

M.A. Mikhailov, T.V. Demina, S.G. Pecherskaya, L.A. Bogdanova

Institute of Geochemistry SB RAS, Irkutsk, Russia,

deminat@igc.irk.ru

Crystals with beryl structure (emerald, cordierite) represent perspective material for quantum electronics [1, 2]. The major demands to these materials are: 1) high transparency; 2) optical and mechanical homogeneity; 3) thermal and chemical stability; 4) meagre thermal expansion; 5) high hardness [3]. The technique to obtain crystals of required quality exemplified by beryllian indialite (BI, $Mg_2BeAl_2Si_6O_{18}$) was produced [4]. The crystals of this phase is crystallochemical analog to beryl and cordierite [5]. Notify that beryl, emerald and cordierite had thermal expansion coefficient $2{,}6x10^{-6}$/°C, $1{,}7\ x10^{-6}$/°C and $0{,}5\ x10^{-6}$/°C, accordingly [6, 7].

The aim of this investigation to obtain monophase ingot, consisting of BI only, from own melt. The BI composition $Mg_{1.63}Be_{1.23}Al_{2.10}Si_{5.97}Cr_{0.04}O_{18}$ was used. This BI growing by flux method is homogeneous in composition and physical properties [4]. These BI individuals was transparency and had unit cell parameters of a=9.575Å, c=9.269Å, colored with chromium as yellowish-green, temperature of melt 1370°C, hardness 1290 kg/mm^2. Emerald is observed on the sides of some large crystals BI as surficial growths. The other conditions of BI growth from a melt: platinum crucible, air atmosphere, transient overheat up to 1400°C/h, endurance at 1370-1380° and rate of cooling - 0.75°/h.

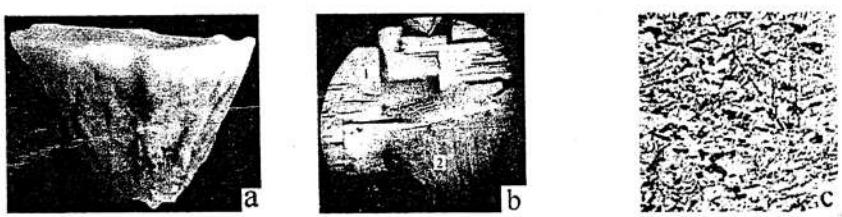

Fig. Appearance of an specimen (a); (b) - detail (a) – boundary between white (1) and green (2) layers; (c) - detail (a) - phenocrysts of an emerald (?) in a green layer of ingot. Magnified to (a) - 2.3^x; (b) – 72^x; (c) - 150^x.

As a result the zonal ingot has obtained (Fig. a), where the white layer was on top and green one was at bottom. A volumetric ratio of bands is (1)/(2) = 1/1.57. Boundary between

layers is distinct (Fig. b). The monomineral layer (1) consists of prismatic colourless (in thinseetion) BI crystals is sized 0.04x0.09mm. (Fig. b). The green band (2) consists of BI, occurring as blocks extended along an ingot and disoriented between each other. In band (2) BI thinsection is also colourless. The small emerald-green prismatic crystals (0.006x0.04mm) probably, emerald, provide green colouring to this layer (Fig. c). Except for these prismatic crystals, BI is penetrated with laths (up to 0.005x0.05mm.) of non-defined phase and spinel skeletal formations. However X-ray phase analysis has shown presence of only BI, and it has not confirmed presence of impurity phases. The composition of last phase will be specified when making X-ray electron microprobe analysis of an ingot. Importantly, that beryllian indialites, generated in the top and bottom layers, differs in cell parameters (Table).

Table

№ of a layer	Parameters of a BI unit cell, Å		Volume, Å^3
	a ±0.004	c ±0.009	V±1.4
(1)	9.575	9.280	736.75
(2)	9.584	9.293	739.15

Characteristically, that the BI parameters of the upper layer are close to BI parameters, which composition became the prototype of a composition for crystallization from a melt.

Our experiments have shown, that a melt of composition adequate to homogeneous BI-based solid solution, obtained by a flux method, probably, liquates at more high-temperature crystallization. The perhaps to obtain homogeneous BI from this melt and colourless BI with chrome presence in initial charge is required further investigations.

The investigations is carry out with the help Integration project of SB RAS № 155.

References

1. Lefever R.A. et. al. / Amer. Mineral., v. 47, № 11-12 (1962) pp. 1450-1453.
2. Solncev V.P. et al./ Spectroscopy and rentgenography of minerals (Novosibirsk, Nauka, 1975) pp. 77-87.
3. Ryabtzev N.G. Materials of a quantum electronics (Moscow 1972) 382 p..
4. Dyomina T.V., Mikhailov M.A., in: Experiment in Mineralogy, v. II, ed. M.B. Apelbaum (IEM RAS, Moscow 1993) pp. 154-187.
5. Smolin Yu.I. et al. // Crystallography. v. 44. №3 (1999) pp. 454-457.
6. Minerals. Reference book, v. III, N 2. ed. F.V. Chuhrov (Science, Moscow, 1981), pp.83-136.

ABOUT THE EQUILIBRIUM FORM OF CRYSTAL

Guskov S.S., Faddeev M.A., Chuprunov E.V.

N.Novgorod State University, N.Novgorod, Russia

Reticular density ρ_R is important parameter of the crystal face. The faces with the most reticular density have a low growth rate [1]. By growing of crystal, the area of these faces increases gradually and defines the crystalline polyhedron form. Hence, the crystals having identical lattices must grow as polyhedrons of identical shape. That is often at variance with the experimental results. Therefore, to describe the growth process of crystal face, it is necessary to introduce into consideration the more detailed characteristic, which takes into account the atomic structure of a growing crystal.

The atomic structure of a crystal is considered approximately as the package of hard spheres. The crystal face is represented as the cross-section of crystalline fragment. Orientation of the face is determined by the Miller indexes (*hkl*). The sum over the cross-section of the hard spheres is calculated per unit of area and is denoted by *S*. For fixed indexes (*hkl*) the cross-section sizes of atomic hard spheres depend on position of the cross-section plane inside the unit cell. Therefore, it is necessary to shift the cross-section plane in the range of the interplanar spacing d_{hkl}. Maximum of *S* can be defined as the filling coefficient *Q*.

We calculated reticular density ρ_R for different kinds of Brave lattices and the coefficient *Q* for several crystalline structures of cubic syngony. The Millers indexes situated in decreasing order of reticular density and of coefficient *Q* are presented in table 1. It is evidently, that these series of indexes do not coincide for different crystals with the same lattice type.

The faces with the highest value of coefficient *Q* have the maximum size for grown crystals. For NaCl and FeS_2 these faces are <100>, for CsCl – <110>, for CaF_2 – <111>. For $KA1(SO_4)_2*12H_2O$ the faces with indexes <100>, <110>, <111> are formed. Thus, the calculation of coefficient *Q* allows to determine the largest faces of the equilibrium form for grown crystal.

For all crystals mentioned above the dependence of growth rate *V* on the coefficient *Q* is described by the following relationship:

$$V = C/Q^3,$$

where C is same dimensional constant.

Table 1. The Millers indexes situated in decreasing order of coefficient *Q* and of reticular density ρ_R.

Primitive cubic lattice				Face-centered cubic lattice		
Q			ρ_R	*Q*		ρ_R
CsCl	FeS_2	$KA1(SO_4)_2 \cdot 12H_2O$		NaCl	CaF_2	
110	100	111	100	100	111	111
100	311	110	110	311	100	100
211	210	100	111	331	110	110

[1]. Modern crystallography. V.3. Moscow, "Science", 1980. (in Russian).

[2]. Portnov V.N., Belyustin A.V. Crystal Growth. Gorky, Gorky State University, 1977. (in Russian).

EXPERIENCE IN APPLICATION OF AHP GROWTH METHODS: THEORY AND EXPERIMENT.

Vladimir D. Golyshev

Center for Thermophysical Researches "THERMO" Alexandrov

e-mail: thermo.ltd@relcom.ru; phone/fax (095 584-58-16)

The present work demonstrates the results of long-term, complex, numerical-experimental researches performed in close cooperation with the Russian and foreign scientists and dedicated to a crystal growth method from a melt under conditions of the Axial Heat flux close to the Phase interface (AHP method) offered by the author.

The AHP method was proposed for solution of two problems. The first problem is obtaining of precisely known conditions close to the melt/crystal interface. The second one is growth of large-sized bulk crystals. This problem arose from attempt to accomplish a task on growth of synthetic mica by a method of spontaneous crystallization when the author worked at VNIISIMS. Mica was grown in crucibles about 50 cm in diameter and 100 cm high.

The method was developed to solve two tasks. The first task was to obtain conditions when variations in diameter and length of a growing crystal did not change crystallization conditions. The second one was to find a way at which it was possible to satisfy the requirements imposed by features of mica growth. It was necessary, at large diameters of a crucible, to provide a small overheating of the melt, high temperature gradient in the melt, and to generate conditions for directional growth of spontaneously mica. In the report, the results found in the field of growth of mica are described.

As a result of change of political regime, lack of financing and later on in connection with the market demands, researches into the AHP method were continued at the CTR "Thermo" basically in the field of investigation into fundamental aspects of crystal growth for solution of problems connected with the growth of semiconductors. Realization of these problems was based on a potentiality to control the interface shape, the pattern of melt flows close to the melt/crystal interface, the boundary conditions, and the simple geometry.

The AHP method was employed to study the interfacial kinetics of layered growth; in situ measurement of supercooling; determination of conditions for morphological instability at the interface; to research the correlation between the character of heat and mass transfer and macro- and microhomogeneity in a crystal; to study fundamentals for crystallization of

concentrated alloys when crystallization conditions are determined by concentration fields; to study crystallization features in growth of anisotropic crystals.

Results of these researches are described by the example of some dielectrics and semiconductors. Examples of high accuracy in the description of heat and mass transfer processes are presented too. The problems arising from application of actual experimental boundary conditions for quantitative modelling are described. It has been shown that the scientific basis of the AHP method is developed in general, and the method is a novel step in the field of crystal growth from the melt; and it can be recommended as a benchmark crystallization process.

The researches have also shown that the method is very promising for growth of homogeneous, bulk crystals of different groups of materials, including crystals of concentrated alloys. Prospects for application of the method in space and as alternative to space researches on the ground are under consideration.

The researches in the field of fundamental investigations have been conducted under financial support of the Science-NASA Program; TM4/4 Theme; RSA (Contract No.007, 19978); RFFR (Projects №№ 02-02-17128 and 97-03-32980); CRDF (Projects ##RE1-2233 and RE1-2480); INTAS (Project No. 99-01814 and Project No.2000-263); and also NASA, Project # 98-HEDS-05092. The researches in the field of development the technology for growth of germanium have been supported by the Project of RFTR (code AHP).

PSEUDOSYMMETRY OF CRYSTALS UNDERGOING PHASE TRANSITIONS

V.A. Ivanov, N.V. Somov, M.A.Faddeev E.V.Chuprunov

Nizhniy Novgorod state university named after N.I. Lobachevsky,. N. Novgorod., Russia

The phase transitions of the II sort in crystals are characterized by continuous change of atomic coordinates in a unit cell that is accompanied by change of a space symmetry-group Thus the space symmetry-groups of high-symmetry G^I and low-symmetry G^{II} phases correspond as group - subgroup. As far as contortions of electron density occurring in the process of the phase transitions of the second sort are usually of a small value, the distribution of electron density in asymmetrical phase should be almost invariant concerning the operations of group G^{II}, i.e. the crystal structure of low-symmetry phase should be pseudo-symmetric.

The parameter of the order (η),which takes on the values distinct from zero in low-symmetry phase and equals to zero in high-symmetry phase [1], is set for the quantitative characteristics of the crystal structure changes at the phase transition.

For the quantitative estimation of the invariance degree for electron density function $\rho(\vec{r})$ relating to the symmetry operations $\hat{t}$ can be used a functional [2]

$$\eta_t[\rho(\vec{r})] = \int_0^1 \rho(\vec{r}) \cdot \rho(\hat{t}\vec{r})d\vec{r} \;/\; \int_0^1 \rho^2(\vec{r})d\vec{r}, \qquad (1)$$

that describes the invariance degree for electron density function relating to the operation $\hat{t}$. If the function $\rho(\vec{r})$ is completely invariant concerning the operation $\hat{t}$, then the functional [1] is equal to 1, if not – then $0<\eta_t[\rho(\vec{r})]<1$.

Thus, a crystal in an asymmetrical phase should have high (close to 1) pseudosymmetry concerning the operations of symmetry $\hat{t} \in G^{II}$, $\hat{t} \notin G^I$. The invariance degree of symmetrical phase concerning these operations is equal precisely to 1. Hence, for an estimation of an order parameter η^* it is possible to use value of $1-\eta_t[\rho(\vec{r})]$. It should be noted, that $\eta_t[\rho(\vec{r})]$ characterizes the value of the order parameter independent on whether the order parameter is a scalar, a vector or a tensor.

In [3] there were analyzed series of crystals belonging to the structural type $KTiOPO_4$ (KTP) undergoing the transition of the II sort. It is shown, that in the viewed crystals of the low-symmetry phase $\eta_t[\rho(\vec{r})] > 0.5$ for all symmetry operations of the high-symmetry phase. Thus temperature of a phase transition rises at increase of a symmetry degree $\eta_t[\rho(\vec{r})]$.

The purpose of this investigation is to examine pseudosymmetry of crystals undergoing a

phase transition represented in structural data banks. These banks contained the pairs of crystal structures with the identical chemical formulas and space groups of symmetry, bound by the relation group – subgroup. Besides the diversion of the unit cell's parameters from a multiple relation at the passage through the point of the phase transition should be insignificant (no more than 5%). For sectional structures the necessary requirements for the phase transition of the II sort, or transition of the I sort, close to the second without the change of transmitting subgroup were fulfilled. The invariance degree of electron density function $\eta_t[\rho(\vec{r})]$ was calculated for the low-symmetry structures relating to the symmetry operations appearing in the supergroup G^{II}. The results of the calculations for 495 inorganic structures are represented as a histogram in a fig.1.

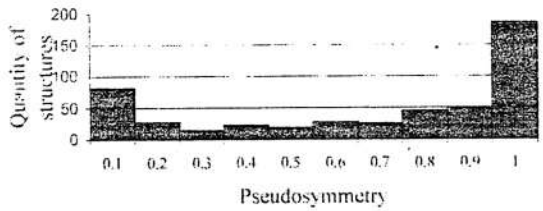

Fig.1. Allocation of explored pairs of inorganic crystals on quantity of pseudosymmetry.

In a databank there was no information about the evidence of the II sort phase transition among the pairs of crystalline structures for which the invariance degree of electronic density concerning the extra symmetry operations has appeared to be below 0.2. We think that in such crystals there is possible phase transition I sort, close to the II sort transition [1].

The similar calculations of pseudosymmetry were carried out for organic structures taken from Cambridge structural data bank, bound by the above-stated conditions. The obtained distribution of the 52 discovered pairs of organic crystals is depicted on fig. 2.

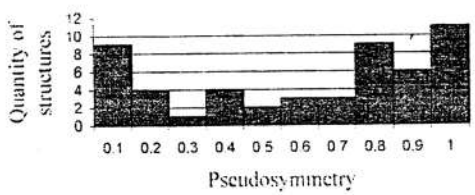

Fig.2. Distribution by degree's value of pseudosymmetry for 52 pairs of organic crystals undergoing the phase transition.

The analysis of crystal structures which pseudosymmetry is close to 1, has shown, that the distinction in a spatial atomic arrangement in both crystals of a pair is insignificant. The difference between the relevant coordinates does not exceed the tenth shares of an angstrom unit, that indirectly points out the existence of II sort phase transition.

Thus, on the basis of the carried out explorations it is possible to state, that the major value of pseudosymmetry concerning the extra operations appearing in the higher symmetry phase is necessary, but insufficient condition for the sectional pairs of crystalline structures to transfer into each other by the II sort phase transition.

The sectional method of the estimation of the order parameter η^* can be used for a prediction of a possibility of the II sort phase transition in crystals. Let the explored crystal have a space group of symmetry G^I. It is clear, that there is a restricted set of space groups G^{II}_i, (i = 1,2, ...), being supergroups for group G^I which the structure can convert into as a result of the phase transition of the second sort. By making the calculations of crystal pseudosymmetry concerning all operations $\hat{t} \in G^{II}_i$, $\hat{t} \notin G^I$ we'll get a set of values η_t. If in a supergroup G^{II} all values of pseudosymmetry η_t will be close to 1, the existence of a modification of an explored crystal, which is crystallized in group G^{II}_i. Thus the modified structure can be connected to the initial phase transition of the second sort. Thus, the proximity to 1 of pseudosymmetry η_t for all operations $\hat{t} \in G^{II}_i$, $\hat{t} \notin G^I$ is probably necessary, though not sufficient to indicate the existence of the phase transition of the II sort.

1. Strukov B. A., Levanuk A.P. // The physical ferroelectric phenomena of the phenomena in crystals. M.: Science. Physmathlit, 1995. 304 p.

2. Chuprunov E. V., KhoKhlov A. F., Faddeev M. A.// Crystallography. M. FM, 2000. 496 p.

3. Katkova M. R., Nosov S. S., Chuprunov E. V., Belokoneva E. L.// Crystallography. M. PM, 2000. V.45. №4. 707 p.

TECHNOLOGY DESIGN FOR CRYSTAL GROWTH FROM AQUEOUS SOLUTION

Boris I. Kidyarov

Institute of Semiconductor Physics SB RAS, Novosibirsk, Russia

A number of requirements have to be met for the successful growth of crystals of useful morphology and good quality from solution [1-2]. Among these requirements, the knowledge of the solubility, the temperature coefficient of solubility, the metastable zone and the nature of the crystal-medium interface are very important. In this report on the base of these empiric data the design of crystal growth technology from aqueous solutions is elaborated.

The studies of the nucleation kinetics of the many lithium, sodium, potash, rubidium, ammonium, cesium and other salts have been carried out particularly by statistical method of many samples in works [1-2]. The general dependencies of the solubility product (SP) and maximum supercoolings ΔT_m (super-solubility) of rubidium 1-1 electrolytes on anionic radii are presented in fig. 1. It is evidently that both dependencies are non-monotonic, and ones are enough similar. The extreme positions also coincide for both curves. But, that is a rare case for 1:1 electrolytes. For all other 1-1 salts these dependencies are not quite similar, and even ones are contrary for lithium salts [18]. It s shown that on a distinct dependence $\Delta T_m = F(SP)$ for rubidium salts these electrolytes are clear divided into two groups on their solubility: 1) parabola with maximum for interval of solubility product «- 2.6 ÷ +1.2» ; 2) parabola with maximum for interval of solubility product «+1.2 ÷ +6». For all other 1-1 electrolytes the dependencies $\Delta T_m = F(SP)$ are indistinct.

The known set of the pair SP- ΔT values for aqueous solution of I-I, II-I and other types of electrolytes is bounded approximately by two direct lines (1-2), fig.2. The certain interrelations into solubility, super-solubility, types of salts crystallisation and possible methods of perfect crystal growth from aqueous solution have been early particularly established [1-2]. At first approximation all salts can be divided into main three parts according to stability of the supersaturated solution:

1. The solutions of the first group (I) have the maximum $\Delta T \sim 85\text{-}110$ °C. Owing to high stability of the supersaturated solutions the crystals of this group can be grown easily from pure solutions by different methods, including accelerated ones (for example KDP) [19]).

2. The solutions of the second group (II) have moderate ΔT ~30-80 °C. In pure solution it is observed usually the growth of imperfect crystals, having many solution inclusions, non-perfect faces, twins. The perfect crystals of this salts group can be grown only in multinary solutions, which contain certain macro- and micro-constituents [4, 16-18].

3. The solutions of III type have the least values of ΔT (7-28 °C). Owing to low stability of these supersaturated solutions the perfect crystals of this salts group can be grown only at precise temperature stabilization ~ 0.01-0.001 °C, or also from multinary solutions [4, 16-18].

In fig.2 the narrow strip (B) along line 3 designate according to Debey-Hückel the ideal solutions ($0 \le q \le 1$, q- extent of non-ideality, $0 \le SP \le 1$). It divide all solutions also into three groups [1-2]. The crystals of salts, which form ideal solutions (B), can be grown more easily, than salts, having low (A), or high solubility (C). Namely the salts, find near line 1, are sleight soluble and we must increase a solubility by addition into solutions certain

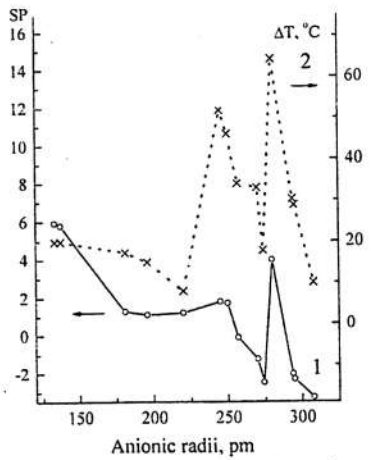

Fig.1. Dependence of the solubility product (SP,curve 1) and the limiting supercooling (ΔT, (curve 2) on the anionic radii for the rubidium salts.

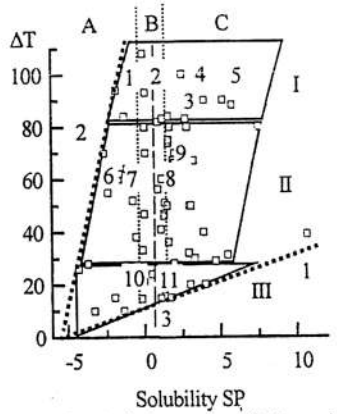

Fig.2. The indistinct set of the pair values of the solubility product SP and the solution super-cooling ΔT (°C) for 1:1 and other salt solution.

macro-constituent. On the

contrary for growth of perfect crystals we must often decrease a solubility of salt, having too high SP (strip C). Thus, the set of all experimental points in fig.2 is separated into

no less than eight-nine characteristic and distinctive sub-fields, in which the conditions for the perfect crystal growth from aqueous solutions can be predict a priory. About 11 examples of the choice of the perfect crystal growth technology are depicted by points 1-11 in Fig. 2 and ones are described particularly in our works [1-2], and works of other authors. So, if we can predict, or estimate **SP** and **ΔT** for different salt solutions, then we can design of crystal growth technology from aqueous solution for novel materials. The investigation results allow predict the crystallization peculiarities of electrolyte solutions, suitable methods and conditions of perfect crystal growth on the basis of known dimensional factors of given salts.

[1] B.I. Kidyarov, J. Korean Crystal Growth and Crystal Technology, 13 (2003) №2, 51.

[2] B.I. Kidyarov, in: Proceedings of the Fifth International Conference "Single crystal growth, heat and mass transfer", in 2 volumes. V.1, ed. V.P. Ginkin (SSC RF IPPE, Obninsk, Russia, 2003) pp.147-155.

INTERRELATION BETWEEN DIAMOND AND CARBONADO

A.B. Makeyev[1], W. Iwanuch[2]

[1]Institute of Geology of the Komi Science Centre of the Ural Division of RAS, Syktyvkar, Russia;

[2]Departamento de Química Fundamental, Instituto de Química, Universidade de São Paulo, Brazil

Fourteen samples of Brazilian carbonado from the states of Bahia (Andarai region), Minas Gerais (r. Macaubas) and Mato Grosso (fasenda Arozsemsal, Nortelandia) were objects of our research. By means of the scanning electron microscope JSM-6400 with the detachable device Link ISIS-300 fragments of metal films (18 kinds) were found both on the surface of carbonado, and inside them as inclusions. They are – Au, Ag, Au-Ag, Sn, Sn-Cu, Bi, Pb-Cr, Fe, Ti, Ni, W, Fe_7Cr, Fe-Ni-Cr, Fe-Sn, Fe-Ni, Ni(Fe,Co), Ni-Cr, W(Fe,Cr,V). Chromatic cathodoluminescence (CCL) of these carbonado samples was investigated. In the collection there were carbonado samples characterizing with CCL of two types. The first type of the cathodoluminescence, which shows a zonal picture of CCL, was observed on a chip of the large carbonado grain, where the colour of zones varies from the centre to the surface of the grain in the following: dark blue – red – green – yellow-green. The same type of zonal CCL as dissemintations of dark blue spots (luminescence of the diamond grains with the size 0.1–0.3 mm) on the green area (carbonado luminescence) was found on the surface of the other sample of Brazilian carbonado from Mato Grosso State. The second cathodoluminescence type is characterized by monotonous azonal and black-orange mottled patterns and is typical for all other samples. The unique phenomenon – overgrowth of rather large (3 mm) plane face octahedral crystal of the diamond by the diamond microgranular unit (carbonado) is found. This find is the convincing proof of relative genesis of carbonado and diamond. There was discovered the face of diamond octahedra that was covered by a thin (0.3 mcm) almost continuous film TiO_2 (rutile) on the chip of carbonado described above with zonal chromatic cathodoluminescence. The film (primarily metal Ti, and then oxidized to rutile) was preserved by the overgrowth of diamond by carbonado. It is one more proof of diamond growth through metallic membranes. The presence of diamond and carbonado together in the same sample was also proofed by the superposition of X-ray luminescence spectra of diamond and carbonado, they are N3 + 520, 575 nm centres. The isotope

composition of carbon $\delta^{13}C$ of studed carbonados (-13.85 – -21.34 ‰) is not adjusted in the interval of variations that are common for Brazilian carbonados. The samples from Minas Gerais State have more lightened isotope composition, than carbonados from the looses of Bahia State. $\delta^{13}C$ of two samples carbonados differ from others by 4-7 ‰ light composition of carbon, which is close to $\delta^{13}C$ of diamonds from eclogites. The inclusion of octahedral crystal of diamond is revealed in one of them. The genesis of carbonado and diamond is closely connected, as their units are known in accretions. Most likely, carbonado crystallizes in kimberlite fluidizate during the transportation of diamonds from the mantle to the Earth crust, and at this time carbonado is able to grow on diamonds.

REFERENCES

Makeev A. B., Iwanuch W., Obyden S.K., Bryanchaninova N.I., Ivannikov P.V., and Saparin G. V. Interrelation of Diamond and Carbonado (Based on the Study of Collections from Brazil and Middle Timan) // Dokl. Earth. Sci. №9. 2003.

DIELECTRIC PROPERTY OF TGS CRYSTALS DOPING BY CO AND CR IN THE PHASE TRANSITION REGION

Malyshkina O.V. and Il'ina E.V.

Tver Stat University, Tver, Russia.

As is known, introduction of impurity during growth of crystals creates in them certain quantity of defects [1], that influences on physical properties of crystals and allows to receive materials with determined properties. The authors [2-4] mark, that the introduction of ions of metals ambiguously influences physical properties of TGS crystals. In the present work influence of ions Co and Cr on dielectric property of TGS crystals in the phase transition region is investigated.

In the given work is shown, that introduction both ions Co, and ions Cr results in reduction of meaning of spontaneous polarization in comparison with analogous meaning for a pure TGS crystal. At the same time the exact concentration dependence is not found out. The double impurity of metals Co and Cr also change meaning of spontaneous polarization, but in this case the meaning of spontaneous polarization both reduction, and increase depending on concentration of impurity in comparison with spontaneous polarization of a pure crystal.

Research of temperature dependences of spontaneous polarization has shown, that temperature of disappearrance of spontaneous polarization, corresponded to Curie temperature, according to the thermodynamic theory, for crystals doping by both ions Co and ions Cr varies about meaning of temperature Curie for a pure crystal. Dependences on concentration in this case is not found out. Introduction of double impurity of metals Co and Cr in TGS crystals results to reduce of Curie temperature in area ferroelectric phase.

In result of research the temperature dependences of the permittivity was found out, that the location of the maximum meaning of permittivity does not depend on concentration of impurity. However the value of a maximum permittivity for doping crystals decrease in comparison with similar meanings for a pure TGS crystal. At the same time distinctly of the concentration dependence is not established.

In work account of internal fields is also made. For this purpose we determined coefficients of thermodynamic expansion in terms of free energy on degrees of polarization (α and β) by temperature relation on reciprocal permittivity and square of spontaneous polarization.

REFERENCES

1. Strukov B.A., Levanjuk A.P. Physics of Ferroelectric Phenomena in Crystals. (Vystaja Shkola, Moscow, 1995) (in Russian)

2. Dabizha T.A., Zharov S.Yu., Korina R.V., Rud'ak V.M. // Ferroelectrics and Piezoelectrics. (KSU, Kalinin, 1981, P.23).

3. Zharov S.Yu.// Ferroelectrics and Piezoelectrics. (KSU, Kalinin, 1984, P.172).

4. Tzedric M.S. Physical properties of crystals of TGS family (depending on growing conditions). (Science and engineering, Minsk 1986.) (in Russian).

INFLUENCE OF EXTERNAL INFLUENCE TO A CONDITION OF POLARIZATION IN A SUPERFICIAL LAYER OF CRYSTALS NIOBATE BARYE STRONTIUM.

O.V. Malyshkina, A.A. Movchikova, B.B. Ped'ko, T.O. Zaznobin
Tver State University, Tver, Russia

The large information of polarization distribution and space charge in surface areas of ferroelectric crystals can be received by investigating frequency dependencies of pyroelectric current. In experiment the frequency dependencies of pyroelectric current were removed by use of modulation of a thermal flow by pulses of the rectangular form in a range of frequencies from 2 up to 400 Hz, that, for crystals of niobate barye strontium (SBN), corresponds to depth of heat penetration in a crystal from 10 ?m up to 180 ?m. The depth of heat penetration in a crystal was calculated by formula: $x = \sqrt{\alpha / \pi f}$, where ? - coefficient of the thermal diffusion, f - frequency of modulation of a thermal flow.

We make the calculation of the coefficient of thermal diffusion on a technique, described by the author's [1]. The value of the coefficient of thermal diffusion for a crystal SBN it equals to 1,9 10^{-7} $м^2/с$.

In the present work the character of distribution of the pyroelectric coefficient in a surface layer of a pure monocrystal SBN and SBN with impurity Cr and Ce was investigated. The measurements were realized on polarized samples and samples, be exposed to a variable electric field ~ 300 V/mm. The poling of crystals realized by effect an electrical field 5 kV/cm in paraelectric phase with further cooling under a field to room temperature. Research of influence the annealing (in air) on character of pyroelectric coefficient distribution in a surface layer of SBN crystals is also made. The annealing in air was made at temperature 200°C. The measurements of pyroelectric coefficient were carried out for the different sides of a sample.

In all polarized SBN samples as with an impurity Cr, and with an impurity Ce, inhomogeneous distribution of the pyroelectric coefficient on a sample thickness is observed. Increase the pyroelectric coefficient in a layer, laying on depth from 30 ?m up to 80-120 ?m (depending on a kind and concentration of an impurity) is found out. Such behaviour the pyroelectric coefficient

means that polarization in this layer more, than near to a surface and in depth of a crystal. Such character of distribution the pyroelectric coefficient can means that the full polarization of a crystal in an external field does not occur. The depth of a crystal remains partially depolarizing. It is not necessary to exclude that fact that the greater meaning of polarization in a layer can be observed at presence near to a surface the volume charge. Results the etching of crystals show, that the surface layer is practically monodomain, whereas deeper etching reveals presence polydomain structure. It confirms the first point of view.

Influence on crystals SBN: Cr and SBN: Ce by a variable electrical field does not result to depolarization of samples, as opposed to pure SBN, in which after the influence of a variable field, pyroelectric response is observed only on the party of a crystal, corresponding to "-" end of a vector of polarization and its value is much less, than at a polarized sample. The great reduction pyroelectric response after influence of a variable field is observed in SBN with a double impurity Cr and Ce too. Research the thermostimulated processes of switching SBN also denotes the essential differences in behaviour of crystals pure and with impurity Cr and Ce.

Research the annealing samples of SBN has shown, that thermal influence results to full depolarization of the doped SBN crystals, they have only small pyroelectric response at heating of one side of a sample on frequencies, large 40 Hz. It corresponds to depth ~ 40 ?m. On a direction pyroelectric current is established, that the polarization in this layer is directed from depth to a surface of a sample. At the same time at a pure SBN crystal, value of the pyroelectric response of the annealing sample correspond to pyroelectric response of the depolarizing crystal, but the direction of polarization with both parties of a sample, is directed from depth to a surface.

It is shown that the laws of a passing of thermal effect Barkhausen much depend on external influence.

REFERENCES

1. A.A. Bogomolov, N.N. Chereshneva, T.A. Pashina, S. Lang // Ferroelectrics and Piezoelectrics. (TSU, Tver, 1993, P.79).

GROWTH RATE OF ROCHELLE SALT FACES IN THE PRESENCE OF THE CU^{2+} IONS

Vorontsov D.A., Kim E.L., Portnov V.N., Chuprunov E.V.

N.Novgorod State University, N.Novgorod, Russia

The impurities influence on the crystal growth has been studying due to the depending of the mechanism of growth and properties of the crystals on the composition of crystallirable substance [1].

Results of measurements of the growth rate of Rochelle salt crystal faces on balls on the $CuCO_3$ concentration in solution and their morphology features are discussed.

The shape of growth rate curves for {001}, {210}, {110}, {100}, {011}, {120}, {101}, {021} faces can be interpreted on the basis of Bliznakov equation with Langmur, Frumkin-Fauler and De Bur isotherms. The best description is obtained with the use of De Bur isotherms. For all curves the equal meaning of adsorption constant is obtained, taking into account the interaction each other of the adsorbed particulars.

The analogues effect is due to $CuC_4H_4O_6 \cdot 3H_2O$. The more strong impurity effect, similar to [2], is observed for the alkali addition in solution.

The photometry of Rochelle salt solutions with Cu-tartrate gives the optic density curve enlarging with wave length increasing. Supplementary addition of NaOH causes the maximum of optic density for 640 nm. This is evidence of complexes $Cu(OH)_6^{4-}$ or $Cu(OH)_4(H_2O)_2^{2-}$ presence [3]. These changes in Rochelle salt solution with NaOH are also fixed in the EPR-spectra. In [4] was shown, that Cu-ions are built into Rochelle salt crystal lattice in the Na-ions position. It may be presumed, Cu-complexes being adsorbed on to crystal faces affect the growth rate, but after that they are dissociated on the growing surface and incorporated into the crystal at another form.

The morphology of {001} and {210} Rochelle salt faces was investigated by AFM. The {001} and {210} faces of crystal, grown from pure solution, are smooth. The dislocation sources were detected. Impurities disturb perfect growth, and the faces of the crystal, grown from impure solution, are consisted from macrosteps of about 5-10 nm on the {001} surface and 20-40 nm on the {210} surface.

[1]. Rashkovich L.N., Kronsky N.V. // J. Crystal growth. 182. 1997. P. 434-441.

[2]. Belyustin A.V. Crystal Growth. V.4. 1964. M., P.10-14.

[3]. Buketov E.A., Ugorets M.Z., Ahmetov K.M. Dehydration of the metals hydroxides in the alkali solutions. Alma-Ata: "Science". 1971.

[4]. Vökel G., Windsch W. Phys. Stat. Sol. V. 17. No. 1. 1966. K.75-78.

PROBLEMS OF MONOCRYSTALS GROWTH IN SYSTEM $TB_2O_3 - GA_2O_3$.

Chemekova T.J., Belousova O.L., Udalov J.P., Rahmankulov R.M.

Institute of chemistry of silicates of the Russian Academy of Science, S-Petersburg

E-mail: chemekova@mail.ru

Occurrence metastaible phases complicate process of crystallization garnet and perovskite structures in systems $Ln_2O_3 - Al_2O_3$ and $Ln_2O_3 - Ga_2O_3$. Steady growth of monocrystals of aluminates and gallates REM is caused as thermal characteristics melt and a crystal and the processes proceeding in melt and at the front of crystallization.

In the present work dependence of stability of growth Tb - Ga a garnet from contents Ga_2O_3, from change of a thermal mode, replacement Tb^{3+}on Y^{3+}, Al^{3+}, Ca^{2+} was investigated. Crystals were raised by Chohralsky method from own melts. Drawing and rotation rates were 3 - 12 mm / h and 8 - 50 rev/min respectively. At stoichiometric composition in this case growth of crystals is unstable structure $Tb_3Ga_5O_{12}$. Evaporation gallium oxide from melt caused of its introduction much in initial mixture in amount from 2 up to 6 wt%. For the compositions containing a lot of 4 wt% Ga_2O_3 transparent monocrystals in diameter of 12 mm and by length 25 mm were received at drawing rate 7 mm / h and rate of rotation 50 rev/min, with a direction of spontaneous growth <211>. Application микрорентгеноспектрального the analysis has allowed establishing that in conditions of experiment ions Ca^{2+} and Y^{3+} do not enter into a lattice of crystals. And in formed firm solutions there is a replacement of a part of ions Ga^{3+} on Tb^{3+}in octahedral positions. Garnet phase in system $Tb_2O_3 - Ga_2O_3$ has the formula $\{Tb_3\}[Ga_{2-x}Tb_x]Ga_5O_{12}$. A phase with perovskite structure $TbGaO_3$, found out only in high-temperature area, has incongruent melting point at 1860°C.

CAPACITOR METHODS OP MEASUREMENT OP ELECTROST A TIC CHARGES AND FIELDS

Michaylov B.A. , V.P. Pronin

Measurement of electrostatic charges and fields, created by them, is made by a method of an electrostatic induction, which is realized by means of various instrument modifications or without transformations of charge induced in circuits of measuring electrodes into an electric current,or with applicatiolJl of parametrical transformation.

Methods and means, intended for measurement of general charge, distributed in comparatively large volume (integrated) and methods allowing to locate area of measurements ир to a share of mm^3 are distinguished. In the latters the parametrical transformation is used, as the charge induced on measuring electrodes is insignificant, especially at density of a charge in object 10-7 - 10-8 coulomb. To increase the sensitivity one should sacrifice resolution.

The features of methods and also basic circuits and designs of devices, intended for panoramic measurement of distributions of density of surface and volumetric charges in layered structures with the linear resolution about 0,1 mm ary considered.

It is shown, that the creation of methods of absolute measurements of a charge is connected with taking into account electrophysical parameters of material. It is possible only with the help of multiparametrical electrocapacitive systems, in which in the area of measurements additional quasi-static periodically varied fields within a frequency range, where dielectric permittivity is constant, are excited. These fields are modulated by low frequency of transformation of induced charge into variable electrical signal or at the expense of changing of distance from measuring electrode (probe) ир to a researched surface on harmonic law, or owing to noncontacting scanning of researched material. Then selection of signal at excitation and modulation frequencies is made. They contain information about diel_ctric permittivity and geometrical parameters and solution of set of equatiolls, made with taking chosen mathematical model into account.

The primary applications of various updatings are considered.

ELECTROCAPACITIVE DEFECTOSCOPY OF DIELECTRIC

Michaylov B.A. V.P. Pronin

Defectoscopy of dielectric, high-resistance semiconductor and composite materials occupies the special place at the control of uniformity of electrical properties of materials and quality of let out production at all stages of its manufacturing, as widely used electromagnetic, acoustic, radioscopy and other methods are intended, basically, for the control of metal products and, as a rule, are unsuitable for research of wide class of sealing materials.

For this purposes the application of electrocapacitive methods allowing to define naturally electrophysical and geometrical parameters of object is most perspective.

Concept of electrocapacitive methods is rather wide, but as a rule integral .
definitions of capacity connected directly with dielectric permittivity, conductivity and geometrical factors, and also indirectly with other physical characteristics of materials, structure, humidity, ageing, filler distribution etc. are considered, it being known that area of averaging of measured quantities is rather great - units of square centimeters and more.

The decision of other classes of problems is connected with the development of various areas of physics and engineering, in particular, electrophysics,microelectronics, physics of semiconductors and dielectric, original ways of record and transformation of the information. For this purpose the methods and means ensuring noncontacting nondestructive measurements of parameters of materials with averaging on respectively small area (from units of sq. mm to hundreds of sq. micron) are required and basic characteristics determining metrological qualities of eletrocapacitive systems are sensitivity and resolution. However to define these characteristics within the framework of traditional approaches is difficult, but in this work these questions are generally solved.

Stillarge infonnation on distribution of electrical properties in materials can be received as a result of study of panorama processes of accumulation and relaxation of a charge in them under influence of various external factors - temp erature , electrical field, electromagnetic radiation and others. 1 t is achieved in the result of uncontacted scanning of a researched surface by a probe ensuring necessary sensitivity and spatial resolutioll.

Stilllarge infonnation on distribution of electrical properties in materials can be received as a result of study of panorama processes of accumulation and relaxation of a charge in them under

influence of various extemal factors temperature, electrical field, electromagnetic radiation and others. It is achieved in the result of uncontacted scanning of a researched surface by a probe ensuring necessary sensitivity and spatial resolution.

Such approach allows to solve many problems, connected with dielectric electrolyzing under action of electrical fields and to investigate features of

thennostimulated polarization and depolarization of various materials, and also solve engineering tasks of realization of unique, but rather simple designs, intended both *for* perfonnance of scientific researches and use in industrial manufacture *for* the control of uniformity of physical properties and geometrical parameters with linear resolution about 0,1 *mm.*

The authors showed that electrocapacitive systems, the part of which is researched dielectric, semiconductive and composite material, naturally reflect changes in its parameters through an electrical signal, induced in circuit of measuring electrodes of a probe.

The . various modifications of electrocapasitive methods are based on excitation of quasi-static electrical field in researched object, or owing to action of an extemal voltage between electrodes, or at the expense of creation of the injected electrical charge on a surface and in volume or by using both of these methods. .

The devices created on the basis of electrocapacitive systems allow to effectively detine uniformity of electrical properties of materials and to carry out scientific researches connected with studying distributions of an electrical charge, practically inaccessible to other wellknown methods.

Electrocapacitive systems *for* panoramic defectoscopy of materials are applied in a wide range of the thickness and electrical parameters changes, however their sensitivity and resolution are antagonistic relations.

Panoramic defectoscopy of materials is based on studying relaxation and accumulation of charge process as a result 6f thennostimulated depolarization and polarization, and also injected charge relaxation under room temperature and by means of excitation of longitudinal or a cross to a layer quasi-static electrical field varied, *for* example, on harmonic law.

INFLUENCE OF LITHIUM NITRATE ON THE CHARACTER OF SECONDARY PHASE MINERAL FORMATION DURING INDUSTRIAL SYNTHESIS OF QUARTZ.

Smirnov A.A., SobolevaT.V., Dikk E.V., Belimenko F.A

Russian Research Institute for the Synthesis of Materials

Lithium nitrate admixtures added into working solution for growing improve the piezo-optical properties of quartz. However, the output of the special-quality crystals is reduced because of the high quantity of solid inclusions in some cases. In 2001-2003 VNIISIMS' scientific workers suggested the technologists of the pilot plant to decrease concentration of the lithium salt impurity admixtures and to reduce it depending on the autoclave-sets to 0.35 –0.80 g/l. It is to ensure stability of growing the high quality blocks and to decrease intensity of decoration using admixture elements of growth dislocation.

Nowadays there is no clear view of the lithium nitrate admixture action mechanism. However, such admixture is widely used when quartz is grown and it also has an effect on quartz quality. If Li^+ ions and especially $LiNO_2$ are available, the concentration of H^+ ions in quartz is to reduce more than in 5 times. In spite of this the high content of lithium is not detected. In Mr. Lodiz's opinion, $LiNO_2$ is adsorbed onto the surface of the growing crystal. They are not caught by crystal itself and don't pass H^+ or OH^+ ions but it allows to improve the piezoelectric properties of quartz [l].

Two groups of minerals formed from solutions at the direct and parallel- serial reactions were chosen among 5 paragenetic mineral associations fixed previously by the authors [2]. It may be found in solutions as suspension and at certain conditions selectively be captured by quartz crystals.

It should be critical (sufficient) concentrations of different metal (Li, Fe, Ca, Al) impurity ions at the direct reactions in solutions. Independent mineral phase can crystallize with the assistance of such ions. Among minerals emeleusite, aegirine, spodumene, kvanefjeldite and quartz microcrystals are the most wide-spread. They have ideal faceting in the form of single crystals in one-hundredth and one-thousandth mm. Diverse-microwavy aggregates of clinoholmquistite, merrihueite, sugilite, which don't influence on violation of synthesis process also form in distinctly subordinate amount.

During parallel-serial reactions primary mineral phases form from solution first, and then they are transformed in another minerals. These minerals form polymineral "flaky"

threadlike-microgranular aggregates.Term "flaky allocations" used by different researchers during few decades in the studying process of solid inclusions in quartz, but its composition and structure weren't studied. Allocations of these minerals make up amoeba-like forms with jagged edges and have sizes from few micrometers to first millimeters. They are diagnosed by microscope observation in preparations, when they have sizes more then 2-3 micrometers.

Mechanism of its formation can be explained in the following way. Foliation (silica polymerization) with atomized (<1-2 mm) hydrogel formation takes place in very concentrated alkaline-siliceous solutions. These high-porous colloids can absorb big amount of Fe and Ca impurity ions and later form consistent range of mineral phases. Mechanism of this process is viewed in work [3]. As a result of such reactions "flaky" polymineral aggregates of alternating composition arise: threadlike-microgranular aegirine + kvanefjeldite + clinoholmquistite + quartz microcrystals + relict solid gels. When lithium concentration in solution is high, these formations are partly or completely replaced by emeleusite, which constitute aciniform aggregates. Single minerals with plane-parallel faces and microsizes can be pressed to growth surface of crystal for a long time by solution stream. As a result of such process obliteration of single crystals by crystallizable layers of quartz takes place. The most part of "flacky" aggregates doesn't capture by growing face [3].

Preliminary research about lithium nitrate role showed the following results:

As a whole optimal additions of lithium promote to quartz quality improvement. The main defects in quartz crystals are conceived, when vessel is put into operation as a result of solid mineral phase depositions on the seed plates, which become the source of linear optical heterogeneity origin (growth dislocations, "perforetions", twin formations, "blue" threads, rays). Emeleusite is predominant mineral among solid inclusions. Some scientists of VNIISIMS consider that, when autoclave optimally put into operation (without abrupt fluctuations in power), emeleusite, falling on the seed plate, is distributed as superfine layer, which consists of smallest isometric crystals, which obviously aren't the source of growth defects in quartz.

Lithium residual amount in "heavy" phase and on vessel sides, remained from previous cycles wasn't taken into account during emperical calculations of optimal additions of lithium reagents. Due to this lithium content in the following cycles considerably increases.

The main role of lithium nitrate "optimal" additions lies in the following. According to our calculations millions of emeleusite smallest crystals are formed, when vessels are put into operation. This mineral contains about 2,5 mass % of Li_2O and 12,0 mass % of Fe_2O_3. So,

abrupt decrease of ferrum ions in solutions takes place during emeleusite formation. It obstructs to aegirine crystallization due to direct reactions. Lithium, which remains after emeleusite formation promotes in some cases to formation of the other plane-faceting minerals, which can be captured later by growing quartz and worsen qualitative caracteristics of crystals.

Research of the lithium nitrate influence on quality of synthetic quartz crystals should be continued. It is necessary to correlate data of x-ray topography with specific content and solid inclusion deposition form on the seed plates. First of all these depositions on the seed plates determine the quality of growing quartz crystals.

References:

1. Lodiz R., Parker R. Single crystal growth. M., Mir, 1974, p.540.
2. Smirnov A.A., Soboleva T.V., in "Crystals: growth, properties, real structure, application". 5th Intern. Conf. (Alexandrov, VNIISIMS, 2001), pp. 86-88.
3. Smirnov A.A., Soboleva T.V., Sopeleva E.G., in "120 years from academician A.E. Fersman's birthday", M., 2003, p. 108.

SOPHISTICATION OF STRUCTURE OF MULTICRYSTALLINE SILICON – INCREASE IN THE QUALITY OF THE SUBSTANCE FOR THE SOLAR ENERGY

B.A. Krasin, A.I. Nepomnyaschikh

Vinogradov Institute of Geochemistry, SB RAS, Irkutsk, 664033, fax 8 (3952) 42 70 50, phone 8(3052) 5114 66, E-mail: krab@igc.irk.ru

Geometrically ideal column structure of profiled silicon as a set of rectilinear monocrystalline pivots is not available in nature. In fact we deal with the complicated spatial ratios of voluminous neighboring crystallites with their total column direction. Our studies of multicrystalline silicon allow revealing some indices of those ratios, their significance as a substance and what is the most significant to obtain the perfect structure in the growing process.

In the macroscopic studies of longitudinal and traverse cross sections of multisilicon ingot we evaluated the following indices:

- Size of crystallites from the beginning to the end (longitudinal cut piece) and correspondingly size of grains (traverse cut piece)
- Inclusions of neighboring crystallites with the deformation of intergrain boundaries
- Break of monocrystalline growth of crystallites
- Appearing of additional chambers of crystal growth including those with sharp change of growth direction

During the microscopic investigations we have evaluated the following indices:

- Polycrystalline density (an indirect characteristics of grain size);
- Change of the crystallographic orientation of neighboring crystallites;
- Features of degrading of monocrystalline growth (dislocations, deformations of intergrain boundaries, extraneous inclusions in crystallite blocks, break in crystallite growth).

To obtain a more perfect structure of multisilicon during the growth using Bridgmen-Stockbarger method we investigated the morphological parameters of the ingot: a) location of the growth zone in the ingot; b) shape of crystallization front (flat, convex, concave); c) direction of column growth of crystallites (along the vertical axis, from walls of crucible towards the radial location); d) start of column growth and rates of their growth; e) monocrystalline areas at the beginning of growth and transitions into column structure in comparison with data of temperature distribution along the axis of heater, temperature

gradient in the growth zone, width of hot zone, location of the crucible with the charge and melt in the heater's field and other conditions of growth (rate of growth, rate of axial rotation, regulating of the heat protection of heat transfer for the upper stock of the container with the charge and melt).

The influence of the above indices of the structure on the electrophysical features of the material is ambiguous. The most significant parameters include crystallite size, break of monocrystalline growth and additional chambers of growth of crystal with the wide-angle deviation. The degradation of the monocrystalline growth also decreases the quality of the electrophysical material. However, the degree of influencing the degrading is different (e.g. number and pattern of dislocations in the body and on the boundaries of the crystallite or inclusions in crystallite blocks of different admixture elements).

As a result the method of obtaining the multisilicon ingot with wide (almost from the beginning of the crystallization) monoblocks and direct intergrain boundaries has been developed. It is based on the application of crystallographically oriented charge of monocrystals on the flat crucible's bottom in temporal adiabatic system ("cold bottom") and for the stable and continuous growth of monocrystallites – ensuring the isothermal character of the system with an optimal growth rate.

Работа выполнена в рамках интеграционного проекта СОРАН № 178

PRESSURE-INDUCED PHAS TRANSITIONS, ELECTRICAL AND SPECTRAL PROPERTIES OF MOLECULAR CRUSTALS OF [60]FULLERENE COMPLEXES.

N.G. Spitsina[1], A.A. Lobach[1], I.V. Kondratieva[3], I.V. Bashkin[4]

[1]Institute of Problems of Chemical Physics RAS, 142432 Chernogolovka, Russia

[2]Russian Chemistry Tehnological University by D.I. Mendeleev, Moscow,Russia

[3]MGU by F.I. Lomonosov, Moscow, Russia

[4] Institute of Solid State Physics RAS, 142432 Chernogolovka, Russia

We have studied the single crystals of pristine C_{60} and its molecular complexes with organic donors bis(ethylenedithio)tetrathiafulvalene (BEDT-TTF or ET) and tetramethyltetraselenafulvalene (TMTSF) by means of ESR, IR and Raman spectroscopy at high pressure. The important changes in the ESR signal of C_{60} have been observed under axial pressure combined with shear deformation. It is shown that the treatment at anisotropic pressure 4 GPa results in symmetry lowering of the C_{60} molecule and formation of radicals. The Raman spectra of the molecular complex C_{60}•TMTSF•2(CS_2) have been measured *in situ* at pressure up to 9.5 Gpa and ambient temperature. The pressure behavior of Raman peaks reveals singularity at 5.0 ± 0.5 GPa related to the softening and splitting of some of phonon modes. The residual softening of the $A_g(2)$ mode is the same as in a case of KC_{60}, which may be an indication that the transition has a charge-transfer character, resulting in the formation of the C_{60}^{-1} anionic state charge-transfer complex.

For the polycrystalline samples of the $ET_2 \cdot C_{60}$ molecular complex, the electric conductivity was measured in dependence on pressure to 7 GPa at temperatures of 20 and 150°C. At room temperature, the electric conductivity increased following the logarithmic law. The data measured at 150°C showed a break of the slope in the lg$R(P)$ curve around 4.5 GPa, which is usually an indication of a phase transformation in the sample.After the high-pressure experiment, the IR spectra were measured at normal conditions as well as the grain structure was studied using the electron microscopy and the chemical composition was characterized by means of the X-ray photoelectron spectroscopy.The data obtained demonstrated that the high-pressure treatment at 150°C leads to decomposition of the molecular complex, precipitation of the ET grains and the C_{60} polymerization. A comparison of the IR spectra of the sample treated under pressure at 150°C and refined from ET using the CH_2Cl_2 solvent with IR spectra of the C_{60} polymeric phases showed the best correspondence to the dimer spectrum.

Acknowledgments. This work was supported by the Russian Foundation for Fundamental Research, grant 02-03-33218.

SYNTHESIS AND INVESTIGATION OF HYDROXYAPATITE/CELLULOSE NANOCOMPOSITE

Ejova J.A., Koval E.M., Zakharov N.A., Kalinnikov V.T.

Kurnakov Institute of General and Inorganic Chemistry RAS,

Leninskjj pr., 31, 119991, Moscow, RUSSIA

E-mail: zakharov@igic.ras.ru, (095) 955-48-84, (095) 954-12-79

Calcified tissue, such as long bone and jaw bone, is considered as a biologically and chemically bonded composite between hydroxyapatite $Ca_{10}(PO_4)_6(OH)_2$ (HA) nanocrystals and biopolymers.

We have succeeded to develop a chemical coprecipitation processes to production of biocompatible nanocomposite materials, in which inorganic filler (HA) is dispersed within the polymer matrix on a nanometer scale [1,2].

The method of HA/cellulose nanocomposite preparation is based upon investigation of systems $CaCl_2$-$(NH_4)_2HPO_4$-NH_3-H_2O-cellulose, $CaCl_2$-$(NH_4)_2HPO_4$-NH_4 HCO_3-NH_3-H_2O-cellulose with constant concentration of $(NH_4)_2HPO_4$ and relation in starting stacks Ca^{2+} : PO_4^{3-} = 1,65-1,67.

The formation of HA/cellulose nanocomposite were confirmed with chemical analysis, IR-spectroscopy, X-ray analysis, scanning electron microscopy. It was demonstrated the production of nanocrystallites of HA and investigated the influence of stock composition on the formation and dimension of nanocrystallites. The existence of nanocrystallites dimensions (about 20 nanometer) was estimated on the base of diffraction lines width determination.

We acknowledge the financial support from Foundation of Presidium of Russian AS (Fundamental sciences to medicine; Synthesis of substances with specified properties).

[1] Ejova J.A., Koval E.M., Orlovskii V.P. The conditions of calcium carbonate hydroxyapatites formation and their association with sodium alginate// Jurnal neorganicheskoi chimii (rus.). 2002. V.47. № 8. P.1246-1251.

[2] Ejova J.A., Koval E.M., Orlovskii V.P. Synthesis and investigation of calcium carbonate hydroxyapatite/collagen biocomposites// Jurnal neorganicheskoi chimii (rus.). 2003. V.48. № 2. P.334-337.

IN SITU MEASUREMENTS OF THE INTERFACE SUPERCOOLING DURING MELT CRYSTAL GROWTH OF THE DIELECTRICS: CURRENT STATE AND PROSPECTS FOR THE FUTURE.

Bykova S.V., Golyshev V.D., Gonik M.A., Tsvetovsky V.B.

Center for Thermophysical Researches "THERMO", Alexandrov, Russia, Institutskay St.1,

Faceted growth is characteristic for a wide range of single crystals of dielectrics, growing from a melt. Determination of kinetic dependence $V=F(\Delta T)$, where V is the growth rate of a crystal and ΔT is facet supercooling, is very important for interpretation of the layered mechanism of interfacial kinetics and technological advancement for growth of crystals. To measure ΔT, a new *in situ* method based on measurement of the interface brightness temperature, T_b, with an optical pyrometer through a growing crystal was offered [1-3]. The procedure is developed for media having an opaque melt and transparent crystal at the wavelength of the pyrometer. Our investigations were conducted for $Bi_4Ge_3O_{12}$ and $Bi_{12}GeO_{20}$ crystals. These crystals were chosen due to successful combination of melt and crystal absorptivity, α. So, for the $Bi_4Ge_3O_{12}$ melt, $\alpha > 200$ см$^{-1}$ and for the $Bi_4Ge_3O_{12}$crystal, $\alpha < 0.03$ см$^{-1}$ [4]. In accordance with the proposed method, ΔT is found from the equation: $T_b^m - T_b^v(t)$, where T_b^m is the brightness temperature measured in the absence of growth and corresponding to the melting point; $T_b^v(t)$ is the brightness temperature at the growth rate V corresponding to the temperature of the supercooled interface, t is time of crystallization. As a result of *in situ* measurement, the dependence of $\Delta T(t)$ is found.

To measure the $T_b^v(t)$ dependence and then to obtain the $\Delta\Delta$ *(t)* dependence, two specially designed optical pyrometers are used. One of them is a double-beam pyrometer with a measuring spot 1.2 mm in diameter (measurement of maximum supercooling) [5]. The second is a pyrometer for simultaneous measurement at 20 points situated within 1.1x20 mm line at the interface (measurement of supercooling distribution along the interface) [6]. The pyrometers have sensitivity more than 0.1K at a level of 1100^{0}C. A standard pyrometer ЛОП-72 with a measuring spot 8 mm in diameter (measurement of average supercooling) was also used. Crystallization during in situ researches of $\Delta\Delta$ *(t)* is conducted with a growth method called as the Axial Heat flux close to the Phase interface (AHP method) [7]. Two crystallization procedures have been used. First one was a decrease of temperature at boundaries of the melt/crystal system; second one was a pulling of a crucible into the cold zone. Application of AHP method allows to use with high accuracy methods of numerical simulation for definition of $V(t)$ dependence. Then, comparison of the calculated dependence $V(t)$ with the experimental dependence $\Delta T(t)$ is done to determine the kinetic dependence

$V=F(\Delta T)$. For numerical determination of $V(t)$, specially developed numerical methods are used [8,9].

In the present work, sources of inaccuracy for dependences of $\Delta T(t)$, $V(t)$ and $V=F(\Delta T)$ are analyzed; estimations of errors for the measured supercooling $\Delta T(t)$ calculated by the simplified one-dimensional model of radiation heat transfer in a semitransparent crystal are presented; features of different numerical models applied for determination of $V(t)$ are considered. Data obtained on $V=F(\Delta T)$ for different facets of $Bi_4Ge_3O_{12}$ are presented and preliminary data on supercooling distribution along the interface during crystallization of $Bi_{12}GeO_{20}$. Experimental and numerical methods to correct experimental data on supercooling for elimination of errors are proposed. Application of laser radiation for local impact on a small part of the interface is discussed. Measurement of distribution of ΔT has shown that the method is very promising not only for determination of layered growth fundamentals but it can also be employed in future as a new technique for control and monitoring the crystallization process.

The work was supported in part by INTAS Project No. 2000-263 and in part by RFBR Project № 02-02-17128.

1. V.D. Golyshev, M.A. Gonik, V.B. Tsvetovsky, Instruments and Experimental Techniques, 41, p 735, 1998, (Translated from Pribory i Tekhnika Eksperimenta, No. 5, p 153, 1998).
2. V.D. Golyshev, M.A. Gonik, V.B. Tsvetovsky, Ya.V. Vasilev, and V.N. Shlegel, J. Cryst. Growth, Vol. 216, pp 428-436, 2000.
3. V.D. Golyshev, M.A. Gonik, V.B. Tsvetovsky, J. Crystal Growth, Vol. 237-239, pp 735-739, 2002.
4. Golyshev, V.D. and Gonik, M.A., Vasilev, Ya.V. and Shlegel, V.N., J. Crystal. Growth, 262 (2004), 202-211.
5. Golyshev V.D., Gonik M.A.// Cryst. Prop. Preparation. 1991. V. 36-38. P. 623
6. S.V. Bykova, V.S. Dozhdikov, V.D. Golyshev, M.A. Gonik, V.A. Petrov, V.N. Senchenko, V.B. Tsvetovsky, Book of Abstracts of Xth Russian Conference on Thermophysical Properties, Kazan, 30 September – 4 October, 2002, pp 54-55.
7. V.N.Senchenko, V.S.Dozhdikov, D.I.Kapustin, V.D.Golyshev, 2004, to be published.
8. S. V. Bykova, V. D. Golyshev, M. A. Gonik, V. B. Tsvetovsky, at all, J. Crystal Growth, (266), 2004, 246-256.
9. S. V. Bykova, V. D. Golyshev, M. A. Gonik, V. B. Tsvetovsky, at all, J. Heat and Mass Ttransfer, 2004 (to be published).

COMPUTERIZED PARAMETRIZATION OF STRUCTURES USING THE CONCEPT OF MULTIFRACTALS

V.U.Novikov, E. M. Eybatova

Moscow State Open University, 22, P.Korchagin st. Moscow, 129805, Russia.

e-mail: vknovik@rol.ru

It has been worked out the procedure of multifractal parametrization of structure materials and production program that permits the determination of fractal dimension characteristic connected with mechanical properties. It has been shown that multifractal analysis reveals high information capacity in the studies of structure materials of various nature.

INTRODUCTION

Much attention is given recently to the fractal analysis of structures in materials that undergo self-organization under various conditions [1-3]. However, in real physical systems self-similarity of structures occurs only over a limited scale, thus calling for the application of a multifractal approach. In this case the fractal measure is represented by interconnected fractal subsets which change following power functions with different exponents [3], meaning that the set we study is structurally uniform and comprises subsets differing in their fractal dimensions. Accordingly, sets of such kind became known as multifractals. The limitations of fractal analysis in the investigation of physical objects (such as metal fracture surfaces) demonstrated earlier [4] suggested the introduction of the characteristics of fracture structure related to the mechanical properties [4-8].

1.PROCEDURE FOR PARAMETRIZATION OF A MULTIFRACTAL SET OF LINES

The fundamentals of computerized analysis of multifractal structures have already been discussed [1-3].The analysis of multifractal characteristics of a two-dimensional structure involves representing it as a population of zeros and unities since each structure element can assume but two possible values corresponding to one bit of information. In order to convert 256-colour image into a monochrome version, the file in question (graphics BMP-format, 512x512 pixels) was loaded into the videomemory of PC. Further, the current range of shades was adjusted so as to fix the required threshold level of grey. Then all shades having an intensity of grey equal to or less than this level were taken is black, all shades exceeding

this level – as white. The monochrome image copied then to the on-line storage represented a two-dimensional array of 512x512 bytes that characterized the given structure.

It is apparent from the following expression [3]

$$\tau(q) = - \lim_{\delta \to 0} \frac{\ln N(q,d)}{\ln \delta} \qquad (1)$$

that the mass index $\tau(q)$ is the derivative of the functional relationship: logarithm of the weighted number of cells N(q,d) versus logarithm of cell dimension δ. As applied to the given procedure, the values of $\tau(q)$ were found in the following way. The structure studied was superposed with sets (2, 4, 8, 16, 32, 64, 128,256) of square cells with side δ_k (k=1, … 8). The characteristic function N(q,d) was calculated for each set as the normalized number of points occupied by the given set in a given cell, then summed up over all cells for given k. The normalizing basis was the total number of cells of the same colour constituting the given set. These calculations were made for all k=1,…, 8 and the dependence $\ln\{N(q,d)\}$ versus $\ln(\delta_k)$ was plotted. Then the least squares procedure yielded the slope which actually was the index of mass τ for the given q. Similar calculations for all q in the range from –40 to 40 in steps of 1 were conducted and the dependence $\tau(q)$ plotted. Finally, the following formulas

$$\alpha(q) = - \frac{d}{dq}\tau(q), \qquad (2)$$

$$f(\alpha(q)) = q\alpha(q) + \tau(q) \qquad (3)$$

were used to calculated f, α and D for each q. The dependence $\tau(q)$ became the basis for determining the spectrum of Reniy dimensions. The measure offered in the algorithm considered here is the area covered by points of one of the two possible colours (black and white), so the initial 256-colour format image had to be converted into a monochrome image. This operation caused a loss of information since a three-dimensional relief was substituted by a planar image.

2. METHODICS FOR MULTIFRACTAL PARAMETRIZATION OF COMPACT AGGREGATED STRUCTURES

This procedure involves the analysis of not a monochrome image, as in the previous case, but rather of the initial 256-colour image of the structure, the intensity of the shade of grey in each image pixel being interpreted as the "depth" or the distance to the observer's eye. The

darker regions with lesser intensity of grey correspond to more distant surface points of the structure studied, whereas the brighter regions correspond to points that are closer to the observer. Thus, the surface of the structure of the structure studied appears to be "immersed" in a layer with a "depth" of 256 arbitrary units each of width correlates with one shade of grey. With the measure reference tending to zero, this surface reveals fractal (multifractal) properties.

In developing this procedure we applied the main principles of the formalism described above. The necessary condition was that the structure studied (surface in the three-dimensional Euclidean space) is covered with a set of elementary parallelepipeds, their bases represented by squares with sides δ_k = 2, 4, 8, 16, 32, 64, 128, 256 shades of grey corresponding to each δ_k. The characteristic function N(q,d) was calculated by summing up over all the cells filling out the 512x512x256 parallelepiped, normalizing was conducted in relation to the total number of image points (512x512), and values of f, α and D were found for each q in the range from –40 to 40. Then we determined the relationship $D_q = f(q)$ and the surface area S of the structure studied expressed in arbitrary units: "size of image pixel per unit shade of grey".

3. COMPUTERIZED PARAMETRIZATION OF GRANULAR AND AGGREGATED STRUCTURES

A photomicrograph of the structure of a material is scanned and converted into a graphical BMP-format file. Much attention is paid to the selection of resolution because the resulting image must include an element sized 512x512 pixels covering the largest possible area. The dependence D(q) produced by computerized analysis of the structure permits the determination of the spectrum of Reniy dimensions: D_0 – characterizing a uniform fractal; D_1 – the informative dimension; D_{40} and D_{-40} characterizing the degree of surface looseness (maximum for D_{40} and minimum for D_{-40}). The difference $\delta_s = D_1 - D_{40}$ (or else $\Pi_c = D_0 - D_{40}$) describes the latent ordering of the structure.

We conducted multifractal parametrization of the granular structure of nonmagnetic austenitic Mn-Ni-Cu-V-C steels varying in Cu/Ni ratio from 0.05 to 0.9 [9]. The dependence of the parameter δ_s on the Cu/Ni ratio was determined, as well as the correlation between the cold brittleness temperature t_{K1} and parameter δ_s. It is obvious that the equality $\delta_{s1}^{max} = \delta_s^*$, as found in the analysis, is the critical parameter controlling the type of the correlation dependence $t_{K1}=f(\delta_s)$: when $\delta_s > \delta_s^*$, t_{K1} decreases with the increase of the degree of latent ordering, but increases when $\delta_s < \delta_s^*$. The apparent inference is that multifractal

parametrization of the initial grain structure can be useful for the optimization of the composition of steel (as well as for other modes of affecting alloy structure).

Another subject of inquiry was the structure of specimens of polymethylmetacrylate (acrylic plastic) and of NiCu catalyst [10]. The problem was to reveal the structure differences from the viewpoint of their multifractality in relation to parameters Π_c and S. The results of this study were as follows:

Material	D_0	D_{40}	$\Pi_c=D_0 - D_{40}$	$S*10^{-6}$
Polymethylmetacrylate	2.703	1.911	0.792	2.702
NiCu catalyst	2.660	2.064	0.596	5.419

It is apparent that the values of D_0 for both specimens are close, but their multifractal structure differs: considering the fractal set with the greatest looseness (parameter D_{40}) planar clusters ($D_{40} < 2$) are predominant in the plastic, whereas three-dimensional clusters ($D_{40} < 2$) prevail in the catalyst. The transition to a volume-aggregate structure decreases the latent ordering of the structure (values of Π_c for the catalyst are lower than those for the plastic). The higher value of S for the catalyst points to the higher sinuosity of its surface compared to that of the plastic.

CONCLUSION

Elaborated methodics and production program has been shown that multifractal parametrization, as a new method of structural studies, holds much promise for improving the structure and properties of materials.

REFERENCES

1. B.B.Mandelbrot. The Fractal Geometry of Nature. W.H.Freeman and Company, New York (1982).
2. T.C.Halsey. M.H.Jensen, L.P. Kadanoff, at al. Phys. Rev. A, 33 (1986) 1141.
3. J.Feder. Fractal, Plenum Press, New York and London. (1988).
4. B.B.Mandelbrot, D.E.Passoja and A.J.Pannlay. Nature 308 (1984) 721.
5. G.V.Vstovskii, A.G.Kolmakov, V.F.Terentiev. Metals, 4 (1993) 164.
6. G.V.Vstovskii, I.J.Bunin, A.G.Kolmakov at al. Dokladi Russian Academy of Science, 343 (1995) 613.

7. V.S.Ivanova. Synergetics. Strenghts and fracture of metallic materials. Nauka, Moscow (1992).
8. G.V.Kozlov, V.U.Novikov. Problems of manufacturing and automatization, 3-4 (1996) 34.
9. O.A.Bannich, V.M.Blinov, M.V.Kostina. Metals, 2 (1995) 62.

MOSSBAUER STUDY OF FE DOPED CBN POLYCRYSTALS AFTER THERMOBAR TREATMENT.

Zalesky A.,Belarus State University

Cubic boron nitride (cBN) is known for its outstanding qualities such as hardness, high melting temperature and wide band gap allowing its wide industrial application. However, such application is often limited with cBN lattice defectness. Thermobar treatment at temperatures and pressures close to those applied during cBN synthesis is an effective method of transformation of defect structure. Mossbauer study of local configurations formed by ^{57}Fe probes in cBN enables the analysis of defectness variations occurring during thermobar treatment.

In present paper samples of policrystalline cBN were prepared from hBN precursor powders by catalytic synthesis with catalisator Al (2 wt %) and Si (2 wt %) with addition of carbonile Fe (3 wt %). After that samples have been subjected to thermobar treatment at T = 1800 °C, P=7.0 GPa.

Investigations have been made using Mossbauer spectroscopy and XRD. Data were processed using program Mosmod 2000. Numerical evaluation has shown, that lattice became more disordered with thermobar treatment, that can be assigned to the formation of vacancies and vacancy complexes. During first stage of the process (1-5min.) ordering of polyinterfaces takes place formation of special-type borders. On the second stage (5-11 min.) disordering of polyinterfaces takes place. This could be attributed to intensive phase formation on the polyinterfaces due to high temperature annealing.

ON CONTOUR TREATMENT IN COMPLEX SPECTRAL LINES IN CRYSTAL VIBRATION SPECTRA

V.M. Voskresensky, P.G. Chufyrev

Instiute of Chemistry and Technology of Rare Elements and Mineral Raw Materials KSC RAS. 184200 Apatity, Russia. E-mail: chufyrev@chemy.kolasc.net.ru

It is possible to obtain important information about the fine process of structural unit ordering in crystals and dynamic changes in this ordering in the case of external attacks by analyzing the behavior of spectral line basic parameters: frequency, intensity, semi width, and the shape parameter. The experimentally observed contours of real spectral lines in the crystal vibration spectrum are essentially overlapping lines of dissimilar shapes and intensity. The parameters of actually observed lines differ from the true ones due to many distorting factors such as the effect of adjacent lines, aperture distortions, background, etc.

Therefore the true parameter values can only be assessed after a special mathematical treatment of the spectrum. Nowadays the most precise and rapid mathematical methods are based on Fourier transforms.

What is usually applied is the integral Fourier transform and discrete Fourier transform. Formulas of these transforms look as follows:

Integral Fourier transform:

$$G(p) = \int F(x) \exp(ipx)\, dx$$
$$F(x) = 1/2\pi \int G(p) \exp(ipx)\, dx$$

- discrete Fourier transform:

$$G_k = \sum Fj \exp(i\, 2\pi jk/N) \qquad k=0,1,\ldots,N \qquad j=0,1,\ldots,N-1$$
$$F_j = 1/N \sum G_k \exp(-i\, 2\pi jk/N) \qquad k=0,1,\ldots,N-1 \qquad j=0,1,\ldots,N$$

Each harmonic parameter is calculated by direct transformation whereas the calculation of the harmonic sum requires reverse transformation.

By harmonics is meant the function:

$$x = A \cos(2\pi t/T + \varphi),$$

where A is the amplitude, T – period, - phase.

In order to pass from sine to cosine it is sufficient to change the phase by $\pi/2$. The amplitude, phase, frequency and period of each of the harmonics are related to coefficients F_k by the formulas:

$$Re_k = A_k \cos \varphi_k,\ Im_k = A_k \sin \varphi_k$$
$$F_k = Re_k + i\, Im_k$$
$$A_k = 1/N\sqrt{(Re_k^2 + Im_k^2)}$$
$$\varphi_k = \text{arctg}(Im_k/ Re_k),$$

where k =0,1…,N-1

This permits to cut the high-frequency section of the spectrum and, using the reverse Fourier transform, to obtain a curve with filtered out noises. However, this may result in severe oscillations – the so-called Gibbs oscillations whereby the smoothness condition is violated. The oscillations can be by more than three orders subdued by applying a special filter to the Fourier transform:

$Wk = 0.4243801+0.4973406*\cos(\pi k/K)+0.0782793*\cos(2\pi k/K)$ при $k<K$,
$Wk=0$ при $k \geq K$.

The filtration degree is set by K parameter whose meaning is the upper frequency boundary.

If the line is not smooth enough and does not fit the requirements, then various interpolation methods can be used. All these methods are called upon to find intermediary values from available values. The tasks of interpolation are solved by constructing the interpolation function L(x) approximately substituting f(x) given in the table, and passing through all the given points –nodes of interpolation. Interpolation involves the following three problems:

1. Selection of the interpolation function l(x)
2. Evaluation of the interpolation error R(x)
3. Permutations of interpolation nodes to attain the highest frequency of the function to reconstruct restore the function.

Selecting of the interpolation function type is generally important. Specifically, it should be remembered that any number of functions can be run through the given points. Therefore the first problem of interpolation is normally resolved by opting for a polynomial, although other functions can also be applied. Interpolation using polynomials is more accurate while spline functions result in smoother interpolation. The difference may become essential when not only the function values but its derivatives are needed.

The narrowing or increasing of the spectrum resolution is achieved by varying the contribution of Lorenz and Gauss components. The Lorenz contribution diminishes the line width; the Gauss contribution broadens it. This method is called the Lorenz-Gauss transform.

There are numerous packages realizing the spectral line treatment, both in Russia and abroad. However, it is difficult to create a system to handle the problems in general. All the programs are mostly developed to solve specific difficulties.

The imperfect methods of analysis and data treatment produce inaccurate information about the processes analyzed. Gaining an insight into the nature of substances calls for perfecting the mathematical apparatus.

The work was performed with the support of RFBR. Grant № 03-03-32964.

INVESTIGATION OF THE LUMINESCENT AND OPTICAL PROPERTIES OF THE SET OF TUNGSTATE CRYSTALS WITH WOLFRAMITE STRUCTURAL TYPE

O.V. Rzhevskaya[1], S.N.Ivanov[1], V.N. Kolobanov[1], V.V. Mikhailin[1], D.A. Spassky[2], B.I. Zadneprovski[3], L. Jönsson[4], G. Svensson[5]

[1] Synchrotron Radiation Laboratory, Physics Faculty, M.V. Lomonosov Moscow State University, 119992 Vorob'evy Gory, Moscow, Russia

[2] Skobeltsyn Institute of Nuclear Physics, M.V. Lomonosov Moscow State University, 119992 Moscow, Russia

[3] All-Russia Research Institute of Mineral Materials Synthesis, Irkutskaya St. 1, Aleksandrov 601600, Vladimir Region, Russia

[4] Physics Department, Lund University, Professorgatan 1, Lund S-22363, Sweden

[5] Department of Inorganic Chemistry, Chalmers University of Technology, Getebörg, Sweden

Depending on the ionic radius of the cation, $r > 10^{-10}$ m or $r < 10^{-10}$ m, tungstate crystals divide into two different structural types – scheelite and wolframite type. In the present work we measured luminescence and reflectivity spectra of a set of tungstates with wolframite crystal structure, namely $CuWO_4$, $CoWO_4$, $NiWO_4$, $FeNa(WO_4)_2$, $CdWO_4$, $ZnWO_4$, $MgWO_4$, in order to study the nature of the luminescent centeres and the electronic structure of the energy bands of these crystals. Luminescence spectra under X-ray excitation were measured at the experimental station on beamline 5.6 of the storage ring "Siberia-2" (electron energy of 2.5 GeV) at the room temperature. White beam of synchrotron radiation through Be-foil was used for the excitation of luminescence. Reflectivity spectra were measured on the VUV-station on beamline 4.3 of the storage ring "Siberia-1" also at the room temperature.

SWITCHING PROCESSES IN TGS and DTGS CRYSTALS IRRADIATED BY HIGH-CURRENT PULSED ELECTRON BEAM.

[1)]Ivanov V.V., [1)]Makarov V.V., [1)]Klevtsova E.A., [1)]Markova T.A., [2)]Tutunnikov S.I., [2)]Efimov V.V.

[1)] Tver State University, Tver

[2)] Joint Institute for Nuclear Research, Dubna

In the present time are the measurements of the polarization reversal occurring after some type of external influence – electric field, temperature, mechanical strain. In work [1] investigates an electronic irradiation effect on dielectric behaviors of single TGS and DTGS crystals accomplished.

In the present work relaxation switching processes in TGS and DTGS crystals irradiated by high-current pulsed electron beam were studied. The method combining the measurements of dielectric permittivity, polarization, coercive field and tanδ with Barkhausen effect method observation has been employed [2]. The dependences of total Barkhausen jumps number and differentiate distribution in irradiated TGS and DTGS crystals by branch of hysteresis loop were obtained. The integrated jumps number during of changing an electric state TGS crystals increases with an electron fluence increase from 0 to $60 \cdot 10^{15}$ electron·cm^{-2}. Similar dependence is observed in all researched interval of temperature. It appears because of an electron fluence increase the imperfections number, and thereof Barkhausen jumps number increases. An analogous relative curves position of integrated jumps number the irradiated and unirradiated DTGS crystals in the interval of an electron fluence from 0 to $70 \cdot 10^{15}$ electron·cm^{-2} are observed. The total Barkhausen jumps number at the switching an external electric field were studied. The time dependence of the Barkhausen jumps number in TGS and DTGS crystals irradiated by high-current pulsed electron beam at the different radiation fluence were observed. It was shown increasing an external electric field accelerates the process of polarization reversal as unirradiated TGS and DTGS, and for irradiated with different fluence value and as increase total number of Barkhausen jumps. Mathematical machining of experimental outcomes has shown the curves of following of Barkhausen jumps are well approximated by the law $N \sim 1 - \exp\left(-\left(\frac{t}{\tau}\right)^{\alpha}\right)$, where τ and $0<\alpha\leq 1$ – constants.

1. Sogr A.A., Kopulova I.B. Izv. RAS. Ser.phys.-1996, T.60, 10, p.150-152. (in Russian)
2. Rudyak V.M. Switching processes in nonlinear crystals. –M.:Nauka, 1986.-248 p.

This work was supported by the program "Universities of Russia" № УР01.01.053.

CRYSTAL GROWTH IN THE SYSTEM LI_3PO_4 – LI_4GEO_4 – LI_2MOO_4 – LIF UNDER THE INFLUENCE OF THE ELECTRICAL FIELD

Dmitry A. Ksenofontov, Ludmila N. Demianets, Alexei K. Ivanov-Schits

Institute of Crystallography of Russian Academy of Sciencies 59 Leninsky pr. Moscow 119333,

The study of the simultaneous influence of heat and electrical field on the crystal growth was performed in the system Li_3PO_4 – Li_4GeO_4 – Li_2MoO_4 – LiF. The special equipment which allowed to apply a direct electrical current for the system "growing crystal-melt" was constructed. The Pt-rod and Pt-crucible served as cathode and anode respectively, thus electrical circuit was the following: current source – crucible – melt – growing crystal – Pt-rod. Growth occurs on the Pt-rod immersed into the flux due to temperature decrease; simultaneous application of direct electrical current (voltage V= 0.08 and 0.15 V) controlled the growth process. Parameters of the crystallization process were: temperature of system melting was 970°C, temperature decrease rate in the range 970-950 °C was 0.1 °C/h, starting chemical components were 40.11g Li_3PO_4, 56.95g Li_4GeO_4, 73.53g Li_2MoO_4, and 23.53g LiF. The electrical current was found to control the compositions and growth conditions of crystallizing phases in the system. Applying the electrical field led to the change of the composition of the growing crystals. Lithium molybdates Li_2MoO_4 and $Li_{1.3}Mo_3O_8$ were crystallized onto the Pt-rod at V=0.08 V while the crystals of lithium germanate, Li_2GeO_3, were grown onto the cathode at V=0.15 V. In the case when Pt-crucible and Pt-rod were served as cathode and anode respectively at V=0.15 V the crystals of lithium germanate, Li_2GeO_3, crystallized on the Pt-rod. Phosphorus remained in the flux forming the vitreous phase.

Thus the presence of the electrical field provides the directional ion migration in the melt. Thus the presence of anode and cathode provides the ion migration in the melt which results in the local change of melt composition and the crystallization of the compounds with various compositions depending on applied electrical field.

The change of the strength of the current was noticed during the process of crystal growth. At the beginning of the process, when Pt-rod was immersed into the flux, I=10 mA; at the end of the crystallization it was one order higher. The explanation of that phenomenon was suggested on the basis of the electrophysical characteristics of the melt. The composition of the melt and its properties changed due to the growth of crystals with definite composition. Crystal growth under simultaneous action of heat and electrical field may be represented as a novel method of crystal growing, which is based on the main principles of the flux growth and electrocrystallization.

The work was performed at partial financial support of Russian Foundation for Basic Researches, Grant N 02-02-16958 and Russian Federation President Grant for supporting the leading scientific school N 1954.2003.2.

ELECTRON SPIN RESONANCE (ESR) OF MELILITE ACTIVATED SINGLE CRYSTALS (NA, CA)(MG, AL,SI)$_3O_7$.

S.F.Nosov, A.O.Semenkovich, M.I.Samoylovich

VNIISIMS, Alexandrov

Two types of melilite synthetical crystals, irradiated by γ-rays with doses $4*10^4$ – $2*10^7$ __ were studied. Chemical composition of the first sample corresponded to akermanite ($Ca_2MgSi_2O_7$), the second sample had blended compound, corresponded to 70% of helenite ($Ca_2Al_2SiO_7$) and 30% of akermanite.

Colorless sample of akermanite became pink, and light-green sample of blended compound became of teapot color under the influence of γ-rays. Radiant color of the second sample vanished and pink color of akermanite became not so intensive during several days.

ESR spectra were observed and recorded with the help of radiospectrometer ER-200-DSRC on frequency 9,8 gigahertz at 300 K. Spectra from two types of centers: hole and electron, were observed in both samples. Spectrum of the hole center is presented by two lines 2 oersteds in width with sextet hyperfine structure (SHS) from 8 equivalent centers, spectrum of the electron center – by 8 lines 3-6 oersteds in width without sextet hyperfine structure (SHS).

Spectrum of the hole center is described by spin Hamiltonian for spin S = ½:

$$H=g\beta HS+AIS,$$

where β - Bohr magneton; g – spectroscopic chipping tensor; H - magnetic intensity; S and I – electron and nuclear spins; I=5/2; A – hyperfine chipping tensor.

The following main valuations of g-tensor are defined: g_1 = 2.0057±0.0005; g_2 = 2.006±0.001; g_3 = 2.0267±0.0005.

Hyperfine structure is isotropic, valuation is obtained for hyperfine coupling constant: A =10.5±0.5 oersteds ($1.05*10^{-3} \pm 0.05$ cm^{-1}).

Spectrum of the electron center is described by Hamiltonian

$$H=g\beta HS$$

The following valuations of g-tensor are found: g_1 = 1.9174±0.0005; g_2 = 1.957±0.001; g_3 = 1.9801±0.0005.

Six-component SHS of the hole centers and hyperfine coupling constant valuation show that they are liable to nucleuses of Al^{27} (prevalence – 100%, nuclear spin I=5/2). This spectrum can be attributed to O^--centers, localized in the nearest surrounding of Al^{5+}-ions, which replace Si^{4+}-ions.

Interpretation of paramagnetic centers is justified by analysis of symmetry properties of structural positions [1] for space group of D_{2d}^3 symmetry of melilite [2].

Oxygen positions have magnetic multiplicity 8, moreover one of the crystallographic axes, namely (001) coincides with magnetic axe. This fact actually takes place for magnetic axe g_3, which coincides with direction (001).

Presence of eight equivalent centers shows that it also connect with oxygen ions. We can expect that these centers present electrons, localized on Al^{3+}-O^{2-} - bonds in Mg-tetrahedrons, where Mg^{2+}-ions are replaced by Al^{3+}-ions.

References:

1. Meyl'man M.L., Samoylovich M.I. Application in spectroscopy of ESR activated single crystals. – M.:Atomizdat, 1977. p.272
2. Bregg U., Klaringbull G., Crystal structure of minerals. – M.: Mir, 1967.

EXPERIENCE IN APPLICATION OF AHP GROWTH METHODS: THEORY AND EXPERIMENT.

Vladimir D. Golyshev

Center for Thermophysical Researches "THERMO" Alexandrov

e-mail: thermo.ltd@relcom.ru; phone/fax (095 584-58-16)

The present work demonstrates the results of long-term, complex, numerical-experimental researches performed in close cooperation with the Russian and foreign scientists and dedicated to a crystal growth method from a melt under conditions of the Axial Heat flux close to the Phase interface (AHP method) offered by the author.

The AHP method was proposed for solution of two problems. The first problem is obtaining of precisely known conditions close to the melt/crystal interface. The second one is growth of large-sized bulk crystals. This problem arose from attempt to accomplish a task on growth of synthetic mica by a method of spontaneous crystallization when the author worked at VNIISIMS. Mica was grown in crucibles about 50 cm in diameter and 100 cm high.

The method was developed to solve two tasks. The first task was to obtain conditions when variations in diameter and length of a growing crystal did not change crystallization conditions. The second one was to find a way at which it was possible to satisfy the requirements imposed by features of mica growth. It was necessary, at large diameters of a crucible, to provide a small overheating of the melt, high temperature gradient in the melt, and to generate conditions for directional growth of spontaneously mica. In the report, the results found in the field of growth of mica are described.

As a result of change of political regime, lack of financing and later on in connection with the market demands, researches into the AHP method were continued at the CTR "Thermo" basically in the field of investigation into fundamental aspects of crystal growth for solution of problems connected with the growth of semiconductors. Realization of these problems was based on a potentiality to control the interface shape, the pattern of melt flows close to the melt/crystal interface, the boundary conditions, and the simple geometry.

The AHP method was employed to study the interfacial kinetics of layered growth; in situ measurement of supercooling; determination of conditions for morphological instability at the interface; to research the correlation between the character of heat and mass transfer and macro- and microhomogeneity in a crystal; to study fundamentals for crystallization of

concentrated alloys when crystallization conditions are determined by concentration fields; to study crystallization features in growth of anisotropic crystals.

Results of these researches are described by the example of some dielectrics and semiconductors. Examples of high accuracy in the description of heat and mass transfer processes are presented too. The problems arising from application of actual experimental boundary conditions for quantitative modelling are described. It has been shown that the scientific basis of the AHP method is developed in general, and the method is a novel step in the field of crystal growth from the melt; and it can be recommended as a benchmark crystallization process.

The researches have also shown that the method is very promising for growth of homogeneous, bulk crystals of different groups of materials, including crystals of concentrated alloys. Prospects for application of the method in space and as alternative to space researches on the ground are under consideration.

The researches in the field of fundamental investigations have been conducted under financial support of the Science-NASA Program; TM4/4 Theme; RSA (Contract No.007, 19978); RFFR (Projects №№ 02-02-17128 and 97-03-32980); CRDF (Projects ##RE1-2233 and RE1-2480); INTAS (Project No. 99-01814 and Project No.2000-263); and also NASA, Project # 98-HEDS-05092. The researches in the field of development the technology for growth of germanium have been supported by the Project of RFTR (code AHP).

ON THE SYSTEMS OF CRYSTAL EXTERNAL FORMS

Smirnova N.L.

Moscow State University

Single crystals – are important materials in modern industry. Investigation of external crystal form system allows designing prognostic scheme that can be useful for growth theory and applications.

The set of external form (EF) vertexes with shared faces is called vertexon. The summary number of all faces meeting at a vertex is called summery valence (SV). The valence of the vertex may be concrete. It may be simple if all faces shared this vertex are n-polygons with the same n. It may be mixed if n-gons shared this vertex are different. Mixed valence is composed of numbers. Every number is the sum of n-gons with the same n. So the vertex may be monovalent or geterovalent. The goal of this work was to examine 195 tetragonal and 246 hexagonal EF, their vertexons, summery and concrete vertex valences.

Six SV were found in 195 tetragonal EF: 3, 4, 5, 6, 7 and 8. Six different VS compose 12 combinations: 3, 34, 345, 346, 347, 348, 35, 36, 38, 4, 45 and 48. One and the same vertex may be repeated in EF 1 – 8 times. The set of SV combinations increase up to 68 if we take into account ratios of vertex repetitions. Different ratios are in angle brackets and numbers of 195 EF with the same ratios are in round brackets: **3** <1 (9), 2 (14), 3 (14), 4 (11), 5 (5), 6 (2)>; **34** <1:1 (19), 1:2 (4), 1:3 (3), 2:1 (15), 3:1 (13), 4:1 (9), 5:1 (2), 6:1 (6), 7:1 (2), 8:1 (1), 2:2 (5), 3:2 (3), 4:2 (4), 5:2 (1), 6:2 (1), 8:2 (1), 2:3 (3), 3:3 (3), 4:3 (3), 5:3 (2), 14:3 (1), 2:4 (1), 3:4 (1), 4:4 (1), 9:4 (1), 3:5 (1), 8:5 (1)>; **345** <1:1:1 (2), 3:1:1 (2), 4:1:1 (1), 1:3:1 (1), 3:2:1 (1), 7:1:2 (1)>; **346** <1:1:1 (1), 2:2:1 (1), 4:2:1 (1), 5:2:1 (1), 6:3:1 (1), 2:3:1(1)>; **347** <7:1:1 (1)>1-1; **348** <1:2:1 (1)>; **35** <1:1 (1), 2:1 (1), 4:1 (1), 5:1 (1), 6:1 (1)>; **36** <4:1 (1)>; **38** <2:1 (1)>; **4** <1 (1), 2 (2), 3 (2), 4 (2)>; **45** <2:1 (1)>; **48** <1:1 (2)>. Number of SV combinations without SV 3 is 10-62-185. The number of EF, that don't contain SV 3 is changing from 3 to 10, when going from the set 12 to set 68 and to set 195.

There are 46 different ratios, among them 6 are 1-ary, 27 binary, 13 – ternary: **1**, 2, 3, 4, 5, 6, **1:1**, 1:2, 1:3, **2:1**, 3:1, 4:1, 5:1, 6:1, 7:1, 8:1, **2:2**, 3:2, 4:2, 5:2, 6:2, 8:2, **2:3**, 3:3, 4:3, 5:3, 14:3, **2:4**, 3:4, 4:4, 9:4, **3:5**, 8:5, **1:1:1**, 3:1:1, 4:1:1, 7:1:1, **1:2:1**, 2:2:1, 3:2:1, 4:2:1, 5:2:1, **1:3:1**, 2:3:1, 6:3:1 and **7:1:2**. The quantity of the set decreases from 46 to 37, if we put ratio ciphers from smaller to lager: **1**, 2, 3, 4, 5, 6, **1:1**, 1:2, 1:3, 1:4, 1:5, 1:6, 1:7, 1:8, **2:2**, 2:3, 2:4, 2:5, 2:6, 2:8, **3:3**, 3:4, 3:5, 3:14, **4:4**, 4:9, 5:8, **1:1:1**, 1:1:2, 1:1:3, 1:1:7, 1:2:2, 1:2:3,

1:2:4, 1:2:5, 1:2:7 and 1:3:6. Ratios may be represented as some arithmetic sequences: **1(1)**, 2, 3, 4, 5, 6; **1:1(0:1)**, 1:2, 1:3, 1:4, 1:5, 1:6, 1:7, 1:8; **2:2(0:1)**, 2:3, 2:4, 2:5, 2:6, 2:8; **3:3(0:1)**, 3:4, 3:5, 3:14; 4:4, 4:9; **5:8**; **1:1:1(0:0:1)**, 1:1:2, 1:1:3, 1:1:7; **1:2:2(0:0:1)**, 1:2:3, 1:2:4, 1:2:5, 1:2:7 and **1:3:6**. Ratios may be represented as line complication scheme, silent ratios are in quotes: **{1:1}**, 2:2, 2:2:1, 1:1:1, 3:3, 4:4, **/3:4/**, **<2:3>**, 2:3:1, **5:8**, **/3:5/**, **[1:2]**, 1:2:1, 2:4:1, 3:6:1, **4:9**, **/2:5/**, 2:5:1, **<1:3>**, 1:3:1, 2:6, **"2:7"**, 2:7:1, **/1:4/**, 2:8, **3:14**, **1:5**, **1:6**, **1:7**, 1:7:1, **1:8**, **{1}**, 2, 3, 4, 5 and 6

The quantity of mono- and mixed valences in the set of 195 tetragonal EF is 17: 3, 12, 111, 4, 13, 22, 112, 1111, 5, 14, 23, 122, 6, 24, 222, 223 and 8. The number of vertexes with different valences is 1-6. Instead of large number combinations from 17 on 1-6 there are only 68 vertexes with different concrete valences: **3**-(0, 4, 13, 22), 13-22, 22-8, **12**-(0, 4, 4-13-22, 4-22, 4-22-112-14, 4-22-8, 4-112, 4-122, 4-24, 13, 13-22, 13-22-24, 22, 112, 8), **3-12**-(0, 4, 4-13-24, 4-22, 4-22-222, 22, 112, 14), **111**-(0, 22, 14), **12-111**-(0, 4, 4-13, 4-22, 4-14, 4-122, 13, 13-112, 22, 22-112, 22-1111, 22-1111-24, 112, 112-1111, 112-223, 1111, 14, 23), **3-12-111**-(0, 4, 4-112, 4-13-22, 4-13-5, 4-22, 4-22-112, 13, 13-23, 22, 112, 112-1111, 112-223, 6), **4**-(0, 22, 22-23, 8). In round brackets are combinations that are added to combinations before brackets. There are 35 combinations in brackets with SV more than four: ***4***, 4-13, 4-13-22, 4-13-5, 4-13-24, *4-22*, 4-22-112, 4-22-112-14, *4-22-23*, 4-22-222, 4-22-8, 4-112, 4-14, 4-122, 4-24, *4-8*, **13**, *13-22*, 13-22-24, 13-112, 13-23, **22**, 22-112, 22-1111, 22-23, *22-8*, **112**, 112-1111, **1111**, **14**, **23**, **6**, **223** and **8**. The combinations that exist as EF are distinguished in italic.

Five SV were found in 245 hexagonal EF: 3, 4, 5, 6, and 7. The 5 different EF compose 11 combinations: 3, 34, 345, 346, 347, 35, 356, 36, 4, 456, and 46. One and the same vertex may be repeated in EF 1 – 11 times. SV 4, 5, 6, and 7 are repeated no more than three times and more often are unique. The set of SV combinations increase up to 72 if we take into account ratios of vertex repetitions. Different ratios are in angle brackets and numbers of 245 EF with the same ratios are in round brackets: **3** <1 (8), 2 (17), 3 (17), 4 (23), 5 (10), 6 (7), 7 (2), 8 (3), 9 (2), 10 (1), 13 (1)>; **34** <1:1 (20), 2:1 (24), 3:1 (16), 4:1 (15), 5:1 (5), 6:1 (5), 7:1 (1), 8:1 (1), 1:2 (1), 2:2 (2), 3:2 (2), 4:2 (2), 6:2 (1), 7:2 (1), 1:3 (1), 3:3 (1), 4:3 (2), 6:3 (1)>; **35** <1:1 (3), 2:1 (1), 3:1 (2), 4:1 (1), 6:1 (1), 7:1 (1)>; **36** <2:1 (2), 3:1 (2), 5:1 (1)>; **345** <1:1:1 (1), 3:1:1 (1), 4:1:1 (2), 1:2:1 (1), 2:2:1 (1), 3:2:1 (1), 7:2:1 (1), 8:2:1 (1)>; **346** <1:1:1 (3), 2:1:1 (1), 3:1:1 (2), 4:1:1 (1), 6:1:1 (1), 1:2:1 (1), 2:2:1 (1) 3:2:1 (2), 4:2:1 (1), 6:2:1 (1), 2:1:2 (1), 4:1:2 (1), 5:3:1 (1), 8:4:1 (1)>; **347**<1:2:1 (1)>; **356**<1:1:1 (1), 2:1:1 (1)>; **4** <1 (1)>; **46** <1:1 (3), 2:1 (2), 3:1 (1)>; **456** <2:1:1 (1)>.

There are 46 different ratios, among them 11 are 1-ary, 18 binary, 17 – ternary: **1**, 2, 3, 4, 5, 6, 7, 8, 9, 10, 13; **1:1**, 2:1, 3:1, 4:1, 5:1, 6:1, 7:1, 8:1, **1:2**, 2:2, 3:2, 4:2, 6:2, 7:2, **1:3**, 3:3, 4:3, 6:3; **1:1:1**, 2:11, 3:1:1, 4:1:1, 6:1:1, **1:2:1**, 2:2:1, 3:2:1, 4:2:1, 5:2:1, 6:2:1, 7:2:1, 8:2:1, **2:1:2**, 4:1:2, **5:3:1**, **8:4:1**. The quantity of the set decreases from 46 to 41, if we put ratios ciphers from smaller to lager. Ratios may be represented as some arithmetic sequences: **1(1)**, 2, 3, 4, 5, 6, 7, 8, 9, 10, 13; **1:1 (0:1)**, 1:2, 1:3, 1:4, 1:5, 1:6, 1:7, 1:8; **2:2 (0:1)**, 2:3, 2:4, 2:6, 2:7; **3:3 (0:1)**, 3:4, 3:6; **1:1:1 (0:0:1)**, 1:1:2, 1:1:3, 1:1:4, 1:1:6; **1:2:2 (0:0:1)**, 1:2:3, 1:2:4, 1:2:5, 1:2:6, 1:2:7, 1:2:8; **1:3:5** and **1:4:8**. Ratios may be represented as line complication schemes, silent ratios are in quotes: **{1:1}**, 2:2, 2:2:1, 1:1:1, 3:3 **/3:4/**, **<2:3>**, 2:3:1, **/"3:5"/**, 3:5:1, **[1:2]**, 1:2:1, 2:4, 2:4:1, 3:6, 3:6:1, "4:8", 4:8:1, **/"2:5"/**, 2:5:1, **<1:3>**, 1:3:1, 2:6, 2:6:1, **2:7**, 2:7:1, **/1:4/**, 1:4:1, 2:8, 2:8:1, **1:5**, **1:6**, 1:6:1, **1:7**, 1:7:1, **1:8**, **{1}**, 2, 3, 4, 5, 6, 7, 8, 9, 10 and 13.

The quantity of mono- and mixed valences in the set of 245 hexagonal EF is 16: 3, 12, 111, 4, 13, 22, 112, 1111, 5, 14, 23, 122, 6, 24, 33 and 25. The number of vertexes with different valences is 1-6. Instead of large number combinations from 16 on 1-6 there are only 72 vertexes with different concrete valences: **3**-(0, 4, 4-6, 4-22-25, 22-14, 5), **12**-(0, 4, 4-13-14, 4-22, 4-22-112, 4-22-6, 4-112, 13, 13-22-6, 13-112, 22, 22-6, 112, 23, 23-6), **111**-(0, 112, 122), **3-12**-(0, 4, 4-22-6, 4-14, 13, 13-112-6, 13-6, 22, 22-1111, 22-112-122, 112, 14, 23, 6), **12-111**-(0, 4-22, 4-22-1111, 4-14, 13, 22, 22-122, 112, 112-33, 112-6, 14, 6), **3-12-111**-(0, 4, 4-13-112, 4-22, 4-112-14, 13, 13-22-6, 13-112, 13-112-14, 22, 22-112, 22-112-1111, 22-6, 112, 112-23, 1111, 122), **4**-(0, 22-14-6, 22-6, 6) and 22 (6). In round brackets are combinations that are added to combinations before brackets. There are 39 combinations in brackets with SV more than four: **4**, 4-13-112, 4-13-14, 4-6, 4-22, 4-22-112, 4-22-1111, *4-22-14-6, 4-22-6*, 4-22-25, 4-112, 4-112-14, 4-14, *4-6*, **13**, 13-22-6, 13-112, 13-112-14, 13-112-6, 13-6, **22**, 22-112, 22-112-1111, 22-112-122, 22-1111, 22-14, 22-122, 22-6, **112**, 112-23, 112-6, 112-33, **1111**, **5**, **14**, **23**, 23-6, **122** and **6** .

At first sight there is the same relations in tetragonal and hexagonal systems, but there are some differences. For instance there are only 17 combinations out of 35 tetragonal and 39 hexagonal sets, that are in both sets: **4**, 4-22, 4-22-112, *4-22-6*, 4-112, 4-14, *4-6*, **13**, 13-112, **22**, 22-112, 22-1111, **112**, **1111**, **14**, **23** and **6.**

Some schemes of external forms and their valences were designed. These schemes are regular. New members will be put in them regularly.

IN SITU MEASUREMENTS OF THE INTERFACE SUPERCOOLING DURING MELT CRYSTAL GROWTH OF THE DIELECTRICS: CURRENT STATE AND PROSPECTS FOR THE FUTURE.

Bykova S.V., Golyshev V.D., Gonik M.A., Tsvetovsky V.B.

Center for Thermophysical Researches "THERMO", Alexandrov, Russia, Institutskay St.1,

Faceted growth is characteristic for a wide range of single crystals of dielectrics, growing from a melt. Determination of kinetic dependence $V=F(\Delta T)$, where V is the growth rate of a crystal and ΔT is facet supercooling, is very important for interpretation of the layered mechanism of interfacial kinetics and technological advancement for growth of crystals. To measure ΔT, a new *in situ* method based on measurement of the interface brightness temperature, T_b, with an optical pyrometer through a growing crystal was offered [1-3]. The procedure is developed for media having an opaque melt and transparent crystal at the wavelength of the pyrometer. Our investigations were conducted for $Bi_4Ge_3O_{12}$ and $Bi_{12}GeO_{20}$ crystals. These crystals were chosen due to successful combination of melt and crystal absorptivity, α. So, for the $Bi_4Ge_3O_{12}$ melt, $\alpha > 200$ см$^{-1}$ and for the $Bi_4Ge_3O_{12}$crystal, $\alpha < 0.03$ см$^{-1}$ [4]. In accordance with the proposed method, ΔT is found from the equation: $T_b^m - T_b^v(t)$, where T_b^m is the brightness temperature measured in the absence of growth and corresponding to the melting point; $T_b^v(t)$ is the brightness temperature at the growth rate V corresponding to the temperature of the supercooled interface, t is time of crystallization. As a result of *in situ* measurement, the dependence of $\Delta T(t)$ is found.

To measure the $T_b^v(t)$ dependence and then to obtain the $\Delta T(t)$ dependence, two specially designed optical pyrometers are used. One of them is a double-beam pyrometer with a measuring spot 1.2 mm in diameter (measurement of maximum supercooling) [5]. The second is a pyrometer for simultaneous measurement at 20 points situated within 1.1x20 mm line at the interface (measurement of supercooling distribution along the interface) [6]. The pyrometers have sensitivity more than 0.1K at a level of 1100^{0}C. A standard pyrometer ЛОП-72 with a measuring spot 8 mm in diameter (measurement of average supercooling) was also used.

Crystallization during in situ researches of $\Delta T(t)$ is conducted with a growth method called as the Axial Heat flux close to the Phase interface (AHP method) [7]. Two crystallization procedures have been used. First one was a decrease of temperature at boundaries of the melt/crystal system; second one was a pulling of a crucible into the cold zone. Application of AHP method allows to use with high accuracy methods of numerical simulation for definition of $V(t)$ dependence. Then, comparison of the calculated dependence

$V(t)$ with the experimental dependence $\Delta T(t)$ is done to determine the kinetic dependence $V=F(\Delta T)$. For numerical determination of $V(t)$, specially developed numerical methods are used [8,9].

In the present work, sources of inaccuracy for dependences of $\Delta T(t)$, $V(t)$ and $V=F(\Delta T)$ are analyzed; estimations of errors for the measured supercooling $\Delta T(t)$ calculated by the simplified one-dimensional model of radiation heat transfer in a semitransparent crystal are presented; features of different numerical models applied for determination of $V(t)$ are considered. Data obtained on $V=F(\Delta T)$ for different facets of $Bi_4Ge_3O_{12}$ are presented and preliminary data on supercooling distribution along the interface during crystallization of $Bi_{12}GeO_{20}$. Experimental and numerical methods to correct experimental data on supercooling for elimination of errors are proposed. Application of laser radiation for local impact on a small part of the interface is discussed. Measurement of distribution of ΔT has shown that the method is very promising not only for determination of layered growth fundamentals but it can also be employed in future as a new technique for control and monitoring the crystallization process.

The work was supported in part by INTAS Project No. 2000-263 and in part by RFBR Project № 02-02-17128.

1. V.D. Golyshev, M.A. Gonik, V.B. Tsvetovsky, Instruments and Experimental Techniques, 41, p 735, 1998, (Translated from Pribory i Tekhnika Eksperimenta, No. 5, p 153, 1998).
2. V.D. Golyshev, M.A. Gonik, V.B. Tsvetovsky, Ya.V. Vasilev, and V.N. Shlegel, J. Cryst. Growth, Vol. 216, pp 428-436, 2000.
3. V.D. Golyshev, M.A. Gonik, V.B. Tsvetovsky, J. Crystal Growth, Vol. 237-239, pp 735-739, 2002.
4. Golyshev, V.D. and Gonik, M.A., Vasilev, Ya.V. and Shlegel, V.N., J. Crystal. Growth, 262 (2004), 202-211.
5. Golyshev V.D., Gonik M.A.// Cryst. Prop. Preparation. 1991. V. 36-38. P. 623
6. S.V. Bykova, V.S. Dozhdikov, V.D. Golyshev, M.A. Gonik, V.A. Petrov, V.N. Senchenko, V.B. Tsvetovsky, Book of Abstracts of Xth Russian Conference on Thermophysical Properties, Kazan, 30 September – 4 October, 2002, pp 54-55.
7. V.N.Senchenko, V.S.Dozhdikov, D.I.Kapustin, V.D.Golyshev, 2004, to be published.
8. S. V. Bykova, V. D. Golyshev, M. A. Gonik, V. B. Tsvetovsky, at all, J. Crystal Growth, (266), 2004, 246-256.
9. S. V. Bykova, V. D. Golyshev, M. A. Gonik, V. B. Tsvetovsky, at all, J. Heat and Mass Ttransfer, 2004 (to be published).

ZNO CRYSTALS: ELECTRON-ION STRUCTURE, DEFECTIVE CENTERS, ELECTROPHYSICAL PROPERTIES.

K.P. Semenov, G.V. Danilova
VNIISIMS, Alexandrov

Electron-ion structure of ZnO matrix and its defective centers are not considered from the position of probability-wave quantum chemistry (its fault postulates are shown in [1,2]) but from the position of neoclassical power structural chemistry. According to it electrons of atoms in crystals oscillate with imposed by resonance frequencies oscillation of particles e^--e^+ in vacuum media in potential traps formed by the forces $F_{e^-i} = q_{e^-} \cdot q_i \cdot \varphi(R_{e^-i})$ (the exact form of the three sections of alternating function $\pm\varphi(R)$ in the range 0.03 Å<R<18Å was determined) and their interaction with charges q_i within the radius 2.1Å. In the coupling — Zn^{2+}———$2e^-$— 0^{6+}— electron pairs 2^{e^-} oscillate with energy 6.8 eV in e^--e^- traps R^{φ}=0.032Å (the distance between their centers of oscillation). Absorbing the photones with energy more than E=3.43 eV electron pairs can be temporarily absorbed in smaller traps in the centers of triangles Zn^{2+} in plane (0001), forming current conducting metal planar [1] Zn^{2+}/e^- couplings. UV irradiation of high-resistance samples with $\rho_i \sim 10^{11}$Ohm·cm the value of ρ_i decreases in $2 \cdot 10^3$ times. In the process of irradiation of such samples by visible light ρ_i decreases in tens times. When ion Zn^{2+} is replaced by metal ion Me^+ one single-electron coupling —Me^+———e^-—06^+— which captures one electron and becomes negatively charged — Me^+——$2e^-$—0^{6+}— coupling. When ion Zn^{2+} is replaced by metal ion Me^{3+} planar $Zn^{2+}Me^{3+}/e^-$, $Zn^{2+}Me^{3+}/2e^-$ and $Me^{3+}/3e^-$ couplings are formed. Ions Al^{3+} decrease ρ_i of zincite to units Ohm·cm. Tetrahedral couplings $Zn^{2+}/2e^-$ and $0^{6+}/6e^-$ on the base of vacancies 0 and Zn conduct current and give absorbtion bands in UV range. On the basis of Zn vacancies — 0^{6+}—$2e^-$—H^+—$2e^-$—0^{6+}— couplings can be formed. They give bands of IR absorbtion. Ions Li^+ e^-—Li^{3+}—e^- can be absorbed in the centers of triangles $(2e^-)_3$ of neighboring parallel to axis C ZnO couplings, forming positively charged $(2e^-)_3/Li^+$ centers. The charge of crystals is displayed in strong asymmetry of volt-ampere curves (VAC):I (+U), resulted in sum of external and internal, proper voltages and I (-U) resulted in subtraction (voltage of the sample is lower than external one). The difference of currents of these VACs reaches 20 times. Hysteresis of direct and reverse movement of VAC is explained by shrinking of proper field $\varepsilon_{prop.}$, caused by the growth of external voltage +U and, vice versa, by extending $\varepsilon_{prop.}$ caused by the growth of –U.

Many crystals when reaching a certain critical voltage (from 25 to 150 V) are noted to have a considerable voltage drop on the samples at first at a slow and then at a sudden growth of current (less 1A) while heating them up to 200-400°C. We connect this drop with the formation of numerous negatively charged Zn^{2+}/e^- centers beside "+" electrode. The steepness of VAC increases along with the growth of mecanical load σ (N/m^2) on the samples. However, good repeatability of curves $\rho_i \sim \sigma$ when they are multiply removed doesn't occur. Gamma-irradiation decreases ρ_i of crystals by order of magnitude.

Initial crystals are not piezoactive. Only after annealing at 500 °C there appear signals "resonance-antiresonance" which reach maximum amplitude after annealing at 650 °C (5-7 times as much as quartz wafer). It is shown that p-type of "hole" conductivity and "+" of Hall's coefficient are not caused by mythical holes in crystals but by the fact that the external field $\varepsilon_{ext.}$ provokes the growth of their own opposite field $\varepsilon_{prop.} > \varepsilon_{ext.}$ which accelerates electrons in the direction opposite to the one when $\varepsilon_{prop.} < \varepsilon_{ext.}$ (n-type).

1. Semenov K.P. Electron-ion structures of crystals. The 5th International Conference "Crystals: growth, properties, real structure, application". Alexandrov: VNIISIMS 2001. pp. 560-603.
2. Semenov K.P. Neoclassic counterrevolution in natural sciences: axiomatics and theory of structures in mathematics, physics, chemistry. Computer copy. Alexandrov: VNIISIMS 2004.

REVERSED COMPLEX DIELECTRIC PERMITTIVITY IN CRYSTALS OF THE ROCHELLE SALT GROUP

A. V. Shil'nikov, V. A. Fedorikhin and N. V. Ratina

Volgograd State Architectural and Engineering University, Volgograd, 400074, Russia

Results of studies of reversed complex initial dielectric permittivity ε_0^* in crystals of the Rochelle salt group are presented in this work, namely, pure (RS), litium-doped Rochelle salt (LRS) and 100% deuterated Rochelle salt (DRS). The measurements have been made on a bridge equipment in ultraweak (≈0,4 V/cm) low and infra-low frequency measuring fields. Unlike the experiments described in [1-2], the temperature points were selected near the lower and upper Curie points in order to the values of spontaneous polarization for the all samples have the same magnitude ($\approx 1 \cdot 10^3$ Кл/м^2). Thereby, at the given conditions isotopic and isovalent impurity and difference of temperature influence mainly on investigated characteristics of our crystals. Before the measurements the samples were exposed to short-time field-effect annealing. The sinusoidal field of 50 Hz was applied to crystals. The amplitude was variated from the saturation field of polarization to zero and then samples were kept without influence during 30 min. Spectra of $\varepsilon_0^*(\nu)$ were obtained at different values of the applied DC bias field $E_=$. For all samples at temperature set-point effective depths of dispersion of the real part of the complex permittivity was determined, namely, frequency effective depth $\Delta\varepsilon'(\nu)=\varepsilon'_{1\Gamma u}-\varepsilon'_{1\kappa\Gamma u}$ and "field-effect" depth $\Delta\varepsilon'(E_=)=\varepsilon'_{max}(E_=)-\varepsilon'_{min}(E_=)$. These data are presented in Table. Here $E_=$ is the value of the applied DC bias field, under which ε' has maximum $\varepsilon'_{max}(E_=)$. Arrows designate the tracing direction of the quasistatic polarization loop. $\varepsilon'_{min}(E_=)$ is the value of the ε' of the sample in the state of the polarization saturation. Obtained results demonstrated that the isotopic and/or isovalent substitution of atoms in Rochelle salt lattice gives rise to higher polarizability of the samples. It should be noted that the differences connected with the value of the domain wall concentration are negligible at the given thickness of the crystals studied here.

SAMPLE	T, °C	$E_=$, V/cm	$\varepsilon'_{min}(E_=)$	$\varepsilon'_{max}(E_=)$	$\Delta\varepsilon'(E_=)$	$\Delta\varepsilon'(\nu)$
RS	-14.4	→ 80	81	291	210	141
		← 1.4	76	308	232	149
	21.3	→ 51.4	91	686	595	537
		← 5.7	97	762	665	609
LRS	-13.4	→ 24.6	51	388	337	201
		← -57.4	55	361	306	201
	20.1	→ 24.6	57	793	736	632
		← -24.6	60	881	821	654
DRS	-18.5	→ 188.9	90	323	233	131
		← -222	71	241	170	61
	30.7	→ 100	98	1085	987	899
		← -77.8	97	1124	1027	937

The studies have been partly supported financially by the grant of RFBR №02-02-16232, the grant of Competitive Centre of Ministry of Education № E02-3.4-424, the grant № 202. 03. 02. 04 "Science investigations of higher school in the priority lines of science and technology" and the grant № 1514.2003.2 of the support to leading schools of science.

1. *E. S. Popov, S. L .Rapoport, A. V. Shil'nikov,* Izv. Akad. Nauk SSSR, Ser. Fiz., **31**, 1199, (1967).
2. *A. V. Shil'nikov, A. P. Pozdnyakov, N. M. Galiyarova, L. A. Shuvalov,* Izv. Ross. Akad. Nauk, Ser. Fiz., **67**, №8, 1117-1123 (2003).

IMPACTS OF VARIOUS TYPE DEFECTS ON LOW AND INFRA-LOW DIELECTRIC RESPONSE OF THE TRIGLYCINE SULFATE GROUPE

A. V. Shilnikov, V. A. Fedorikhin, B. A. Strukov* and N. V. Ratina

Volgograd State Architectural and Engineering University, Volgograd, 400074, Russia

* Moscow State University, Moscow, 119992 Russia

Dielectric responses of several crystals are compared in this work, namely, of nominally pure (TGS), chrome-doped triglycine sulfate (TGS+Cr^{3+}) and (TGS+Cr^{3+}) crystals irradiated with the characteristic CuK_α radiation (at a dose of ≈80 kR) - (TGS+Cr^{3+})R. The measurements have been made on a bridge equipment in ultraweak (E_0≈0,4 V/cm) low and infra-low measuring fields both wide temperature range and near phase transition (PT). Experiment results show general and different properties of investigated single crystals. The temperature dependence of the real part of the complex permittivity $\varepsilon'(T)$ of all samples has typical λ-shaped peak and $1/\varepsilon'(T)$ obeys the Curie-Weiss law. However, $\varepsilon'(T)$ и $1/\varepsilon'(T)$ show that (TGS+Cr^{3+}) has more diffusion PT then other. Besides, X-ray irradiation of the crystals results in "radiation annealing" which increases their polarization and diminishes diffusion of the PT. Curves $\varepsilon'(T)$ and maximum values ($\varepsilon'_{(TGS)max} > \varepsilon'_{(Cr)Rmax} > \varepsilon'_{(Cr)max}$) confirm this fact.

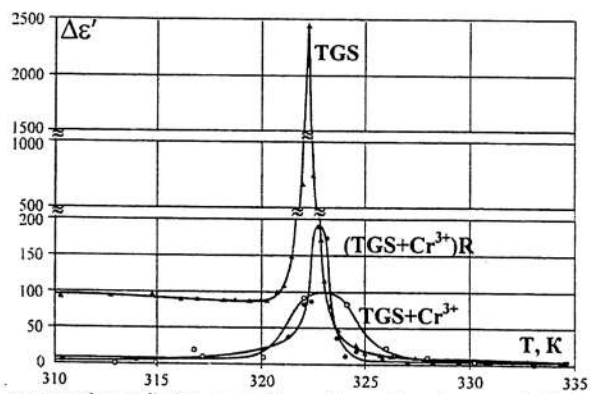

Figure shows curves of temperature dependence of the effective depth of dispersion ($\Delta\varepsilon' = \varepsilon'_{1Hz} - \varepsilon'_{1kHz}$). It illustrates that the region of pronounced dispersion of ε* is observed mainly in the temperature range near the PT. Therefore, one can assume that radiation annealing only partly reduces unipolarity of the (TGS+Cr^{3+}) crystal. Table indicates the comparative dielectric characteristics of crystals obtained in heating treatment. C_p and C_f are Curie-Weiss constants determined for the para- and ferroelectric

phases, respectively.

Parameters	ε'_{max}		C_P, K		C_F, K		T_c, K from $1/\varepsilon'=f(T)$		C_p / C_f	
Sample	1 kHz	1 Hz	1 kHz	1 Hz	1 kHz	1 Hz	1 kHz	1 Hz	1 kHz	1 Hz
TGS	12899 ±129	15331 ±153	2788 ±46	2805 ±49	1056 ±61	1211 ±63	322,25 ±0,02	322,55 ±0,02	2,64 ±0,12	2,32 ±0,11
TGS+Cr^{3+}	3002 ±30	3084 ±31	3173 ±3	3288 ±4	919 ±4	928 ±4	323,10 ±0,02	322,85 ±0,02	3,45 ±0,03	3,54 ±0,03
(TGS+Cr^{3+})R	3905 ±39	4076 ±41	2584 ±26	2695 ±25	851 ±3	912 ±5	322,92 ±0,02	322,89 ±0,02	3,04 ±0,07	2,95 ±0,05

The studies have been partly supported financially by the grant of RFBR №02-02-16232, the grant of Competitive Centre of Ministry of Education № E02-3.4-424, the grant № 202. 03. 02. 04 "Science investigations of higher school in the priority lines of science and technology" and the grant № 1514.2003.2 of the support to leading schools of science.

INVESTIGATION OF PREPARETION OF Mg-CONTAINING HYDROXYAPATITES, CARBONAT- HYDROXYAPATITES AND COMPAUNDS ON THE BASE OF THESESUBSTANCES AND COLLAGEN

Ejova J.A., Koval E.M., Zakharov N.A., Kalinnikov V.T.

Kurnakov Institute of General and Inorganic Chemistry RAS,
Leninskjj pr., 31, 119991, Moscow, RUSSIA
E-mail: zakharov@igic.ras.ru, (095) 955-48-84, (095) 954-12-79

Biomaterials and tissue engineering are becoming increasingly important in biomedical and chemical practice. It is clear that cellular response to materials depend on composition and structural properties of the material at both micrometer- and nanometer scale.

We developed a method (solubility of I.V. Tananaev) to produce biocompatible inorganic materials with different compositions and compounds on the base of a biocompatible phosphates and biopolimers. Our method is based upon investigation of systems $CaCl_2$-$MgCl_2$-$(NH_4)_2HPO_4$-NH_3-H_2O, $CaCl_2$-$MgCl_2$-$(NH_4)_2HPO_4$-NH_4 HCO_3-NH_3-H_2O and systems $CaCl_2$-$MgCl_2$-$(NH_4)_2HPO_4$-NH_3-H_2O-collagen, $CaCl_2$-$MgCl_2$-$(NH_4)_2HPO_4$-NH_4 HCO_3-NH_3-H_2O-collagen with constant concentration of $(NH_4)_2HPO_4$ 0,05 mol/l and relation in starting stocks $n_1 = Ca^{2+} : PO_4^{3-} = 1,63\text{-}1,65$, $n_2 = Mg^{2+} : PO_4^{3-} = 0,0083; 0,0167$; $n_3 = CO_3^{2-} : PO_4^{3-} = 0,033$, pH = 9,7-10,4.

Experimental data (chemical analysis, IR-spectroscopy, X-ray analysis) have shown formation in solid states of inorganic substances - nonstoichiometric hydroxyapatites with compositions:

$Mg_{0,1}Ca_{9,8}(PO_4)_6(OH)_{1,8}\cdot xH_2O$ ($n_4 = 1,63$); $Mg_{0,05}Ca_{9,85}(PO_4)_6(OH)_{1,8}\cdot xH_2O$ ($n_4 = 1,64$); $Mg_{0,1}Ca_{9,9}(PO_4)_6(OH)_{1,8}\cdot xH_2O$ ($n_4 = 1,65$); $Mg_{0,1}Ca_{9,8}(PO_4)_6(CO_3)_{0,2}(OH)_{1,4}\cdot xH_2O$; $Mg_{0,05}Ca_{9,85}(PO_4)_6(CO_3)_{0,2}(OH)_{1,4}\cdot xH_2O$; $Mg_{0,1}Ca_{9,9}(PO_4)_6(CO_3)_{0,2}(OH)_{1,6}\cdot xH_2O$;

and compaunds on base of these substances and collagen:

$Mg_{0,1}Ca_{9,8}(PO_4)_6(OH)_{1,8}\cdot z$ collagen $\cdot xH_2O$; $Mg_{0,05}Ca_{9,85}(PO_4)_6(OH)_{1,8}\cdot$ z collagen $\cdot xH_2O$; $Mg_{0,1}Ca_{9,9}(PO_4)_6(OH)_{1,8}\cdot$ z collagen $\cdot xH_2O$; $Mg_{0,1}Ca_{9,8}(PO_4)_6(CO_3)_{0,2}(OH)_{1,4}\cdot$ z collagen $\cdot xH_2O$; $Mg_{0,05}Ca_{9,85}(PO_4)_6(CO_3)_{0,2}(OH)_{1,4}\cdot$ z collagen $\cdot xH_2O$; $Mg_{0,1}Ca_{9,9}(PO_4)_6(CO_3)_{0,2}(OH)_{1,6}\cdot$z collagen $\cdot xH_2O$.

In investigated systems origined only carbonat-hydroxyapatites of A-types. The substitution of PO_4^{3-} by CO_3^{2-} in solid state under considered conditions is not take place.

We acknowledge the financial support from Foundation of Presidium of Russian AS (Fundamental sciences to medicine; Synthesis of substances with specified properties).

STUDY AND REVEALING LAWS OF NUCLEATION OF CALCIUM OXALATE IN AQUEOUS SOLUTION

O.A. Golovanova, Department of Chemistry, Omsk State University, Omsk, Russia
E.V. Rosseyeva , Department of Chemistry, Omsk State University, Omsk, Russia

The study of crystallization and nucleation of substances in aqueous solutions is one of the actual directions in modern research, but at present they are poorly investigated. Calcium oxalate is one of the most popular salts, which is crystallizing in organism. The feature of urinary stones composition in Omsk region (Russia) by the methods of X-ray diffraction, infrared spectroscopy and Ion-Exchange Chromatographer was studied. On the base of data about quantitative and qualitative composition of urine and physicochemical properties of crystallization phase thermodynamic and mathematical crystallization models for some urinary stones mineral phase was built. It was established, that the dominant part of urinary stones is presented with calcium oxalate (60%), which has two main forms: $CaC_2O_4\cdot H_2O$ and $CaC_2O_4\cdot 2H_2O$. In our research we studied the peculiarities of nucleation and growth of calcium oxalate monohydrate (COM) crystals in aqueous solutions with presence of albumin and amino acids which are components of solution where COM crystals are formed in human organism. In our analyses we worked under conditions whenever possible to *in vivo*. The results obtained in the experiments permit us to assume that presence of albumin, Glycine and Glutamine acid in aqueous solutions decreased general reaction order, nucleation time and rate constant of nucleation COM and inhibited growth and aggregation rates of its crystals.

HEXAGONAL AND CUBIC PHASES OF SOME ALKALI METAL PNICTIDES

O.K.Gulish[1], O.V.Kravtshenko[1], M.E.Leonova[1], L.G.Sevastyanova[1], A.I.Medovoj[2]

[1]Department of Chemistry, Moscow State University, Leninsky Gory, 119899 Moscow, Russia

[2]Russian Academy Natural Science

The most part of alkali metal pnictides Me_3Pn (Me÷ Li, Na; Pn÷ P,As, Sb, Bi) under atmospheric pressure and ambient temperature have hexagonal strukture.

These compounds where found to undergo reversible phase transition from hexagonal to denser cubic phase under high pressure [1-3].

Existence of the correlation constancy Kc for isostructural pnictides Me_3Pn has been established:

$$Kc = a_i^H / a_j^H = c_i^H / c_j^H = a_i^C / a_j^C, \text{ where}$$

a_i^H and c_i^H - parameters of the lattice for hexagonal phase of some pnictid;

a_i^C - parameter of the lattice for cubic phase of this pnictid;

a_j^H, c_j^H, a_j^C - parameters of the lattice for hexagonal and cubic phases of other isostructural pnictid.

A correlation constancy makes possible the evaluation of unknown parameter of the lattice.

The calculated values a^C of Na_3Sb and Na_3Bi are found to be in good agreement with experimental results {Table }.

Compounds	Parameters hexagonal phase, Å (known}		Parameters cubic phase, Å		
	a^H	c^H	a^C(known}	a^C(calculated}	a^C{experimental}
Li_3P	4,26	7,54-7,58	-	-	5,88-5,93
Li_3As	4,39	7,81	-	6,06	-
Li_3Sb	4,71	8,32	-	-	6,57
Li_3Bi	-	-	6,71	-	-
Na_3P	4,98	8,80	-	-	-
Na_3As	5,09	8,98	-	7,05	-
Na_3Sb	5,37	9,52	-	7,47	7,40-7,46
Na_3Bi	5,45	9,66	-	7,59	7,60-7,65

This method we hope can be use in some other application.

The work was carried out the financial support of the Russen Foundation for Basic Research (Project Noc. 00-15-97457 and 02-02-17915).

[1] Beister H.J., Haag S., Kniep R. et al.//Angew. Chem. 1988.V.100.P.1116.

[2] .Leonova M.E., Sevastyanova L.G., Gulish O.K., Burdina K.P.//Inorg. Mater. 2001.V.37. PP.1270-1273.

[3] Leonova M.E., Bdikin I.K., Sevastyanova L.G. et al //Vestn.Mosk.Univ., Ser.2: Chem. 2000.V.41. PP.334-337.

DEVELOPMENT OF A TECHNIQUE OF COMPRESSION OF GASES AND LIQUIDS UP TO HYPERHIGH PRESSURE

V.A.Mukhanov

It is known that many technological processes are considerably accelerated under high pressure, however the big problems arise at compression of gases and liquids.

The purpose of this work is to create a cell for processing various materials by high pressure of gases in wide temperature range.

The object in view was achieved by compression of gases in the condensed condition (solid or liquid) in a copper (or from beryllic bronze) ampoule. Edges of a beaker of an ampoule were executed as the V-shaped ledge, and in a cover there was a deepening conterminous to a ledge.

The reactionary cell is shown on fig. 1. In ampoule *1* there is a sample *2*. The ampoule with a sample is cooled by liquid nitrogen - (-196^{0}C), close to cover *4*. After evaporation of liquid nitrogen the cover *4* opens and quickly brings in the ampoule necessary quantity of the condensed gas *3*, then the ampoule closes cover *4*, and is repeatedly cooled up to-196°C and together with the cooled (-196°C) face electroinputs 5 is inserted in the container from a lithographic stone or pyrophillite *6*.

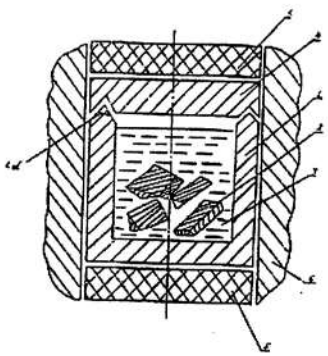

A Fig. 1. A reactionary cell for compression of condensed gases.

1 - beaker of an ampoule from copper or beryllic bronze (at compression of oxygen the beaker is made from aluminium); 2- processable gases by high pressure material; *3* - compressed gas;4- *-cover* from copper, beryllic bronze (at compression of oxygen from aluminium); 5-composition electroinputs; 6-container from a lithographic stone or pyrophillite.

The equipped container is put between two hard-alloy matrixes and compress by the pressure 2.0-2.5 GPa, maintains 2-3 minutes that the cell has got ambient temperature, and

then compress up to the necessary pressure (calibration on pressure by a standard technique). After compression by transmission of an electric current through a reactionary cell manufacture its warming up to necessary temperature on the given capacity (preliminary calibration with the help of the thermocouple chromel-alumel).

After endurance during necessary time heating disconnect, pressure reduces to atmospheric. Methane, nitrogen, argon, ammonia, carbonic gas, various liquids can be compressed up to 4,3-4,5 GPa with warming up to 1300^{0}C in volumes up to 2 cm^3 by the described technique. At compression of oxygen it was marked its vigorous (especially at heating) interaction with copper that interferes with hermetic sealing of the cell.

Copper begins intensively to pass hydrogen at pressure 4.0 GPa already at 700-800°C.

It is established, that the gases having boiling point are higher-196°C, it is possible to compress down to 10.0 GPa, using the developed technique.

To compress oxygen it was possible in an aluminium ampoule. In this case on the surface of aluminium under action of the compressed oxygen extremely strong film of oxide protecting metal from the further oxidation is formed. Thus it is established, that having heated cells it is possible to carry out up to melting point of aluminium, at pressure 2.0 GPa it is possible to heat a reactionary cell up to 760°C, at 4.0 GPa up to 980°C, at 6.0 GPa up to 1050°C, at 10 GPa up to 1300°C. At higher temperatures it is possible explosive decompression of cells.

For the same reasons the aluminium ampoule is steady against influence of fluorine, fluorine hydride, xenon bifruoride, nitroden dioxide.

In an aluminium (or duraluminium) ampoule it is possible to make up at high temperature and at hyperhigh pressure of oxygen various compounds: in particular, high-temperature superconductors. So, at processing $YBa_2Cu_3O_{6,9}$ (T_c = 89 K) at 4.0 GPa oxygen and at temperatures up to 570°C) oxygen up to composition $YBa_2Cu_3O_{7,8}$ (T_c=91 K). At higher temperatures passes the oxygenolyse this compound with formation $YCuO_3$ and $Ba_2Cu_2O_5$. The bismuthic and thallic superconducting compounds are exposed to oxygenolyse at 300°C under pressure of oxygen 2.0 GPa with formation of compounds with pentavalent bismuth, trivalent thallium and trivalent copper. Superconducting properties at trioxide of thallium Tl_2O_3 (part of a superconducting phase is ~0.01 %)were established at 77 K.

Compression of the liquefied ammonia with mixture of hexagonal boron nitride and magnesium diboride carried out in copper ampoules with inner diameter 17 mm and inner height 10 mm and reactionary volume V = 2.27 cm^3. Use of such ampoules allows to obtain in ammonium - thermal process up to 15-17 carat of cubic boron nitride in every 3-5-minute cycle. It is possible to obtain the alloying semiconducting (p-type or n-type) crystals of BN_c by using reactionary mixture with additions of Be_3N_2 or Si_3N_4 respectively.

SYNTHESIS OF SMALL HIGH-STRENGTH CRYSTALS OF DIAMOND.

Mukhanov V.A., Filippova E.B.

For carrying out the most efficient and economic way of cutting of solid and super-solid crystals of sapphire, silicon carbide, titanium nitride – multi-blade or wire cutting up, and also polishing these materials, the diamond micro-powder measuring from 40/28 microns up to 14/10 microns as an abrasive is used.

The single-crystal micro-powder with the raised strength characteristics is preferable, allowing to manufacture the greater number of sawing up cycles.

In the monography [1] the micropowder of DSMIQ type (Diamond synthetic mono-crystaline of high quality) appropriating to such requirements has been described and the assumption of expediency of use contained as a source of carbon at target synthesis of natural graphite, and also application of the metal - solvent preliminarily saturated with carbon. It is necessary to note that on the data [1] crystals of DSMIQ type surpass in abrasive ability crystals of ASN type (GOST 9206-80) in size range sizes between 5/3 microns and 20/14 microns (1,5-3 times), and the diamond micro-powder measuring 28/20 microns and above does not differ from diamonds of ASN type (GOST 9206-80) .

The purpose of the present work is to create an efficient technique for the synthesis of small diamonds of the raised toughness at high overall yield from one sinter (not less than 2,5 carates) with the maximal maintenance of crystals of graininess 20/10 microns.

The analysis of many experimental cycles of sintering showed that it is possible to reach an object in view when following the conditions listed below:

1. Use as a source of carbon at synthesis of natural graphite of GSM type preliminarily processed in a disintegrator, graininess less than 40 microns.

2. Application of eutectic NiMn alloy of PRGN-40A type (with particle size less than 40 microns) as metal - solvent.

3. Optimal composition of fusion mixture for synthesis of diamond micro-powders has been determined as a ratio 30-40wt. % of carbon and 60-70wt. % NiMn.

4. Pre-award heat treatment of fusion mixture is entered in vacuum at 960^0C within 0,5-1,5 hours for impregnation of black lead by metal and carbonization of metal - solvent.

5. Ready fusion mixture is charged in the container with reactionary volume $1,2 \cdot 10^{-6}$ m^3 by using the end heaters providing an optimal temperature schedule of synthesis at constant submitted capacity.

6. The optimal time mode of synthesis is determined as 50-90 seconds.

The yield of crystals of diamond from such cycle of sintering reached to 4 ct (at the maintenance in fusion mixture 40 weight. % of graphite). The part of the basic granularity 28/20 microns made 30-35 weight %, and the part of granularity 20/14 reached to 20 weight %. At maintenance of maximal initial pressure in high pressure chamber (HPC) and, accordingly, increase of number of nucleuses, it is possible to achieve displacement of a maximum of grain distribution in a zone 20/14 microns.

At work on similar fusion mixture in HPC of toroid type (P~8,0 GPa) it is easy for configuration to displace a maximum of grain distribution up to 5/3 microns [2]. However, at rather low pressures (~4,5 GPa) it is impossible to displace maximum of grain distribution lower than 20/14 microns.

To reach this purpose it is required to put into the fusion mixture for synthesis a strictly fixed quantity of diamond crystals measuring between 3 and 7 microns. Putting only 1 weight. % of 5/3 micron diamond as padding nuclei in fusion mixture heat-treated in vacuum allows to displace a maximum of distribution to a grain 14/10 microns. (~30wt. %), and overall yield of sizes 20/14 and 14/10 micron to finish up to 57wt. %).

Obtained diamond crystals have mainly well cube-octahedral forms and in 1,5-2 times higher abrasive ability in comparison with grains of powders ASN for sizes 28/20, 20/14, 14/10 microns, but concede on this index to values DSMIQ declared in [1] for graininess of 14/10 microns a little.

On the basis of given technological indexes it is possible to recognize the stated technique enough efficient for industrial use. Excretion of diamonds from sinters proceeds rather easily and with minimum losses when using the standard technologies of washing out. Obtained diamond crystals may be efficiently used by multi-blade or wire cutting up and polishing of solid and super-solid materials.

References.

1. Synthesis of diamonds. Novikov N.V., Fedoseev D.V., Shul'zhenko A.A., Bogatyreva G.P et al. Kiev: Naukova dumka, 1987, v.1, p. 42-46.
2. Sanzharlinskij N.G., Mukhanov V.A., Nosukhin S.A. Crystallization of diamond in quasi-isothermal conditions. In: Synthesis of minerals: Alexandrov,VNIISIMS, 2000. v.3, p. 144-178.

INTERRELATION OF THERMODYNAMIC CHARACTERISTICS OF SUBSTANCES WITH THEIR STRUCTURE AND PROPERTIES

V.A.Mukhanov, VNIISIMS, Alexandrov

Good conformity between calculated and experimental values (10 – 20 %) has been obtained when carrying out the work on determination of interrelations between thermodynamic characteristics of substances and their properties (hardness **H**, compressibility **b**, factor of linear thermal expansion **a)** [1,2]. Calculations of **H,b,a** for more than 100 simple and complex substances have been carried out by using formulas (1-3).

$$H = \frac{2,038 \cdot \Delta G_{атом}}{VN} AB \qquad (1)$$

$$A = \left[\frac{2 \cdot \Delta G_{атом}}{NV98,14}\right]^{0.00715\left[\frac{VN98,14}{\Delta G_{атом}}\right]^{1,935}} \qquad (1a)$$

$$B = \left(\frac{2X_C}{X_C + X_Д}\right)^2 \qquad (1b)$$

$$\alpha(T) = \delta \cdot \frac{V(T)}{3\Delta G_{атом}(T)\sqrt{B}} \qquad (2)$$

$$a(T) = \frac{Cp(T)}{Z\Delta G_{атом}(T)\sqrt{B}} \qquad (3),$$

where $\Delta G_{атом}$ - free energy of atomization of compound $C_m D_n$; **V** - molar volume, **N** - coordination number, **X** - Pauling electronegativity , $X_C < X_Д$; $C_p(T)$ - heat capacity; **δ, Z** - express factors [1,2].

The determined interrelations may be used in scientific and practical work for estimating properties of new materials.

1. Mukhanov V.A. Interrelation of hardness of substances with their structure and thermodynamic characteristics. – Proceedings of VNIISIMS Alexandrov, 1998, v. 15, pp. 145-154.

2. Mukhanov V.A. Hardness of materials - Proceedings of IV Int.Conf."Crystals: growth, properties, real structure and application, 18-22.10.1999,. Alexandrov. VNIISIMS v.2, pp. 295-308.

THE ADVANCEMENT OF DIAMOND REMOVAL FROM DIAMONDCONTAINING SINTERS

Mukhanov V.A.

VNIISIMS, Alexandrov

The technique of chemical diamond removal from diamondcontaining sinters is described. It includes the following stages:

1. Crushing of sinters till the sizes less than 2 mm.
2. Sieving of a crushed material on granularity 2000/630, 630/315 and less 315 micrometers.
3. Heat treatment of sinters on air at 580-590^{0}C within 0,5-1,5 hours scattered on pallets.
4. Chemical treatment of sinters (each granularity separately) 30 % muriatic acid in 13-liter plastic containers (on 2 kg of sinters) at ambient temperature.

Thus occurs self warming reactionary volume.

5. Washing and drying of the obtained rest from a mix of diamond, graphite and traces of metal.
6. Heat treatment of this mix (if necessary with the catalyst 1 weight. % of mix KOH: KNO_3 = 1:1) on pallets with thickness of layers no more than 20 mm at 570÷600^{0}C within 1-2 hours.
7. Heat treatment in a melt of alkali NaOH with addition of KNO_3 an obtained concentrate with the subsequent wash by cool water.
8. Acid treatment of obtained diamond, washing and drying.
9. Filtering off all diamondcontaining clouds for prevention of losses.

The technique practically excludes losses of diamond, there is no necessity to use ecologically dangerous compounds of hexavalent chrome and nitric acid, the specific consumption of chemical reagents contracts in comparison with other ways at 2-10 time.

The described way is used for reception of diamond in VNIISIMS since 1993.

Very large quantity of diamondcontaining sapphire slimes is formed by multiblade cutting of sapphire crystals with help of mixture of industrial oil and diamond powders.

The technique of diamond removal from the oily sapphire slimes, includes the following stages :

1. Burning off of oil.

2. Processing by muriatic acid for removal of iron.

3. Alkali treatment (in melt KOH with addition KNO_3), water wash of a melt, washing of a precipitate by water.

4. Processing of a washed precipitate by an muriatic acid, fallout of all finely divided diamond on a bottom of a vessel together with initial silicate gel, separation of diamondsfree gel, washing diamondcontaining gel water, processing by water solution of its potassium alkali for removal of silicon compounds , water wash, aqueous classification of diamond, drying.

The offered technique of diamond removal is cheap and allows to remove practically all diamonds more than 3 micrometers in size.

INTERACTION IN SYSTEM B - N-H IN THE CONDITIONS OF HIGH PRESSURE AND TEMPERATURE

V.A.Mukhanov, V.L.Solozhenko

VNIISIMS, Alexandrov, Institute of superhard materials, Kiev, Ukraine

The transformation process from graphitelike hexagonal boron nitride (BN_h) to cubic boron nitride (BN_c) runs under the pressure more than 4GPa and at a temperature over 1100^0C sufficiently quickly only in presence of traditional catalysts ($Mg_3(BN_2)_2$, Li_3BN_2, AlN, MgB_2).

The presence of ammonia in the reaction mixture reduces the P,T- parameters in this process and accelerates its velocity. It was possible to obtained cubic boron nitride with degree of transformation 0,90-0,98 from mixtures of BN_h (90 wt.%) and catalyst MgB_2 (10 wtv.) already under 2,5-2.9 GPa and at 1000-1100^0C.

The yellow powder of BN_c is formed with particle size from 1 to 100 micron. The particle size increases when the pressure decreases and the part of ammonia in reactionary mixture grows.

We use anhydrous hydrazine N_2H_4 or its mixture with ammonia 1:1 (the one weight part of hydrazine dissolves one weight part of ammonia at 0°C) in quality ammoniaforming substances for system BN_h+ MgB_2 with the purpose of increasing the processibility. However hydrazine is extremely poisonous what interferes with introduction of this technique in production.

The synthesis of BN_c is carried out to increase the processibility from a mixture of magnesium diboride with BN_h and urea or melamine.

It is established that transformation of BN_h to BN_c is promoted in water presence. The process runs under the pressure above 3.5 GPa while the temperature is over 1100°C. The catalyst of transformation is water - ammonia – boron oxide mixture:

$BN_h + 2H_2O = NH_3 + HBO_2 = NH_4BO_2$.

Small tetrahedral (2-3 microns) crystals of BN_c are formed during this process.

Amorphous and rhombohedral boron reacts with ammonia at 700 °C and pressure 0.20-3.5 Gpa forming rhombohedral boron nitride BN_r. On data of x-ray diffraction the part of the BN_r phase is 98-99 %, a =2.504 Å, c =10.00 Å. Under a higher pressure of ammonia (from

above 3.5 GPa), temperature is higher 1100 °C and long heat treatment of rhombohedral BN_r passes in BN_h . A degree of three-dimensional ordering obtained in BN_r researches routinely makes 0.7-0.9. Besides these samples contain a significant amount of hydrogen.

Tentative estimations show that 1 atom of hydrogen on 1000 atoms of boron and nitrogen suffices to make favourable "rhombohedral" (ABC ABC) an arrangement boronnitrogen layers. However rhombohedral modification is unstable. It passes to BN_h after a long heat treatment under high pressure in ammonia. This process is considerably accelerated in the presence of water: at 3% of H_2O in the mixture the reaction passes completely BN_r in BN_h for 3 minutes.

Rhombohedral modification is always formed as an intermediate phase at interaction of ammonia or hydrazine with boron or its connections.

It is necessary to note that so-called mesographitic m-BN with a degree of three-dimensional ordering from 0.2 up to 0.7 crystallizes disorder forms that at low temperatures (less than 800^0 C) in systems B + NH_3 , B_4C+NH_3, BP+NH_3, MgB_2 + NH_3. At higher temperatures it passes in BN_r.

The wurzite boron nitride BN_w is recrystallized at 4.0 GPa and 1100^0C in ammonia in a mix of BN_h and BN_c, and in the presence of traditional catalysts it passes completely in BN^c, therefore BN_w is absent on diagrams of crystallization B + NH_3, MgB_2 + NH_3 .

BN_r is formed also at thermal decomposition of borazol $B_3N_3H_6$ and borohydride ammonium NH_4BH_4 in ammonia at pressure 1.5-3.5 GPa and temperatures is higher 900 °C (at lower temperatures the part of m- BN is great), and process goes more softly in the presence of the gaseous nitrogen connecting forming hydrogen.

It is necessary to note that pyrolytic boron nitride undergoes action of ammonia (3.0 GPa, 1100 °C 15 minutes) significant ordering in a direction of an c-axis , flake boron nitride slit on thin leaflets: half-width of a reflex (002) decreases from 0.7-1.2 ° (Θ) till 0.15-0.18 °(Θ) (at axial compression by half-width of this reflex decreases till 0.5-0.6 ° (Θ)). (At BN_h half-width of a reflex is 0.12 °). It is indicate on the possible intercalation of ammonia into pyrolytic boron nitride and deintercalation out.

During studying solubility BN_c in systems MgB_2 - NH_3 and Mg_3N_2-NH_3 it was established, that at use of surplus of ammonia by the dissolving agent compound $Mg_3(BN_2)_2 \cdot 4NH_3$ is solubility in which makes in the first system 3.5 ± 0.5 weight. %, and in the second

system 4.5 ±1.0 weight. %. Distinction is caused by presence at the first system of a significant amount of the hydrogen forming at interaction of magnesium diboride with ammonia.

From the analysis of obtained results it follows that at interaction during 300-500 c within the searched systems spontaneous crystallization of BN_c is observed down to pressure about 2.0 GPa. If pressure is higher 2.5 GPa, a degree of transformation of BN_h to BN_c achieves values 0.90-0.98. The high degree of transformation and the small sizes of formed crystals testify to passing process of crystallization of cubic white graphite in the field of its thermodynamic stability far from a line of equilibrium.

It was not possible to fix spontaneous crystallization BN_c, under a pressure lower 2.0 GPa, however the experiments (which have been carried out in pressure range 0.5-2.0 GPa and temperatures 1200-1300^0C) with use of single crystals BN_c touch-hole and diamond touch-hole have shown a possibility of crystal growth of BN_c on a surface of injected seeds in the tetrahedral form with sizes 10-20 microns.

It is observed that the epitaxial growth of tetrahedral microcrystals BN_c with formation both collateral and twinning (on spinel to the law) accretions an octahedral surface of diamond single crystals 0.1-0.2 MPa and temperature 1130-1200^0C in system Li_3N-BN-NH_3

Thus the behaviour of synthesis BN_c in the presence of a fluid phase allows essentially to expand P, T-area of formation BN_c. Thus the experimental results contradict standard phase diagram BN Corrigan-Bundy [1] and well coordinate to the diagram designed in [2], it proves the credibility of our experimental data [3, 4].

References.

1. **Corrigan F. R., Bundy F. P.** Direct transitions among the allotropic forms of boron ni-tride at high pressure and temperatures//J. Chem. Phys. 1975. V. 63. N 9. P. 3812-3820.

2. **Solozhenko V.L.** About the phase diagram of boron nitride //Doklady Acad. nauk USSR. 1988. V. 309. N 1. P. 147-149.

3. **Solozhenko V.L., Mukhanov V.A., Novikov H. A.** P, T- area of the sphalerite boron nitride formation // Doklady Acad. nauk USSR. 1989. V. 308. N 1. P. 131-133.

4. **Solozhenko V.L., Mukhanov V.A., Novikov H. A.** Interaction of ammoniak and nitrogen with boron and its compounds in the high pressure and temperatures conditions // Doklady Acad. nauk USSR. 1990. V. 312. _N 3. P. 630-633.

STUDY OF VEIN QUARTZ SAMPLES FROM DEPOSIT ZHELANNOE BY ELECTRONIC MICROSCOPE.

V.G. Balakirev, G.I. Krylova, N.G. Sharov

VNIISIMS, Alexandrov, e-mail: sharova@list.ru

Deposit Zhelannoe is one of the most important Russian quartziferous objects. Considerable supplies of vein quartz, which have wide application as charge material for synthetical single crystal growing are found there. According to genesis vein quartz of this deposit belongs to metamorphogene-hydrothermal formations. It is very turbid and has coarse-grain (up to giant-grain) constitution and various deformations and according to behavior of structural deformations is referred to radiationally unstable type.

Samples of vein quartz, presented by white and gray fragments were studied. According to the obtained data white color of quartz is determined by light scattering on gas-liquid inclusions, pores and partly on associate minerals, localized in cavities of gas-liquid inclusions. Interfaces in cracks and intergranular cavities occur in gray quartz more often; obviously, light scattering on it creates gray color effect.

Defects, typical for vein quartz of the other deposits: gas-liquid inclusions, pores on the borders of grains and in its volume, break surface on the borders of grains and healed cracks, strain dislocations with frequency distribution ~10^4-10^5 cm^{-2} are observed in vein quartz samples from deposit Zhelannoe. Cavities of natural etching are absent on quartz of deposit Zhelannoe; features of quartz growth are showed distinctly. Mica-like formations are found often. Atypical drop-shaped formations, which weren't occurred anywhere earlier and have considerable volumes in scales of electronic microscope are found out in preparations, obtained from charge material, delivered by firm "Ranova". Round faces and growth stages are observed on it, that's why it's supposed that they crystallized from very concentrated fluids at the moment of fresh spalled spot preparing (probably, it was of technogenic origin, due to processing of quartz pieces by aggressive reagents). Apical growth forms of impurity phase are unusual (non-quartz) condensed along surface of intergranular cavity.

As a whole, a great amount of impurities, localized in gas-liquid inclusions, intergranular cavities in the form of friable aggregates or disintegrate particles are present in quartz of deposit Zhelannoe. Appropriate raw material requires application of special scheme of enrichment for its precision valuation.

REFLECTION OF GEODYNAMICAL SITUATIONS IN INDICATED PROPERTIES OF QUARTZ.

Bydtaeva N.G., Boroznovskaya N.N.*, Kiselyova R.A., Mileyeva I.M.

VNIISIMS, Alexandrov,

Quartz of oreless quartz veins in limits of Ural-Mongolian belt is studied: vitreous quartz of Sakmarskiy quartziferous area with enclosing eclogite-glaucophane-shaly complex, granular quartz of Ufaleyskiy eclogite-gneissic complex, vein quartz of seam zone of Garganskaya block framing (Eastern Sayan). The main methods of quartz studying were atomic-adsorptive, thermoluminiscent, gas-chromatographic and vacuum dekreptophonik.

Quartz vein formation of Ufaleyskiy complex took place in subduction zone of oceanic core under the continental block at regressive stage of metamorphism at increased pressures. Granular quartz has structure of tectonite and characterizes by low content of mineral and structural impurities. Own structure defects of excitonic type are prevalent. Water is prevailing in composition of inclusions at subordinated role of CO_2.

Quartz veins of Sakmarskiy area formed in subduction zone under island arc block in rocks of oceanic, island arc, and continental-slope formations at conditions of glaucophane metamorphism. Low content of chemical impurities are characteristic for quartz. AlO_4^{4-}/ Li^+ are prevalent in structural impurities. Increased content of water in inclusions are characteristic, as the reflection of low-temperature metamorphism.

Quartz of Dzhabyk-Karagayskiy quartziferous region is localized in Sugomaksko-Katsbakhskaya seam zone in dislocated rocks of apoultramaphite-greenschist formation (serpentinite mélange). Quartz differs by structural heterogeneity, in structural impurity composition AlO_4^{4-} centers with Al, Li, Na compensators are prevalent. Own defects role is decreased; nitrogen, methane, carbon oxide are present in inclusions as well as water and carbonic acid.

Nontraditional quartz material – monomineral quartzites, localized in rocks of silicocarbonic formations is found out in limits of Garganskaya block. The latter were formed in conditions of shallow shelf. Siliceous rock transformation in to granular (recrystallized) quartz occurred in conditions of mantle-overthrust tectonics, caused by ophiolite obduction on the Garganskiy microcontinent. Development of granular quartz in silicocarbonic thick mass is irregular and belongs to local structures, formed in conditions of compression in limits of shift zone. Increased amount of water and carbonic acid are present in fluid composition; increased content of carbon oxide and methane are characteristic. Roentgenoluminiscence of own defects of quartz are characteristic for chemically pure quartz. The concomitance of structural impurities is presented by Al^{3+}, Ge^{3+}, Na^+, Li^+, Mn^{2+}.

Study of quartz showed regular changing of its composition and properties in dependence of various geodynamical situations.

CHEMICAL ENRICHMENT OF VEIN QUARTZ OPAQUE VARIETIES BY ACIDIC LEACHING OF THE IMPURITIES.

Sharov N.G., Astafyev V.N., Krylova G.I.

VNIISIMS, Alexandrov, Russia, e-mail: sharova@list.ru

Treatment by acids or so called acidic leaching with the use of different acids and variants of its combinations, concentrations, temperatures of treatment is included at certain stages in all schemes of quartz enrichment [1]. Nowadays, traditional chemical methods of enrichment because of considerable toughening of requirements to quartz material quality under the contents of elemental and mineral impurities for quartz of melting type are not proved enough. Complex researches for optimization and selectivity of acidic treatment either at the initial stages of conversion, or at the finishing stages of precision purification are actual, because existing approaches to quartz material enrichment not always allow to obtain competitive concentrates and stable physical-chemical indexes of finished production. Appropriate problems are studied in VNIISIMS on the material with high content of gas-liquid inclusions on an example of opaque coarse-grain vein quartz of deposit Zhelannoe. It is known that this material is difficult to enrich, and the best results were achieved mainly due to treatment of quartz grits of standard size (+0,1-0,4 mm) by reagents, containing fluorine, in acid medium [2], at the final operations of enrichment schemes. Thus, considerable decrease of finished concentrate output was noticed.

As known, acidic leaching of elemental and mineral impurities assumes process and ecological difficulties [1-3], and also deficit of reagents. However, we can't be sure in obtaining of precision purification of enriched quartz grits without using hydrofluoric acid HF for the given types of quartz. That's why, it was decided not to retract from using of medium, containing HF, considering initial comparative purity of material and "favorable" discover of considerable part of some elemental impurities (mainly – Na, Ca, Mg, K) in the composition of gas-liquid inclusions and also diverse defects of quartz. We made this work during limited time of treatment (1-5 hours) in combinations with the other mineral acids at indoor temperature with forecatalyst and at increased T-parameters. This was made with account on long-dated and sparing application of equipment on the base of fluoroplastic-4 and isotactic polypropylene with intensive agitation of reacting mass, including supersonic treatment.This envisages an opportunity of higher output of concentrate at optimal rate of purification and regeneration of hydrofluoric acid from silicofluoride (IV) of hydrogen.

Concentrate purity in 24-25 ppm from original 42-45 ppm is achieved in sum of 13 elemental impurities.

It is known that mineral acids can efficiently purify surface-film pollutions and selectively dissolve some mineral impurities without use of HF-reagents, it makes possible to use mineral acids at initial stages of quartz material conversion, especially during "washing from ferrum" . It is detected that use of weaker oxalic acid instead of strong inorganic acids (HCl, HNO_3, H_2SO_4) during acidic treatment doesn't give optimal removal of impurities with low solubility producing, specifically of iron compounds [4]. Acidic leaching of elemenal impurities at the same parameters of quartz processing showed that efficiency of operation depends a little on the composition and concentration of strong inorganical acids in the range of concentrations 11-73 mass %.

Study of different acids and conditions of their application seem to be prospective for quartz of low transparence. They are particularly important for early stages of enrichment, because optional use of acids can promote the appearance of insoluble phases and another effects, which make difficult the complete puryfication of raw material from elemental impurities.

References:

1. Kravets B.N. Special and combined enrichment methods. M. Nedra. 1995, pp. 101-122.
2. Saltykova E.A., in "Perfecting of technology and machinery for vein quartz recycling". Kyshtym. 1988, pp.35-39.
3. Ryss I.G. Chemistry of fluorine and its inorganical compounds. M. Goskhimizdat. 1956.
4. Lidin R.A., Andreeva L.L., Molochko V.A. Reference-book on inorganical chemistry. M. "Khimiya". 1987. pp. 237-238.

RESOURCE BASE OF QUARTZ RAW MATERIAL IN RUSSIA.

Yu. A. Shatnov, I. S. Tigetova
VNIISIMS

Balance of mineral resources supplies of Russia includes deposits of piezooptical quartz, rock crystal, transparent recrystallized and granular quartz for melting, milky-white quartz for optical glass manufacture. Supplies of piezoquartz and rock crystal for melting are concentrated in deposits of the South and Subpolar Urals and the South Yakutia. Its quantity is rather limited, and these supplies aren't developed as there is no demand. Supplies of transparent recrystallized and granular quartz are estimated at millions of tons (accordingly more than 1,6 t. and about 3,0 m.t. in vein mass). Deposits of transparent quartz are presented by objects of the Subpolar Urals and partly – of the South Urals. Objects with granular quartz have been explored in the Middle and South Urals, in the region of Lake Baikal. Base of milky-white quartz with total supplies of more than 10 m.t. is presented by deposits of the South Urals, Karelia, and partly – of the Subpolar Urals.

Supposed resources of quartz raw material on 01.01.2003 are estimated by objects of piezoquartz, rock crystal and vein quartz for melting. Resources of the most important deposits (objects of the South Urals), or resources of developing composite deposits of the Subpolar Urals (Zhelannoye, Dodo, Puyva) are taken into account for piezooptical quartz or rock crystal. Although geologic perspectives in the respect of quartziferous mineralization also remain for a range of objects in other regions of Russia. Namavara in Belomorskiy area, Man'-Khambo in the North Urals, objects of Verkhoyanye and Momskiy area in Yakutia, Ket-Kapskiy and Omolonskiy area in the Far East, separate objects of Verkhne-Aldanskiy area, etc.

Specificity of the transparent recrystallized (glassy) and granular quartz resource base is determined by the fact that these resources do not meet contemporary demands of industry. Resources are not divided into directions of use and don't give an idea of mineral resource base status of the quartz raw material scarcest varieties (specifically, especially pure quartz, high qualitative charge for the synthesis). Well-founded data about resources of highly demanded quartz raw material at the present period is absent in spite of formally considerable scales of this base (transparent vein quartz – about 6,7 m.t., granular quartz proper – about 5,2 m.t.).

State of Russian mineral resources base is reflected on accompanying resource maps of piezoquartz – rock crystal and vein quartz. Maps show location of deposits and appearances which are taken into account, data on raw material supplies (in tables) and supposed resources (on circular diagrams) with quartziferous formations, presented by them. Electronic versions of Russian resource map are created with the use of scanning and subsequent vectoring of image by means of model of programs Easy Trace®. Digitized material is exported in the form of shp-files. Attributive information about deposits and appearances is presented in the form of dbf-files in WIN1251 coding. Assemblages for creation of resource maps hard copies of 1:7500000 scale have been worked out.

TIPOMORPHIC DEFECT COMBINATIONS OF QUARTZ HAVING DIFFERENT GENESIS AND THEIR INFLUENCE ON TECHNOLOGICAL PROPERTIES.

Krylova G.I., Balakirev V.G., Rakov L.T., Mitrophanov A.A.

VNIISIMS, Alexandrov; VIMS, Moscow; OAS "Polar Quartz", Moscow. Russia

Tipomorphic properties of quartz removed from genetically different formations have been studied. Their formations have the following ranges of TP-conditions: quartz veins are < 300 - 550°C, 2,5 – 8 kbar; pegmatites are < 550- 650°C, 6 – 8 kbar; silexites are ≤ 550°C, 5 kbar ; granite-porphyries are ~ 730°C, 1,5 kbar; quartzites are 400-600°C, 2-9 kbar. Complex of mineral-geochemical and spectroscopic techniques, X-ray topography and electronic microscopy was used.

Differences between quartz varieties are defined with maximum values of elements-impurities, with their proportion and position into quartz matrix. Com-bination and behaviour of defects depend on crystallinity degree caused by quartz genesis. When the aggressive action is available to quartz, the peculiarities of radiation instability are sharply changed.

Using electronic microscopy the density changes of deforming dislocations were revealed in the range of $10^5 - 10^9$ cm^{-2} (single instance to $10^{10} - 10^{15}$ cm^{-2}) including tendency of growing with TP-conditions for quartz forming. Variations of pore dimensions are to >3 orders achieving peaks at 3-4 μm. The total volume of pores is estimated as ~ 0, 0001% of the quartz volume. The amorphous rates are changed from 1-5 to >35 min.

Information of defect combinations is of great importance when the way of raw quartz processing and profile of its application in industry are chosen. Based on peculiarities of quartz defects the methods of their study using EPR, X-ray IL, IRS are required to adapt.

PECULIARITIES OF THE IMPURITY COMPOSITION OF THE VEINED NON-METALLIFEROUS QUARTZ IN BLACK SCHIST SERIES.

Krylova G.I., Skobel L.S.

VNIISIMS, Alexandrov; OAS "Polar Quartz", Moscow. Russia

A part of quartz veins is located in the carbonaceous rocks (black schist) in the quartz-bearing districts of the Urals. The significance of such rocks can be defined with physics-mechanical, geochemical barrier functions. They make an appreciable contribution at the level of the local criteria as they are to stimulate transformation of the fluid conditions caused quartz formation in its turn.

The veined quartz located in the carbonaceous strata has specific differences from quartz connected with the another rocks. Based on the chemical analysis they contain great amount of Mn, Ge, Cr, often Cu, Tl. It happens that value of Al, Ti, Na or Ca is decreased. The gas phase analysis contain great amount of CH_4, NH_3, CO which is rather higher than in quartz background. Mass-spectrometric analysis are to fix fall of water content to ~ 82 % against ~ 88 % in quartz that is removed from the veins of another rocks. Using X-ray IL technique the special centers of luminescence suppression are revealed. Such specific composition of the mine-rals - accessory veins is essentially changed. The veins being in the carbonaceous schist are very seldom crystal bearing

USE OF MAGNETIC PROPERTIES FOR IDENTIFICATION OF JEWELLER STONES

Artemjev G.G., Veretin V.S., Gerasimenko N.I.

Russian Academy of Economics named after G.V. Plekhanov, Moscow, Russian Federation

The magnetic properties of crystals are remarkable by that they depend not only on laws of crystal structure, but also from a condition and behavior of atoms, composing it. The researches of magnetic properties widely use with detailed study of real crystal structures with all by their deviations from the idealized circuits.

With definition of jewels quite often there are useful most unusual methods of research. One of such methods - definition of magnetic properties of jewels. Under magnetism gemmologers mean a quantitative measure of power reaction of a crystal on presence of a magnetic field. Magnetism in any measure reminds a magnetic susceptibility of a crystal. A small constant magnet and suitable scales of a nonperiodical type allow easily, though not inexactly to estimate magnetism of a stone.

In these experiments it is important to avoid distortion of results because of that, that some details industrial of scales are sometimes made from ferromagnetic materials.

The measurements are made as follows. On a cup of scales we place a high plastic support. The scales must be put to zero point. After that on a support we establish a researched stone and slowly bring to it a small magnet as long as it does not touch almost surface of a stone. If the mineral has appreciable magnetism, the balance of scales will be disturbed, when the magnet will be from a stone on distance of several mms. Write down weight, which stone "has lost" from action of a magnet. The difference between it and true weight will characterize an attraction of the given stone to a magnet.

This measurement is easiest for carrying out on scale of nonperiodical of a type, from which scale, it is possible continuously to read out the indications of weight.

For definition of magnetism of a stone it is possible to take advantage of the empirical formula

$\Delta P / \sqrt{P} \times 100$.

The practical value even of rough measurements is doubtless, since due to this measurment it is possible to distinguish stones having identical appearance and difficult to identify by usual methods of identification.

In a jeweler industry the limited number of minerals is actively used and they are easy to classify by method offered by B. Anderson, though, empirical formula, offered by him for definition of magnetism is questionable.

In table 1 the basic stones having appreciable magnetism are given.

Table 1

	Name	Given on B. Anderson	Data of the authors
Strong magnetic	Almandine	290-410	300
	Spessartine	250-360	320
	Rodonite	280-370	290
Middle magnetic	Chrisolite	50-75	40
	Pirope	40-100	50
	Turmaline dark green	50-70	40
Low magnetic	Green turmaline	10-20	8

The additional attractive party of the given method is the opportunity of its use even on stones inserted in frame.

The most successful results of application of the given technique were recognition of the following pairs stones given in table 2. They not only can have identical appearance, but also hardly identified by usual methods of diagnostics:

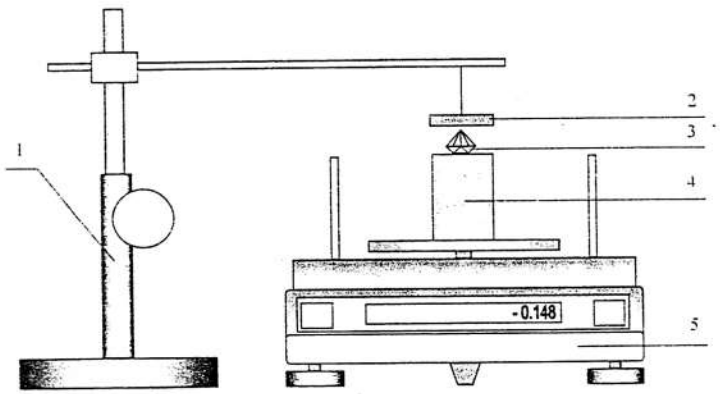

Fig. 1 Installation for measurement magnetism of crystals. 1 - bar - holder of a magnet, 2 - magnet, 3 - researched crystal, 4 - support from a nonmagnetic material, 5 - electronic scales.

DEFINITION OF AN INDEX OF REFRACTION OF JEWELLER STONES.

Artemjev G.G., Gerasimenko N.I.

Russian Academy of Economics named after G.V. Plekhanov, Moscow, Russian Federation

Correctly to identify a jeweler stone it is possible in an outcome of measurement it of the physical characteristics. One of the major optical characteristics of minerals is the index of refraction. For various jeweler stones this value essentially differs, therefore it is used as one of effective criterions of diagnostics and expertise of jeweler stones.

Passing light through the transparent environment rather precisely can be described by the laws of geometrical optics. It is based on concept of an optical ray as trajectories of light particles - fotons. Though from a point of view of the wave theory an essence of refraction is not the deviation of light from an initial direction, and change of length of a wave. The latter is observed, also with a normal falling of light on boundary of the unit of the environments, i.e. when the refraction is not observed.

For a research of jeweler stones, when there is enough accuracy of an index of refraction up to two decimal signs, it is necessary to stop on two methods: a method full of internal reflection and so-called direct method.

In jeweler practice large distribution has received refractometer, the principle of which is based on an appearance of so-called full internal reflection. A method fast and rather exact. Full internal reflection is observed in a lamina of a special immersion liquid ploted on a surface of a researched sample. Unfortunately, the index of refraction for majority of liquids, which can be used as an immersion, is insignificant. It limits possible values of an index of refraction to the value 1, 81 - 1,86. Besides transparent liquids with high values of an index of refraction, as a rule, is very toxic, that also limits area of their active application.

Less often and without a due physical substantiation the so-called direct method is applied. It used with a research of jeweler stones with an index of refraction larger, than 1,8. Diamond (n = 2, 42) and its main simulators fianite (n = 2,12) and muassanite (n = 2,69) belong to this group. And these stones especially first two, - are in the lead in jeweler business.

Practically in all issuings on gemmology for measurements the direct method recommends to use microscope. The researched sample should be transparent and have on itself

the grinded platform. It is attached to glass so that the platform is parallel to glass and is placed on the table of microscope. The essence of a method consists in matching the real height of a sample (that it is possible to make and with the help of micrometer) with an apparent height. The index of refraction presumably is equal to the ratio of the real height to an apparent height.

The absolute index of refraction of the environment is defined as the ratio of speed of light in vacuum to speed of light in the environment, or the ratio of lengths of waves of light in vacuum and environment or, that follows from it, as the ratio of sine of an angle of incidence to sine of a corner of refraction.

In a fig. 1 the course of rays creating the image is shown.

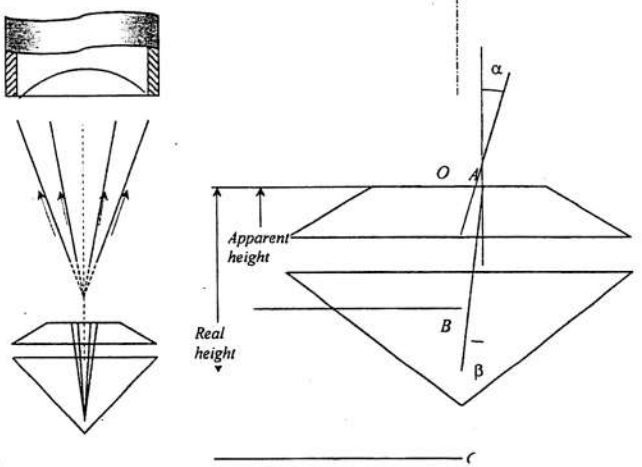

From triangles OAB and OAC, having the common leg OA it is possible is to receive the ratio of the real height of a chip to a height apparent and equally it will be to the ratio of a tangent of an angle of incidence to a tangent of a corner of refraction. For small (not exceeding 3 - 5 degrees) corners the tangent is approximately equal to sine. Therefore ratio of sines which are included in the law of refraction is possible in the first approximation to replace by the ratio of tangents. The

requirement of a smallness of corners, thus, is main, defining bounds of applicability of a technique.

The lens of microscope differ by the angular apertures. The more resolving power of lens, the more its the angular aperture. (Angular aperture - corner between extreme rays of a conic light bundle which is included in the system.) the depth of sharpness ensured by the lens, is in inversive relation from its aperture. Therefore requirement of a smallness of corners for rays used with a construction of the image, limits the use of lens with large allowing, so, with insignificant depth of sharpness.

The error of a method is significant. It is defined not only by difference of numerical value of sine from numerical value of a tangent, but also by large depth of sharpness of lens, having the small aperture, and, in the last queue, accuracy of measurement of moving basement of microscope. It is necessary to select the lens proceeding from the compromise between depth of sharpness and value of an aperture corner. To increase accuracy of measurement of moving of basement of microscope it is possible, by attaching to it modern electronic micrometer, permitting to define the linear sizes with accuracy of 0,01 mm. Thus, it is possible to receive quite satisfactory outcomes.

FORMATION OF ANDRADITE DEPENDING ON THERMODYNAMICAL PARAMETERS OF SYNTHESIS

J.V. Sankova[1], M.S. Kozlov[1], L.N. Demianets[2], E.V. Zharikov[1]

1- D. Mendeleyev University of Chemical Technology of Russia, 125047, Russia, Moscow, Miusskaya Sq., 9, sankova@rctu.ru

2 - The Shubnikov Institute of Crystallography of the Russian Academy of Sciences, 119333, Russia, Moscow, Leninskii prospect, 59

Beauty and unusual intensity of colour of gemstones always attracted attention of the mankind. An emerald and demantoid distinguish among stones having green colour. In contrast to synthetic emeralds, which are successfully growing by hydrothermal method, the technology of preparation of synthetic demantoid is not developed so far.

Demantoid represents a variety of andradite $Ca_3Fe_2Si_3O_{12}$ containing the chromium impurity up to 1,5wt%. The study of the diagram of ternary system CaO-Fe_2O_3-SiO_2 shows an incongruent character of andradite melting: the melting point is 1180^0C, and at temperature 1150^0C the decomposition of substance begins. Besides the given compound cannot be fabricated at normal atmospheric pressure, that speaks about inapplicability melt - growth methods.

On the basis of the analysis of geological features of andradite formation was chosen the hydrothermal method of synthesis of these crystals.

Several series of experiments on synthesis of andradite, with use of charge from oxides of iron (III) and silicon, and also with use various calcium - containing components are carried out: $CaCO_3$, $Ca(OH)_2$, $CaCl_2$, CaO, $CaSiO_3$. The water solutions $CaCl_2$, NH_4Cl, NH_4OH, Na_2CO_3, NH_4F, KOH, $LiNO_3$ and $LiCl$ of various concentrations were used as the solvent.

Yield of andradite crystals was investigated in dependence on the following thermodynamical parameters: temperatures from 250 up to 550^0C, pressure from 600 up to 1600 atm. On the data of X-ray analysis the maximum yield of andradite (95%) was achieved at the use of $CaCO_3$ as a calcium - containing component, at temperature 550^0C and pressure 1600 atm. At given thermobarical conditions at application of other calcium-containing components the

yield has made: for $Ca(OH)_2$ - 89%, for CaO - 85%, for $CaSiO_3$ - 83%. In addition to andradite among products of synthesis are found: $FeO(OH)$, $CaFeSi_2O_6$, $Fe(OH)_3$, which are reducing a yield of a main product of reaction.

At lower temperature and pressure (250^0C and 600 atm) the andradite formation is found only at use $CaCO_3$ and CaO as a source of calcium. The yield achieved was10 and 27% correspondingly. It allows to make the assumption that the boundary of andradite crystallization region begins below 250^0C. In the given conditions the reaction has ran not completely, what confirmed by the presence of the not reacted starting components of charge in the products of reaction. Besides that the following by-products of reaction were formed during synthesis: Ca_2SiO_4, Fe_3O_4, $Ca_6Si_6O_{17}(OH)_2$.

The analysis of the experimental data obtained at various pressures allows to make a conclusion about insignificant influence of pressure on formation of andradite and region of its crystallization.

The experiments carried out by us have shown that the lower temperature boundary of andradite crystallization region lies in limits from 250 (and below) up to 400^0C depending on a kind of starting calcium - containing components of charge and upon composition of the solvent.

NATURAL TYPES OF TURQUOISE – THE MAIN FACTOR IN CHOOSING METHOD OF IMPROVEMENT.

Soboleva T.V., Suchkova E.M.

Russian Research Institute for the Synthesis of Materials

No large deposit of turquoise has been developed during the recent years. In literature there are reports only about its discoveries of scientific importance [3, 4]. Turquoise supplies in the world are limited and irreplaceable, as well as other jewellery stones. At the same time turquoise remains highly demanded, occupying stable niche on the market of jewellery stones. Fall in demand of turquoise isn't prognosticated soon.

Jewellery turquoise forms 5-10 % of the deposit total mass. As a result of this, problems of improving of its quality become more significant. A great amount of improving methods are described in literature [1, 6]. Since turquoise as gemmological object is a polymineral material, so results of improving directly depend on its natural types, determined by mineral composition [7]. Turquoise, which preserves texture and characteristic peculiarities of natural turquoise is the most demanded. According to experimental data opalized turquoise, which is wide-spread on tekhutskiy (earlier kal'makyrskiy) industrial type in the rocks of porphyric formation with copper-molybdenum and polymetallic mineralization and possesses the largest effective porosity can be improved by such method (without violation of stone wholeness) [2, 5].

According to own results and analytical processing of literary data, natural (which contains quartz, opal, allophane) and corrresponding process types of turquoise are presented at deposits of various industrial importance in different degree of occurence.

Availability and degree of occurence of any process type of turquoise on the deposit allow us to prognosticate its profitability, taking into account choosing of optimal improving methods.

References:

1. Balitskiy V.S., Lisitsyna E.E. Synthetical analogues and imitations of gems. M., Nedra, 1981, 158.
2. Ivicheva S.N., Astafjeva N.V., Soboleva T.V. et al., in: "Crystals: growth, properties, real structure, application". 3rd Intern. Conf. (Alexandrov, VNIISIMS, 1997), vol.1, pp. 198-207.

3. Kleymenov D.A., Pekov I.V., Chukanov N.V. "Mineralogy, gemmology, art". Izd-vo Sankt-Petersburg, Saint-Petersburg, 2003, pp.33-34.
4. Popov V.A., Spirin A.N. Uralskiy Mineralogicheskiy sbornik, № 2 (1993), pp. 78-81.
5. Soboleva T.V., Makhina I.B., Astafjeva N.V., in: "Real structure and properties of acentric crystals". 2nd Intern. Conf. (Alexandrov, VNIISIMS, 1995), pp. 524-530.
6. Sorokina S.L., Balitskiy V.S., Tovmasyan A.I. et al., in: Abstracts of 1st gemmological conference (Chernogolovka, 1985), pp. 78-79.
7. Yakhontova L.K., Soboleva T.V., Plyusnina I.I. et al. ZVMO, part 118 (1989), № 2, pp. 83-93.

PRECISION REFINE OF THE $Sr_3TaGa_3Si_2O_{14}$ CRYSTAL STRUCTURE

V.V. Yunin, B.A. Maximov *, V.N. Molchanov *, B.V. Mill **, T.I.Ovsetsina, E.V. Chuprunov

Nizhniy Novgorod State University, N.Novgorod, Russia

* Institute of Crystallography RAS, Moscow, Russia

** Moscow State University, Moscow, Russia

The $Sr_3TaGa_3Si_2O_{14}$ single crystal belongs to trigonal acentric crystals of langasite family (structural type $Ca_3Ga_2Ge_4O_{14}$, the space group P321). Pure and activated ions of transitive elements the langasite crystals have interesting physical properties. They are - piezoelectricity, luminescence, laser and optical properties [1, 2]. The given structure has been determined [3], but R = 4,7 % is a little overestimated. The purpose of the given paper is precision structure refine by the x-ray diffraction data: an atomic structure of $Sr_3TaGa_3Si_2O_{14}$, monocrystal including chirality definition.

The crystal was grown by Czochralski method, rolled in sphere (d = 0,28мм). An experimental file of reflections and the specified meanings of parameters of an elementary cell were received in X-Ray laboratory IC RAS.

For initial the coordinates of atoms from [3] were taken. The crystal was determined in the space group P321. The refine was spent with use of extinction model of the 1-st type with Lorentz distribution of mosaic blocks.

At the account of thermal movement of atoms in isotropic approximation, in the basic atoms STGS was appear the distribution of residual electronic density, characteristic for harmonic of thermal fluctuations, is observed. Responsiveness of anisotropy of thermal fluctuations for all atoms of structure in harmonic approximation results in disappearance practically of all peaks of residual electronic density in the nearest vicinities of atoms and important by Hamilton criterion to decrease R/Rw to meanings 2.10/2.47 %.

On a final stage size of relative volume inverted components of a crystal (parameter Flack [4]) makes 0.03. At specification of inverted structural model R/Rw = 5,83/6,03 %. By results of these tests, it is possible to ascertain, that the absolute structure of the investigated crystal STGS meets to initial model and the coordinates of basic atoms of structure in the right system of coordinates characterize its absolute structure.

The crystal structure $Sr_3TaGa_3Si_2O_{14}$ is typical of langasite family. A basis of a skeleton are tetrahedron layers formed by oxygen tetrahedron of two grades: fineer 2d

(symmetry of a position - 3), engaged by atoms Si, and larger 3f (2), engaged by atoms Ge. The association of layers, translationally identical in a direction [001] = c, is carried out oxygen octahedron, inside which there are atoms Ta. Coordination polihedra of large atoms Sr, the occupying emptiness of a skeleton, have eight tops and can be submitted deformed by Thomsons cubes (dodecahedron with triangular sides).

The langasite structural type is characterized wide isomorphism in all cation positions. Refine of structural parameters of model at replacement of Ta atoms by Ga atoms 1a position results in R-factor increasing, that shows, that Ta atom completely occupies 1a position. By results of definition of the occupation of the 3f tetrahedra and 2d have made: 3f - ($Ga_{0.98(1)}$ $Si_{0.02(1)}$), 2d - ($Si_{0.97(1)}$ $Ga_{0.03(1)}$).

Thus, precision study of STGS crystal structure with refine of absolute structure is executed. The received meanings of coordinates of atoms and interatomic distances will be well coordinated to the data [3] at much higher accuracy. One may to note some distinctions in size and anizotropy of thermal fluctuations of atoms and more reasonable meaning of distance Ta-O.

The work is maintained by the grant RFFI 03-02-17075 and Program of conducting scientific schools (NS- 1642.2003.2).

References

1. B.V. Mill, Yu. V. Pisarevsky. // Proc. 2000 Int. IEEE/EIA Frequency Control Symp., Kansas City, Missouri, USA. 2000. P. 133.

2. A.A. Kaminskii, B.V. Mill, S.E. Sarkisov. // Physics and spectroscopy of laser crystals. M. Science.. 1986. P. 197.

3. H. Takeda, J. Sato, T. Kato et all. // Mater. Res. Bull. 2000. V. 35. P. 245.

DEPENDENCE OF GEMMOLOGICAL INDICES OF CHAROITE ON MORPHOLOGY AND INTERNAL STRUCTURE OF ITS AGGREGATES (PSEUDOCRYSTALS).

Smirnov A.A., Soboleva T.V.

Russian Research Institute for the Synthesis of Materials

Importance of gemmological indices of jewellery semiprecious charoite – commercial name of charoite rock, is determined mainly by mineral charoite and less by accompanying minerals, which influence on gem decorative properties isn't viewed.

Mineral charoite doesn't form single crystals. Its macrodepositions are presented by pseudocrystals or aggregates. They are built by submicrone-thread- like aggregates of parallel-fibrous individuals 30-40 nm in thickness and up to 1-2 cm in length. Therefore, according to fiber sizes charoite on one hand can be related to submicrone formations (cross-section), on the other hand – to thread-like (elongation). So superfine fibrous individuals of charoite can be characterized as new, not knowing earlier natural variety of thread-like crystals, notable for hyperanomalous elongation [4].

Hydrothermal-metasomatic origin of charoite caused the formation of different morphological types of its aggregates. Its sizes vary in wide limits: length changes from one-tenth mm up to 10-12 cm, width – from one-hundreth mm up to 1-3 cm [5].

Along with epigenetic changes of aggregates (plastic deformation, recrystallization) distortion of its original forms and appearance of some new types (fibrous-flaky, fibrous-laminar, etc.) takes place.

Authors have determined seven types of natural (geological) types and about 50 charoite varieties according to morphological types of charoite aggregates, petrogenetic conditions of its formation and some other parameters. Hereafter, they became the base for development of quality estimation criteria of charoite material and separation of jewellery and semiprecious stone sorts [2]. The following natural types have been picked out: aphanitic, fibrous, parquet-like (laminar), rossette-like, parallel-columnar, plicated and eye.

Main gemmological indices of charoite are: colour saturation, intensity of silver shade (silky or pearly), pattern and durability. They are determined by morphology and aggregate sizes, internal structure and structural-textural peculiarities of charoite rock.

Rate of colour saturation and intensity of silver shade are closely related. They are showed in laminar, columnar and radial aggregates with the sizes more than 0,5-1,0 cm in full measure. Strongly parallel packing of charoite fibrous individuals, minimal content of fine-dispersed dissemination of relict and superimposed minerals (aegirine, orthoclase, calcite, apophilite) are characteristic for them. Such semitransparent aggregates provide appearance of

saturated lilac, violet and brown colours and intensive silky shade ("running" line effect). However, when parallelism of fibers in aggregates is disrupted as a result of postmineral deformations, colour saturation decreases and pearly shade is observed instead of silky. The latter is characterized by isotropic and smooth light dispersion index without sharp maximums [1].

Patterns, created by different charoite aggregates, are extremely various and original [3]. Aggregates should have relatively large sizes, sufficient for psyhophysical perception with human eyes. The most beautiful patterns are created by radial, laminar, columnar and mis-shapen fibrous-goffering aggregates. However, unique patterns by decorative properties and contrast range are observed in aggregates with well-developed silver shade and dichroism. Due to this effects charoite colour changes accoding to optical orientation of aggregates from dark-violet, lilac to silver-white with gradual transitions. When orientation of polished sample changes, "running" silver line effect (silky shade) appears and wide gamma of colours of different luminosity (dichroism) is observed.

For the most part jewellery semiprecious charoite possesses low durability, which vastly decreases the possibility of its use in stone-cutting manufacture and first of all for jewellery settings manufacture. Aphanitic charoite, built by fine-acicular aggregates, less common on deposit, possesses very high durability [6]. Aggregates with relatively small sizes (not more than 0,5-1,0 cm): radial, interwoven fibrous, laminar, are not so durable, but suitable for jewellery setting manufacture. Postmineral deformation of aggregates vastly decreases the durability of charoite. That's why as a result of mechanical treatment flacky- and goffering-fibrous aggregates "crumble" easily and often are not suitable for big products manufacture.

1. Bukhtiyarova E.V., Smirnov A.A., Indutniy V.V., Taran M.N. Mineralogicheskiy zhurnal, vol. 14 (1992), №2, pp. 95-99.
2. Smirnov A.A., Soboleva T.V., Bukhtiyarova E.V., in: "Crystals: growth, properties, real structure, application". Intern. Conf. (Alexandrov, VNIISIMS, 1997), vol. 2, pp. 526-535.
3. Smirnov A.A., Soboleva T.V. Works of VNIISIMS, vol. XVI (2000), pp. 164-171.
4. Smirnov A.A., Soboleva T.V. "Mineralogiya Rossii" Tezisy dokladov God. Sobraniya Mineralogicheskogo obshchestva pri RAN (Saint-Petersburg, 2000), pp. 226-227.
5. Smirnov A.A., Soboleva T.V., in "Crystals: growth, properties, real structure, application". 5th Intern. Conf. (Alexandrov, VNIISIMS, 2001), pp. 255-257.
6. Smirnov A.A., Soboleva T.V. "Mineralogy, gemmology, art". Izd-vo Sankt-Petersburg, Saint-Petersburg, 2003, pp.66-67.

COLORED GEMSTONES:
SOME PECULIARITIES OF RAW MATERIAL, GEOLOGY AND DEPOSITS GENESIS,NATURAL RESOURCES

Kovalenko I.V., Kostelova T.G., Shulyaeva L.N.

VNIISIMS, Russia

Colored gemstones as the commercial minerals are characterized with the specific peculiarities. First of all, there is a lot of gems varieties and the ways of their formation. At the modern stone-cut industry over 100 names of gems are used. They belong to the different groups : minerals, mineral aggregates, rocks, bio-mineral aggregates, synthetic materials and improved gemstones The value of gems raw material depends not only on its decorative characteristics but also it is defined by their scarce in nature, current fashion, national-historic traditions, de-mands and business condition.

Colored gemstones depending on their quality are used in the different fields of jewelry and stone-cut industry. They are applied as technical raw material (dia-mond, corundum, garnets, agates, chalcedonies etc.). Classification developed by Kievlenko [1] is the most available one among the present systematization of the colored gemstones. It is based on the cost value and the application fields of gems. There are three groups there: jewelry (precious), jewelry – ornamental and orna-mental. It should be added that the ornamental stones can be used as a decorative material and sometimes as building one. In addition the ornamental stones have sections of high quality material that are used in jewelry industry.

Rarity and unequal location of the colored gem deposits on the earth surface, their small dimensions and sharply contrast gems composition in comparison with the rock totality are to testify their formation caused by the geological processes. Nowadays the saved up knowledge on geology, genesis and peculiarities of gems formation have been generalized by Kievlenko as the geology-industrial classifi-cation of the colored gems deposits [1]. It is based on the genetic grades and geo-logical position of deposits, ore-bearing and ore-generating formation. Such way allows to have an idea of the practical significance of objects, their scales and to contribute directions to predict, to prospect and to estimate these objects.

It's very difficult to characterize the geology-genetic peculiarities of some de-ficit gems. However we should pay attention to the following deposit peculiarities:

- Gemstones formation. Such gems as chrysolite, amethyst, garnet, corundum belong to the polygenic formation and occur into different formation comp-lexes. In fact their significant accumulations belong to the special geology-genetic types of deposits and connect with the restricted set of the geological formation.

- The original sources of the majority of jewelry, jewelry – ornamental gems are the small bodies of the complicated morphology having uneven distribu-tion of the commercial minerals. As a rule, they don't form the large indust-rial accumulations and are the material sources for placers that are the im-portant type of deposits, especially for the faceted stones.
- Colored gemstones (excluding the own deposits) form the industrial con-centrations at the deposits of the another commercial minerals. They are removed as the favorable component there.

Our country has the significant reserves of alexandrite, amethyst, demantoid garnet, emerald, jadeite, chrysolite, chrysoprase, agate, amazonite, lazurite, ne-phrite, rhodonite, charoite, amber, serpentine and jasper. Russia has the world reserves of charoite and about 90% of the world amber reserves.

The brief analysis of the mineral resource base (MRB) and gems market [2,3] shows that the current reserves can provide Russia with the leading positions at the world market to the specific kinds of gems. The Urals' demantoid, the Sayany nephrite, the Yakutyay chrome-diopside and charoite, the Baltic amber are of great interest.

The mineral resource base of Russia excludes the deposits and conformably the reserves of alexandrite, topaz, chrysoprase, turquoise, zircon, spodumene and others. The deposits of ruby, sapphire, noble opal, beryl, jewelry jadeite are very small by the reserves volume. In addition they are not able to rival at the world market by the raw material quality.

In conclusion we should say the following:

- The perspectives of MRB extension are connected with the worse know-ledge of the territories at the Eastern-Siberia, Southern- Siberia, Northern-West and the Far East regions.
- The prospecting work in the East has caused the new discovery of the fa-ceted garnet and chrysolite, beryl, agate, rhodonite etc. and increase the predicting resources.
- The perspectives of the reserves increase depend on exploration the flanks and deeper horizons of the famous deposits.
- The technogenic deposits and application technologies successfully deve-loped at VIISIMS to improve natural gemstones (beryl, opal. corundum, jadeite. charoite, chrysoprase and others) can be used as additional source for gems, in particular for faceted raw material.

1. Kievlenko E.Ya. Geology of gemstones, EKOST, 2001, M., 582.
2. Kovalenko I.V. V International conference «Crystals: growth, properties, real structure, application»,v.2 Alexandrov, VNIISIMS, 2001, 458-468
3. Yusipov A.A. «Mineral resources of Russia. Economy and management», № 4, 1999, 52

JADEITITE TREATMENT

Kovalenko I.V., Vniisims

Jadeitite is relatively scarce in nature and its industrial accumulation is very rare. There are some famous deposits such as Pyserka and Left Kechpel at the Polar Ural, Urivok at the Northern Caucasus and Borusskoe in the mountains of the Western Sayany at the territory of Russia. Jadeitite is interested as a gemstone by its green color, translucency in fine chips, structural pattern, high velocity and transparency. So called «imperial», the emerald-green translucent jadeitite variety, is highly estima-ted among all jadeitite gemstones.

At the Russian deposits the high-grade jadeitite amounts the first interests and the jewelry raw material contains 0,001- 0,04% of the jadeitite body volume. In this con-nection to develop methods for increasing quality of the raw material having the low one is very actual nowadays. To use successfully the present methods is to allow to enlarge volume of application the raw jadeitite at the stone-cut industry. In the final analysis it is to rise efficiency of the deposits exploitation.

The target of the raw jadeitite treatment is to improve its decorative properties, namely: to intensify green color of gemstone, to obtain more contrast texture pattern, to reduce color of the thick dyed gemstones (dark green, grayish –dark-green) varie-ties and to increase the level of the jadeitite translucency keeping its green color. We studied modifications of the low quality raw jadeitite based on the comprehensive analysis of the matter composition, decorative properties of the natural varieties of the Polar-Ural, Eastern-Sayny and Kazakhstan deposits. To consider mineral compo-sition, grain character, texture peculiarities and color of the initial rocks (involved into experiments) are required to choose the technique of treatment.

There are the following technological types for systemizing natural raw jadeitite by possibility and process of its improvement:

- light-gray of different hues fine-grained jadeitite (homogeneous, marbly natu-ral types); they are improved by thoroughly painting into green color;
- light-greenish-gray and grayish –light-green jadeitites (weak pattern, streaky and uniformed-spotted natural types); they are improved by color intensity and contrast range of the textural pattern;
- thick-dark-green, bluish-gray-dark-green to the black jadeitites (marbly, landscape natural types); they are improved by reducing color, sometimes with the further paint into green one;

- gray of different hues, monomineral jadeititic by the rock content; modification is the double phase transition method to obtain the translucent sinters, to paint them thoroughly into green color [1].

In conclusion it's necessary to note that the most stable results on treatment of the raw jadeitite having low quality were obtained by means of the surface thoroughly painting (methods of green color intensity and contrast range of the textural pat-tern). This method allows to change the raw jadeitite having low quality into semi-precious one and to increase the reserves of the high quality material in 2-6 times. Method of the double phase transition is a rather long-term way to grow jewelry jadeite. It's required to continue researches for processing the optimal technological parameters.

To compare the results of the surface thoroughly painting of the jadeitite samples from the different deposits has caused to repeat experiments based on the raw mate-rial from the Borusskoe and Levokechpelskoe deposits and also the Pusierka one having the low quality material.

Literature

1. Muhanov V.A., Kovalenko V.S., Kovalenko I.V. III International conference «Crystals, growth, properties, real structure, application», v.1, Alexandrov, 1997, 190-197

GEOLOGICAL AND ECONOMIC MAP FOR COLOURED GEMSTONES OF RUSSIA.

A.V.Turasheva (VNIISIMS)

The numerous publications of the last years demonstrate that the Russian geological service is carrying out a statistical and cost analysis of all kinds of mineral resources (journal «Mineral resources of Russia». Economics & Management. 1998-2004).

Researches conducted by VNIISIMS in cooperation with "Centrequartz", "TsNIIgeolnerud" are aimed at creating a comprehensive information storage on Russian coloured stones and their place in the world hierarchical gradation. These specialized surveys have been made since the beginning of the 1990s, including economic issues since 1999, unfortunately, insufficient due to financial problems.

The geological-economic analysis of the Russian jewellery coloured stones of the 1st order (according to Kievlenko's classification), which are a priority on the foreign market is made to the present time: sapphire, ruby, emerald, alexandrite, fenacite and zircon. The main methodological principles are explained in the «Exploration and conservation of mineral resources» № 1. 2004 [4]. Here we would like to point out that cost estimations for different kinds of mineral raw material are not standardized, so it is possible to use some other methodical approaches.

The set of researches already conducted is an initial stage for compiling a draft of a geological-economic map on deficient kinds of Russian gemstone raw material. Prospective variant – large-scale maps-incision for separate industrial regions (Ural, Far East etc.) on the basis of «Summary resource map of coloured stones of Russia » of the scale 1: 5.000 000 made by the specialists of VNIISIMS (I.V. Kovalenko and all [3]).

This report attempts to generalize the estimations on concrete gemstone raw material objects and provinces [4] and create an illustrative block of the geological-economic information on precious stones. Furthermore, in the process of studying other kinds of coloured stones this block will be replenished and corrected.

Taking VIEMS methodical recommendations [1,2] as the main technical-economic indices describing separate types of mineral resources and their share in the general balance of gemstone raw material production, it is supposed to take into account the following information in diagrams and graphs:

Quantitative indices:

- the quantitative composition of the mineral resource base (number of objects - deposits and displays, including perspective by geological criterions and economically profitable);
- a degree of industrial development of reserves and their share by kinds of a useful mineral in the general balance;
- the annual output (reached and expected) of colour stones;
- the cost of annually extracted gemstone raw material;

Qualitative indices:

- the potential recoverable cost of minerals (in the explored reserves and in the expected recourses);
- the cost of 1 unit of ore (crystal raw material) calculated for each useful component (faceted, cabochon, collection sorts) and dependent on useful component ores, ore technological effectiveness and prices on products;
- minimal price of a unit of product;

Economical indices:

- possible annual income (without taxes) from the development of deposits;
- net profit from the development of deposits;
- investments necessary for the development of gemstone reserves.

Out of the common 121 objects only 9 deposits with balance reserves where about 68 % of resource base is concentrated are suitable for economical open exploitation. Emerald deposits are the most explored ones, while the worst explored are alexandrite and sapphire deposits. Potential value of natural precious stones is about $96.6 m, of which the explored and estimated reserves make up $62.7 m (65 %), and active near-surface part - $24.6 m (25 %). Small investments will make it possible to improve the shallow Ural accumulations of ruby and sapphire.

The summary geological-economic analysis and the map on its basis represent a synthesis of the accumulated knowledge for rating and selection of gemstone objects, for regulating the system of licensing of the mineral resource use, for the development of a strategy of geological exploration considering the present infrastructure of Russian regions.

References.

1. V.P.Vasilenko, V.A.Aliskerov, M.N.Denisov, K.G.Stafeev (VIEMS) Compiling a geological-economic map. Economics & Management. №3. 1999.

2. A.S.Savin Evaluation of mineral resources. Geological studies and use of minerals. Information reference book. Vol. 4, pp. 44-52, 1999.
3. I.V.Kovalenko, T.G.Kostelova, L.N.Shulaeva, Z.A.Bagrova, I.S.Tigetova «Resource map of Russian coloured stones». «Razvedka i okhrana nedr» №1.2004.
4. A.V.Turesheva. Geological and economic analysis of mineral base for basic types of gemstone raw material of Russia. «Razvedka i okhrana nedr». №1.2004.

DISPERSION OF DIELECTRIC PERMITTIVITY OF THIN FERROELECTRIC FILMS OF STRUCTURE $PB(TI_{0.45}ZR_{0.53}\ W_{0.01}CD_{0.001}\ )O_3$

A.A. Bogomolov[1], M.O. Verezhnikov[1], S.G. Gakh[2], V.A. Aleshin[2], I.N. Zaharchenko[2]

[1]Tver State University, 170000 Tver, Sadovyi Lane, 25, Russia
[2]SII of Physics of Rostov-on-Don State University

The work is devoted to the study of dielectric permittivity dispersion in $Pb(Ti_{0.45}\ Zr_{0.53}\ W_{0.01}Cd_{0.001}\ )O_3$ films having different electrodes such as steel and aluminium. Dielectric relaxation studies provide information about the character of the distribution of electric parameters on the film thickness [1] and also about the condition and properties of "dead" layers [2].

The $Pb(Ti_{0.45}\ Zr_{0.53}\ W_{0.01}Cd_{0.001}\ )O_3$ (PZT-1) films on stainless steel substrates were prepared by the method of high-frequency cathodic sputtering of a target from hot-compressed ceramics of the same composition. Sputtering was carried out in an atmosphere of oxygen at a pressure of 100-180 Pa. The temperature of the substrate was varied in the limits from 500 to 600 ^{0}C. X-ray phase analysis carried out on the diffractometer DRON-3M (Cu K_α filtered radiation) confirmed that the films were single phase with perovskite structure. The films were supplied by an aluminum (Al) counter-electrode with diameter D = 2 mm. The film thickness was $d = 10^{-4}$ cm.

Frequency dependence of ε' and ε" was measured in a frequency range from 100 Hz to 1 MHz. The Cole-Cole diagrams constructed from the experimental data have the shape of an arch at high-frequencies and a linear part in the low-frequency area. The data are presented for the temperature interval from 20 to 200 ^{0}C. The estimated times of relaxation were found to be in agreement with [1].

Literature

1. V.K. Yarmarkin, S.P. Teslenko. Phys. Solid State, 40 (10) (1998).
2. A.M. Bratkovsky, A.P. Levanyuk. Phys. Rev. B 63, 132103 (2001).

IMPROVEMENT OF NATURAL CUTTING CORUNDUM.

E.M. Kozhbakhteev, S.N. Ivicheva, G.I. Krylova, A.A. Marin
O.V. Repina, A.A. Reu
VNIISIMS, Alexandrov, Russia

At the present time the share of high-quality gemstone resources on the world market is constantly decreasing while the quantity of modified and improved raw material is increasing. Russia possesses considerable deposits of corundums the most part of which requires improving. This paper dwells upon the nature of corundum's colour and the methods of treatment which allow to improve the jewellery properties of this raw material.

The conducted experiments permitted to develop a working variant of the gemmological and technological classification for 20 types of corundum deposits in Russia including recommendations on the most optimal techniques for their improvement with regards of the conditions for heat treatment, thermal diffusion or combined treatments.

GROWING OF THE LARGE CRYSTALS $MgAl_2O_4$, USING HORISONTALLY DIRECTED SOLIDIFICATION METHOD.

Ivanova O.A., Smirnova S.A.
VNIISIMS Alexandrov

Crystals of the aluminium-magnesium spinel - $MgAl_2O_4$ - successfully com-bine such technically important properties as high hardness (Moh's scratch hardness number - 7,5 - 8), density (4 g/cm^3), chemical stability and non-hyg-roscopicity, isotropy, a large zone of the optical transparence. It enables to ap-ply spinel crystals in various acoustic and optoelectronic devices as dielectric and optical media , substrates for the epitaxial growing of semiconductive films etc. [1,2]. The coloured varieties of spinel are the beautiful materials for jewel-ry.

In contrast to such basic crystals as ruby, sapphire, garnet the spinel applica-tion is rather restricted at the pointed out fields. It's associated that the applied methods for growing spinel - Verneuil method and growth from the solutions into melt - are not allowed to grow large crystals of good quality.

For the first time we have grown the spinel crystals using horizontally direc-ted solidification method. Crystals have the shape of plates which monocrys-talline zone is comparable with the crucible dimension (70 x 160 x 20 mm).

Crystals were grown using the grower " Sapphire -2MG" at the inert gas at-mosphere (gauge pressure is 0,5 atm.) into molybdenum container having sha-pe like boat. Previously tableted magnesium and aluminum oxides mixed as the required stoichiometric formula of spinel were used as an infant material. A seed was fixed at the container's narrow part. The process of growing includes the following: melting the infant material, making the homogenized solution and slightly melting the infant material. Then the crucible containing the melt is slowly removed from heating zone to more cold one of the growing chamber where crystal is to be cooled and annealed.

The grown crystals are colorless and transparent They captured gas inclusions in the close part proximity to the bottom. In addition we grew spinel crystals doped with cobalt and chromium side by side with the non-doped one.

To grow spinel single crystals as large plates is to allow to open the new fields of application.

1. C.F. Akhmetov et al. Solid State Physics. 1977, v.17, is.1, p.308-309
2. K. V. Yumashev, I.A. Denisov, N.V. Kuleshov. Optical Society of America, washigton DC. 2000, vol. 34, p.236-239

AN INVESTIGATION OF THERMAL AND DEFORMATION PROPERTIES OF QUARTZITE AT THE TEMPERATURE INTERVAL OF POLYMORPHIC α-β TRANSITION BY MEANS OF NEUTRON DIFFRACTION AND ACOUSTIC EMISSION

A.N. Nikitin[1], R.N. Vasin[1], A.M. Balagurov[1], G.A. Sobolev[2], A.V. Ponomarev[2]

[1] Joint Institute for Nuclear Research, Dubna

[2] Scmidt United Institute of Physics of the Earth RAS, Moscow

The process of preparation and development of an earthquake source cannot be completely understood and described without creating more accurate and complicated physical models of the geological medium. The phenomena of instability of the rocks under influence of high temperatures and pressure are especially badly investigated, including during phase (polymorphic transition). So, studying of abnormal physical properties of the rockforming minerals at high temperatures and pressure, for example, of the nature of abnormal behaviour of polycrystalline quartz at the temperature interval of α-β transformation (560 - 600 °C) is actual. The behavior of natural polycrystalline quartz (Shokshinskiy quartzite) was investigated by means of time-of-flight neutron diffraction and acoustic emission at the SKAT-TKOS measuring complex installed at the beamline 7a of fast pulsed reactor IBR-2. Also, the neutron diffraction measurements were performed with the quartz powder sample at the HRFD diffractometer. The changes of the lattice spacing of quartz during the α-β transition were measured and values of lattice stresses were estimated. It is shown that the transition occurred at the temperature interval 540 to 573 °C and the sample was completely consisted of β-quartz at a temperature above 600 °C. Short splashes of acoustic emission (AE) were observed when the phase transition was completed. The intensity of splashes exceeds by two orders the level of AE, caused by the thermal bursting of quartzite under heating; dynamics of these splashes may be described by dependence of the relaxation type. The behaviour of AE splashes is similar to the known sequence of seismological events: main event – aftershocks. It is possible, that such phenomena can promote the development of earthquake source due to the stress state changes in medium or to the trigger effect.

FLUID INCLUSIONS IN QUARTZ VEINS OF THE LEGADEMBI AND SACARO GOLD DEPOSITS (SOUTHERN ETHIOPIA)

Shatagin N.N., Sobolev R.N., Teka S.H.

The Legadembi and Sakaro gold deposits are of gold-quartz type. They are situated in the limits of the Arabian-Nubian shield (southern Ethiopia). Wall rocks form here narrow strips within Megado gneisic belt. They were formed during the neo-Proterozoic Wilson cycle. These rocks were metamorphosed in the conditions of the lower greenshist or the upper amphibolite faces and later overworked by retrograde metamorphism of the greenshist faces and tectonic deformations.

Wall rocks of the Legadembi deposit are: nodulous gneisses, quartz-sericite schists, talc-tremolite-actinolite schists, quartz-biotite-actinolite-talc schists, graphite-quartz-mica schists and amphibolites. Quartz veins locate in quarts-biotite-actinolite-talc rocks. The course of the ore zone is NNW. The angle of inclination is 60-65° WSW.

The Sakaro gold deposit locates on the distance near 5 km to south of the Legadembi gold deposit. The gold body is represented by two parallel quartz veins. Graphite muscovite schists represent the wall rocks here. These veins were emplaced along an anticlinal fold having N-S trend. Fractures have trend NW, plunge SW and branch southwards. They control emplacement of the quartz veins. Gold and sulphide minerals within the veins occur along fracture zones and quartz grain's boundaries.

Fluid inclusions were carried out of auriferous quartz veins from the Legadembi and from the Sakaro gold deposits. Fluid inclusions from both gold deposits are very similar, so we describe them together.

There are 5 principal types of inclusions: 1. Primary liquid CO_2 inclusions, 2. Primary two-phase CO_2 – H_2O inclusions, 3. Three-phase CO_2 – H_2O inclusions, 4. Naturally decripitated inclusions and 5. Secondary two-phase CO_2 – H_2O inclusions. Types 1, 2 and 4 were divided on subtypes.

Type I. Primary liquid CO_2 inclusions.

Among this type we divide two subtypes: type *I-a* consists only of liquid inclusions CO_2 and type *I-b* consists of liquid CO_2 and one or some solid phases.

Type I-a. Inclusions of liquid CO_2 have oval shape. They have 10—30 μm longs. About 90-95% of inclusion's volume consists of CO_2 and only 5-10% of volume is represented by H_2O. It is impossible to establish homogenization's temperature because inclusions explode before the disappearance of phase's frontier.

Type I-b. Inclusions consist of mineral's crystals + liquid CO_2. The last one is always in crystals. The size of the inclusion depends of crystals' size and can be up to 50-70 μm. The size of liquid CO_2 usually is much less in comparison with the size of the crystal. Usually such crystals are amphiboles (tremolite-actinolite) (90%). Other minerals are chlorite and albite and very rare calcite, halite and rutile. The last mineral passes from inclusion to surrounding quartz. These mineral-inclusions were formed in the process of sedimentation actinolites, thremolites and other minerals on the quartz's faces. These minerals captured drops of liquid CO_2. Quantity of liquid CO_2 is up to 90 % of inclusion's volume but quantity of H_2O is less than 10%.

The decripitation's temperatures as for subtype I-a (200 – 300°C) are below homogenization's temperatures.

Type II. Primary two-phase CO_2 - H_2O inclusions are very similar to subtype I-a. They are elongate and oval. Their size usually is less than 20 μm. Quantity of liquid CO_2 and H_2O is more or less the same (40 – 60 %). Sometimes in inclusions is gaseous bubble but its volume is less than 10 %. Homogenization's' temperatures vary in the limits 325 - 390°C, the average temperature is near 350°C.

Type III. Three-phase CO_2 - H_2O inclusions are very similar to type II. For these inclusions are typical presence of gaseous bubbles. Averaged formula of such inclusions is the following: L(H_2O - 30-40%) + L(CO_2 - 30-40%) + G(CO_2 - 30-40%). The temperature of complete inclusions' homogenization varies from 300 to 350°C with the average near 320°C. On the basis of the morphology it is possible to divide inclusions of this type into two subtypes: *(type III-a) oval three-phase inclusions and (type III-b) three-phase inclusions with negative facetting.*

Type IV. Naturally decrepitated inclusions in quartz are very typical for both deposits. Such type of inclusions is usual thing in metamorphic formations. Their formation is a result of excess of inner pressure in inclusion, which appear in the process of rocks moving from the big depth to the surface of the earth.

Type IV-a. Decrepitation's clusters of fluid inclusions.

Excess of inner pressure in fluid inclusion can form microcracks which as an excess in comparison with hydrostatic pressure. If during such a process an inclusion will be open, then form very specific three-dimensional figures so-called decrepitation's clusters. New daughters inclusions form after explosion. They have very different phase composition. This process took place on deposits Legademby and Sacaro: inclusions in quartz were formed during several stages.

Type IV-b. Inclusions of «fragment's» shape. This type of inclusions forms as a result of main inclusion's explosion. The shape of inclusion formed in the process of explosion is very complex and the most typical is "fragment's" shape.

Type IV-c. Inclusions with elongate branch pieces. This specific form of inclusion is typical for secondary inclusions, which are result of natural decrepitation of primary fluid inclusions

Type V. Two-phase gaseous-aqueous inclusions are of the secondary origin and related to cracks and boundaries of grains.

Thermodynamic parameters of minerals formation.

The study of fluid inclusions of both deposits gives possibility to establish the following succession of its formation: one-phase CO_2 ⇒ two-phase H_2O-CO_2 ⇒ three-phase H_2O-CO_2 ⇒ main part of two-phase H_2O inclusions.

Both subtypes of one-phase CO_2 inclusions are of early stage and syngenetic with quartz. These inclusions decrepitate at 200°C and possibly they were formed by the pressure near 2 Kb.

The temperature of two-phase H_2O-CO_2 formation was near 350°C and pressure was near 4 Kb. So, the part of quartz veins was formed at the progressive stage of regional metamorphism. Only the secondary inclusions were formed on the regressive stage of metamorphism. But for all that the decrease of pressure took place quicker than temperature. This was the reason for formation naturally decrepitated inclusions.

Conclusion

Quartz veins of Ligademby and Sakaro gold deposits were formed in condition of tremolite-actinolite stage of the progressive regional metamorphism. Gold-quartz veins' formation relates to retrograde stage (greenschists) of regional metamorphism. The decrease of pressure was more intensive in comparison with temperature. These data are in good agreement with results by using divers geothermometers and geobarometers.

ADVANCES AND TRENDS IN THERMOBAROGEOCHEMISTRY STUDIES IN UZBEKISTAN

V.S. Polykovsky Y.B.Turmuratov, R.A. Sharipov, R.B.Freylih, L.R. Ismailov

Society of Fluid Inclusion Research of Uzbekistan

International Academy of Mineral Resources "Goskomgeo".

Thermobarogeochemistry is a new branch of geochemistry, its development in Uzbekistan can be divided into three stages.

The first stage is from the 20^s to the 50^s of this century, the charasteristics of this century is that geologists draw more attention to the genesis of metal deposits. They solved these problems by using the results of fluid inclusion studies achieved by the scientists from the UK, Russia, Germany and other countries. In the middle of 50^s of this century, the Academican Kh.M. Abudulaev from Uzbekistan, the founder of the studies, of ore genesis initiated and carried out the research of the thermobarogeochemistry, he studied gas-liquid inclusions in fluorite from the Aurakhmat deposit which is located 90km North-East off Tashkent. This work was completed by B.G.Gruskanli. The academician A.G.Betkhtin used these data twice in this books of **"Mineralogy and Distribution Law of ore Deposits",** due to the careful work of the former. He used these data as samples to explain great possibilities of the forming conditions of the endogenic deposits.

The third stage began from 1962. Supported by N.P. Ermakov and K.Ya.Babaev, V.S. Polykovsky built up the first thermobarogeochemistry laboratory in the Research Institute of Middle Asia Geology and Mineral Raw Materials.

Today, many institutes in Uzbekistan are carrying out studies of thermobarogeochemistry. They include "The Geology of Tashkent" (V.S.Polykovsky, N.A.Ivanova) which is subordinated to the National Committee of Mineral Resources Council of Ministers; State University of Technology in Tashkent (H.A. Akbarov); Tashkent Univercity (Jivaev); Research Institute of Geophysics of the Uzbek Academy. The laboratory equipment in these units include "Ermakov" and "ВИМС" homogenisation thermometer, "Луч" sound wave decrepitater, "ЛХМ-80" chromato-spectrometer, "V.A. Kormushin"cooling stage and photographic equipment for the thermobarogeochemistry studies. Following is a brief introduction of rescarch directions of thermobarogeochemistry in Uzbekistan:

-The research in thermobarogeochemistry conditions of deposit forming of gold, silver, tunsten, copper, lead, fluorite, diamond and other deposits of endogenetic origin.

-The research on thermobarogeochemistry conditions of deposit forming of carbonatite and related rare earth deposits.

-The research on thermobarogeochemistry conditions of deposits forming of epigenic and valcanogenic deposits.

-The study of forming conditions of oil and gas.

-Developing new methods of thermobarogeochemistry, blind ore deposit finding by thermohalos.

-The application of thermobarogeochemistry on geological survey, ore reconnaissance and prospecting.

-Standartisation of the working regulations in the research works of thermobarogeochemistry in different stages of field and laboratory work.

-Developing and applying mathematical methods for the data processing ofthermobarogeochemistryresearch results, patically the methods developed by the combination of traditional geology, geochemistry, petrology and others with the thermobarogeochemistry.

-The professinal education for the students from state Tashkent Universityof Technology and the students from State Tashkent University, to become mainstay of the thermobarogeochemistry research;The professional training to the workers who are working in the education or research units subordinated to the National Committe of Mineral Resources under the Council of Ministers;The drafting of the educational programs and the editing of text books of "Practical thermobarogeochemistry" for the university students in geology.

-The publication of the periodical achievments (through Geologycal Journal of Uzbekistan and the Journal of Uzbekistan Mineralogycal Society) to upgrade the level of research and practical application methods of thermobarogeochemistry, to present in the professional symposium on thermobarogeochemistry, to attend the international conference of geology and international technological assistance projects.

The mineral-forming fluids at the gold-ore polystadial deposit Tarynskoe (The Sakha-Yakutiya).

Krylova T., Akimov G.

IGEM RAS, Staromonetny per. 35, Moskow, Russia

The vein-disseminated gold deposit Tarynskoe represents a new type of the large-scale gold mineralization in the Verkhne-Indigirskii area.. The main gold reserves are connected with the practically quartzless zones of disseminated, visually not detected thinly needle-like arsenopyrite hosted by tectonized aleurolites and argillites. Besides, at the deposit a vein-like mineralization is manifested in form of Au-quartz (low-sulfide), Au-berthierite, Au-berthierite-quartz, Au-Ag-tetrahedrite-jamesonite-pyrrhotine-quartz, and pyrite-marcasite-chalcedony-quartz veins and vein-veinlet zones.

The hydrothermal mineralization was formed in following five mineralization stages: I - Au-sulfide disseminated ores in compression zones and Au-quartz vein-stockwork ores in conjugated tension zones; II - Au-rare metal; III - Au-Sb; IV - Ag-base metal (+Au); V - marcasite-chalcedony-quartz mineralization; the superimpozition of the latter on the Au-Sb-bearing veins results in the bertherite and antimonite re-deposition. Gold in stage I is manifested as invisible in arsenopyrite and native, in others - only as native gold.

A number of indications unites the deposit Tarynskoe with the most large gold-ore deposits of an area studied. The combination of Au-quartz vein-stockwork and disseminated Au-sulfide ores reminds of the deposit Natalka (the Kolyma region); disseminated mineralization character and stadiality bring the deposit Tarynskoe closer to the deposit Maiskoe (the Chukotka region).

The physical and chemical conditions of mineral formation were studied by microthermometry of fluid inclusions (FIs). Microthermometry was carried out using thermocriochamber Linkam THMSG-600 with long-distance lens (x 80, Olympus), installed on the microscope equipped by videocamera, at the temperatures between -196 and 600^{0}C. For syngenetic FIs of one- and two-phase composition the pressure was calculated using V. Kalyuzhnyi's method and computer code FLINCOR. The samples studied contain FIs sizing no more than 15-20 μm .

A typical feature of the deposit is that main vein mineral is represented by the milky-white quartz (stage I) with superimposed later mineralisation including ore one. The quartz is broken by numerous fractures, which are traced by very small (lesser than 5-7 mkm) secondary FIs. The latter are not suitable for determination of the physical and chemical parameters of the deposit formation. The deposition of ore minerals of all the subsequent stages is accompanied by early quartz re-crystallisation, resulting in the formation of quartz

"clear" zones with FIs syngenetic to the ore minerals; it is these FIs that mirror the formation conditions of the superimposed mineralization.

Two-phase FIs have the melting eutectic temperature (Tm eut) between -34.1 and -22.2^{0}C. Part of them contain Na-chloride solution. But another Fis part has the melting process not characteristic for the solutions with prevailing Cl-ion. At the moment of eutectic melting ice disappears; under further heating practically continuous process of the re-crystallization of solid phases, occupying up to 40-60 % of FIs volume, may be seen. The final melting occurs at temperatures above 10-11^{0}C. It is known that sulfate and bicarbonate crystallohydrates melt in the field of positive temperatures. The presence of great amount of CO_2-bearing FIs allows to consider that these FIs contain bicarbonate-chloride solutions. The salinity is rather high: its values are placed between saturated solution concentration and eutectic one. Its specific values, as is recommended by A. Borisenko (1974), were not determined owing to difficulty of diagnostics of the solids in FIs sizing smaller than 15 μm.

The disseminated Au-sulfide and vein-type Au-quartz ores were formed during one process (stage I). The needle-like gold-bearing arsenopyrite was crystallized at the process beginning in temperature range of 290-240^{0}C in heterogenous medium consisted of prevailing CO_2-CH_4 fluid and high-saline Na-bicarbonate-chloride solution under 670-520 bar stipulated by tectonic compression. The native gold was deposited toward the process end under temperatures of 190-160^{0}C from homogenous hydrothermal low-saline (4.8-3.2 wt. %) Na-chloride fluid and pressure of 10-6 bar as a result of tectonic tension.

As a rule, the vein-type ores of subsequent stages were deposited in heterogenous environment. The CO_2-bearing fluid contained CH_4 variable amounts (up to 20 mol.%); water solution had a Na-chloride or Na-chloride-bicarbonate composition under salinity significant variations (on an average of 7-10 wt. %). The native gold in these stages was deposited under temperatures less than 240^{0}C.

At present period of study conducted, the FIs investigations do not give a complete picture of the mineral-forming process dynamics. At the same time, the temperatures, received during FIs measurements, are in good agreement with temperatures, obtained for the same samples using chlorite geothermometers. Combined these data, it can be assert the ore deposition of each new stage to be accompainied by temperature and pressure increasing, the deposition of minerals of each stage being occured against the temperature decreasing backdown. The deposit polystadiality is a result of repeated tectono-magmatic activization after formation of the Au-sulfide disseminated and Au-quartz vein-type ores (stage I).

This study was financially supported by the filial of the SAGME "Vostochno-Yakutskoe" (contractas 136 - 2002 and 131 -2003) and RFBI grants (03-05-64095 and 04-06-64539).

TERMOBAROGEOCHEMICAL OF FEATURE AND ROLE PALEO TEMPERATURE OF A GRADIENT AT FORMATION SELBUR AMETHYST OF A FIELD (SOUTHERN TIEN-SHAN)

Oimahmadov I.S.

Institute of geology, Tajik Academy of Sciences

ilhomjon55@yahoo.com, amethyst@ac.tajik.net

In the Selbur amethyst - bearing area two mineral-forming stages are established . At first stage the quartz veins and lodes of lenght 5-25m and thichness 5-10sm are formed along North West faults. Veins are plate-shaped and rarely lense-shoped. Quartz occurs as dense, massif similar to hornfelse masses of milk-white, sometimes gray shade colour (quartz I) and pole-shaped, congestion-radiant units borrowing to peripheral parts of veins and lodes (quartz II).

In the second stage were formed productive quartz - amethysts zone of mineralization (Central, Northern, Western I, Western II, Western III, East, Selbur - Dalniy), exclusively drawn to explosive infringements sub-meridian of orientation. The quartz - amethysts mineralization forms plate-shaped, lenticular, branchy, sometimes of wrong configuration, veins and lodes from 0,5 up to 6m of thickness and from 30 up to 550 m extension. The products of the second stage were formed on a background multistage opening of cracks, in which there was a repeated faltering receipt a hydroterm, to what the presence of four quartz generations testifies, in particular. The quartz III is characterized by petty-granularity structure, massive dense texture and milk-white up to gray-white colour, occupying the basic central parts of veins. The quartz IV occurs as mid-grained, petty-poles (2-6mm), milk-white, grayish and in some places of translucent units, forming veins and lodes, located in wall-veins parts quartz veins of early generation.

Two subsequent of generation of quartz (V-VI), which were formed in the final periods of mineral forming process, concern to actually amethyst mineralization. The quartz V is amethystized as big-granularity, spotty-isometric (2-10mm) and pole-shaped (from 5x3x3mm up to 40x20x15mm) units carries out the central parts veins and lodes, which adjoin to quartz origin of the fourth generation of matter. Pole-shaped units of amethystized quartz grow towards each other before filling fracture of space. The colour of a mineral here is changing from light -violet, pale-lilac up to rich-violet. Thin more light and grey strips (1-5,5mm) on a dark - violet background sometimes are present and show crust-stripped texture due to pulse characte of acting hydro thermal solutions. It is characteristic for units of quartz of this generation.

One of basic type-morfing features of quartz VI (amethyst) formation is its spatial and

genetic connection with residual cavities, which formation is connected with inside-stages tectonic motions. The cavities are mainly located in wall-veins and central parts quartz veins of early generations. In cavities crystallization of amethyst occurred under rather quiet conditions, the ideal shape of amethyst crystals in druses and brushes show this condition. Crystals of amethyst are characterized by prizm form with prevailing development of romboedrs by the size from 0,5-1 up to 2-4 cm. The size of crystals is various, average from 1-3 up to 5-10см. The colouring in crystals and parallel-poles units amethyst is distributed rather non-uniformly and changes from pale - violet, lilac up to rich - violet. There are regular painted intervals in violet tone of average colour density crystals. The crystals and parallel-pole units amethyst quite often are characterized by zone distribution of colouring, changing one other from of milk-white, to lilac and violet colours.

The formation quartz and quartz- amethyst mineralization in Selbur amehtyst area occured on a background of change of physic-chemical parameters both in time, and in space. Crystallization of quartz from hydro thermal mineral forming solutions of the first stage (the quartz I and II) occured at temperatures 450-340^{0}C and pressure 970 -750 atmospheres. As results of the analyses, have shown threefold water extraction quartz formation hydro terms of the first stage are characterized by the high contents Cl^- (56 equal. %) at appreciably low concentration HCO_3^- (28 equal. %) and SO_4^{2-} (14 equal. %). In cation group $Na^+ + K^+$ + are prevailing (69 equal. %) as well as Ca^{2+} + (30 equal. %). According to temperatures of eutectic freezing of gas-liquid inclusions, mineral forming fluids of the first stage were characterized by chlorid-sodium composition. The concentration of salts in solution of inclusions is changing from 31-18 (quartz I) up to 18,5-13,2 weights. % (quartz II). pH of solutions of inclusions is closes neutral.

The products of the second (productive) stage minazalization were formed at lower physic-chemical parameters. Crystallization of quartz in the second stage occurred in a range of temperatures 435-110^{0}C and pressure 720-150 atmospheres. Productive stage are characterizedby in side-stages motions, cycles of which is fixed by consecutive change of temperature, pressure, structure and concentration of mineral forming solutions from early mineral generations to late. Early generation of quartz of a productive stage have following termobaric parameters: quartz III - 435 - 385^{0}C, P- 720-710 atmospheres and quartz IV -320-275^{0}C, P- 700 -465 atmospheres.

Amethyst, being a product of the final periods of a productive stage, is characterized by the lowest meanings of thermobaric parameters: quartz V (amethystized) - 235 - 180^{0}C, P - 490 -410 atmospheres, quartz VI (crystals and in parallel - poles units amethyst) - 195 -110^{0}C, P- 450 -150 atmospheres.

In all investigated generation of quartz of a productive stage the change of temperatures crystallization in a horizontal direction is accompanying with the paleo

temperature gradient equal to 5,5-13,6^{0}C on 100m. In vertical section of the Central quartz - amethyst zone is revealed the natural increase of temperature with depth, and in time of formation the quartz – amethysts veins the change of a temperature gradient is observed. So, the paleo temperature gradient (average) for quartz III is equal 8,5^{0}C, quartz IV - 10,5^{0}C, quartz V - 14^{0}C and quartz VI - 20^{0}C/100m. On a basis of paleo gradient, the depth of formation quartz – amethyst mineralization from modern erosive surface is appreciated for on quartz III -530 –410m, quartz IV -430 –240m, quartz V - 355 –320m and quartz VI -300 – 225m. Paleo gradient helps to calculate level of cerosion for size quartz - amethysts of zones Northern, Western II. East and Selbur - Daliny, which for quartz III corresponds to 60-119m, quartz IV-145-190m, quartz V-34-105m and quartz VI-50-75m.

Thus, between vertical drop of mineralizetion and paleo temperature gradient for each generation of quartz of a productive stage observes direct dependence: the less size of paleo gradient, the more vertical drop of mineralizetion on lodes revolt.

In composition of a liquid phase hydro thermal of solutions of this stage an active role is played by Cl^-, HCO_3^-, SO_4^{2-} and NO_3^-. With fall termobaric of parameters the contents Cl^- (quartz III-50,6-42,4 egul %, quartz VI-48,7-32,2 egul. %), decreases in mineral-bearing solutions and is increased HCO_3^- (quartz III-40,2-34,9 egul %, quartz VI-54,1-29,5 egul %) and SO_4^{2+} (quartz III-21,5-11,8 egul %, quartz VI-23,6-6,9 egul %). In composition of solutions cation prevails $Na^+ + K^+$ (quartz III-81,1-58,5 egul %, quartz VI-74,2-60,3 egul %). The less importance has Ca^{2+} (quartz III-41,5-18,9 egul %, quartz VI-39,7-25,8 egul %). Thus, at formation of the second stage the hydro thermal mineral-bearing solutions had bi-carbonate- cher-calcium-sodium –potassium composition. The results of criometric research have shown to complex composition of hydro thermal fluids which from quartz and amethyst mineralization on the area Selbur amethyst area. Mineral-bearing solutions, at essential prevalence of NaCI and KCI, also are enriched with such components as $MgCl_2$ and $NaSO_4$.

From early generations to late in a productive stage, the gradual difference of concentration of mineral-bearing solutions is observed also. It is equal in quartz III 21,5-9,8 weight. %, quartz IV -19,8-15, quartz V-17,5-9,5 weight. % and quartz VI-14,5-5,8 weight. % .pH of solutions 7,4-6,8.

Thus, amethyst on the area Selbur amethyst of a field crystallized at temperatures 235-110^{0}C and pressure 490-150 атм from sulphate-bi-carbonate-chloride-calcium solutions with concentration of salts 17,5-5,8 weights. %.

In summary we shall note, that established thermobarogeochemical parameters of amethyst formation, alongside with general geological factors of the mineralisation control, can be used for contouring of amethyst-bearing squares both conducting prospecting search and estimated works for this kind of mineral.

ONCE AGAIN ABOUT TEMPERATURE FORMATION OF BARIT (ON EXAMPLE OF DEPOSITS KARAMAZAR, TAJIKISTAN)

Gadoev M.L., Fayziev A.R.

Institute of geology, Tajik Academy of Sciences

mustafog@yahoo.com, must@ac.tajik.net

Around of meanings of temperatures received for barite by a method of homogenization of gas-liquid inclusions, there is a discussion that they not always reflect real conditions crystallization of this mineral connected to the contents in him abnormal conservates of mineral forming fluids. These scientists consider, that barite crystallizes from hydrothermal solutions at temperatures which are not exceeding 200^{0}C (Bagratashvili, 1961; Uchameishvili, 1980; Roedder, 1972). In their opinion, the meanings of temperatures exceeding this digit are abnormal and should be excluded from consideration. However of long standing of research barits from deposits and ore occurences of various genetic types of Tajikistan do not confirm this assumption. The data, received by us, unequivocally specify that barits could be formed and at temperatures considerably exceeding 200^{0}C.

In the beginning this question we shall consider on an example barits from occurences of various mineral and genetic types Karamazar barit-bearing area of Northern Tajikistan.

Barite mineralization in Karamazar (Deposit Baritovay gorka, Severnay jila, Akmagol and Muzbek) is observed among rocks of various age, since lower Carboniferous and finishing Tertiary formations. However majority of industrial deposits barite was formed in late Paleozoic and is located in various on structure and age intrusive and effusive rocks. The containing rocks thus were exposed by intensive change and are expressed in sericitization, chloritezation, kaolinization, beresit formation, silicification, carbonatization and, in a smaller scale, ferrification, albitization and feldspatization.

Alongside with actually barite deposits and occurences, submitted quartz - barite, barite-galenite and quartz-barite-fluorine deposits, this mineral meets in significant amounts and in fluorine (Naugarzan, Kengutan etc.) and silver - basicmetals (Big Kanimansur, Zambarak etc.) deposits. Besides barite is found out in skarns molybdenite-wolframs (Chorukhdairon) and polymetal (Altintopcan, Kansai, Kurusai, Turangli and ets.) deposits, in which barite is not the basic component of ores. He is connected here with finishing ore process by stages of mineralization and it is in their top horizons.

Thermometric research have shown, that basic morfogenetic types of inclusions mineral forming solutions in barite are submitted, mainly, liquid and gas-liquid konservates. Bitumen inclusions meet occasionally. Dominant types among them are one-phase inclusions with the various sizes.

Primary gas-liquid inclusions in barite are irregular distributed ones and groups. The ratio of phases in such inclusions vary from 1:4 till 1:14. Their sizes is very fine. Sometimes reach (achieve) up to 0,05 mm. The form of inclusions in them various. It are marked basically sharp-angled, oval, triangular, square and lengthened. Crystall-form prizmatic-shaped and shape of isometric inclusion meet sometimes.

Temperatures of homogenization of inclusions in barits from various deposits are different (see table).

Table

Temperature of barite formation барита in deposits and occurences in Karamazar area

Deposit	Generation	Temperature, ^{0}C	
		Homogenization	Decrepitation
Baritovay gorca	I I I	175-250 90-130	- -
Severnay jila	-	185-255	-
Tereklitau	-	160-230	-
Koshmagat	-	170-235	-
Akmogol	-	190-245	-
Naugarzan	-	100-165	-
Kanimansur -//- -//-	I I I I II	185-230 130-155 65-125	180-225 - -
Zambarak	-	135-155	180-270
Tariecan	-	160-200	250-270
Chorukhdairon	-	150-270	200-300
Turangli	-	170-245	200-280
Orlinay gorca	I I I	190-265 -	- 130-200

The study of inclusions mineral forming solutions in barits of the barite deposits shows, that crystallization of this mineral occured in a wide range of temperatures 90-255^{0}C. Early generations of barite were formed at temperatures 160-255^{0}C, and late - 90-165 ^{0}C.

As against of barite of properly barite deposits, range of temperatures of formation of this mineral in deposits of other types in our region wider. Temperature of homogenization of inclusions in barits from these deposits is equal to an interval 65-270^{0}C. Among them the maximal meanings of temperatures are characteristic for barite of Chorukhdairon deposit. Here temperature of homogenization of inclusions is equal 150-270^{0}C (Alidodov, 1982).

For barits of deposits in Kurusai ore field the meaning of temperatures of homogenization are raised: 182-238 and 198-250^{0}C (Sazonov, 1962) also is characteristic, in comparison with barits from Naugarzan and Zambarak deposits. In the latter it has appeared as lowered a little and changes from 100 up to 165^{0}C. Inclusions of mineral forming fluids in barits of various generation from a deposit Big Kanimansur is homogenizing accordingly at temperatures 185-230^0, 130-155^0 and 65-125^{0}C (Fayziev, Fozilov, Gadoev, 2001). Let's note, that reliability of temperatures of homogenization of inclusions in investigated barits was supervised on other minerals (quartz, fluorine, calcite), taking place with it in close paragenetic of association.

Temperature of intensive cracking barits occured in intervals 130-200^{0}C (Orlinay gorca), 180-225^{0}C (Kanimansur), 250-270^{0}C (Tariecan) and 200-300^0 C (Chorukhdairon).

It is necessary to note, that in barits from Karamazar deposits really quite often abnormal gas-liquid inclusions are marked, and distinguished from "normal" gas-liquid inclusions by a unequal ratio of gas and liquid phases quite often taking place beside each other. The origin of such inclusions, probably, is connected to physical properties (fragility, cleavage) mineral. It is possible to explain occurrence of abnormal inclusions by action on them of high-temperature solutions of later stages mineralization, therefore inclusions in barits was cracing and there was an outflow of a liquid phase through formed micro-cracks. Where barite contacts with other minerals (quartz for instance), the abnormal high-temperature inclusions occur there.

The study barits from fluorite deposits of Central Tajikistan shows on an interval of temperatures of homogenization of primary gas-liquid inclusions in them, equal 75-310^{0}C (Fayziev, 1991). To higher meanings of temperatures of homogenization of inclusions characterize barite from gold deposit Sasic (Central Pamir). Primary gas-liquid inclusions in crystals barite from this deposit with gas filling 25-46 % and size up to 0,1 mm in length

homogenized within the limits of temperatures 275-365^0 C (Fayziev, Alidodov, Iskandarov, 1972).

It is known, that in the most part of deposits linked with carbonatites, barite is one of the basic minerals in ore bodies. The formation of these deposits occured from high density (60-75 and more weight. %), saturated by volatile components, silicat-salt, melts, melt-salts and solutions – brine at temperatures more than 600^{0}C (Fayziev, Iskandarov, Gafurov, 2000). Barite is crystallized at temperatures higher 600^{0}C, for example on a deposit Dunkeldic (East Pamir).

The temperatures crystallization barite more than 200^{0}C is confirming by some examples from the references on detailed researches of A.I. Gomelauri with the co-authors (1974) both A.G.Tvalchrelidze and V.I. Sheglova (1990) on deposits of Georgia; the intervals of temperatures crystallization barite 220-280 and 242-302^{0}C are established. D. Rife's (David, 1971) study of inclusions in this mineral from a deposit to a Cartersville (the state Georgia, USA) has established a limit of temperatures of homogenization of inclusions 127-297^{0}C. On the data O.A.Kovrigo (1973) formations barite on Ridder-Sokolniy deposit occured at temperatures 330-360^{0}C. On G.I. Belikovoy etc. (1978) temperatures of formation barite of deposits of Bashkiria occured in a range of temperatures 155-300^{0}C, and Orlov deposit - 250-330^{0}C (Jilinskaye, Kormushin, 1971), Zarechenskogo and Average polymetal deposits (Rudniy Altai) - 250-320^{0}C (Borisenko, 1988), deposits Atasuyskogo such as - 200-250^{0}C (Kulinich, Mukhanov, etc., 1988), deposits Zakarpatye -100-250^{0}C (Platonova, Kovalishin etc., 1976).

Thus, the given examples show, that barite could crystallize from mineral forming solutions and at higher temperatures, than 200^{0}C.

LITERATURE

1. Алидодов Б.А. Месторождение вольфрама и молибдена // Минералогия, геохимия и генезис некоторых эндогенных месторождений Таджикистана. Душанбе: Дониш, 1983. С.201-226.
2. Багратишвили Т.Д. некоторые вопросы минералогии баритовых месторождений Западной Грузии // Тр. геол. ин-та АН Груз. ССР. Мин.-петр. сер., 1961.Т.5.
3. Беликова и др. Физико-химические условия образования баритов в Башкирии // Термобарогеохимия земной коры и рудообразование. М.: Наука, 1978.С.122-127.

4. Борисенко А.С.Физико-химические параметры формирования баритовой минерализации Алтае-Саянской складчатой области // Тр. Института геологии и геофизики. Новосибирск, 1988. Вып.733. С.165-177.
5. Гомелаури А.И., Гуниава В.Д., Аревадзе Д.В. Температура образования некоторых баритах месторождений Западной Грузии // Вестн. МГУ. Сер. геол. 1974. №5. С. 113-116.
6. Жилинская И.И., Кормушин В.А. Температура образования барита и флюорита на Орловском месторождений (Рудный Алтай) // Изв. АН Каз. ССР. Сер. геол. 1975. №2. С. 56-58.
7. Ковриго О.А. Термометрия включений в рудообразующих минералах Риддер-Сокольного месторождения // Новые данные по геологии медных и полиметаллических месторождений Казахстана. Алма-Ата, 1973. С.79-87.
8. Кулинич В.В., Муканов К.М. и др. Физико-химические параметры формирования баритов различных генетических типов на месторождениях Атасуйского типа (Центральный Казахстан) // Прикладная термобарогеохимия. Матер. межвед. Семин. Алма-Ата, 2-4 июня 1987. Ч.1.Алма-Ата, 1988. С. 160-164.
9. Платонова Э.Л., Ковалишин З.И., и др. Условия образования баритов в Закарпатье // V всесоюзное совещание по термобарогеохимии (тезисы докладов). Уфа, 1976. С.200.
10. Сазонов В.Д. Некоторые физико-химические особенности процессов гипогенной минерализации на примерах отдельных месторождений Таджикистана // Автореф. дис. …канд. геол.-мин. наук. Душанбе, 1962.
11. Твалчрелидзе А.Г., Щеглов В.И. Минералого-геохимическая модель жильного баритового рудогенеза // ЗВМО.1990.Вып. 2. Ч. 119. С. 21-34.
12. Учаймешвили Н.Е., Малинин С.Д., Хитаров Н.И. Геохимические данные к процессам формирования баритовых месторождений. М.:Наука, 1984.124с.
13. Файзиев А.Р., Алидодов Б.А., Искандаров Ф.Ш. Некоторые физико-химические особенности формирования Сасыкского золоторудного месторождения (Центральный Таджикистан) // Минерал. сб. Львовск. госун-та. 1972. Вып.4. №26. С.378-387.

14. Файзиев А.Р. Минералогия, генезис и закономерности размещения флюоритовых месторождений центрального Таджикистана. Душанбе: Дониш, 1991. 314с.

15. Файзиев А.Р., Искандаров Ф.Ш., Гафуров Ф.Г. Минералогия, термобарогеохимические условия становления и генезис редкоземельно-флюоритового место-рождения Дункельдык (ВосточныйПамир) . Душанбе, 2000. 174 с.

16. Файзиев А.Р., Фозилов М.М., Гадоев М.Л. Баритовая минерализация месторождения Большой Канимансур (Северный Таджикистан) // Труды ИГ АН РТ. «Геология и минерально-сырьевые ресурсы республики Таджикистан». Душанбе. 2001. С.185-189.

17. Rife David L. Barite fluid inclusion geothermometry. Carters Ville mining district. // Econ. Geol. 1971. Vol 66. №8. P.822-824.

18. Roedder E. Barite fluid inclusion geothermometry, Carters Ville mining district, Northwest Georgia, Discussion // Econ. Geol. 1972. Vol 67. P.821-822.

GAS-CHROMATOGRAPHY AND RADIOSPECTROSCOPY OF VEIN QUARTZ OF SOME INDUSTRY DEPOSITS

E.N.Kotova, S.N.Shanina, S.K.Kuznetsov

The vein quartz used as raw material for synthesis of monocrystals and smelting of a glass, is characterized by a wide variety of the constitution and properties. This variety is caused by variations of physical and chemical parameters of mineral formation. The composition of gas-liquid inclusions and structural elements-impurity in vein quartz from several deposits of Ural, Kazakhstan and Karelia were analysed by gas chromatography and electron spin resonance (ESR). This investigation is of interest not only for the analysis of mineralgenesis conditions. but also for an estimation of quality of quartz raw materials.

The analyses of gas-liquid inclusions were carried out by gas chromatograph Tsvet 800. The sample to be analysed was fragmented into pieces with 0.25 – 0.5 mm in diameter, was loaded into the special quartz reactor and were heated up in the atmosphere of rare gas. Preliminary they were heated at 100°C during 6 hours for removal of water that may be absorbed on a sample surface. Spectroscopic researches of quartz were made by ESR. ESR spectra of the powder preparations of the quartz were recorded at room temperature and boiling-point of liquid nitrogen with the commercial radiospectrometer SE/X 2547 (RadioPAN, Poland). Sample weight was ca. 200 mg. Error of measurement of the absolute value of the concentrations of the centres was ca. 20%.

Results of gas chromatographic analysis of the vein quartz from various quartz deposits are shown in table 1. The basic gas components emitted from the quartz in the both fields of low (100-600°C), and high (600-1000°C) temperatures are water and carbonic gas. At the same time with them nitrogen, carbon monoxide, metane, hydrogen and heavy hydrocarbons (hh) are fixed. In vein quartz from Kuznechikhinskoe and Bercutunskoe deposits the total contents of gases are 49.7-73.8 μg/g, in vein quartz from Zhelannoe deposit it is much higher - 331.0 μg/g. The highest contents of gases was established in the vein quartz of Aktas deposit - 919.4-1074.0 μg/g.

The main part of gases is released from vein quartz in low temperature interval (100-600°C). Obviously, in this interval rather large gas-liquid inclusions are opened. In the field of higher temperatures gassing greatly decrease. In this area, probably, there is an opening of the smallest gas-liquid inclusions, and removal of structurally connected water as well.

Table1

Composition of gases released during heating of quartz from some deposits

Deposit	N	T, °C	Contents, μg/g							
			N_2	CO	CH_4	CO_2	H_2O	H_2	hh	amount
Zhelannoe	k1	100-600	0,78	2,43	0,64	23,34	261,52	–	8,59	297,30
		600-1000	–	4,70	0,03	1,72	27,00	0,28	–	33,73
Kuznechikhinskoe	k4	100-600	–	1,54	0,16	5,02	48,13	–	1,35	56,20
		600-1000	–	3,09	0,03	1,58	12,84	0,11	–	17,65
	k5	100-600	0,94	1,18	0,17	4,97	42,17	–	0,98	50,41
		600-1000	0,19	4,32	0,02	1,55	16,71	0,21	–	23,00
Berkutinskoe	k8	100-600	0,06	1,41	0,15	4,86	28,32	–	1,05	35,85
		600-1000	–	2,15	0,02	1,13	10,55	–	–	13,85
Aktas	k9/1	100-600	0,37	1,17	0,25	9,45	857,67	0,06	0,60	869,57
		600-1000	0,37	5,57	0,38	2,08	40,57	0,22	0,61	49,80
	k9/2	100-600	0,31	1,31	0,28	19,57	954,96	0,07	0,83	977,26
		600-1000	0,18	2,48	0,05	14,70	78,50	0,45	0,40	96,76

According to the ESR studies after γ-irradiation in vein quartz probes of all deposits were founded Al- and Ge- paramagnetic centers (tabl. 2). Along with the aluminum and germanium in the quartz structure there are sodium, lithium and hydrogen ions acting as compensators of deficiency of a charge and included in these structural defects.

The aluminium centers are prevailing. The contents of Al-centers in the samples of quartz annealed at 530°C and irradiated by γ-rays doze 30 Mrad, fall within the interval 7.4–72.4 ppm. After annealing (1000 °C) and irradiation within a doze 30 Mrad the contents of the aluminium centers grows at 1.1-2.1 time. Their ratio in the vein quartz of various deposits are constant.

The concentration of germanium centers in the vein quartz structure varies in range from 0.02 to 0.19 ppm. Quartz of the Rukh-Navolok, Aktas, Kuznechikhinsk, Berkutinsk deposits contains relatively low consentration of these centers, does not exeed 0.7 ppm. The vein quartz from the Zhelannoe and Nicolay-Shor deposits have higher concentrations of Ge-centres – 0.12-0.19 ppm.

The results of the researches testify to some features of formation of the vein quartz of the considered deposits. The vein quartz of the Uralian deposits as raw material for a glass melting has higher quality, than the quartz of the Aktas and Rukh-Navolok deposits.

The investigation was made within the financial support of the Russian Foundation for the Basic Researches, (grant RFBR #02-05-64747) and the integral project of the Earth Science Department of the Russian Academy of Sciences.

Table 2

Concentration of paramagnetic centres in the vein quartz from some deposits on ESR data

Deposit	N	Ge/Li, ppm	Al, ppm		
			Al_1	Al_2	Al_3
Zhelannoye	k1	0.12	0	23.4	35.2
	56_86	0.13	0	7.4	14.4
	58_86	0.17	0	16.6	21.5
	69_86	0.14	0	18.0	30.0
Nikolay-Shor	2062	0.13	0	35.5	38.2
	2064	0.15	0	19.1	29.2
	2065	0.19	0	17.5	22.0
Kuznechikhinskoye	k4	0.06	0	10.5	16.8
	k5	0.06	0	11.0	31.7
Berkutinskoye	k8	0.07	0	16.0	22.9
Aktas	k9	0.02	0	54.1	83.6
Rukh-Navolok	k11	0.06	0	110.7	159.8

The note. Concentration of paramagnetic aluminium centres was measured in the initial probes – Al_1; in the annealed (530 °C) and the irradiated (30 Mrad) probes – Al_2; in the annealed (1000 °C) and the irradiated (30 Mrad) probes – Al_3.

References

1. Balitsky V.S. Experimental study of crystal formation processes. M., Nauka, 1978, p. 144.

2. Vinogradov V.V., Danchevskaya M.N., Kolmogorov J.V., Kosoruchkin G.V., Kreysberg V.A., Rakcheev V.P. Influence of gas-impurities in quartz raw material on quality of silica melting // Electronic industry. 1985. V. 6, p. 3-33.

3. Methods of study and estimation of deposits of quartz raw material / Minestry of geology of USSR; VNIISIMS, Editors.: E.P. Melnikov, S.V. Kolodieva, M.F. Yarmak et. al.-M.: Nedra, 1990, p. 168.

GEL INCLUSIONS IN SILICA MINERALS

Kulchitskaya A., Chernysh D.

Institute of Geochemistry, Mineralogy and Ore Formation
of National Academy of Science of Ukraine

In spite of the fact that strong tendency of silica acid to polymerization causes formation of sols and gels in a wide pH range – from 1 to 12, reports about gel inclusions (Kalyuzhnyi, 1968) are rather unique. Size of inclusions is not always favorable for specification of their physical state, and only colloform textures testify to colloid origin of inclusions (Dolgov, 1959; Ermakov, 1972).

Literature data analysis, our own experiments and observations over natural systems gave us the possibility to expand the fixed notion of gels: a) Gels of silica should not necessarily be jelly-like. Dry on the surface, rigid hydroxylated silica is formed in a very acid medium; b) CO_2, CH_4, N2 and other compounds could be contained together with (or without) water in disperse medium; c) Gels are formed not only in the result of coagulation of colloid solution. Interaction of true solutions, that contain soluble silica, as well as oxidation of silanes, and saponification of silica tetrachloride and many other reactions result in the formation of jelly-like silica. d) While pressure increases temperature boundaries of gel existence also widen; e) Trapping mechanism of gel inclusions differs from the same for true solutions inclusions.

Inclusions of non-dried silica gel (with disperse medium) were observed in vitreous opal resembling hyalite. Contents of inclusions is more mobile form of silica (in comparison with opal matrix), which formed as the result of silica gel differentiation by the composition of volatile and non-volatile admixtures. Volatile components contribute to silica transportation in the region of light compaction. Differentiation processes became apparent also inside inclusions that finally caused isolation of crystalline silica (quartz) and gas phase in the center.

Inclusions of non-dried silica gel were also observed in quartz, especially in low-temperature quartz, crystallization of which took place against a background of rapid PT-parameters change. They are remarkable for their large size that is several times larger than the size of fluid inclusions, surrounding them. Gel inclusions are also remarkable for the way of their behavior during cooling. Even if the size is huge, it is practically impossible to notice phase transitions in inclusions, or they could be observed only in a narrow spaces between

silica gel and vacuole walls. Water in dispersion medium is proved by deformation of gas bubble and by the change of its size while the temperature crosses 0°C. If there is no gas phase from the very beginning, it could appear in the result of gel compaction after several sequential cycles of heating-cooling. In natural conditions such inclusions transfer into water inclusions with anomalous gas bubble. CO_2 in disperse medium is also fixed by the temperature of phase transitions. Density of CO_2 inside gel inclusions differs significantly from CO_2 density in the nearest fluid inclusions. Silica gel inclusions with different disperse medium could be contained in one crystal. Inclusions of non-dried silica gel in quartz are also the result of silica differentiation by the content of volatile admixtures.

Undoubtedly, gel inclusions should be widely represented in the nature, especially among vein quartz formations. It is only prolonged period of quartz crystallization that does not preserve them. They are transformed to ordinary families of fluid inclusions: clusters, swarms, necked inclusions, "healed" with inclusions cracks.

PYROLYSIS OF MINERALS AND FLUID COMPONENTS OF INCLUSIONS

Kulchitskaya A., Voznyak D.

Institute of Geochemistry, Mineralogy and Ore Formation
of National Academy of Science of Ukraine, Kyiv

Volatile elements are important components of mineral-formation medium, and their composition is the most reacting to the changes of its physical-chemical parameters. The minerals containing volatile components, fix these changes. Therefore, composition of pyrolysis products of minerals and rocks should reveal the conditions they were formed (transformed) in. The problem is – to discover the regularity of composition change of pyrolysis products according to one or another formation condition.

Data we gathered include several thousands of chromatographic analysis of gas pyrolysis products of mineral samples, conducted on one instrument, by one method and in the same conditions. The last is very important as the composition of pyrolysis products depends on analysis conditions, first of all on fraction size, temperature and time of heating. **Pyrolysis products of minerals do not correspond with the composition of volatile components in mineral-formation medium, they could only be used for comparison of mineral samples, formed in different conditions.**

The method of step-up heating of mineral samples from 50 to 1050C with stepwise analysis of pyrolisys gas in fixed temperature intervals seemed to be rather informative. While gradually increasing the temperature, we involve in the pyrolysis process the components, which are stronger held by a mineral and for their separation more energy is needed. Physically adsorbed gases are the first that come off (from the surface of a mineral and opened pores), then – chemically adsorbed components (pyrolysis products in fact). Thus, we receive a series of discrete gas portions that characterize the composition of volatile components in different layers of mineral fragment, starting with a surface layer. Analysis results allow us to receive the apportionments curves of pyrolysis primary components – H_2, N_2, CO, CH_4, CO_2, H_2O and secondary C_2H_4, C_2H_6, H_2S, SO_2 – according to the temperature, in a way metric characteristic of the sample.

Accumulated material proves that every mineral sample has a stable composition of volatile elements and their volatile compounds. The more uniform mineral composition of the sample is, the more stable analysis results are. Standard deviation of containment of CO, CO_2 and H_2O does not exceed 50% and only for H_2 it could reach 100%.

If to combine temperature intervals, one can follow the change of gas composition as far as high- and low-temperature pyrolysis products accumulate, from the external to internal layer and visa verse. Composition of some compounds could be replaced by their ratio. Volatile elements are irregularly distributed among the minerals, that is why we should consider this while comparing compaunds of different elements. We have received the most demonstrative results when used the ratio of different compounds of one element, for instance H_2/H_2O, CO/CO_2, H_2S/SO_2, which does not depend on the mineral composition of the sample. Curves of the change of composition of hydrogen and carbon compounds illustrate how contrasting metric characteristics of one and the same matter (SiO_2) could be (pictures). Phosphorite and apatite, glauconite and biotite are remarkable for the composition of pyrolysis products. Biotite curves differ by disposition on value axis, if biotite is contained in different rocks. The form of the curves could change. Pyrolysis products of all crystalline substances, we have researched, are notable for higher H_2/H_2O value against CO/CO_2. It has been also noted that deeper the rocks are formed the higher this excess is.

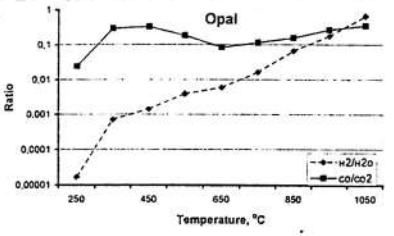

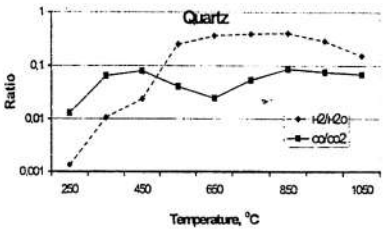

Volatile components of fluid inclusions have a definite position within pyrolysis products. Step-up heating enables to differentiate adsorbed gases and fluid components of inclusions a bit conventionally. Inclusions are retained in the mineral by a mechanical force. They come off between physical and chemical desorbing. Maximum decrepitation of inclusions is observed in the interval 250-450° but can vary for different minerals. Notable bend of the curve H_2/H_2O points to decrepitation of inclusions. The worked out test system enables to define rather confidently methane, nitrogen, carbon dioxide, hydrogen sulphide in inclusions, but does not allow to define the correlation between the components of inclusions. In general, fluid inclusions are not favourable for thermal analysis. Fluid inclusions increase the deviation of composition of pyrolysis products from the mean value. Not all minerals contain fluid inclusions, thus mineral samples are not identical.

TRIMETHYL ACETIC ACID IS SOURCE OF NATURAL DIAMOND FUSES

Murogova Raisa N.

JSC "GAZPROMGEOFIZIKA" Industrial branch "MOSGAZGEOFIZIKA"

8a, Burovaya St., Shchyolkovo, Moscow Region, 141100

Tel/fax: (095)-745-01-44, (09646)-3-41-35

Many scientists in various times think that organic matter from rocks take part in diamond genesis. This article devote to search of specific carbonaceous matter are fuse for natural diamond genesis.

Only some organic joints are stable to temperatures of diamond genesis. These are carbon asids, composite ethers and related to them joints – amides.

In the table 1 there are temperatures of existence of some carbon acids from rock exposed to heating in the temperature range 100-1010°C. The step of heating was 20-30°C.

Table 1

T,°C	**Carbon acids which pyrolysis products are stated by gas analysis during destruction of organic matter from rocks**
740	HCOOH, CH3COOH, C4H9COOH, C2H5COOH, C4H9COOH, C3H7COOH (isobutyric)
770	HCOOH, CH3COOH, C4H9COOH, C2H5COOH (propionic), C4H9COOH (methyl ethyl acetic)
900	HCOOH, CH3COOH, C4H9COOH (trimethyl -acetic)
1010	HCOOH, CH3COOH (acetic)
	HCOOH, CH3COOH
	HCOOH (formic)

Acetic acid and formic acid wasn't completely destroyed at 1010°C but products of pirolisys of trimethyl acetic acid wasn't discovered at temperatures higher 900°C. Trimethyl acetic acid is interesting because its carbonic lattice contains 5 atoms which attitude position similar to diamond lattice. External carbon atoms edged by hydrogen, which can be beat out only by corpuscular oxygen during destruction of trimethyl acetic acid's molecule.

$$C_4H_9\text{-}C(=O)\text{-}OH + 3O^{2-} = 5C + 5H_2O \quad (1)$$

Products of pyrolysis will be diamond and water. Simultaneously the decay of acetic acid and formic acid is occurring. These chemical reactions are:

$$CH_3\text{-}C(=O)\text{-}OH \rightarrow CH_4 + CO_2 \quad (2)$$

$$H\text{-}C(=O)\text{-}OH \rightarrow CO + H_2O \quad (3)$$

$$H\text{-}C(=O)\text{-}OH \rightarrow H_2 + CO_2 \quad (4)$$

$$CH_3\text{-}C(=O)\text{-}OH \rightarrow CH_2{=}CH_2 + 2O^{2-} \quad (5)$$

$$CH_3\text{-}C(=O)\text{-}OH + H_2 \rightarrow CH_3\text{-}CH_3 + 2O^{2-} \quad (6)$$

$$CH_3\text{-}C(=O)\text{-}OH + H_2 \rightarrow CH_3CH_2OH + O^{2-} \quad (7)$$

The maximum of corpuscular oxygen may well take by decay of country carbonate rocks.

Nitrogen will be obligatory product of amides decomposition. All these gases and water are present in gas inclusions from diamonds.

All aforementioned facts are explain a presence in nature early-aged light isotope-enriched (C^{12}) diamonds due to carbon from trimethyl acetic acid.

THE QUARTZ FORMING CONDITIONS OF GRANITIC PEGMATITES WITHIN BASIC ROCKS IN NORTH-WESTERN PART OF THE UKRAINIAN SHIELD (OBTAINED BY DATA OF FLUID INCLUSION RESEARCH)

Larysa R.Red'ko, Ihor M.Naumko

Institute of Geology and Geochemistry of Combustible Minerals of National Academy of Sciences of Ukraine and of National Joint-Stock Company "Naftogaz of Ukraine"
Naukova Str., 3a, 79601, Lviv, UKRAINE
e-mail: igggk@ah.ipm.lviv.ua

The north-western part of Ukrainian Shield in the same way as in other regions is the area of considerable development of pegmatites genetically and spatially with granitoid complexes. However the felsic pegmatite formations within rocks of basic composition are wide spread here too. It was found some accesory minerals in them and sufficient albitization process was established that were genetically related to formation of numerous pegmatites ores and the scale of this process development usually is used for pegmatite veins and bodies evaluation (Lazarenko, Pavlishin, 1974). This fact defines the necessity of further studies of these rock units and in particular the genetic features of their mineral-forming processes (based on the fluid inclusions in quartz and mineral parageneses) as the principal hopeful search and evaluation criteria.

Quartz crystal from pegmatites occured within anortosites and gabbro-anortosites of **Golovins'kyi quarry** are characterized by clear zoning: the matrix of crystal comprised by pegmatite of graphic structure, the internal zone is composed by light to dark-smoky quartz variety and external zone by ice-coloured one.

The diversity of fluid inclusions inclusions types in quartz can be summarized as follows.

Multiphase inclusions with minerals-daugthers occur as individual groups in crystal matrix without visible relations to filled fractures suggesting for their primary nature (early-secondary). Phases ratios and compositions are rather variable. Th = 420-450°C L.

Also primary features are displayed by tube-like inclusions situated immediately close to crystal surface. These are predominantly two-phase diverse-filled inclusions of CO_2 (from $81L_1 + 19G$ to $7.5L_1 + 92.5G$), rarely complex of type $L + L_1 + G$. $ThCO_2$ ($15L_1 + 85G$) = 24.9°C G.

The secondary inclusions are presented by the next types:

- complex CO_2 ones with phase relations from $10L + 60L_1 + 30G$ to $1L + 19L_1 + 80G$. The finding of syngenetic complex inclusions CO_2 ($75L + 25\text{-}20L_1 + 68\text{-}75G$, $ThCO_2$ = 29.5°C G, Th = 267°C G) and vapour-liquid inclusions (85L + 15G, Th = 250°C L, C = 4.2 weight per cent of NaCl) allows to define pressure of mineral forming that is about 30 MPa;
- sufficiently carbon dyoxide inclusions from $40\text{-}30L_1 + 60\text{-}70G$ ($ThCO_2$ = 23°C G) to $60\text{-}70L_1 + 40\text{-}30G$ ($ThCO_2$ = 27.5°C L_1);
- vapour-liquid inclusions overfilled with latest solutions: 97L + 3G, Th = 100°C L, whole concentration 17-18 weight per cent of NaCl;
- multiphase inclusions with mineral-satellite (goethite) and composition of 93L + 5-6G + 2-1B;
- essentially vapour and essentially liquid inclusions.

There were solid inclusions of goethite and underfined mineral found in ice-coloured quartz as well as primary vapour-liquid inclusions 85L + 15G, total salt concentration (by cryometry) 22-23 weight per cent with composition close to $CaCl_2$ + NaCl.

In quartz from pegmatite veins met by drill holes in **Kirov-Kocherivs'ka structure-metallogenic zone** vapour-liquid inclusions predominate having almost constant filling: early-secondary – volumetric with form close to corresponding negative crystals and composition of 60-65L + 35-30G, Th = 260-280°C L, rarely 340-350°C L (when unsoluble up to T = 380°C solid phases presents); secondary of different forms, 75L + 25G, Th = 190-220°C L.

In some cases within a single fracture several inclusions associate with phase relations from 70-75L + 30-25G to 10-15L + 90-85G as well as minute complex inclusions CO_2 where liquid CO_2 content is 30-40 per cent, water solution – 40-50 per cent.

As one can see the most important component of volatile phases of fluid inclusions in quartz is CO_2. Its content increases from early to late units: pegmatites of graphic structure → internal crystal zone → external crystal zone or pegmatite of graphic structure → of pegmatoid one → of micro-block one (see below).

Location	Composition of volatile, vol. per cent			
	CO_2	N_2	CH_4	H_2
Pegmatites from Golovins'kyi quarry				
Of graphic structure	59.1	38.5	1.2	1.2
From internal zone of crystal of quartz	84.4	14.6	0.2	0.8
From external zone of crystal of quartz	93.1	5.5	1.0	0.4
Pegmatites from Kirov-Kocherivs'ka zone				
Of graphic structure	50.0	50.0	0.0	0.0
Of pegmatoid structure	87.2	12.8	0.0	0.0
As above	100.0	0.0	0.0	0.0
Of micro-block structure	91.5	7.4	1.1	0.0

As above	96.5	3.5	0.0	0.0

It should be noted that the analogous behavior of carbon dyoxide content changes and its importance in the regulation of the mineral-forming medium acidity-alkalinity (Naumov et al., 1972) was found when reconstructions were provided by quartz formation in rock-crystal chamber-type pegmatites (Kalyuzhnyi, Kovalishin, 1967) and rare-metal vein pegmatites (Naumko, 1986; Vynar, Kalyuzhnyi, Naumko et al., 1987; Naumko, Matviyenko, Vynar et al., 2001) of the Ukrainian Shield in rocks of felsic composition.

The next conclusions on quartz forming conditions of granitic pegmatites within basic rocks may be suggest based on the results of fluid inclusion research and generalization of data from their typomorphic features with aggregate state, composition, PT-conditions etc. Mineral was formed in unstable environments of postmagmatic stage of pegmatite process preferentially under influence of heterogenization of mineral-forming fluids at general decrease of temperature and exchange of fluids concentration and their composition (with predominance of alkaline elements, chlorine and carbon dyoxide). On the whole the established temperature and geochemical parametres are close to those of ones in pegmatite bodies and veins related to felsic rocks (for example Volodars'k-Volyn' and Korostyshiv pegmatite fields in north-western part of the Ukrainian Shield).

FLUID INCLUSIONS IN VEIN QUARTZ OF ZHELANNOYE DEPOSIT, THE SUBPOLAR URAL

N.V.Sokerina, S.N.Shanina
Institute of Geology, Syktyvkar

Domestic industry is now facing an acute problem of raw quartz supply, the problem being due to the absence of pure transparent quartz reserves. The problem can be resolved by using low-quality vein quartz. The quality of quartz is known to be strongly dependent on its fluid inclusions. There are abundant data on fluid inclusions in rock crystal of Zhelannoye deposit, including those on the homogenization temperature, types and morphologies of inclusions. The major task for the authors has been a detailed study of fluid inclusions in vein quartz of the deposit. There are a lot of rock crystal-bearing veins composed of coarse-grained and columnar quartz divided in three types by its transparency and texture-structural features: gray, milky-white and translucent. The latter was the later among them, it is related usually to the start of rock crystal-forming process. With this purpose in mind, we have studied fluid inclusions in vein quartz of various generations, classified fluid inclusions into types, established temperature of their homogenization, character of decrepitation, and morphology of fluid inclusions. Analysis of homogenization temperature and frequency of its occurrence (Fig. 1) has revealed that histograms for grey and milky-white quartz have a mode in the 171–190°C range. Histogram for translucent quartz shows a mode in the 206–228°C range (number of intervals was calculated according to Sterdges formula). Gas chromatography (Tab. 1) has revealed a typically high H_2O content. A tendency to an increase in CO_2 and decrease in N_2 content has been observed from grey to translucent quartz. In order to estimate the total content of gases released on heating, the samples were subjected to decrepitation without pumping out the released gas. Total gas content was measured. It was found to be from 130 to 179 c.u. for grey quartz, 111 to 187 c.u. for milky-white quartz, and 131 - 154 c.u. for translucent quartz. Aqueous extract data indicate an increase in relative contents of alkaline constituents and sulphates and decrease in nitrate amount from early to later stages in quartz formation. Salts dissolved in fluid inclusions of this deposit are of essentially potassium-sodium chloride-bicarbonate composition.

a)

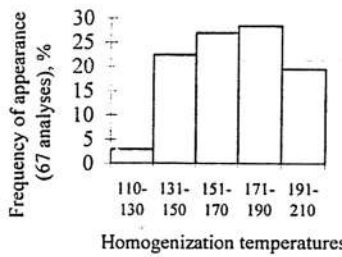

b)

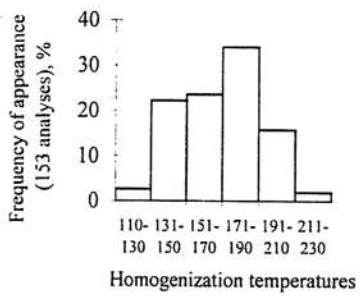

c)

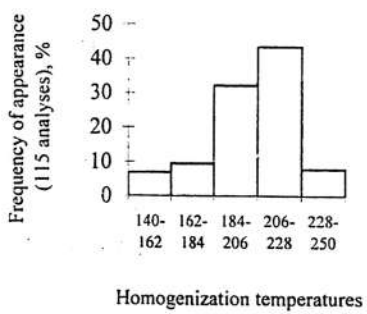

Fig. 1. Histogram of homogenization temperature frequency:

a – grey quartz, b – milky-white quartz, c – translucent quartz.

Table 1

Chemical composition of fluid inclusions in vein quartz of Zhelannoye deposit, μg/g

sample	species	N_2	CO	CO_2	H_2O	Σ
2230	grey	0,16	0,03	1,44	30,1	31,73
2231	grey	0,16	0,03	1,36	44,7	46,25
2319	grey	3,04	0	0,93	70,2	74,17
1758	grey	2,4	0	2,97	17,6	22.97
	x	1,44	0.02	1,68	40,65	43,78
		3,3	0,05	3,8	92	
	Vx	104,23	115,47	53,25	55,60	51,21
2225	milk-white	0,35	0,06	4,33	4	8,74
2224	milk-white	0,35	0,14	2,89	24,5	27,88
2229	milk-white	0,16	0,06	2,38	47,9	50,5
2226	milk-white	0,38	0,14	1,7	4,1	6,32
2210	milk-white	0,26	0,17	1,7	3,4	5,53
2214	milk-white	0,32	0,23	1,36	10,3	12,21
2212	milk-white	2,11	0	1,11	106,3	109,52
2215	milk-white	3	0	2,89	37,6	43,49
	x	0,87	0,10	2,295	29,76	33,02
		2,6	0,3	6,9	90	
	Vx	123,67	82.98	46,12	118.26	107.27
2236	translucent	0,06	0,06	0,85	38,3	39,27
2232	translucent	0,45	0	4,59	12,95	17,99
	x	0,26	0,03	2,72	25,63	28,63
		0,90	0,10	9,50	89.50	
2233	crystal	0,03	0,03	0,34	15,2	15,6
2234	crystal	0,19	0,14	0,34	8,4	9,07
	x	0,11	0.09	0.34	11,8	12,34
		0,89	0,69	2,76	95,66	

Notice. Vx – correlation coefficient; x – average, numerator - absolute value, μg/g, denominator - relative number, %

GENETIC ASPECTS OF ZN-CU MASSIVE SULFIDE DEPOSITS OF VERKHNEURALSKY ORE DISTRICT, SOUTHERN URALS ON DATA OF FLUID, MELT INCLUSION AND ISOTOPE STUDIES

V.S.Karpukhina[1], I.V.Vikentyev[2], V.B.Naumov[1]

[1] - V.I. Vernadskii Institute of Geochemistry and Analytical Chemistry, Russian Academy of Sciences, 19 Kosygin street, Moscow 117334, Russia

[2] - Institute of Geology of Ore Deposits, Petrography, Mineralogy and Geochemistry, Russian Academy of Sciences, 35 Staromonetny per., Moscow 119017, Russia

Volcanogenic massive sulphide (VMS) deposits of Verkhneuralsky ore district are located in the northern part of Magnitogorsk ensimatic trough and host by arc-related calc-alcalic rhyolite-dacite series $D_2gv_1^2$, underlying by Na-basalts $D_2gv_1^1$. Small zones of sericite-quartz and sericite-chlorite-quartz rocks occur in the footwall of the ore bodies. In elaborated genetic models the origin of VMS deposits is connected with small-depth acid magmatic chamber. However many aspects of this connection remain debatable. Melt inclusions in quartz phenocrysts were studied in samples of dacite, rhyodacite and rhyolite. Fluid inclusion studies in minerals from ore bodies and in quartz phenocrysts (secondary inclusions) from altered country rocks have been carried out in addition to earlier investigations (Karpukhina, Baranov 1995). Primary and secondary fluid inclusions were analyzed for their homogenisation temperatures (T_{hom}) with an accuracy of $\pm 2^0$C. Salinites were obtained from measured ice melting point with an accuracy of $\pm 0.2^0$C , eutectic temperatures - $\pm 1.5^0$C, using the technique of Borisenko (1977). The pressure was estimated from CO_2-phases and PVT data.

Fluid inclusion study

Usually secondary fluid inclusions in quartz phenocrysts or in minerals of ores (quartz, barite, anhydrite) are not exceeded 10 μm. Inclusions are liquid-rich and rare liquid with CO_2-phases. T_{hom} of liquid-rich inclusions lie in the range of 380-120^{0}C. A thermometric analyses in the ore bodies and in altered country rocks have shown that ore bodies have been formed over discharge channels approaching sea floor or at subbottom position from high temperature (up to 380^{0}C) hydrothermal solutions. High temperature fluid flows (380-250^{0}C) are local - their width up to a few tens meters. Palaeothermal gradient in the central zones ranges up to

150-100^{0}C/100 m, decreasing till 10-20^{0}C/100m on the flanks, where T_{hom} did not exceed 190-150^{0}C. High temperature patterns are also defined for the handing wall rocks.

Primary inclusions in quartz, barite and carbonates from ore are liquid-rich. The observed T_{hom} (375-137^{0}C) in the ores are not connected with the ore composition, but reflect grade of epigenetic transformation of ores. T_{hom} of inclusions in fine-grained ores with colloform texture relicts are lower (137-200^{0}C) then in recrystallized coarser grained aggregates (200-300^{0}C) and vein-form, which have temperatures 270-375^{0}C.

Two main types of fluids were distinguished: I - hydrocarbonate-chlorite and II - chloride with prevalence Na. Salinities in the range from 2 to 8 wt % Na equiv., being 2-3 times greater than that of marine water. Fluids (I) are distributed in ores and altered rocks mainly in high-temperature zones, (II) on flanking zones of underlying altered rocks. Fluid (I) can be interpreted as juvenile based on chemical composition and spatial distribution. Fluid (II) is interpreted to reflect transformed sea water. Sulfur contents in fluid of vacuoles ranges from 160 to 250 mg/l, and copper - from 0.3 to 1.2 g/kg of solution.

Evidence for boiling of hydrothermal solution while approaching the sea-floor were revealed in the host rocks. H_2O-CO_2-bearing inclusions are found in a wide zone which decrease downwards, extending to a depth of >500 m. The pressure values seem to be ranged 0.6-1.0 kb, that corresponds to buried, subbottom conditions of ore genesis.

Melt inclusion studies

Melt inclusions in quartz phenocrysts are from 5-10 μm to 150 μm diameter. Two main types of melt inclusions are discovered: the most widespread the devitrified inclusions, and rarely found glasses, some of them contain the ore globules of magnetite and also sulphides, represented by pyrrhotite, pentlandite, chalcopyrite and bornite, defined by electron microprobe. Melting of glasses occurred at 600-720^{0}C, homogenisation at 900-1110^{0}C, when devitrified inclusions at 750-820^{0}C and 950-1210^{0}C accordingly. Glasses and homogenised devitrified inclusions were analysed by electron microprobe for major elements and F,Cl. Composition of glasses in melt inclusions (data of electron and ion microprobe) are differing considerably from the composition of felsic volcanites by higher contents of SiO_2, K_2O and lower contents of other components (FeO, MgO,CaO). The melts of K-Na composition (K_2O/N_2O=0.3-0.7; K_2O+Na_2O=2.5-5.1) are most widespread; Na-composition (Na_2O till 5.5 wt %) and K-composition (K_2O up to 9.7 wt %) are rare. Sulphur concentration in glass of inclusion with sulfide globule is 0.03 wt %, corresponding to sulphur solubility in acid melt.

The content of water in melts may reach 6 wt%, taking into consideration total of oxides, the data were confirmed by ion microprobe (4.6-4.7 wt %). The content of trace elements was defined by ion microprobe also (in ppm): Li 0.30, Be 0.35, B 115, Sr 100, Y 34.2, Zr 105, Nb 1.11, Ba 355, La 5.04, Ce 13.0, Nd 8.46, Sm 2.61, Eu 0.90, Dy 3.98, Er 2.80, Yb 3.12, Th 0.94.

Sr and stable isotope studies

$^{87}Sr/^{88}Sr$ ratio for carbonates corresponds to a primary one because of the absence of ^{87}Rb in the composition. $(^{87}Sr/^{88}Sr)_0$ for carbonates (0.7048-0.7063) were found to be close or exceed those for acid volcanites of the ore field (0.7041-0.7064, Bobokhov et al., 1989). Very narrow range of $(^{87}Sr/^{88}Sr)_0$=0.70597-0.70625 indicating a lower involvement of marine and higher input of magmatic water are characteristic for ores and host rocks of the lower level; the smaller values occur in carbonates of latest quartz-carbonate veins in diabase dykes. Isotope compositions of O and C of carbonates ($\delta^{18}O$= +13 to +26.5 ‰, $\delta^{13}C$= -28 to +1 ‰ for massive ores and $\delta^{18}O$= +9 to +27 ‰, $\delta^{13}C$= -20 to -1‰ for altered igneous rocks) confirm the conclusion of a marked addition of magma-derived components. Results from limestones samples, from the unit overlaying ore bodies of the upper ore level, demonstrate that hydrothermal endogenic input occurred during their formation: the footwall of the limestone layer has $\delta^{18}O$= +26 ‰ and samples from further up have $\delta^{18}O$= +27.5 to +28.5 ‰, approaching the field of isotope composition of marine carbonates. Values of $\delta^{34}S$ in sulfides of ore bodies range from -11.3 to +11.1 ‰ CDT. Such large variations of $\delta^{34}S$ in sulfides exclude input of sulfur to hydrothermal fluid from single homogeneous source (e.g. magmatic chamber or marine water). The isotopic compositions of H in sericite (8 samples) and O and H in chlorite (2 samples) from altered rocks of Uzelginsk deposit were investigated. The δD values of fluid water (its temperature was taken as T_{hom} of inclusions in associated quartz) vary from -1.6 to -37 ‰. The δD values of fluid below 250°C (-3.7 to -1.6 ‰) roughly coincide with those of oceanic water. In fluid of 290-330°C, δD values decrease to -29 to -30 ‰. Two values of $\delta^{18}O$ calculated for fluid (+1 and +4 ‰) are intermediate between marine and magmatic oxygen.

Conclusion

VMS deposits of Verkhneuralsky region are an example of a long-term ore-forming systems. Primary ores were deposited on oceanic floor as well as in subbottom position under the covering of limestones, cherts and siltstones from hydrothermal chlorine solutions at T=150-380°C and P=0.6-1.0 kbar. Heterogeneity in fluid inclusion composition was established. Sr and stable (S,O,C) isotope studies revealed dual (oceanic and juvenile) nature of ore-forming fluid source. Isotope data indicate that the main input of magmatic components arise at the final stage of ore genesis from the late-volcanic processes that manifested itself in the formation of igneous-explosive breccia and basic dykes. Occurrences of copper-bearing phases within sulfide globules found in melts inclusion in felsic rocks indicates increased copper content in parent magmatic melt and are evidence of important role of magma-derived metal components in ore formation.

Acknowledgements

The authors wish to thank E.Baranov, A.Chugaev, A.Dervirts, A.Ignatiev and L.Nosik for cooperation. This study was supported by the Russian Foundation for Basic Research (03-05-65005) and Russian Science Support Foundation.

References

Bobokhov A.S., Gorozhanin V.M., Kuzmin S.A., 1989. *Strontium isotope data for acid volcanics of Magnitogorsk synclinorium of the South Urals*. Ufa: Nauka (In Russian).

Borisenko A.S., 1977. Criometric technique applied by studies of the saline composition of solution in fluid indusion in minerals. *Geologia and Geophysika* 8, 16-27 (in Russian).

Karpukhina V.S., Baranov E.N., 1995. Physical and chemical conditions of formation of the massive sulfide ore deposits of the Verkhneuralsky ore area, Southern Urals. *Geochemistry Intern.* 1: 48-63.

THERMODYNAMIC CONDITIONS OF EVDIALITE FORMATION IN VARIOUS TYPES OF PEGMATITES IN HIBINY'S MASSIF.

A. A. Samsonov, D. V. Lisitsin (Federal State Museum "Samotzvety")

S. F. Trufanova, R. N. Murogova (Production division "Mosgasgeophysics")

Alkaline pegmatites from a Kola Peninsula (Hibiny region) are met practically in all types of rocks and, as a rule, are grouped in the extensive fields associated with the most fluviopermiable zones. Irrespective of structure of containing rocks and presence of the late imposed processes all alkaline pegmatites can be divided into two groups, which initially vary between themselves.

The first group is vein pegmatites, described by coarse-grained structure and rather simple mineral structure, which usually corresponds to the structure of containing rocks, including basic accessories. Characteristic minerals of such pegmatites are nefelines, coarse-crystalled pyroxene or amphibole, kalium feldspar, enigmatitis, sphene, titanium magnetitis, evdialite, rincitis, astrophyllite or lamprophyllite. These are high-temperature pegmatites formed during a magmatic stage from the residual fusion slightly enriched with volatile compositions.

Pegmatites of a second group are in a lump characterized by zonal and mineral structure not corresponding to structure of containing rocks. Pegmatites of a second group can form veins, lenses and isometrical bodies, sometimes irregular-shaped bodies with numerous subdivisions (apophises). One of characteristic features of these pegmatites is a presence of needle-like egyrine among rock-forming minerals, which compositionally are almost identical to pure $NaFeSi_2O_6$. The second group of the subdivision consists of differentiated pegmatites from Hibiny region with zeolitic or ultraagpaites nuclei.

One of the dazzling representatives of decorative collection minerals from alkaline pegmatites is *evdialite.* Met in various types of pegmatites from Hibiny region evdialite is found as well formed crystals of pink and crimson color, small outcrops in rocks, veiny and monomineral formations of significant capacity.

Two samples of evdialite from different groups of pegmatites are investigated.

The first group pegmatite is located in foiaites from the mountain called Jukspor in the central part of a massif. Pegmatite is presented as a veiny body (5 m in length and about 0,4-0,5 m in capacity) of essentially feldspar-pyroxene composition with honey-yellow nodules of sphene, black enigmatites, druses and separate brownish - red crystals of evdialite, plates of astrophyllite, grains of gray nepheline. Feldspar of kalium-sodium composition (orthoclase-pertite); pyroxene crystals (egirines-diopside) usually have a joint growth surface with a

feldspar. Enigmatite crystals are idiomorphic in comparison to other pegmatitic minerals that attributes to its earlier crystallization.

Pegmatite of a second group is located in the hibinytes of the mountain Putelichorr in the northwest part of a massif. Pegmatite is presented as an extended lens of about 20 m in length, mainly of feldspar-egirines composition with the separate sites drastically enriched with evdialite. Evdialite forms well faceted crystals up to 10 centimeters in diameter in a mass of thin-needled dark green egirines and small grains in accretion with light coloured kalium feldspar. Throughout the volume of pegmatite there are separate lamellar crystals of lamprophyllites up to 6 centimeters in length.

Modeling is carried out in the laboratories of PD " Mosgasgeophysics" in the temperature interval between 50-900°C with the measurements of a gas component taken every 20°C throughout with the purpose of definition of the crystallization temperature of evdialite.

From the results of modeling (tables 1, 2) it is visible that formation of two investigated pegmatites occurred in various physical and chemical conditions and to various speed.

Pegmatitic process on the mountain Putelichorr went through slowly, gradually. Direct genetic connection of pegmatite with the magmatic melt is traced. The final stage of an actual magmatic process is fixed at 820°C being accompanied by a precipitation of a solid phase (presumably of a nepheline). A first mineral of the subsequent pegmatitic (postmagmatic) process becomes kalium feldspar (740°C). An actual pegmatitic process, which begins at a fixed 740°C, comes to an end at 400°C, transforming on the way into a hydrothermal. Crystallization of evdialite occurred in a rather wide temperature interval: between 500-540°C and 660°C.

We observe another picture on the mountain Jukspor. Forming of pegmatites occurred here to a greater speed than on the mountain Putelichorr. The border separating magmatic processes from postmagmatic (pegmatitic) passes at the temperature 740°C, as well as in the previous case (precipitation of a kalium feldspar). Evdialite crystallizes in a short interval of temperatures, being one of the last minerals of the pegmatitic association. After 420°C hydrothermal process begins.

By results of the research it is possible to draw the following conclusions:

1. Three stages of pegmatitic formation are allocated corresponding to the different temperature intervals set in the margins from 380-420°C (pegmatitic-hydrothermal associations) to 740-800°C (magmatic – pegmatitic association).
2. There is a direct genetic connection with the magmatic melt.

3. Evdialite is formed in various thermodynamic conditions of the pegmatitic process.
4. Mineral formation in pegmatite proceeded also at low temperatures (hydrothermal process).

The literature

А.В. Щербакова, Р.Н. Мурогова, С.Ф. Труфанова Условия образования минеральных парагенезисов хромитовых месторождений Полярного Урала по газовой составляющей пород Материалы X международной конференции по термлбарогеохимии с.61-78 ВНИИСИМС г.Александров 2001.

С.Ф. Труфанова, Р.Н. Мурогова, Ф.П. Мельников, А.В. Щербакова Температурные условия образования флюорита (по данным термогазохроматографии). Материалы XI международной конференции по термлбарогеохимии с.188-191 ВНИИСИМС г.Александров 2003

Лисицин Д.В., Добровольская М.Г., Цепин А.И. и др. Сульфидная минерализация в высокощелочных пегматитах г.Коашва (Хибинский массив, Кольский п-ов) Геология рудных месторождений Т.44 №5 с.437-449, 2002

Table 1

Geochemical characteristics of temperature barriers in pegmatitic mineral formation at the Putelichorr mountain

Temperature barrier, T°C	Temperature of crystallization of a mineral, T°C	Mineral	Geological process	Geochemical parameters	Note
180-240			Hydrothermal	O_2 N_2	
280-320				C_2H_4 C_3H_6 iC_5H_{12} C_5H_{10} III IV iC_6H_{14} III nC_7H_{16} H_2CO_2	K_2=C_2H_2/ C_3H_6
340-360	340-360			K_5 K_2 K_3 K_4 C_3H_8 C_4H_{10}	
400 420 460	420	Egyrine	Pegmatitic	II C_6H_{14} III K_5 C_5H_{10} I	K_3=C_3H_6/ C_3H_8
500-520-540	500-540	Lamprophyllite, evdialite		K_4 K_2 K_4 K_5 CH_4 C_2H_4 nC_4H_{10} C_4H_6 I II $неоC_5H_{12}$ nC_5H_{12} C_5H_{10}III nC_6H_{14} iC_8H_{18} nC_8H_{18} CO_2 H_2	
660-680-700	660-700	Evdialite, feldspar		K_2 K_3 K_5	
740-780	740	Kalium feldspar		K_2 K_5	
820-860	820-860	Pyroxene, nepheline	Magmatic (hibinytes)	K_3 K_2	

Table 2

Temperature barrier, T°C	Temperature of crystallization of a mineral, T°C	Mineral	Geological process	Geochemical parameters	Note
100-120			Hydrothermal	iC_4H_{10} неоC_5H_{12}	
200	200			K_3	K_2=C_2H_2/ C_3H_6
260-300	269-300			K_2 K_3 K_4 K_5	
380-420				iC_7H_{16} iC_8H_{18} CO_2	
440				CO_2	K_3=C_3H_6/ C_3H_8
460	460	Evdialite		NC_4H_{10} iC_5H_{12} iC_6H_{14} III	
480				K_4 nC_4H_{10}	
				C_2H_2 C_3H_8 C_4H_8 I II C_5H_{10} II III nC_7H_{16} nC_8H_{18}	
600-640	600-640	Sphene, enigmatite	Pegmatitic	K_3 K_4	
				K_2	
660				CO_2 C_2H_6	
740	740	Orthoclase		K_5	
800				iC_6H_{14} II	
860-880			Magmatic (foiaites)	CH_4 C_2H_6 C_4H_8 I C_5H_{10}IV N_2 C_3H_6	

TEMPERATURES OF MINERALIZATION IN HYDROTHERMAL Au-Ag DEPOSIT: EVIDANCES FROM FLUID INCLUSION DATA

D.M.Voinkov, R.N.Murogova

State Scientific Center of the Russian Federation – VNIIgeosystem

Gold-silver deposit bases in Kharamazarsky ore region in North Tadjikistan. Area of deposit is packed by late-paleozoic vulkanic formations, presented by andesic porphyries, liparites, dacite and liparite-dacite porphyties. This vulkanic formations are intruded by dykes of granite-porphyries and diabasic porphyries, which hase late-permian – early-triassic age.

The deposit is localized approach by areas of regional fault. Quartz-carbonate veins, which has thickness from 1-3 m before 20-30 m and crowds of fine quartz or carbonate veinlets are appears ore-bearning. There are 4 ore bodies in the deposit. Ore bodies № 1, 2, 3 are place in Main ore zone. Ore body № 4 is locate in Parallel ore zone. Ore body № 1 is lengest. It length is 220 m to eztend and 180 m to cross dip. Ore bodies № 2, 3, 4 are blind. The length ore body

№ 2 is 400 m in horizontal and 60 m to cross dip. Ore body № 3 is characterized by gentle dip to north under angle 15-25^0. It length in stretching out is 170 m and 40 m – in falling. Ore body

№ 4 is locate in steeply diping Parallel ore zone, locating on 35-40 m southward from the west flank of Main ore zone.

Morphological all ore bodies of deposit are presented by sufficiently self-possessed plane lenses, lying according to ore-bearing zones of crushing and schist. Borders of ore bodies are coincides with contacts of carbonate-quartz veins and accompanying their zones of silification. Distribution of useful components inside ore bodies is irregular.

On the deposit are installed three stages of mineral forming: pre-ore, ore, post-ore.

Pre-ore stage is characterized by pick out propilite mineral assemblages, which has albite-calcite-sericite-chlorite composition with fine grains of pyrite. This pecular to close-to-surface gold deposites.

Ore stage is approach by carbonate-gold-quartz assmblage with rare grains of pyrite, sphalerite, arsenopyrite, galenite, gray antimony and sulphosalts.

Post-ore stage is approach by barite-quartz-carbonate assemblage.

Warm-up mode of mineral-forming is studied for ore stage. All explored inclusion are two phase, gas-fluid. They situated on removing from edges of quartz grains and unconnected with fratures. Centainly studing including are primary. All inclusion homogenizing in the fluid phase. Temperatures of gomogenization of gas-fluid inclusion are determined in the

quartz ore (productive) assemblage with comparatively high contents of gold (grams, tens, hundreds g/t).

As a whole for deposite productive mineral assemblage is formed in the interval 270-125^{0}C.

In samples of quartz of ore body № 1 are fixed temperatures of homogenization comprising of interval 270-155^{0}C, in ore body № 2 – 265-155^{0}C, in valance ore body № 3 – the most low temperatures 145-125^{0}C. In steeply diping Parallel ore zone in the ore body № 4 temperatures of homogenization of inclusion are ranging 255-140^{0}C.

Gas composition of the samples of ore quartz (analysis of the content of CH_4, C_2H_6, C_2H_4, C_3H_8, C_3H_6, iC_4H_{10}, nC_4H_{10}, C_4H_8, iC_5H_{12}, nC_5H_{10}, iC_6H_{14}, H_2, O_2, N_2, CO_2 was determined in the VNIIYAGG laboratory of physical and chemical analysis (Ramenskoe, Moscow region) by the thermal gas chromatography using Tsvet-500 unit.

Thermal dynamics of mineralization is studied based on the temperature of the inter-atomic bond breakage in the complicated structures of organic matter. As known, organic associations in the form of hydrocarbons, graphite, and other modifications of carbon are present in all the types of ore deposits. Thermal intervals relating to formation of ore bodies are estimated from the features of gas component of ore samples when modeling the destruction of organic matter in the temperature range of 100 to 860°C.

Ore body 1 was sampled at three levels: surface, horizon I (50 m to the surface), and horizon II (100 m to the surface). The following temperature intervals of ore formation were found for this body at different depth: 380-460°C - surface; 380-480°C - horizon I; and 500-520°C – horizon II. The temperature gradient for ore body 1 is as much as 60-120°C per the depth of 100 m.

Ore body 2 is characterized by the ore formation temperature of about 480-500°C (close to that of ore body 1) within horizon I.

Ore body 3 features a gentle dipping and is only 40 m in length along the dip. It is characterized by the highest temperature of ore formation within horizon I ranging from 560 to 580°C.

Ore body 4 is embedded in the steeply dipping tectonic zone, it is characterized by the ore formation temperature of 380-400°C.

From the results of modeling of organic matter destruction it follows that ore formation temperature range for ore bodies of the deposits under study is higher than estimate found by homogenization of gas-fluid inclusions.

According to all signs and temperatures of mineral-forming the deposit belongs to the near-surface low-sulphur deposites of gold-silver formation.

TEMPERATURE OF MANGANOCALCITE FORMING OF PARNOKSKOYE DEPOSIT (ARCTIC URAL)

N.N. Zykin

Geological Faculty, Moscow State University, Moscow, Russia

e-mail: nznz@yandex.ru

There are different notions on forming conditions of Parnokskoye iron-manganesian deposit. Opinions of researchers disperse as on separate questions of the geology (structure, age of host rocks and time of ore formation, source of materials etc), as on the genesis of the deposit, moreover the notions on its origin covers all known genetic types of manganesian ores - from hypergenesian to skarn [1-3, 5-7, 9-11]. Considerable part of mineral formation of the deposit was formed as a result of metamorphism of primary oxide (hausmannite-pyrochroite), carbonate (mainly rhodochrosite) and silicate-carbonate (tephroite-rhodonite-cariopilite-rhodochrosite) ores The most wide-spread mineral for metamorphic stage of the deposit is manganocalcite. Multiple veins, rifts, schliere are filled with this mineral, forming brecciform and stringer srtuctures by lamellar, concretion and lenticular- laminated colloform primary ore aggregates. There are hot pink well-crystallized translucent crystals of elongated cross-grained and tabular forms. The are detected two its generations by cross relation. Investigation by means of X-ray microanalyser (MSU) did not reveal any significant differences in the composition of these generations.

In manganocalcite there were discovered two-phase fluid inclusions available for studying by the size 1-17 mkm. The mycrothermometric study of water fluid was fulfilled in mycrothermocamera THMSG-600 company "Linkam" by Prokof'ev V.Yu. (IGEM RAS). Studies of isotope composition of water and gas phases of inclusions in manganocalcite were fulfilled by existing method [4, 8] in the VIMS laboratory of stable isotopes (analysts Zykin N.N., Erokhin V.E.). In all cases inclusions were uncovered by the thermal method with the heating upto 380 °C. °C in the high vacuum for removing void, sorption and other waters.

Studies of isotope composition of water in inclusions have shown that its δD have values -70 ‰ (SMOW). Methane δD in the gas phase = -414‰, methane $\delta^{13}C$ = -30,3‰ (PDB). Inclusions $\delta^{13}C_{CO2}$ is from -4 to -8,5‰. Composition of manganocalcite $\delta^{18}O_{carb.}$ from different horizons ranged between +9,8 and +17‰, $\delta^{13}C_{carb.}$ are characterized mainly by low values (to -14‰), in average form -10‰, but generally have positive correlation with isotope composition of enclosing limestones and carbonaceous ores, which are replaced by

manganocalcite. If pure calcite participates in the system and the system is in equilibrium the isotope data obtained give ore-forming fluid temperatures as 200-300°C.

Table

Results of studies of manganocalcite fluid inclusions of Parnokskoye deposit (Arctic Ural).

N Sample	Mineral	n	Temperature,°C			C_{salts}, g/cm^3	d, mass.% equiv. NaCl	Temperature, °C with correction on 540 bar
			homogenization	eutectic	melting of ice			
T-2	manganocalcite	7	186	-36	-4.7÷ -3.5	0.93	7.5÷ 5.7	236
11-2	manganocalcite	8	184	-32	-3.0	0.92	5.0	234
11-41	manganocalcite	2	187	-31	-2.5	0.91	4.2	237
	-«-	4	162	-32	-2.1	0.94	3.6	212
	-«-	7	154	-31	-2.4	0.94	4.0	204
11-32	manganocalcite	3	119	-31	-1.6	0.96	2.7	169
	-«-	7	180	-31	-1.9	0.91	3.2	230
C-24-1	manganocalcite	2	230	-26	-0.6	0.83	1.1	280
	-«-	3	218	-24	-0.2	0.84	0.4	268
	-«-	7	208	-22	-0.1	0.85	0.2	258
	-«-	3	117	-26	-2.7	0.97	4.5	167

The data obtained show that metamorphism of Parnokskoye deposit ore is valued as low-temperature (prehnite-pumpellyite facies), and haved an isochemical nature.

Reference

1. Брусницын А.И., Калинина О.Г. Физико-химический анализ минеральных ассоциаций марганцевых руд Парнокского месторождения (Полярный Урал)// Геология и минеральные ресурсы европейского северо-востока России. Т.IV, Сыктывкар. Материалы XIII Геологического съезда Республики Коми, 1999, с.12 – 16
2. Брусницын А.И., Калинина О.Г.. Метаморфизм марганцевых и железных руд Парнокского месторождения (Полярный Урал). // Металлогения древних и современных океанов – 99. Рудоносные системы. Миасс: ИМин УрО РАН, 1999. Стр.54-59.

3. Герасимов Н. Н., Наседкина В.Х., Онищенко С.А., Шишкин М.А. Минеральный состав руд Парнокского железомарганцевого месторождения // Геология рудных месторождений, 1998, Т. 41, №1. С. 84-96.
4. Ерохин В.Е., Зыкин Н.Н. Масс-спектрометрическое определение изотопов углерода и кислорода в карбонатных рудах. Методические рекомендации. Москва, ВИМС, 2002, 21 с.
5. Зыкин Н.Н. Изотопный состав углерода и кислорода руд и вмещающих пород Парнокского железо-марганцевого месторождения (Полярный Урал) в связи с его генезисом. // М.: Вестн. Моск. ун-та. Сер. 4. Геология. 2002. № 2, С. 32-39.
6. Зыкин Н.Н.. Геологическое строение и генезис Парнокского железо-марганцевого месторождения (Полярный Урал). // М.: Вестн. Моск. ун-та. Сер. 4. Геология. 2004.
7. Контарь Е.С. и др. Марганцевые месторождения Урала. / Екатеринбург, 1999, 118 с.
8. Методика изотопного анализа лёгких элементов (С, О, Н) разных фаз веществ из одной пробы горных пород, минералов и молодых осадков. Методические указания. М.: ВИМС, 1994, 28 с..
9. Силаев В.И., Ширяева Л.Л. Парнокское железо-марганцевое месторождение: мифы и факты.// Геология рудных месторождений, 1997, т.38, № 4, с.387 – 393.
10. Шишкин М.А., Герасимов Н.Н. Парнокское железо-марганцевое месторождение (Полярный Урал) // Геология рудных месторождений, 1995, том 37, № 5, с.445-456.
11. Шишкин М.А., Герасимов Н.Н. Парнокское железо-марганцевое месторождение: геологическое строение, характеристика руд, пути освоения // Народное хозяйство Республики Коми. Сыктывкар, 1994. Т. 2. № 2. С. 208-223.

LATITUDE OF PARNOKSKOYE DEPOSIT (POLAR URALS) IN PERMIAN PERIOD

N.N. Zykin

Geological Faculty, Moscow State University, Moscow, Russia

e-mail: nznz@yandex.ru

It is well known, that there is a correlation between δD and $\delta^{18}O$, described by the equation $\delta D = 8\delta^{18}O + 10$ ‰ (SMOW), called Meteoric Water Line (MWL) for the water isotopic composition of precipitation and meteoric water on the continents. For the first time this relation was noticed by H. Craig [1]. He generalized it from a lot of experimental data, so the regression line δD and $\delta^{18}O$ is often called in literature the "Craig line". It was also noticed that the most "heavy" meteoric waters are found in low latitudes. The isotopic composition of these waters is close to that of the average ocean water, δD and $\delta^{18}O$ being equal to 0 ‰ and in isotope investigations taken as a the standard SMOW (Standard Mean Ocean Water). At the same time, the farther from the equator, the lighter the isotopic composition of the meteoric water becomes. The "lightest" water both on δD and on $\delta^{18}O$, is found in icecaps and icebergs in the northern and southern Earth poles where the lowest values of heavy isotopes δD = - 420 and $\delta^{18}O$ = - 55‰ (SMOW) were fixed. Besides the dependence on geographical latitude (latitude effect), isotops also depend on the terrain heights , where precipitating occurs (altitude effect), and the remoteness from the ocean (continental effect), because the isotopic fractionation increases the dependence on the number of the "evaporation - condensation" cycles. The above dependencies can be generalized as a climatic or geographic effect.

Numerous investigations have show that isotopes hydrogen kept in rock in most cases corresponds to that of the local meteoric water, i.e. marks the same geographic effect [2 - 4, 6, 9, 10]. This dependence is correlated both for the ancient hypergenic, hypogenic (hydrothermal) formation and for modern active volcanic and hydrothermal systems. Water isotope studies have led to the conclusion that in ore deposits formation, whose source of matter is thought to be juvenile, it was the meteoric water that took part in the convection more often.

The investigation of the fluid inclusions in minerals is as a rule concentrated on the studying only of the hard and gas phases of the inclusion and water chemical composition, i.e. the solvents are also studied. Meanwhile, the water, often forming the greater part of the inclusion volume, is unnoticed by the researchers. The water of the fluid inclusions from the

very moment of their formation is in the "preserved" state. So it can be presumed that it can give information not only as a solvent (density of solution, composition, temperature, etc), but, under certain conditions, it may also give some information of geographic nature. As has been shown above, it indicates the meteoric water' isotope composition at the moment of the inclusion and mineral formation. Therefore the isotope water composition of the fluid inclusions can also characterize the paleolatitude of their formation. However, certain correction should be made due to the existence of the continental and latitude effects.

For a number of years the author has been studying Parnokskoye iron-manganese deposit (Polar Urals) The author [7 etc.] suggests that the deposit belongs to the sedimentary genetic type although there are other assumptions as to its origin [11].

The studies of the isotope water composition of hypergenic minerals have shown that their δD is –130 to –170 ‰ (SMOW), which is typical of the meteorite water of the circumpolar latitudes. The given observation all but confirms the general rule. Along with the sediment oxide – silicate - carbonaceous protores of the deposit, there are numerous metamorphogene mineral forms represented mainly by manganocalcite. In many of the fractures, veins, schlieres and so on, which had developed in the primary ores and formed brecciaform, vein and other textures. In manganocalcite there have been observed two-phase fluidal inclusions mainly in a liquid phase. The studies of the isotope composition of hydrogen made by the author, have shown that the water of the inclusions is much heavier than the stable isotope of other minerals and the local meteoric water and is characterized by δ D = –70 ‰ (SMOW). It was found by using the method of gas and ion chromatography (table, O.F. Mironova), that F/Cl ratio for the metamorphogenic fluids is equal to 0,176, and is higher than the analogous equation in the sea in 20000 times. $(0{,}24 - 1{,}5) \times 10^{-4}$ [5]. The observation in question makes it possible to state that ir was not the sea water which had formed the manganocalcite.

The isotopic composition of the water of the inclusions is much heavier not only than δ D water of the Polar Urals region (-130 ‰, 65-66 m.l.), but also it is heavier than δ D of mean latitudes (the water of Moscow region – 56 m.l. - has the meaning of $\delta D \mp -105$ to –95 ‰). This kind of composition is typical of the latitudes of modern Middle Asia [4, 9, 10]. Thus, the paleolatitude of manganocalcite forming is estimated as 30-40° North. The area of a deposit at those latitudes on the data [8] was at the end of Perm time - the beginning Trias. At the same time it is known that the Urals folding occurs to be in the Carboniferous –Trias Period (with the main stage in the Permian time). Thus, the formation of secondary minerals coincides with the folding stage of the given region.

Reference

1. Craig H.. Isotopic Variations in Meteoric Waters // Science, Volume 133, 1961, p.p. 1702-1703.

2. Kokubu N., Mayeda T. and Urey H.C.. Deuterium content of minerals, rocks and liquid inclusion from rocks. // Geochimica et Cosmochimica Acta. 1961, vol. 21, p.p. 247-256.

3. Stable Isotopes as Applied to Problems of Ore Deposits: Economic Geology and the Bulletin of the Society of Economic Geologists: vol. 69, September-October, 1974, № 6.

4. Ветштейн В.Е.. Изотопы кислорода и водорода природных вод СССР. Л.: Недра, 1982, 216 с..

5. Виноградов А. П.. Введение в геохимию океана. - М.: Наука, 1967. - 213 с.

6. Есиков А.Д.. Изотопная гидрогеология геотермальных систем. М: Наука, 1989, - 208 с..

7. Зыкин Н.Н.. Геологическое строение и генезис Парнокского железо-марганцевого месторождения (Полярный Урал). // М.: Вестн. Моск. ун-та. Сер. 4. Геология. 2004

8. Печерский Д.М., Диденко А.Н.. Палеоазиатский океан; петромагнитная и палеомагнитная информация о его литосфере. М., ОИФЗ РАН, 1995, 298 с

9. Селецкий Ю.Б., Поляков В.А., Якубовский А.В., Исаев Н.В.. Дейтерий и кислород-18 в подземных водах (масс спектрометрические исследования). М., Недра, ВСЕГИНГЕО, 1973, 144 с.

10. Ферронский В.М., Дубинчук В.Т., Поляков В.А. и др.. Природные изотопы гидросферы. М.: Недра. 1975. 280 с..

11. Шишкин М.А., Герасимов Н.Н.. Парнокское железо-марганцевое месторождение (Полярный Урал). // Геология рудных месторождений, том 37, № 5, 1995, с. 445-456.

THE MAJOR REGULARITIES IN FLUORITE FORMATOIN

F. Ya. Korytov, D.M. Voinkov

IGEM RAS, Moscow

State Scientific Center of Russian Federation – VNIIgeosystem, Moscow

The major regularities in fluorite formation can be used in forecasting all these types of deposit; the factors leading to the localization of the mineralization include geotectonic, geophysical, geochronolological, magmatic and mineralogical ones.

Geotectonic factors. There are global fluoritebearing belts at the margins of all the continentsaround not only the Pcific but also the Atlantic, the Indian and the Atctic oceans | 1 |. These polyformational belts contain deposits of various minerals, including oil and gas, and they are regularly related to Mesozoic-Cenozoic rifting and ocean formation. There are also intracontinental and transcontinental mineralogenic belts, which can be traced into the ocean floor. An example is provided by the Ural-Iran-Oman transcontinental belt of extensive magmatism and mineralization. In all these ore belts, the fluorite deposits are usually associated with intersections between mainly submeridional and sublatitudal faults and ring structures.

Geophysical factors. These represent a regular relation between fluorit-bearing zones or regions and megablocks showing extensive rifting and marked changes in thickness in the crust or individual iayers. There are rift structures in many orebelts and regions in Transbaykalia, the Gornyy Altai, Cisbaykalia, South Yakutia, Mongolia, Primor'ye, the Pamirs, South Kazakhstan, the Ukraine and so on, where these structures indicate regions of anomalous mantle (usually decosolidated | 2 |. Certain mineralized belts are associated which transmantlefauits such as the Ural-Iran-Oman line, which mark the boundaries between major inhomogeneities at the surface of the earth's core |3 |. Fluorite-bearing belts and regions are usually complicated in structure (mosaic and angular structures) and have complicated geophysical fields (gravitational and magnetic). Most of the fluorite deposits are associated with the margins of strong geophysical anomalies, which are usually of annular or vortex form in plan and reflect tubular tectonomagmatic structures.

Geochronological factors. These are associated with epochs of extensive fluorite formation, where there are regular signs of evolution in the scales and compositions of the mineralization (from Precambrian to Cenozoic). Over 70% of the ores in many deposits, very varied in composition and origin, are associated with Late Mesozoic to Cenozoic tectonic and magmatic activation, when many fluorite deposits were formed, particularly the following

types: pegmatite, carbonatite, greisen, hydrothermal, hydrothermal-sedimentary, mineralized salt doum, and multistage types.

Magmatic factors. There is a paragenetic relationship between fluorite deposits of many typesin many regions, not only one with another but also with plutonic and volcanic rock complekxes highly differentiated in composition (granites, liparites, desalts, perlites, kimberlites, lamproites and so on), which may have elevated contens of water, alkalis, halides and other elements. All these depositsand igneous rocks have been produced by various mantle and transmantle magmas and fluids, with the latter released from the earth's core initially as plasma jets, which have migrated in the mantle and crust while subject to ongoing alteration and differentiation, which has given rise to the mineralized, saline and petroleum-bearing brines, ultimately determining the great variety of deposits of many different minerals.

Mineralogical and thermobarogeochemical factors. Here there is a relationchip between the mineral composition of the ores and the age, structural position, or deep structure of the region. The largest deposits, with ores varied in composition, are comparatively young (Mesozoic-Cenozoic) rift deposits, where the ores and the fluorite have the highest levels of the rare earths, gold, silver, the platinoids, uranium, beryllium, chlorine and other elements. There is a correlation between the concentrations of these elements in the fluorite and the morphology or color of the crystals, as well as with the formation temperature. The distribution of the fluorite and the other minerals in the deposits or the individual orebodies is usually accompanied by marked horizontal and vertical zoning, whose exact type may vary (straight, combined, etc.), but which is most frequently inverse, where the late and relatively low-temperature minerals are increasingly important with depth (quartz, calcite, sulfides, anhydrite, etc.).

An example is provided by the multistage Mushugay Khuduk deposit in Mongolia, where magmatic rare-earth-fluorite-magnetite-apatite mineralization (carbonatitoids of Jurassic age is overprinted by Cretaceous hydrothermal-metasomatic barite-celestite-calcite-fluorite mineralization.

Inclusion data | 4 |, have shown that fluorite depositscristallized from highly concentrated chloride solutions (30-75 wt.% NaCl) at 1100-80° C and 1.0-2.5 kbar.

Conclusions

The regularities in fluorite formation, which can be used in forecasting and prospecting, indicate that all the continents have provinces promising for various types of

fluorite deposit. In the Russia, one may note particularly the areas of the Northeast, Kamchatka, Sakhalin, the Caucasus, Gornaya Shoriya, the Kola Peninsula, the Yenisey ridge, central and eastern parts of the Russian platform and various other regions. In particular, there are the wellknown fluorite-bearing provinces in Transbaykalia, Central Asia, Primor ye and so on, where the flanks and deep horizonts of the orefields and individual deposits are also promosing for discovering ores containing adularia, sellaite, zeolites, anhydrite and other minerals.

References

1. Korytov F.Ya. Ore-bearing belts around the oceans. In *Mttallogeniya i novaya global'naya tektonika (Metallogeny and the New Global Tectonic).* VSYeGYeI, Leningrad. 1973. pp.147-148.
2. Korytov F. Ya. The relation between mineragenic belts and heterogeneity in the earth,s mantle. *Doklady AN SSSR*. 1985. Vol. 281, № 1, pp. 127-129.
3. Korytov F. Ya. And Ovchinnikov L. N. Uralo-Irano-Omanskiy mineragenicheskiy poyas. *Doklady AN SSSR*. 1986. Vol. 290, № 5, pp. 1175-1178.
4. Ontoyev D. O., Kandinov M. N. and Korytov F. Ya. Formation temperatures for the apatite-fluorite-rare earth mineralization in southern Mongjlia. . *Doklady AN SSSR*. 1977. Vol. 234, № 5, pp. 1164-1166.

SYNTHETIC FLUID INCLUSIONS: THE SYSTEM H_2O-NAF-SiO_2

Kotelnikova, Z. A., Kotelnikov, A. R

Institute of Marginal Seas of RAS, Staromonetny, 22, Moscow, 119108. Russia..

Institute of Experimental Mineralogy of RAS, Chernogolovka, Moscow district, 142432. Russia

kotelnik@iem.ac.ru)

The experimental research of properties of H_2O-SiO_2-NaF system has been conducted by the synthetic fluid inclusions method. In order to obtain experimental evidence on fluorine-containing fluids, we synthesized fluid inclusions in natural quartz under T = 500-800°C and P=0.5-2 kbar in solutions, containing NaF or NaF+NaCl, by cracks healing method. We used ampullaceous technique. Fluid-generative mixture was 0.5M (2.1 wt %) NaF solution or dry-through solid NaF and water (solubility is 4.1 wt % under room temperature). NaCl was put as 1M or 2M solution. The measurement accuracy was ±50 bar for pressure and ±5° for temperature. Lead-in into experimental mode took 1.5-2 h, tempering - 5-8 min for exoclave and 20-30 min for autoclave. The overall experiment duration was 23-35 days.

NaF has inverse solubility dependence on temperature: under room temperature it is 4.1 wt %, under 374°C - about zero. Under even higher temperatures, solubility is unknown. H_2O-NaF state diagram is of the P-Q (II) kind: the critical phenomena are observed in saturated solutions. Three-phase equilibria S+L+V or S+L_1+L_2 exist under temperatures less than lower critical point P or greater than higher Q. Critical phenomena and three-phase equilibria do not exist in P-Q interval, where above-critical F or F+S is present. In such systems saline solubility drastically increases for temperatures and pressures near to Q critical point. Moreover, under high parameters, the interaction between NaF and SiO_2 becomes possible - which leads to quartz incongruent solubility.

Results

500°C, pressure0.5-2 kb

The homogenization of inclusions trapped under 500 bar from 2.1 wt % NaF solution occurred in both L and V phase, sometimes during boiling, under 356-380°C - in the conditions close to critical isochor. Inclusions' nature, trapped under different pressures shows that NaF solubility under constant temperature of 500°C increases with pressure up to 5 wt % in the pressures interval of 500-1000 bar.

Under pressure of 2 kbar we found in the samples four-(three)-phase inclusions, containing "glassy" phase (G), besides gas, solid and liquid (Fig. 1). This phase boundary with liquid had a form of regular meniscus, and by view these inclusions were similar to natural melt inclusions with very high fluid component. But it was trapped under temperature about 1000° lower than quartz melting temperature.

Sometimes, crystalline phase was also present. The amount of inclusions containing "glassy" phase was not high, 2 to 10 over the whole sample. Under heating, the fluid phase homogenized with liquid, while "glassy" phase didn't show observable changes up to 400°C. The further heating was not conducted, to avoid inclusions' opening.

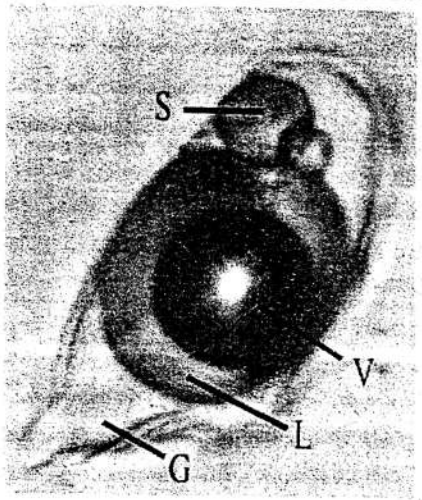

Fig. 1. Fluid inclusion synthesized under 500°C, 2 kbar from NaF+NaCl solutions. Heating leads to homogenization of V+L; "glass" and solids don't change.

Besides that, we met two-phase gas-liquid (V+L) inclusions, homogenizing with liquid in the interval covering the homogenization temperatures fluid phase of multi-phase inclusions with "glassy" phase. Homogenization temperatures spread was quite high - up to 20-30°. These inclusions were placed not only along partially healed cracks, but also in the neogenic part of the sample. In several cases, under heating of gas-liquid inclusions higher than 160°C, the crystal became visible, growing in size with temperature increase and shrinking back to the full invisibility with temperature decrease.

The obtained results show that under t=500°C and P=2 kbar the active interaction of fluid with quartz began, leading to formation of sodium fluorine silicates and hydrosilicates. If it took place under lower temperatures, the used experimental technique did not allow for finding it. So, with temperature and pressure increase, it is impossible to speak about the system under study as binary H_2O-NaF, but only as ternary system H_2O-NaF-SiO_2 , because quartz is no more inert.

When we added NaCl solution to NaF-solution, the heterogenization of fluid into phases L and G occurred. Phase L of the pure H_2O-NaCl system contains 32.2 wt % NaCl (solid NaCl disappears from the V+L+S inclusions under 210°C). In our case solids were dissolved at 241-301°C and total homogenization was at 533-554°C. V+L inclusions homogenized both in

G (392-454°C) and L (428-449°C). The reason for anomalous nature of inclusions can be capture of the products of interaction between fluid and quartz. In the case of presence of NaCl in the solution, the pressure required for appearance of "glassy" phase decreased to 500 bar.

1000 bar, 450-700°C

In all the experiments up to 700°C we found same type inclusions V+L (homogeneous fluid), under 725°C - coexisting V+L и V+L+S (immiscible fluid). As far as the temperature in Q point minimal for upper three-phase domain, T_Q for water solutions of NaF can be taken as 710°C.

Under heating up to 360°C some of V+L inclusions synthesized under 750-800 °C the crystalline phase clearly appeared. Under cooling down to 244°C this phase solved - apparently, these are NAF crystals. Concentration of NaF in V+L inclusions synthesized under 750 °C is about 2 wt %, as evidenced by criometry. The estimate of V+L+S inclusions composition showed 60-70 wt %.

V+L inclusions trapped at 700° homogenized at L at 376-378°C and at 378-382°C in V: the evidence of near-critical parameters. Under pressure of 1 kbar "glassy" phase was found in the samples of experiments conducted under temperature of 750°C and higher.

When we added NaCl to the solution, the homogenization temperatures of V+L inclusions increase, compared to pure fluorine inclusions, synthesized under similar conditions. For example, inclusions trapped from NaF solutions under 600°C homogenize under 366-373°C, while from NaF+NaCl solutions – under 394-412°C (both in L). Under 700°C, as in pure NaCl system, heterogenization takes place. Solid phase is present by two types of crystals, but the reliable estimate of solubility temperature was made for NaCl only - in 3 experiments with different Cl/F ratio it corresponded to 44-53 wt % NaCl (in the pure H_2O- NaCl system, L phase contains 49% of saline).

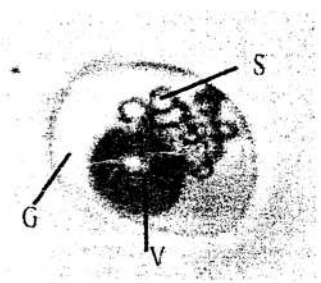

Fig. 2. Fluid inclusion from run 800°C, 2 kbar, 2.1wt% NaF. Under heating liquid phase springs up around gas bubble. Than "glass" decays and liquid volume grows. At 400-500°C some inclusions decrepitated.

2 kb, 500-800°C

In all the samples we met V+L inclusions. Their homogenization occurred: 500°C run – at 290-315°C (in L); 700°C run – at 352-364°C (in L); 750°C run – at 378-382°C (both in L and V); 800°C run – 376-390°C(in L), 385°C in V, 365-379°C –boiling. Besides that, in all the samples we met inclusions with "glassy" phase: V+L+G (Fig. 2) and/or V+L+G+S, and in the 800°C run - V+G additionally.

Heating of such inclusions synthesized under 500 and 700°C leads to homogenization of vapor and liquid (in L) under 306-313°C and 339-345°C respectively (i.e. inside the interval of coexisting V+L inclusions homogenization); no changes in phase G detected. As a rule, we didn't observe solution of crystalline phase up to 500-550°C.

However, in inclusions trapped under temperature greater than T_Q in the presence of heterogeneous fluid, "glassy" phase showed different behavior. Under 140-160°C on its surface appears "shagreen" pattern, and in certain cases it is clearly seen that bubbling in the "glass" occurs. With temperature increase, phase boundary liquid-"glass" becomes rough, here and there toothed, and liquid phase volume grows at the expense of "glass", and, partially, gas. This allows for suggestion that "glass" composition includes crystalline hydrates of sodium hydrosilicates, chipping water off under heating. In V+G+S inclusions, liquid "list" appears around the gaseous bubble. Under temperature about 350°C in glass occur phenomena, similar to eutectic melting: instantaneous melting of one of the phases is accompanied by appearing of multiple solids in the liquid. During further heating, a part of them melts, but, about 400°C, many inclusions open.

Apparently, in H_2O-NaF-SiO_2 ternary system, equilibria $V+L_1+L_2+S_{NaF}$ or $V+L_1+L_2+S_{SiO2}$ are possible, absent in boundary binary systems; in critical points of ternary system minimum temperature and pressure for critical equilibria correspond to $L_1=L_2+V+S_{NaF}$ and $L_1=L_2+V+S_{SiO2}$, and not to the Q point with $L_1=L_2+S_{NaF}+S_{SiO2}$ equilibrium. SiO_2 solubility in this system is quite high in the wide range of temperatures and pressures. Practically, the "heavy fluid" was trapped in the inclusions, which is a low-temperature silicate melt containing much water. Under the capture of "heavy fluid" inclusions looks similarly to the natural melt inclusions

Financial support: grant RFBR 03-05-62027

TERMOBAROGEOCHEMICAL OF FEATURE AND ROLE PALEO TEMPERATURE OF A GRADIENT AT FORMATION SELBUR AMETHYST OF A FIELD (SOUTHERN TIEN-SHAN)

Oimahmadov I.S.

Institute of geology, Tajik Academy of Sciences

In the Selbur amethyst - bearing area two mineral-forming stages are established . At first stage the quartz veins and lodes of lenght 5-25m and thichness 5-10sm are formed along North West faults. Veins are plate-shaped and rarely lense-shoped. Quartz occurs as dense, massif similar to hornfelse masses of milk-white, sometimes gray shade colour (quartz I) and pole-shaped, congestion-radiant units borrowing to peripheral parts of veins and lodes (quartz II).

In the second stage were formed productive quartz - amethysts zone of mineralization (Central, Northern, Western I, Western II, Western III, East, Selbur - Dalniy), exclusively drawn to explosive infringements sub-meridian of orientation. The quartz - amethysts mineralization forms plate-shaped, lenticular, branchy, sometimes of wrong configuration, veins and lodes from 0,5 up to 6m of thickness and from 30 up to 550 m extension. The products of the second stage were formed on a background multistage opening of cracks, in which there was a repeated faltering receipt a hydroterm, to what the presence of four quartz generations testifies, in particular. The quartz III is characterized by petty-granularity structure, massive dense texture and milk-white up to gray-white colour, occupying the basic central parts of veins. The quartz IV occurs as mid-grained, petty-poles (2-6mm), milk-white, grayish and in some places of translucent units, forming veins and lodes, located in wall-veins parts quartz veins of early generation.

Two subsequent of generation of quartz (V-VI), which were formed in the final periods of mineral forming process, concern to actually amethyst mineralization. The quartz V is amethystized as big-granularity, spotty-isometric (2-10mm) and pole-shaped (from 5x3x3mm up to 40x20x15mm) units carries out the central parts veins and lodes, which adjoin to quartz origin of the fourth generation of matter. Pole-shaped units of amethystized quartz grow towards each other before filling fracture of space. The colour of a mineral here is changing from light -violet, pale-lilac up to rich-violet. Thin more light and grey strips (1-5,5mm) on a dark - violet background sometimes are present and show crust-stripped texture due to pulse characte of acting hydro thermal solutions. It is characteristic for units of quartz of this generation.

One of basic type-morfing features of quartz VI (amethyst) formation is its spatial and genetic connection with residual cavities, which formation is connected with inside-stages tectonic motions. The cavities are mainly located in wall-veins and central parts quartz veins

of early generations. In cavities crystallization of amethyst occurred under rather quiet conditions, the ideal shape of amethyst crystals in druses and brushes show this condition. Crystals of amethyst are characterized by prizm form with prevailing development of romboedrs by the size from 0,5-1 up to 2-4 cm. The size of crystals is various, average from 1-3 up to 5-10см. The colouring in crystals and parallel-poles units amethyst is distributed rather non-uniformly and changes from pale - violet, lilac up to rich - violet. There are regular painted intervals in violet tone of average colour density crystals. The crystals and parallel-pole units amethyst quite often are characterized by zone distribution of colouring, changing one other from of milk-white, to lilac and violet colours.

The formation quartz and quartz- amethyst mineralization in Selbur amehtyst area occured on a background of change of physic-chemical parameters both in time, and in space. Crystallization of quartz from hydro thermal mineral forming solutions of the first stage (the quartz I and II) occured at temperatures 450-340^{0}C and pressure 970 -750 atmospheres. As results of the analyses, have shown threefold water extraction quartz formation hydro terms of the first stage are characterized by the high contents Cl^- (56 equal. %) at appreciably low concentration HCO_3^- (28 equal. %) and SO_4^{2-} (14 equal. %). In cation group $Na^+ + K^+$ + are prevailing (69 equal. %) as well as Ca^{2+} + (30 equal. %). According to temperatures of eutectic freezing of gas-liquid inclusions, mineral forming fluids of the first stage were characterized by chlorid-sodium composition. The concentration of salts in solution of inclusions is changing from 31-18 (quartz I) up to 18,5-13,2 weights. % (quartz II). pH of solutions of inclusions is closes neutral.

The products of the second (productive) stage minazalization were formed at lower physic-chemical parameters. Crystallization of quartz in the second stage occurred in a range of temperatures 435-110^{0}C and pressure 720-150 atmospheres. Productive stage are characterizedby in side-stages motions, cycles of which is fixed by consecutive change of temperature, pressure, structure and concentration of mineral forming solutions from early mineral generations to late. Early generation of quartz of a productive stage have following termobaric parameters: quartz III - 435 - 385^{0}C, P- 720-710 atmospheres and quartz IV -320-275^{0}C, P- 700 -465 atmospheres.

Amethyst, being a product of the final periods of a productive stage, is characterized by the lowest meanings of thermobaric parameters: quartz V (amethystized) - 235 - 180^{0}C, P - 490 -410 atmospheres, quartz VI (crystals and in parallel - poles units amethyst) - 195 -110^{0}C, P- 450 -150 atmospheres.

In all investigated generation of quartz of a productive stage the change of temperatures crystallization in a horizontal direction is accompanying with the paleo temperature gradient equal to 5,5-13,6^{0}C on 100m. In vertical section of the Central quartz - amethyst zone is revealed the natural increase of temperature with depth, and in time of

formation the quartz – amethysts veins the change of a temperature gradient is observed. So, the paleo temperature gradient (average) for quartz III is equal 8,5^{0}C, quartz IV - 10,5^{0}C, quartz V - 14^{0}C and quartz VI - 20^{0}C/100m. On a basis of paleo gradient, the depth of formation quartz – amethyst mineralization from modern erosive surface is appreciated for on quartz III -530 –410m, quartz IV -430 –240m, quartz V - 355 –320m and quartz VI -300 – 225m. Paleo gradient helps to calculate level of cerosion for size quartz - amethysts of zones Northern, Western II. East and Selbur - Daliny, which for quartz III corresponds to 60-119m, quartz IV-145-190m, quartz V-34-105m and quartz VI-50-75m.

Thus, between vertical drop of mineralizetion and paleo temperature gradient for each generation of quartz of a productive stage observes direct dependence: the less size of paleo gradient, the more vertical drop of mineralizetion on lodes revolt.

In composition of a liquid phase hydro thermal of solutions of this stage an active role is played by Cl^-, HCO_3^-, SO_4^{2-} and NO_3^-. With fall termobaric of parameters the contents Cl^- (quartz III-50,6-42,4 egul %, quartz VI-48,7-32,2 egul. %), decreases in mineral-bearing solutions and is increased HCO_3^- (quartz III-40,2-34,9 egul %, quartz VI-54,1-29,5 egul %) and SO_4^{2+} (quartz III-21,5-11,8 egul %, quartz VI-23,6-6,9 egul %). In composition of solutions cation prevails $Na^+ + K^+$ (quartz III-81,1-58,5 egul %, quartz VI-74,2-60,3 egul %). The less importance has Ca^{2+} (quartz III-41,5-18,9 egul %, quartz VI-39,7-25,8 egul %). Thus, at formation of the second stage the hydro thermal mineral-bearing solutions had bi-carbonate- cher-calcium-sodium –potassium composition. The results of criometric research have shown to complex composition of hydro thermal fluids which from quartz and amethyst mineralization on the area Selbur amethyst area. Mineral-bearing solutions, at essential prevalence of NaCI and KCI, also are enriched with such components as $MgCl_2$ and $NaSO_4$.

From early generations to late in a productive stage, the gradual difference of concentration of mineral-bearing solutions is observed also. It is equal in quartz III 21,5-9,8 weight. %, quartz IV -19,8-15, quartz V-17,5-9,5 weight. % and quartz VI-14,5-5,8 weight. % .pH of solutions 7,4-6,8.

Thus, amethyst on the area Selbur amethyst of a field crystallized at temperatures 235-110^{0}C and pressure 490-150 атм from sulphate-bi-carbonate-chloride-calcium solutions with concentration of salts 17,5-5,8 weights. %.

In summary we shall note, that established thermobarogeochemical parameters of amethyst formation, alongside with general geological factors of the mineralisation control, can be used for contouring of amethyst-bearing squares both conducting prospecting search and estimated works for this kind of mineral.

ONCE AGAIN ABOUT TEMPERATURE FORMATION OF BARIT (ON EXAMPLE OF DEPOSITS KARAMAZAR, TAJIKISTAN)

Gadoev M.L., Fayziev A.R.

Institute of geology, Tajik Academy of Sciences
mustafog@yahoo.com, must@ac.tajik.net

Around of meanings of temperatures received for barite by a method of homogenization of gas-liquid inclusions, there is a discussion that they not always reflect real conditions crystallization of this mineral connected to the contents in him abnormal conservates of mineral forming fluids. These scientists consider, that barite crystallizes from hydrothermal solutions at temperatures which are not exceeding 200^{0}C (Bagratashvili, 1961; Uchameishvili, 1980; Roedder, 1972). In their opinion, the meanings of temperatures exceeding this digit are abnormal and should be excluded from consideration. However of long standing of research barits from deposits and ore occurences of various genetic types of Tajikistan do not confirm this assumption. The data, received by us, unequivocally specify that barits could be formed and at temperatures considerably exceeding 200^{0}C.

In the beginning this question we shall consider on an example barits from occurences of various mineral and genetic types Karamazar barit-bearing area of Northern Tajikistan.

Barite mineralization in Karamazar (Deposit Baritovay gorka, Severnay jila, Akmagol and Muzbek) is observed among rocks of various age, since lower Carboniferous and finishing Tertiary formations. However majority of industrial deposits barite was formed in late Paleozoic and is located in various on structure and age intrusive and effusive rocks. The containing rocks thus were exposed by intensive change and are expressed in sericitization, chloritezation, kaolinization, beresit formation, silicification, carbonatization and, in a smaller scale, ferrification, albitization and feldspatization.

Alongside with actually barite deposits and occurences, submitted quartz - barite, barite-galenite and quartz-barite-fluorine deposits, this mineral meets in significant amounts and in fluorine (Naugarzan, Kengutan etc.) and silver - basicmetals (Big Kanimansur, Zambarak etc.) deposits. Besides barite is found out in skarns molybdenite-wolframs (Chorukhdairon) and polymetal (Altintopcan, Kansai, Kurusai, Turangli and ets.) deposits, in which barite is not the basic component of ores. He is connected here with finishing ore process by stages of mineralization and it is in their top horizons.

Thermometric research have shown, that basic morfogenetic types of inclusions mineral forming solutions in barite are submitted, mainly, liquid and gas-liquid konservates.

Bitumen inclusions meet occasionally. Dominant types among them are one-phase inclusions with the various sizes.

Primary gas-liquid inclusions in barite are irregular distributed ones and groups. The ratio of phases in such inclusions vary from 1:4 till 1:14. Their sizes is very fine. Sometimes reach (achieve) up to 0,05 mm. The form of inclusions in them various. It are marked basically sharp-angled, oval, triangular, square and lengthened. Crystall-form prizmatic-shaped and shape of isometric inclusion meet sometimes.

Temperatures of homogenization of inclusions in barits from various deposits are different (see table).

Table

Temperature of barite formation барита in deposits and occurences in Karamazar area

Deposit	Gene-ration	Temperature, ^{0}C	
		Homogenization	Decrepitation
Baritovay gorca	I II	175-250 90-130	- -
Severnay jila	-	185-255	-
Tereklitau	-	160-230	-
Koshmagat	-	170-235	-
Akmogol	-	190-245	-
Naugarzan	-	100-165	-
Kanimansur -//- -//-	I II III	185-230 130-155 65-125	180-225 - -
Zambarak	-	135-155	180-270
Tariecan	-	160-200	250-270
Chorukhdairon	-	150-270	200-300
Turangli	-	170-245	200-280
Orlinay gorca	I II	190-265 -	- 130-200

The study of inclusions mineral forming solutions in barits of the barite deposits shows, that crystallization of this mineral occured in a wide range of temperatures 90-255^{0}C. Early generations of barite were formed at temperatures 160-255^{0}C, and late - 90-165 ^{0}C.

As against of barite of properly barite deposits, range of temperatures of formation of this mineral in deposits of other types in our region wider. Temperature of homogenization of inclusions in barits from these deposits is equal to an interval 65-270^{0}C. Among them the maximal meanings of temperatures are characteristic for barite of Chorukhdairon deposit. Here temperature of homogenization of inclusions is equal 150-270^{0}C (Alidodov, 1982).

For barits of deposits in Kurusai ore field the meaning of temperatures of homogenization are raised: 182-238 and 198-250^{0}C (Sazonov, 1962) also is characteristic, in comparison with barits from Naugarzan and Zambarak deposits. In the latter it has appeared as lowered a little and changes from 100 up to 165^{0}C. Inclusions of mineral forming fluids in barits of various generation from a deposit Big Kanimansur is homogenizing accordingly at temperatures 185-230^0, 130-155^0 and 65-125^{0}C (Fayziev, Fozilov, Gadoev, 2001). Let's note, that reliability of temperatures of homogenization of inclusions in investigated barits was supervised on other minerals (quartz, fluorine, calcite), taking place with it in close paragenetic of association.

Temperature of intensive cracking barits occured in intervals 130-200^{0}C (Orlinay gorca), 180-225^{0}C (Kanimansur), 250-270^{0}C (Tariecan) and 200-300^0 C (Chorukhdairon).

It is necessary to note, that in barits from Karamazar deposits really quite often abnormal gas-liquid inclusions are marked, and distinguished from "normal" gas-liquid inclusions by a unequal ratio of gas and liquid phases quite often taking place beside each other. The origin of such inclusions, probably, is connected to physical properties (fragility, cleavage) mineral. It is possible to explain occurrence of abnormal inclusions by action on them of high-temperature solutions of later stages mineralization, therefore inclusions in barits was cracing and there was an outflow of a liquid phase through formed micro-cracks. Where barite contacts with other minerals (quartz for instance), the abnormal high-temperature inclusions occur there.

The study barits from fluorite deposits of Central Tajikistan shows on an interval of temperatures of homogenization of primary gas-liquid inclusions in them, equal 75-310^{0}C (Fayziev, 1991). To higher meanings of temperatures of homogenization of inclusions characterize barite from gold deposit Sasic (Central Pamir). Primary gas-liquid inclusions in crystals barite from this deposit with gas filling 25-46 % and size up to 0,1 mm in length homogenized within the limits of temperatures 275-365^0 C (Fayziev, Alidodov, Iskandarov, 1972).

It is known, that in the most part of deposits linked with carbonatites, barite is one of the basic minerals in ore bodies. The formation of these deposits occured from high density (60-75 and more weight. %), saturated by volatile components, silicat-salt, melts, melt-salts and solutions – brine at temperatures more than 600^{0}C (Fayziev, Iskandarov, Gafurov, 2000). Barite is crystallized at temperatures higher 600^{0}C, for example on a deposit Dunkeldic (East Pamir).

For barits of deposits in Kurusai ore field the meaning of temperatures of homogenization are raised: 182-238 and 198-250^{0}C (Sazonov, 1962) also is characteristic, in comparison with barits from Naugarzan and Zambarak deposits. In the latter it has appeared as lowered a little and changes from 100 up to 165^{0}C. Inclusions of mineral forming fluids in barits of various generation from a deposit Big Kanimansur is homogenizing accordingly at temperatures 185-230^0, 130-155^0 and 65-125^{0}C (Fayziev, Fozilov, Gadoev, 2001). Let's note, that reliability of temperatures of homogenization of inclusions in investigated barits was supervised on other minerals (quartz, fluorine, calcite), taking place with it in close paragenetic of association.

Temperature of intensive cracking barits occured in intervals 130-200^{0}C (Orlinay gorca), 180-225^{0}C (Kanimansur), 250-270^{0}C (Tariecan) and 200-300^0 C (Chorukhdairon).

It is necessary to note, that in barits from Karamazar deposits really quite often abnormal gas-liquid inclusions are marked, and distinguished from "normal" gas-liquid inclusions by a unequal ratio of gas and liquid phases quite often taking place beside each other. The origin of such inclusions, probably, is connected to physical properties (fragility, cleavage) mineral. It is possible to explain occurrence of abnormal inclusions by action on them of high-temperature solutions of later stages mineralization, therefore inclusions in barits was cracing and there was an outflow of a liquid phase through formed micro-cracks. Where barite contacts with other minerals (quartz for instance), the abnormal high-temperature inclusions occur there.

The study barits from fluorite deposits of Central Tajikistan shows on an interval of temperatures of homogenization of primary gas-liquid inclusions in them, equal 75-310^{0}C (Fayziev, 1991). To higher meanings of temperatures of homogenization of inclusions characterize barite from gold deposit Sasic (Central Pamir). Primary gas-liquid inclusions in crystals barite from this deposit with gas filling 25-46 % and size up to 0,1 mm in length homogenized within the limits of temperatures 275-365^0 C (Fayziev, Alidodov, Iskandarov, 1972).

It is known, that in the most part of deposits linked with carbonatites, barite is one of the basic minerals in ore bodies. The formation of these deposits occured from high density (60-75 and more weight. %), saturated by volatile components, silicat-salt, melts, melt-salts and solutions – brine at temperatures more than 600^{0}C (Fayziev, Iskandarov, Gafurov, 2000). Barite is crystallized at temperatures higher 600^{0}C, for example on a deposit Dunkeldic (East Pamir).

The temperatures crystallization barite more than 200^{0}C is confirming by some examples from the references on detailed researches of A.I. Gomelauri with the co-authors (1974) both A.G.Tvalchrelidze and V.I. Sheglova (1990) on deposits of Georgia; the intervals of temperatures crystallization barite 220-280 and 242-302^{0}C are established. D. Rife's (David, 1971) study of inclusions in this mineral from a deposit to a Cartersville (the state Georgia, USA) has established a limit of temperatures of homogenization of inclusions 127-297^{0}C. On the data O.A.Kovrigo (1973) formations barite on Ridder-Sokolniy deposit occured at temperatures 330-360^{0}C. On G.I. Belikovoy etc. (1978) temperatures of formation barite of deposits of Bashkiria occured in a range of temperatures 155-300^{0}C, and Orlov deposit - 250-330^{0}C (Jilinskaye, Kormushin, 1971), Zarechenskogo and Average polymetal deposits (Rudniy Altai) - 250-320^{0}C (Borisenko, 1988), deposits Atasuyskogo such as - 200-250^{0}C (Kulinich, Mukhanov, etc., 1988), deposits Zakarpatye -100-250^{0}C (Platonova, Kovalishin etc., 1976).

Thus, the given examples show, that barite could crystallize from mineral forming solutions and at higher temperatures, than 200^{0}C.

LITERATURE

1. Алидодов Б.А. Месторождение вольфрама и молибдена // Минералогия, геохимия и генезис некоторых эндогенных месторождений Таджикистана. Душанбе: Дониш, 1983. С.201-226.
2. Багратишвили Т.Д. некоторые вопросы минералогии баритовых месторождений Западной Грузии // Тр. геол. ин-та АН Груз. ССР. Мин.-петр. сер., 1961.Т.5.
3. Беликова и др. Физико-химические условия образования баритов в Башкирии // Термобарогеохимия земной коры и рудообразование. М.: Наука, 1978.С.122-127.
4. Борисенко А.С.Физико-химические параметры формирования баритовой минерализации Алтае-Саянской складчатой области // Тр. Института геологии и геофизики. Новосибирск, 1988. Вып.733. С.165-177.
5. Гомелаури А.И., Гуниава В.Д., Аревадзе Д.В. Температура образования некоторых баритах месторождений Западной Грузии // Вестн. МГУ. Сер. геол. 1974. №5. С. 113-116.
6. Жилинская И.И., Кормушин В.А. Температура образования барита и флюорита на Орловском месторождений (Рудный Алтай) // Изв. АН Каз. ССР. Сер. геол. 1975. №2. С. 56-58.

The temperatures crystallization barite more than 200^{0}C is confirming by some examples from the references on detailed researches of A.I. Gomelauri with the co-authors (1974) both A.G.Tvalchrelidze and V.I. Sheglova (1990) on deposits of Georgia; the intervals of temperatures crystallization barite 220-280 and 242-302^{0}C are established. D. Rife's (David, 1971) study of inclusions in this mineral from a deposit to a Cartersville (the state Georgia, USA) has established a limit of temperatures of homogenization of inclusions 127-297^{0}C. On the data O.A.Kovrigo (1973) formations barite on Ridder-Sokolniy deposit occured at temperatures 330-360^{0}C. On G.I. Belikovoy etc. (1978) temperatures of formation barite of deposits of Bashkiria occured in a range of temperatures 155-300^{0}C, and Orlov deposit - 250-330^{0}C (Jilinskaye, Kormushin, 1971), Zarechenskogo and Average polymetal deposits (Rudniy Altai) - 250-320^{0}C (Borisenko, 1988), deposits Atasuyskogo such as - 200-250^{0}C (Kulinich, Mukhanov, etc., 1988), deposits Zakarpatye -100-250^{0}C (Platonova, Kovalishin etc., 1976).

Thus, the given examples show, that barite could crystallize from mineral forming solutions and at higher temperatures, than 200^{0}C.

LITERATURE

1. Алидодов Б.А. Месторождение вольфрама и молибдена // Минералогия, геохимия и генезис некоторых эндогенных месторождений Таджикистана. Душанбе: Дониш, 1983. С.201-226.
2. Багратишвили Т.Д. некоторые вопросы минералогии баритовых месторождений Западной Грузии // Тр. геол. ин-та АН Груз. ССР. Мин.-петр. сер., 1961.Т.5.
3. Беликова и др. Физико-химические условия образования баритов в Башкирии // Термобарогеохимия земной коры и рудообразование. М.: Наука, 1978.С.122-127.
4. Борисенко А.С.Физико-химические параметры формирования баритовой минерализации Алтае-Саянской складчатой области // Тр. Института геологии и геофизики. Новосибирск, 1988. Вып.733. С.165-177.
5. Гомелаури А.И., Гуниава В.Д., Аревадзе Д.В. Температура образования некоторых баритах месторождений Западной Грузии // Вестн. МГУ. Сер. геол. 1974. №5. С. 113-116.
6. Жилинская И.И., Кормушин В.А. Температура образования барита и флюорита на Орловском месторождений (Рудный Алтай) // Изв. АН Каз. ССР. Сер. геол. 1975. №2. С. 56-58.

7. Ковриго О.А. Термометрия включений в рудообразующих минералах Риддер-Сокольного месторождения // Новые данные по геологии медных и полиметаллических месторождений Казахстана. Алма-Ата, 1973. С.79-87.
8. Кулинич В.В., Муканов К.М. и др. Физико-химические параметры формирования баритов различных генетических типов на месторождениях Атасуйского типа (Центральный Казахстан) // Прикладная термобарогеохимия. Матер. межвед. Семин. Алма-Ата, 2-4 июня 1987. Ч.1.Алма-Ата, 1988. С. 160-164.
9. Платонова Э.Л., Ковалишин З.И., и др. Условия образования баритов в Закарпатье // V всесоюзное совещание по термобарогеохимии (тезисы докладов). Уфа, 1976. С.200.
10. Сазонов В.Д. Некоторые физико-химические особенности процессов гипогенной минерализации на примерах отдельных месторождений Таджикистана // Автореф. дис. …канд. геол.-мин. наук. Душанбе, 1962.
11. Твалчрелидзе А.Г., Щеглов В.И. Минералого-геохимическая модель жильного баритового рудогенеза // ЗВМО.1990.Вып. 2. Ч. 119. С. 21-34.
12. Учаймешвили Н.Е., Малинин С.Д., Хитаров Н.И. Геохимические данные к процессам формирования баритовых месторождений. М.:Наука, 1984.124с.
13. Файзиев А.Р., Алидодов Б.А., Искандаров Ф.Ш. Некоторые физико-химические особенности формирования Сасыкского золоторудного месторождения (Центральный Таджикистан) // Минерал. сб. Львовск. госун-та. 1972. Вып.4. №26. С.378-387.
14. Файзиев А.Р. Минералогия, генезис и закономерности размещения флюоритовых месторождений центрального Таджикистана. Душанбе: Дониш, 1991. 314с.
15. Файзиев А.Р., Искандаров Ф.Ш., Гафуров Ф.Г. Минералогия, термобарогеохимические условия становления и генезис редкоземельно-флюоритового место-рождения Дункельдык (ВосточныйПамир) . Душанбе, 2000. 174 с.
16. Файзиев А.Р., Фозилов М.М., Гадоев М.Л. Баритовая минерализация месторождения Большой Канимансур (Северный Таджикистан) // Труды ИГ АН РТ. «Геология и минерально-сырьевые ресурсы республики Таджикистан». Душанбе. 200i. С.185-189.

17. Rife David L. Barite fluid inclusion geothermometry. Carters Ville mining district. // Econ. Geol. 1971. Vol 66. №8. P.822-824.

18. Roedder E. Barite fluid inclusion geothermometry, Carters Ville mining district, Northwest Georgia, Discussion // Econ. Geol. 1972. Vol 67. P.821-822.

PHYSIC -CHEMICAL PARAMETERS OF MINERAL-BERRING PROSESS ON DEPOSITS MARBLE ONYX FROM SOUTHERN TYAN-SHAN

F.A. Malakhov, A.R.Faiziev

The investigation on fluid inclusions was carried out to establish the physic-chemical parameters of mineral-forming solution on marble onyx deposits. The main object for thermobarogeochemistric researches was calcitic marble onyx. Other accompanying minerals - celectite, barite, fluorite and quartz - were investigated too.

It is necessary to note that thermobarogeochemistric researches at study conditions of formation marble onyx are accompanied with the certain difficulties: limitation of inclusions in the mineral (calcite), their small size, and also insignificant distribution of paragenetic minerals, suitable for researches. Besides thinsections of onyx under microscope very dark, often is observed "twinning" of the images of inclusions, owing to strong two-refraction of a mineral.

The study of marble onyx samples from various genetic types of deposits (vein, bedded and carst cave formation) show the following types of microinclusions: 1) water solutions (one-phase and two-phase); 2) carbon dioxide and carbon dioxide - water; 3) hydrocarbons and 4) hard phase.

The hard inclusions in marble onyx are situated in dolomite, native sulfur, gypsum, celestite, magnesite, hydromagnesite, sulfide, hydroxides of iron, oxides of silicon, the clay minerals etc. They are usually met rarely. The exception is the clay minerals, which are contained in a plenty in so-called "clay" layers. It is necessary to note that as hard inclusions there are not only minerals - companions, but also fragments of host rocks seized at precipitation of marble onyx (for example, pieces of limestone or grains of plagioclase).

The hydrocarbon inclusions sited in marble onyx constantly and in various quantities is one of characteristic features of marble onyx mineralization. They were marked in the majority of the investigated samples of various genetic types of marble onyx deposits. These inclusions are distributed irregular and, as a rule, are located in more dark strips of marble onyx, having primary character. They settle down separately and as group on 2-4 and more inclusions. There are marked also in group of inclusions located as chains, for which the non-uniform redistribution of phases, making them as characteristic. These chains are placed without any laws under the relations one to another or relatively to some structure - texture elements of growing zones in onyx. Probably, these inclusions have secondary character.

The forms of hydrocarbons inclusions basically are irregular, rarely lengthened ovoid. There are conservats having the forms of negative crystals as curve-faced round-shaped

secretions of rhombohedric and scalenohedric habits. The size of hydrocarbon inclusions is varying from 0,015 up to 0,1 mm, sometimes reaching 0,3-0,4 mm. As a rule, sin-genetic (primary) inclusions are round-shaped, ovoid with elements of negative fasing. The secondary inclusions have drop-shaped and irregular forms. Aggregate state of hydrocarbon inclusions are seen as following: one-phase (oil, bitumen), two-phase (oil + gaseous; oil + aqueous solution; oil + bitumen) and multiphase (oil + aqueous solution + gaseous; oil + bitumen +gaseous; oil + + bitumen +gaseous). Besides the mentioned above, one sample shows the hydrocarbon inclusion with two liquids not mixing up phases. Hydrocarbon inclusions are characterized by absence of any laws on the redistribution of its phases: amount and contents of those or other phases are changeable and can vary over a wide limit. For example, the contents of a gaseous phase changes from 3 up to 75 % and more.

Under heating of two-phase (oil + gaseous) hydrocarbon inclusions, disappearance of vapor (gas) bubble, i.e. their homogenization, occurred at temperatures 90 - 116^{0}C. The heating of two-phase inclusions, such as oil + bitumen, spent to dissolution of hard phase at temperature 199 $\pm$ 3^{0}C. Heated bitumen inclusions are lightened from dark brown up to light - yellow.

The presence of organic substance well fixed at IR spectroscopy in marble onyx samples. Their IR spectra contains strips of absorption with maxims 3000-2800 cm^{-1} probable for fluctuations of link in C-H-group of hydrocarbon structures; strip of absorption 2700-2500 cm^{-1} belongs to OH- group; strip of absorption 2800 cm^{-1} characterize C-O-group anhydride-carbon acids; strips of absorption in an interval 1400-1100 cm^{-1} are observed as valent fluctuation of C-O-group. Onyxes, except for hydrocarbons, contain also organic substance with oxygen-bearing functional groups. The strips of absorption in an interval 2350-2400 cm^{-1} are connected with carbonic acid; the latter is established in inclusions by the chromatographic analysis.

The amount of bitumen A (amorphous) in samples marble onyx was determined by luminescent - bitumenological analyses, which hesitate in limits from 0,0012% up to 0,008% (average - 0,0032 %). A ratio of an chloroform extract to an alcohol-benzole is 1:3. Specific composition of bitumen substances in marble onyx is seen as increased amounts of an oil fraction, hydrocarbons prevail in its structure. For an chloroform extract the presence of oil - *resinous* (oils up to 50 % and above is characteristic, it is a lot of pitches), resinous (there are a lot of pitches, traces asphaltenes) and, in a less degree, light (free bitumen A) bitumen types. The similar characteristics have bitumen in an alcohol-benzole extract too. As a rule, the organic substances are submitted to various chemical changes, including interactions between

components of considered media system. Many from them collapse with the certain speed directly depending on meaning of temperature. Therefore, the change in time from temperature determines composition and modular state of hydrocarbon inclusions, specifying for their probable source of an origin. Usually for more high-temperature formation is characterized contents of light bitumen, oily-resinous and resinous types are characterized for most low-temperature and hypergenic mineralization. In our case the prevalence of oily-resinous type bitumen specifies that its redistribution occurs in thermodynamic conditions zone of hypergenes. The source of organic matter, as well as calcium carbonate, was served host rocks, is especial if to take into account, that the majority of marble onyx deposit are located in oil-bearing sediments of Paleogene and Cretaceous. It was specified by us earlier (Малахов, Файзиев, 2003).

Carbon dioxide and the carbon dioxide-aqueous inclusions are distributed in marble onyx irregular; they are most advanced in veins and lens-shaped bodies. The size of them vary from 0,005 mm up to 0,05 mm. Carbon dioxide inclusion are mainly one-phase, less two-phase isolations. The homogenization of two-phase inclusions is reached at temperature 24-30^{0}C in a gaseous phase. Occasionally there are three-phase carbon dioxide-water inclusions with sharp prevalence of water solution. The partial homogenization of these inclusions occurs at temperature 28-30^{0}C. The meanings of pressure of mineral-forming solutions were appreciated in these inclusions. Carbon dioxide and water - carbon dioxide inclusions are isolated, as a rule, in result of boiling solutions.

The mineral-forming inclusions of media in marble onyx are being both primary, and secondary. Their belonging to this or that genetic class were established by the basic attributes, according to genetic classification N.P. Ermakov (1972), where to primary inclusions suggested the inclusions located separately, without connection with cracks, and also located in elements cutting of minerals. The primary inclusions located under mineral inclusions of various accompanying minerals and contacts with them. These inclusions are focused in parallel to direction striping, occupying more often interstitial space. To secondary and pseudo-secondary inclusions, according to this classification, located in healed cracks. They usually are one-phase liquid.

The primary inclusions are dated, as a rule, as light, mainly re-crystallized strips in marble onyx. Alongside with one-phase liquid, the individual two-phase gaseous-liquid inclusions are found among them. The one-phase liquid inclusions are of various forms. Prevail round-shaped, round-extended and lengthened, with elements of facing. The size changes from 100-th up to the tenth shares of millimeter, seldom reaching 1 mm. The

gaseous-liquid inclusions have lengthened, tubular, ovoid, three and four-angle forms. Less often they have an irregular configuration. Occasionally inclusions have the form of negative crystal, mainly trigonal prism and rhombohedr. The size of inclusions is the 100-th and tenth shares of millimeter. The ratio of a gaseous phase to liquid one in two-phase inclusions changes from 1:35 up to 1:6. Their homogenization occurs in an interval of temperatures 50-150^{0}C as the first type (table). Geterogenization of them comes under cooling of thin section until 10-50^{0}C. Such wide area of temperature of geterogenization is connected to presence of volatile, first of all carbon dioxide (Наумов, 1982), which is revealed in marble onyx by the chromatographic analysis, and also presence of its strip of absorption (2350-2400sm^{-1}) in IR-spectra of marble onyxes. Among two-phase inclusions mineral-forming media, there are also abnormal inclusions with the sharply increased contents of a gaseous phase. At their heating to temperature 380^{0}C, complete homogenization was not reached though some reduction of a gaseous phase. Some abnormal inclusions has relation of gas to a liquid is 1:3 -1:5; its homogenization is coming at temperatures up to 350-370^{0}C, phases ratio restore to former by their cooling. There are also inclusions with essential content of vapor, homogenizing in a gaseous phase. As the main condition of genesis of abnormal inclusions, it is necessary to consider the transformations of the tubular and lengthened inclusions due to their splitting. The occurrence of such abnormal inclusions is connected with adjournment of related substance on walls of vacuole. However, considering low concentration of solutions of inclusions, it will doubtful some essential influence of this process on temperature homogenization in a case of fast rate of heating.

Quite often under microscope in the thin plates of marble onyx the group of different-completed inclusions from only water up to essential of gas content is observed. Their presence is marked in vein-shaped and stratyform bodies of marble onyx. The origin these different-completed inclusions is connected with boiling of solutions (Бакуменко, 1982). Thus the isolating phases in inclusions can grasp additional, immmiscibiable under the temperature of capturing, phase. These inclusions are not suitable for definition of temperature and pressure by them, including at the moment of boiling of solutions, though they have primary character (Наумов, 1982).

Proceeding from the received data, the top limit of temperature of homogenization of inclusions in marble onyx reaches 150^{0}C. The judging by the data in the table of homogenization temperature, such meanings have insignificant distribution, and the formation of onyx mineralization occurred mainly below 150^{0}C. And the most intensive allocation marble onyx from vein type deposits occurred in an interval 110-70^{0}C. In marble onyx from

stratyform deposits fluid inclusions homogenized mainly at temperatures up to 100^{0}C with peak of temperatures in an interval 90-70^{0}C. Alongside in marble onyx of the marked types of deposits, there are also numerous one-phase *liquid* inclusions showing that mineral-forming process in these deposits proceeded at temperatures below 500^{0}C. In marble onyx from carst type deposits the two-phase gaseous-liquid inclusions meet less often and homogenized mainly below 80-90^{0}C.

Table Homogenization temperature of fluid inclusions in marble onyx

Deposit	An interval of homogenization, ^{0}C	Deposit	An interval of homogenization, ^{0}C
Ishma	68-140	Dangara	70-125
Patru	60-150	Shurkhok	75-135
selboor	60-150	Poshoom	70-150
Takob	50-145	Karluk	65-135
Khojaobigarm	64-140	Garmchashma	55-67
Ziddeh	65-135	Kuhi Lal	55-95
Rikky	75-137	Yory	68-76
Yagnob	65-138	Zuman	80-120
Jilay	65-95	Gaurdak	80-110

Decrepitation of inclusions in marble onyx (both thermo-sound and thermo-vacuum) occurs in a range of temperature from 125 up to 300^{0}C and above. The peaks of decrepitation of inclusions at temperature 125-150 and 200-225^{0}C are observed. On the decrepitation curve some samples is fixed also with very weak gas issuing at rather low temperatures (60-85^{0}C). Decrepitation under temperatures more than 300^{0}C is connected, apparently, with cracking of abnormal inclusions and disintegration of substance on clivage and was not considered.

The results of chriometric researches of individual liquid inclusions in marble onyx show that the complete thawing of hard phases presented anizotropic needle crystal occurs at temperature -3,7 - -3,10. Under the diagram of solubility in system NaCl - $NaHCO_3$ - H_2O (Борисенко, 1977) the concentration of salts in solutions of inclusions makes the first percents sometimes reaching 6-8 w. % in an equivalent of NaCl. The data of the chemical analyses of triple aqueous extracts show, that in cation part of salt composition solutions of liquid inclusions prevails Ca^{2+}, and subordinated amount Mg^{2+}, Na^+, K^+ and NH_4^+ are present. In anion group HCO_3^- and SO_4^{2-} dominate, F^- and Cl^- are present as a lesser degree. Last is marked only in aqueous extract of separate samples, where increase the contents of Na^+ and K^+ also is simultaneously observed, is especially in a sample from Gayrdak deposit. The

highest concentration of F^- are marked in aqueous extracts from deposits Takob, Ziddeh and Yagnob (6.8, 9.36 and 8.4 %-equivalent accordingly). A sulfate-ion in most cases is a leading component of solution in aqueous extracts. Its high contents usually are marked in deposits, where there was an allocation sulfate (celectite, barite and especially, gypsum). The revealed law is precisely fixed in aqueous extracts from Karluk deposit. The increased contents Mg^{2+}, apparently, is connected with containing magnesium-bearing rocks and serves as the indicator of presence of magnesium minerals (dolomite, magnesite and hydromagnesite). In some aqueous extract presence Sr^{2+}, Ba^{2+}, Cu^{2+}, Zn^{2+}, S^{2-} and other ions are revealed. The spectral analysis of the dry rests aqueous extracts show presence Si, Al, Ti, Mn, Cu, Sr, Ba, and also Zn, Pb and other elements. The oxidation-reduction of regime in solutions aqueous extracts is near neutral or has sub-alkaline (pH 7-7,8).

In a gaseous components of inclusions, on the data of gas chromatography, the carbon dioxide prevails, which presence is established also by IR specters of marble onyx. The total contents of other components (CH_4, H_2, CO, N_2 etc.) is insignificant. Some increase of their relative role is observed in inclusions from samples connected with low-temperature sulfide mineralization. There is marked the general downturn contents of CO_2 in a gas component of inclusions from deposits marble onyx of vein via stratyform to karst type.

Meaning of pressure determination on a method of R. Nakken with interpretation of V.A.Kalyujny (1953), it has made 40 - 45 bars for stratyform deposits, less often than 50-55 bars, and for vein ones, mainly 50-70 bars, rarely reaches 100-150 bars. The similar meanings of pressure are received by definition with boiling of aqueous solutions.

The similar physic-chemical parameters of mineral-forming process were received by study of celestite, barite, fluorite and quartz too.

Thus, the received data testify that the formation of marble onyx occurs from low-concentrate low-temperature hydrothermal solutions, having calcium-sulfate-bicarbonate composition.

1.Малахов Ф.А., Файзиев А.Р. Генетические особенности образования проявлений мраморного оникса Южного Тянь-Шаня и прилегающих территорий//Док. АН РТ. Серия геол. - 2003. -№7-8.-С.56-66.

2.Ермаков Н.П. Геохимические системы включений в минералах -М.: Недра, 1972, 175 с.

3.Наумов В.Б. Возможности определения давления и плотности минералообразующих сред по включениям в минералах. Использование методов термобарогеохимии .... -М.: Недра, 1982. -С. 89.

4.Бакуменко Т.И. Сопутствующие, комбинированные и аномальные включения, критерии их познания и возможности использования. В кн.: Использование методов термобарогеохимии....М.: Недра, 1982, с.126-140

5.Борисенко А.С. Изучение солевого состава растворов газово-жидких включений в минералах методом криометрии//Геология и геофизика.-1977.- №8. -С. 16-28

6.Калюжный В.А., Колтун Л.И. Некоторые данные о давлениях и температурах при образовании Нагольного Кряжа (Донбасс)//Мин. сб. Львовского геол. общ.- 1953.- №7. -С.67-74

THE QUESTIONS OF THE IMPROVEMENT ACOUSTIC DEKREPTOMETRICHESKOY EQUIPMENTS IN PURPOSE OF INCREASING TO EFFICIENCY SEARCHING FOR HIDDEN MINERALLIZATION.

V.S. Polickovsky, I.A. Novikov, S.M. Strelitsov, R.A. Sharipov, R.N. MurogovaP, L.R. Ismailov

Uzbekiston branch of International Assosiation Thermobarogeochemistry studies in country of the Asia and Ocean, International Academy Mineral Resource, Tashkent Uzbekistan.

Dekreptometricleskiy acoustic method thermometric studies used at searching for hidden mineralization halo get steamin due to its objectivity, expressive and informatively is broadly used in practical person geology-searching for of the work. However, at the last 15 years of the essential work on improvement decreptometricle equipments was not conducted.

Called on analysis of the nature of the necessary corrections and improvements of the separate nodes decreptometricle equipment has shown need of the new constructive developments goal-directed on following sections:

1. The Reduction level influences stranger noise on effect decrepitation (D), got at microexhlosions gas-fluid inclusions..
2. The Reduction of the nonlinear distortion.
3. Increase frequency and dynamic range.
4. The Simplification of the assembly and adjustments of the equipment.
5. The Development device for regulation of the velocities of the heating of the test.
6. The Development device for automatic ascent of the temperature under D-analysis of the test in assigned temporary mode under constant interval of the heating from 0 before 700 degrees.
7. The Development of the new system of the adjustment decreptometr by change earlier used adjustment on master quartz.
8. The system Development automatic record result D-analysis in digital importances and in graphic performance.
9. The Improvement to general design acoustic decreptometr with provision for achievements maximum comfort in work.

10. The Development of the design of the separate nodes and whole installation as a whole creation to stationary laboratory model and small-dimensioned portable decreptometr, suitable for transportation and following work in field condition.

In 1998r. I.A. Novikovym and S.V. Levinym have offered broadly to use computer technologies under laboratory Termobarogeohimicheskih (TBG) study.

Created by them models decreptometre is used computer of the type IBM with processor PENTIUM 2-800 MHZ, operative memory 256 Megabytes, Winchester'''''''''''''''''''''''''' by capacity 30 Gigabytes and 16 битной by sound card. The Programs were created by means of VISUAL BASIC -6.0, VISUAL C++ and worked WINDOWS 98, as well as were used program for compression acoustic file, recorded in format * WAV*, * MPEG 3* and back.

Sensitivity decreptometre increased As a result of use электретного mike in 8 - 10 once without use additional cascade reinforcements.

Herewith vastly were reduce noise pickups on input chain, due to that that, amplifier was collected on little-making opa-amps and is in close proximity mike. Leaving the mike was connected through sound card of the first computer channel with sampling rate 44.1 кГц, where was produced record and processing the signal by means of special programs.

The Received signal with thermocouples, escalated similar amplifier was connected to 2-channel of the sound card through amplitude modulator. Need of its use is explained that that sound cards do not allow to carry in COMPUTER EBM signals of the direct current, since they have an operating range 18-22000 Hz.

The three-dimensional function of the amplitude is built depending on frequencies of the got bleeps and follows with fixed by temperature.

At count of the number microexplosions depending on the temperature possible to automate and thereby to define the correlation with result other experience got by means of other programs.

Using the modern computer technology permits the conservation directly measured signal and undertaking his(its) repeated recalculation with provision for that particularities, on which researcher will consider necessary to pay earnest heed.

However, collations result D-analysis, got at study of the factions -1-0.5 mm of the master quartz Mogov deposit (Tadzhikistan), and passed complex in process of the studies of the standard master natural material * KVARC-74 *, offered by V.A. Kormushin, have shown insufficient sensitivity of the amplifier, designed on scheme I.A. Novikova - S.V. Levina. Particularly, this

concerns, D-activities in interval 220 degrees Celsius. Considering aforesaid, in scheme of the amplifier designed by I.A. Novikov- S.V. Levin were enclosed some additions.

This has allowed to agree the results D-analysis of the master natural material * KVARC-74 * with result got by means of new dekreptometre with designs I.A. Novikova and S.V. Levinym.

Thereby, on the grounds of called on studies characterized in data thesis possible with confidence to recommend the continuation of the studies on improvement dekreptometre acoustic D-equipments with use the achievements of the modern computer technology. One of the importance of the component parts of this functioning must be a fabrication master artificial quartz, its natural analogue), which must be certain reproducible and certification in accordance with requirements of the metric service.

1. Bozhko M.T., Polikovsky V.S. and others Small-dimensioned D-installation SAIGIMS-2 in collection of the study miniralgeneration solution and melts on inclusions in mineral. Alexander. 1971.
2. Ermakov N.P., Dolgov YU.A. Termobarogechemistry. The Depths. Moscow. 1979.
3. Levin S.V. Computer dekrepitaciya. *The Geology and exploring 2. Moscow. 1998.
4. Lyahov YU.V., Pavluny N.N. and others Termobarogeochemistry of gold. * Will WREATHE *. Livov. 1995r.
5. Polickovsky V.S., Strelicov S.N., Smiyanov V.A. Acoustic decreptometricle LUCH-11. The Works second TBG-symposium APIFIS. Tashkent. 1998.
6. Polikovsky V.S., Strelicov S.N., Smiyanov V.A, Shapiro R.A., Kombarova L. To question about improvements acoustic decreptometrly equipments. The Material XI International Conference on thermobarogeochemistry.
7. Redder E. Flyuidnye inclusions in mineral.
8. Shriek P. Reference manualч sound schemetechiques. The World. Moscow. 1991.

PTCR EFFECT IN FERROELECTRICS-SEMICONDUCTORS

V.B.Kvaskov and A.S.Sigov

Moscow State Technical University of Radioengineering, Electronics, and Automation, MIREA, 78 Vernadsky Ave., 119454 Moscow, Russia

We present a short review of some important results in the field of physical properties, preparation, and possible applications of ferroelectrics-semiconductors with Positive Temperature

Coefficient of Resistivity (PTCR).

The PTCR effect was first observed in semiconducting barium titanate by P.W.Haaijman, R.W.Dam, and H.A.Klasens (Philips) in 1953, but due to the patent procedure the results had not been published. Analogous results were reported by H.A.Sauer and S.S.Vlasens at the Electronic Components Symposium (Washington, 1956), and since that time the semiconducting barium titanate became an object of extended investigations as well as applications: more than 1000 of papers and several hundreds of patents are known, nevertheless the nature of the PTCR effect still has not been described in a non-controversial manner.

We discuss a number of experimental results on the PTCR effect and related phenomena: the influence of doping by different elements (Ce, Pr, La, Sm, Gd, Y, Dy, Nb, Ta, Nd, Sb, Mn, Fe, Cr, et al.) on the electrical conductivity of barium titanate at different temperatures, including the phase transition region, the role of local surface states and internal/external mechanical stresses; the frequency dispersion of PTCR value in both paraelectric and ferroelectric phases; the dependence of thermal electro-motive force on temperature; the nonlinear effects in a wide temperature region.

A special attention is paid to a critical analysis of the existing models of PTCR effect: Saburi-Kinase; Peria, Bratschun, and Fenity; Heywang-Jonker, as well as many others. It is shown that the band model theory is not applicable to semiconductors with low mobility of charge carriers, and in this case the alternative models based upon the possibility of polaron conductivity in single-crystal and ceramic samples can play the leading part.

To our opinion, the most promising approach to a self-consistent model of temperature-dependent conductivity of semiconducting barium titanate should be the consideration of charge carriers movement as a stochastic process, but there is a lack of data for such a consideration at present.

MESSBAUER INVESTIGATION OF QUARTZ DOPED BY IRON-57

S.K. Dedushenko[a*], I.B. Makhina[b], A.A. Mar'in[b], V.A. Mukhanov[b], Yu.D. Perfiliev[a]

[a] Department of Chemistry, Moscow State University, Lenin Hills, Moscow 119992, Russia

Russian Research Institute for Synthesis of Materials, Aleksandrov, Vladimir Region 601650, Russia

Artificial coloured quartz is of great importance for the present-day jewellery industry. In particular iron-doped quartz allows obtaining violet, yellow, green and brown gemstones. The position of an iron impurity in the crystal structure, the electronic structure of the metal ion as well as the general content of iron and proportion between its different forms are the main factors causing the colour and thus influencing the value of the crystal.

Amethyst is the most popular variety of coloured quartz. Its red-violet colour has been known since antiquity but till now the nature of this colour is not well established. Amethyst can be synthesised artificially by growing the quartz in the presence of Fe^{3+}-ions followed by X-ray irradiation of the crystal obtained. The formation and decomposition of the colour were thoroughly investigated by numerous techniques including EPR and optical absorption. But the answer to the question about the oxidation state of iron in this mineral has no definite answer.

Mossbauer spectroscopy is a very useful technique for the determination of the oxidation state of iron. But the content of iron in natural and artificial amethysts is very low and sensitivity of this technique is insufficient for the analysis.

To make the Mossbauer study of amethyst possible we synthesised the quartz crystal doped by ^{57}Fe. It allowed us to record informative Mossbauer spectra. Iron-doped quartz was found to contain a number of iron forms. X-ray irradiation of the crystal leads to changes in its Mossbauer spectrum. These changes can be interpreted as conversion of a part of trivalent iron into tetravalent state.

GROWTH AND OPTICAL PROPERTIES OF CALCITE SINGLE CRYSTALS

V.L. Borodin and I.V. Nefedova

All-Russian Research Institute for Synthesis of Materials(VNIISIMS)

Single crystals of the transparent mineral variety of calcium carbonate $CaCO_3$ (Iceland spar) are widely used in optics due to their high birefringence and transmission in a wide range of wavelengths. They are used at manufacturing polarizers, beam splitter elements, laser shutters and other optical units.

The problem of synthetic growing is of great practical significance. It is most efficiently solved with the hydrothermal method, which is used for mass α - quartz production. Using this method calcite was grown in the USSR [1], in USA [2], in France [3], in Japan [4]. But it was possible only in VNIISIMS (Russia) to develop in detail the technology and grow large crystals of optical calcite at industrial scale [5].

Calcite developed technology is to provide for using seed plates parallel directed to the rhombohedron faces $\{10\ \bar{1}1\}$. However the rhombohedrons are less convenient for making polarizers because of the great deal the expensive raw material waste. For successful crystals growing on pinacoidal $\{0001\}$ and prismatic $\{11\ \bar{2}0\}$ seeds, the configurations of single blocks are to provide for the most economic machining crystals for optical units. This kind of crystals are less useful for making polarizers because of the amount of waste that results and which increases the price of products.

In this work, dispersion of refractive indices (dependence of No and Ne on the length of light wave) was measured and optical inhomogeneities indicated by refractive indices of calcite single crystals were studied.

As the process of hydrothermal crystallization was carried out in aggressive solutions with respect to the steel autoclaves, lined inserts were used for the calcite synthesis. To protect autoclaves (24. 500, 1500 l volume) intended for long experiments, the inserts were made of the special titanium alloy ensuring the reactor corrosion stability and mechanical strength. The insert is the thin-walled autoclave (3, 100 and 500 l volume) placed in the steel bearing one. In the whole experience the operating conditions (pressure, temperature, temperature difference) were withstood constant owing to the autoclave heating up, the solvent thermal expansion in the lining and the inert medium (water) in the autoclave.

The hydrothermal method of calcite growing was carried out in aqueous solutions of NH_4Br at temperature 280-290°C and pressure 60-80 Mpa. In this solutions calcite has a positive factor of solubility, therefore the synthesis were performed under the "direct" temperature differences. The charge, made of fragments of the natural crystals, was loaded in the zone of dissolution (the lower part of reactor) and the seed plates of the Iceland spar large crystals (accurate to ± 30′) were charged in the zone of crystallization (the upper part of reactor). By thermal convection, the saturated solution was transpired from the higher temperature zone of dissolution to the lower temperature zone of crystallization (ΔT= 5-10 °C). Due to over saturation at the temperature of the crystallization zone, the excess of dissolved $CaCO_3$ was deposited on the seeds.

In order to measure the dispersion of refractive indices from single crystalline layer grown on a rhombohedral seed a trigonal prism with face dimentions 20x20 mm was used. Its lateral edges were oriented parallel to the optical axis of calcite. The results of measurements obtained by the prism method at temperature 293K on a goniometer with accuracy 5 angular sec.

Optical inhomogeneities indicated by refractive indices in calcite crystals grown on a prism seed were examined by interferometer of Twayman and Green. To exclude any influence of the surface pattern on measurement flat surfaces of the sample were processed in

the range of 2λ. Then they were covered by flat glasses which caused the distortion of the wave front not more than 0.05λ.

The transmission spectra of natural and synthetic calcite samples were recorded using polarized light in the range of 200-900 nm with a spectrophotometer. The light transmission (T, %) and the factor of light absorption (K, cm^{-1}) in the ultraviolet and vision range of spectrum were determined taking into account reflection losses from the sample surface.

On the basis of the developed technique of growing, we have grown crystals parallel to $\{10\ \bar{1}1\}$, $\{11\ \bar{2}0\}$, $\{0001\}$ faces. The absolute values of the growth rates were changed depending on the physicochemical conditions of the synthesis in the following range: $V_{11\bar{2}0}$ - from 0.05 to 0.25 mm/day; $V_{10\bar{1}1}$ - from 0.05 to 0.20 mm/day; V_{0001} - from 0.05 to 0.10 mm/day. The duration of experiences was 300 days. These crystals have $\{10\ \bar{1}1\}$ and $\{02\ \bar{2}1\}$ rhombohedrons, prism $\{11\ \bar{2}0\}$ and pinacoid $\{0001\}$ faces.

The values of refractive indices of synthetic calcite are close to the values of Iceland spar, but these properties of synthetic calcite are more stable than that of natural calcite.

Crystals grown parallel to the prism faces are characterized by extremely small distortion of the wave front in the direction perpendicular to the layers. Inhomogeneities according to refraction indices make up not more than $3x10^{-6}$ in a sample 7 mm thick. This is distinctly visible from the straight lines of interferograms in «o» and «e» beams.

The study of natural and synthetic crystals in the range of wavelength above 500 nm shows that light transmission is determined with structural features of $CaCO_3$ and is not connected neither to impurities nor to defects of crystal structure. On the contrary, the curves of light transmission in the short-wave range of spectrum are sensitive to various structure infringements and to the presence of impurities depending on the deposit geochemical peculiarities and the physicochemical conditions of crystal growth. Therefore, the synthetic calcite has a higher light transmission and a less statistical spread in T % values than the natural Iceland spar in the range of 340-500 nm.

The main objective of the developed method of calcite hydrothermal growth is to allow to reduce essentially the quantity of waste when manufacturing optical products, in order to increase the economic efficiency of growth. The light transmission and the values of refractive indices of the synthetic calcite are close to the values of Iceland spar, but these properties of synthetic calcite are more stable than that of natural calcite.

References

[1] N. Yu. Ikornikova, Hydrothermal synthesis of crystals in chloride systems, Nauka, Moskow 1975, pp.118-149.

[2] D. R. Kinloch, R. F. Belt, R.C. Puttbach, Hydrothermal Growth of Calcite in Large Autoclaves, J. of Crystal Growth, 24/25, 610, (1974).

[3] F. Gener, M. C. Bricard, R. Lemetre and R. Aumont, Recristallisation hydrothermale de la calcite dans des solution d'halogenuers d'ammonium, High Temperatures-High Pressures, vol. 6, 657-662. (1974).

[4] K Kikuta, S. Hirano, Hydrothermal growth and dissolution behavior of calcite single crystals in nitrate solutions, J. of Crystal Growth, 99, 895, (1990).

[5] V. I. Lyutin, V. V. Dronov, V. L. Borodin, V. E. Khadzhi, Proceeding of the VI International Conference on Crystal Growth, Moscow 1980, 4, p. 169.

THE CATHODOLUMINESCENCE PROPERTIES OF ZINC OXIDE CRYSTAL AND GETHEROSTRUCTURES ON IT BASE.

***Chukichev M.V.*[1], *Kolonius S.D.*[1], *Kortounova E.V.*[2], *Lyutin V.I.*[2], *Chvanski P.P.*[2]**

1. Department of Physics, Moskow State University, 119992, Moscow
2. Russian Research Institute for the Synthesis of Materials, Alexandrov

Zinc oxide single crystals have of wide spectrum of properties that allow to use in semiconducting equipment, optics as piezoelectric transducers, etc. Zinc oxide crystals were grown in hydrothermal conditions. We used autoclaves, that have inside the liners from special metals to protect autoclaves walls against corrosion by the alkalis. The temperature of crystallization was 350 ^{0}C, the temperature gradient was 8 ^{0}C, pressure was 30 Mpa. Crystallization was carried out using a solution of potassium hydroxide in presence of Li+ and NH4+ ions.

In work cathodoluminescence spectra of crystals and films of zinc oxide (ZnO) and getherostructures on his basis are investigated.

It is shown, that the spectrum of the cathodoluminescence in all investigated samples consist of the ultra-violet band formed by radiation exitonic recombination and green emission band of impurity centers with a maximum 500-520nm.

The nature of the centers of a luminescence and an opportunity of application of crystals and getherostructures of zinc oxide in optoelectronics is discussed.

GROWTH LOW DISLOCATION QUARTZ ON ROD SEEDS

Chvanski P.P.*, Gordienko L.A.*, Tsinober L.I.*, Zinkovskaya T.N.*, Polaynski E.V.* Orlov O.M.**

* Russian Research Institute for Synthesis of Minerals (VNIISIMS),

** OAO "Piezo", Moscow,

This paper deals with a way growing new updating of quartz crystals which are intended for manufacturing perspective devices. The new crystallographic orientation of one-zone growth of crystals were offered and determined with the purpose of obtaining low dislocation of quartz.

The new type of a seed material assumes a rod form orientated in length along a direction {10-11}. Grown quartz crystals are submitted mainly by material of negative rhombohedron and have received the name r/r-bar.

The estimation of experiment results was carried out on the basis of structural - morphological study of the grown crystals and the definition Q-factor by a method IR - spectroscopy. The distribution of a not structural and structural impurity in volume of crystals was investigated by methods x-ray γ-irradiation and termodecoration.

CONTENTS

AUTHOR INDEX